Event-Triggered Consensus and Formation Control in Multi-Agent Coordination

Qingchen Liu

Australian National University

A thesis submitted for the degree of
Doctor of Philosophy
The Australian National University

May 2018

Except where otherwise indicated, this thesis is my own original work.
The nature and extent of collaboration have been outlined in this thesis.

Qingchen Liu
29 May 2018

To my father, Miezi Liu, and my mother, Bihua Yu.

Declaration

My doctoral studies have been conducted under the guidance and supervision of Assoc. Prof. Changbin (Brad) Yu, Dr. Jonghyuk Kim and Prof. Jiahu Qin. This thesis contains no material which has been accepted for the award of any other degree or diploma in any university.

Most of the results in this thesis have been published at refereed international journals or international conferences. Some of these results have been achieved in collaboration with other researchers. Co-authored publications as a result of parts of my thesis research are listed as below:

Refereed Journal Papers

1. Z. Sun, **Q. Liu**, C. Yu and B. D. O. Anderson. Cooperative Event-Based Rigid Formation Control. In revision, to be submitted to IEEE Transactions on Network Science and Engineering.

2. **Q. Liu**, M. Ye, J. Qin and C. Yu. Event-Triggered Algorithms for Leader-Follower Consensus of Networked Euler-Lagrange Agents. Accepted by IEEE Transaction on Systems, Man and Cybernetics: Systems.

3. **Q. Liu**, J. Qin and C. Yu. Event-based Agreement Protocols for Complex Networks with Time Delays under Pinning Control. Journal of The Franklin Institute, vol. 353, no. 15, pp. 3999-4015, 2016.

Refereed Conference Papers

4. P. Fang, **Q. Liu**, X. Hou, J. Qin and C. Yu. Edge-Event-Based Multi-Agent Consensus with Zeno-free Triggers under Synchronized/Unsynchronized Clocks. Accepted, to be presented at the 56th IEEE Conference on Decision and Control (CDC'17), Melbourne, Australia, 2017.

5. **Q. Liu**, M. Ye, Z. Sun, J. Qin and C. Yu. Coverage Control of Unicycle Agents under Constant Speed Constraints. Proc. of the 20th IFAC World Congress (IFAC WC'17), pp. , Toulouse, France, 2017.

6. C. Huang, **Q. Liu** and C. Yu. Uniform Upper Bound of the Spectrum of Rooted Graphs. Proc. of the Australian Control Conference (AUCC'16), pp. 105-109, Newcastle, Australia, 2016.

7. **Q. Liu**, M. Ye, J. Qin and C. Yu. Event-Based Leader-Follower Consensus for Multiple Euler-Lagrange Systems with Parametric Uncertainties. Proc. of the

55th IEEE Conference on Decision and Control (CDC'16), pp. 2233-2239, Las Vegas, USA, 2016.

8. **Q. Liu**, J. Qin and C. Yu. Event-Based Multi-Agent Cooperative Control with Quantized Relative State Measurements. Proc. of the 55th IEEE conference of Decision and Control (CDC'16), pp. 2240-2246, Las Vegas, USA, 2016.

9. **Q. Liu**, Z. Sun, J. Qin and C. Yu. Distance-Based Formation Shape Stabilization via Event-Triggered Control. Proc. of the 34th Chinese Control Conference (CCC'15), pp. 6948-6953, Hangzhou, China, 2015.

10. Z. Sun, **Q. Liu**, C. Yu and B. D. O. Anderson. Generalized Controllers for Rigid Formation Stabilization with Application to Event-Based Controller Design. Proc. of the European Control Conference (ECC'15), pp. 217-222, Linz, Austria, 2015.

Acknowledgments

Firstly and foremost, I would like to express my sincere gratitude to my principal supervisor, Assoc. Prof. Changbin (Brad) Yu, who has been incredibly supportive since I first met him. I was recruited by Brad in Shandong Computer Science Center (SCSC) in late 2012 as a team member under his leadership. This precious opportunity to work with a young, creative researcher from a world-leading group benefits me a lot from various perspectives. At this stage, Brad also provides me a lot of support in my PhD application and suggestions in the future research directions, which paved a smooth way for me to start a PhD journey at ANU. In my four years life at ANU, Brad endowed me lots of freedom to explore the research topics of my own interest and offer me invaluable discussions on these topics. He also provides me great opportunities to attend international conferences so that I can get in touch with cutting-edge research topics and discuss with worldwide researchers. Besides research, Brad would also like to share his life experience with me in our numerous hot pot "banquets", which brings me more insights on different aspects of lives.

Secondly, I would also like to thank my co-supervisor, Prof. Jiahu Qin, for his great help and support in my research journey. During these four years, he would always like to sacrifice his time to discuss with me on my research topics or answer my questions, no matter how busy he was. We had discussions at midnights, at the time he was at airports or train stations. My training as a research student would not be complete without his guidance. Jiahu's life attitude also affects me a lot, from which I learnt how a researcher balances his time between work and family.

Thirdly, I would like to thank my friends and colleagues, Dr. Zhiyong Sun and Mr. Mengbin Ye, for sharing their knowledges with me. I started to work with Zhiyong in SCSC and have always received his great help since that. Zhiyong is the person who inspired me to find my PhD research direction: distributed event-triggered control for multi-agent systems. He would always like to share his research experience with me and help me at all the aspects in research. Mengbin is my best partner in research. His cautious attitude to work really benefits me a lot.

I also take this opportunity to thank Dr. Jonghyuk Kim, for his kind help and suggestions during my PhD study and Prof. Brian D.O. Anderson, for his invaluable comments to my research papers. I would also thank Prof. Sandra Hirche, for hosting me as a visiting student in her group where I gained different insights to my research topics by interacting with a robotic researcher.

My time as a PhD student at ANU is with so much happiness by interacting with many nice friends. They are Dr. Yun (Gavin) Hou, Dr. Xiaolei (Eric) Hou, Dr. Junming (Jamie) Wei, Dr Yiming Ji, Yonhon Ng, Pengfei Fang, Dr. Chao Huang, Dr. Yinqiu Wang, Dr. Pan Ji, Dr. Gao Zhu, Yaoxian Song, Zhixun Li at ANU, Dr. Na

Huang (Peking University), Prof. Junliang Shao, Dr. Yinjun Zhang (Beijing Jiaotong University), Wanxin Jin (Technical University of Munich), Qingkai Yang, Xiaodong Cheng (University of Groningen), Wei Bo (Harbin Institute of Technology).

My PhD research has been supported by an ANU-CSC scholarship awarded jointly by ANU and China Scholarship Council. The financial support from this scholarship is greatly appreciated. I am also thankful to Mr. Linlan Ma, who is a secretary in the education office of China Embassy in Australia, for his kind help in dealing with various issues regarding my scholarship.

Lastly but most importantly, I want to thank my parents for their love, patience and encouragements without which I could not make it this far. This thesis is dedicated to my parents.

Abstract

The focus of this thesis is to study distributed event-triggered control for multi-agent systems (MASs) facing constraints in practical applications. We consider several problems in the field, ranging from event-triggered consensus with information quantization, event-triggered edge agreement under synchronized/unsynchronized clocks, event-triggered leader-follower consensus with Euler-Lagrange agent dynamics and cooperative event-triggered rigid formation control.

The first topic is named as event-triggered consensus with quantized relative state measurements. In this topic, we develop two event-triggered controllers with quantized relative state measurements to achieve consensus for an undirected network where each agent is modelled by single integrator dynamics. Both uniform and logarithmic quantizers are considered, which, together with two different controllers, yield four cases of study in this topic. The quantized information is used to update the control input as well as to determine the next trigger event. We show that approximate consensus can be achieved by the proposed algorithms and Zeno behaviour can be completely excluded if constant offsets with some computable lower bounds are added to the trigger conditions.

The second topic considers event-triggered edge agreement problems. Two cases, namely the synchronized clock case and the unsynchronized clock case, are studied. In the synchronized clock case, all agents are activated simultaneously to measure the relative state information over edge links under a global clock. Edge events are defined and their occurrences trigger the update of control inputs for the two agents sharing the link. We show that average consensus can be achieved with our proposed algorithm. In the unsynchronized clock case, each agent executes control algorithms under its own clock which is not synchronized with other agents' clocks. An edge event only triggers control input update for an individual agent. It is shown that all agents will reach consensus in a totally asynchronous manner.

In the third topic, we propose three different distributed event-triggered control algorithms to achieve leader-follower consensus for a network of Euler-Lagrange agents. We firstly propose two model-independent algorithms for a subclass of Euler-Lagrange agents without the vector of gravitational potential forces. A variable-gain algorithm is employed when the sensing graph is undirected; algorithm parameters are selected in a fully distributed manner with much greater flexibility compared to all previous work concerning event-triggered consensus problems. When the sensing graph is directed, a constant-gain algorithm is employed. The control gains must be centrally designed to exceed several lower bounding inequalities which require limited knowledge of bounds on the matrices describing the agent dynamics, bounds on network topology information and bounds on the initial conditions. When the Euler-Lagrange agents have dynamics which include the vector of gravitational potential

forces, an adaptive algorithm is proposed. This requires more information about the agent dynamics but allows for the estimation of uncertain agent parameters.

The last topic discusses cooperative stabilization control of rigid formations via an event-triggered approach. We first design a centralized event-triggered formation control system, in which a central event controller determines the next triggering time and broadcasts the event signal to all the agents for control input update. We then build on this approach to propose a distributed event control strategy, in which each agent can use its local event trigger and local information to update the control input at its own event time. For both cases, the trigger condition, event function and trigger behaviour are discussed in detail, and the exponential convergence of the formation system is guaranteed.

Contents

List of Figures

Chapter 1

Introduction

1.1 Research background

Multi-agent systems (MASs) in general refer to a large-scale system consisting of multiple autonomous agents, which coordinate their actions to achieve a group objective. The word "agent" can refer to autonomous robots, unmanned aerial vehicles (UAVs), or mobile sensors, depending on different control context. The control algorithms designed for MASs are usually required to be implemented in a distributed manner, since it is undesirable to collect and process the global information, compute and allocate the control tasks, within a centralized processor. Over the past decade, the development and investigation of MASs has become extremely popular in various research communities (e.g. control, power systems, computer science, social science) due to their great capacity for a broad applications [Ren and Beard, 2008; Nagata and Sasaki, 2002; Ferber, 1999; Pan et al., 2007].

In control community, there are two fundamental tasks in the study of MASs:

- **Consensus**, where the aim is to reach an agreement regarding certain quantities of interest that depend on the states of all agents via local interaction rules. Successful applications of consensus algorithms are found in spacecraft attitude alignment [VanDyke and Hall, 2006; Ren and Beard, 2004], in smart grids [Zhang and Chow, 2012; Rahbari-Asr et al., 2014] and in wireless sensor networks (see [Oliva et al., 2013; Qin et al., 2017a] for a clustering problem) and [Carli and Zampieri, 2010; Seyboth and Allgower, 2013] for a clock synchronization problem). Some excellent surveys of recent progress on the research of multi-agent consensus can be found in [Cao et al., 2013; Knorn et al., 2016].

- **Formation control** aims to design distributed control algorithms such that a group of agents can achieve some pre-defined formations defined by geometric relationships between the agents. The distributed formation control strategies are usually classified into two types: displacement-based approach [Ren, 2007; Dong and Hu, 2016], in which the desired formation is specified by a set of inter-agent relative positions, and distance-based approach [Anderson et al., 2008; Sun et al., 2015b; Oh and Ahn, 2014] [1], in which the desired formation is

[1] In this thesis, we use 'rigid formation control' to represent formation control using a distance-based approach.

specified by a set of inter-agent distances. The two approaches have their own distinct properties. We refer the readers to an excellent survey paper [Oh et al., 2015] for detailed discussions on formation control.

In practical applications, agents in MASs are usually resource limited. The resource here mainly refers to the agents' on-board devices, such as microprocessors (for processing information and generating control signals), wireless communication devices (for exchanging information among agents), sensors (for measuring relative information between neighbouring agents) and actuators (for driving the agents). The resource limitations partly arise from the fact that these on-board devices are composed of digital components whose performance are restricted by the frequency of the clock references. Thus the procedures of information collection, exchange and processing as well as the generations of control signals can only be implemented in a discrete-time manner even though the agents' self dynamics are continuous. According to the above observations, it is necessary to design distributed algorithms with discrete updating time instants for MASs. The classical approach is to use time-scheduled control scheme (or sampled control scheme) [Isermann, 2013]. When using time-scheduled control scheme, the control updates are determined by a constant sampling period, and between updates the control signals are held constant via zero-order hold techniques. Some recent effort regarding the application of time-scheduled control in MASs can refer to [Xie et al., 2009; Liu et al., 2010; Yu et al., 2011; Gao and Wang, 2011; Xiao and Chen, 2012]. However, using time-scheduled control may be conservative in terms of the number of control updates, since the constant sampling period has to guarantee stability in the worst-case scenario [Seyboth, 2010]. Under this background, the event-scheduled control scheme [Tabuada, 2007; Heemels et al., 2008; Lehmann and Lunze, 2009; Donkers and Heemels, 2012; Wang and Lemmon, 2011] have been introduced into the field of MASs. While both schemes update at discrete time instants, in comparison with the time-scheduled scheme, the event-scheduled scheme has a distinctive advantage when applied in MASs as it can generate updating events aperiodically and adaptively, which has the potential to reduce as much the requirement of processing and actuating resources as possible. Some brief introduction for the recent progress regarding event-triggered control in MASs can be found in [Qin et al., 2016]. In **Chapter** 2, we will also provide a detailed review on the basic event-triggered schemes for MASs, appeared in recent literature. We note that there also have been some work that reports successful applications of event-triggered strategies in different coordination tasks [Guinaldo et al., 2013; Araújo et al., 2014; Wang et al., 2017a].

Event-triggered control for MASs is a relatively new research direction with numerous problems to be explored. In this thesis, we hope to extend this research direction by following its original motivation, that event-triggered control is introduced to be applied on practical agents. Thus we introduce several practical constraints in this thesis, ranging from information quantization, unsynchronized agent clocks and non-linear agent dynamics, which are commonly existed in practical application scenarios. These practical constraints are mainly proposed in combination with

consensus tasks (results are presented in **Chapters** 3-5). We then solve a distance-based formation control problem, by using event-triggered control algorithms. Note that the distance-based formation control problem was proposed under a practical constraint that agents cannot share a knowledge of a global coordinate system. Our proposed event-triggered algorithms can deal with this practical constraint, as well.

1.2 Contributions and Outline

In this section, we present the outline and summarize the main contributions, of the thesis. We remark that at the beginning of each main chapter, a more detailed literature review with comparison to existing work will be provided for each research topic.

Chapter 1 presents a general introduction to the research background and some motivations for the research topics to be discussed in this thesis.

Chapter 2 provides mathematical notations and theoretical preliminaries on graph theory (which focuses on undirected graphs). A general revisit to the event-triggered consensus problem with the review of relevant literature is also provided in this chapter.

Chapter 3 develops two event-triggered control algorithms with *quantized relative state measurements* to achieve consensus for a multi-agent system where each agent is modelled by single integrator dynamics and the network topology is captured by an undirected graph. Both uniform and logarithmic quantizers are considered.

The main contributions of this chapter are summarised as follows:

- We propose event-triggered control algorithms in which the updates of the control inputs and calculations of the trigger conditions are both implemented with only *quantized relative information*.
- We establish the fact that the offsets added to the trigger conditions are necessary to eliminate Zeno behaviour for each agent when designing distributed, event-triggered consensus algorithms with quantized information and presents detailed discussions on how to design constant offsets with a priori knowledge of the graph topology and quantization gain.

Chapter 4 presents novel edge-event-triggered algorithms to achieve multi-agent consensus with Zeno-free trigger events. The control inputs and triggering conditions for each agent are designed based only on relative state measurements in each agent's own local coordinate system. Two cases, namely the synchronized clock case and the

unsynchronized clock case, are studied. In the synchronized clock case, all agents are activated simultaneously to measure the relative state information over edge links under a global clock. Edge events are defined and their occurrences trigger the update of control inputs for the two agents sharing a link. We show that average consensus can be achieved with our proposed algorithm. In the unsynchronized clock case, each agent executes its control algorithm under its own clock which is not synchronized with other agents' clocks. An edge event only triggers control input update for an individual agent. We show that all agents will reach consensus in a totally asynchronous manner.

The main contributions of this chapter are two-fold:

- The synchronized clock case provides new insights to the edge-event-triggered consensus problem with much simpler trigger conditions. Moreover, when employing our algorithm, agents only need to use relative information measured in its own local coordinate frame.

- The unsynchronized clock case provides a generalised framework for edge-event-triggered algorithms where agents can be activated to execute the consensus task at different starting times. The case involving synchronized clocks thus can be regarded as a special case.

Chapter 5 proposes three different distributed event-triggered control algorithms to achieve leader-follower consensus for a network of Euler-Lagrange agents. We first propose two model-independent algorithms for a subclass of Euler-Lagrange agents whose dynamics do not have the vector of gravitational potential forces. A variable-gain algorithm is employed when the sensing graph is undirected. When the sensing graph is directed, a constant-gain algorithm is employed. When the Euler-Lagrange agents have dynamics which include the vector of gravitational potential forces, an adaptive algorithm is proposed.

Our main contributions in this chapter are the following:

- A globally asymptotically stable variable-gain model-independent algorithm is proposed for agents on undirected graphs. The variable-gain controller allows for fully distributed and arbitrary design of parameters in both the control algorithm and trigger function.

- A model-independent, constant-gain algorithm applicable for directed graphs is proposed to achieve leader-follower consensus for networked Euler-Lagrange agents semi-globally, exponentially fast. The control gains are designed to exceed several lower bounding inequalities which require limited knowledge of bounds on the matrices describing the agent dynamics, bounds on network topology information and bounds on the initial conditions.

- We propose a globally asymptotically stable adaptive algorithm for use when the gravitational term is present in the agent self-dynamics on directed net-

works. The algorithm requires more information about the agent dynamics but allows for uncertain agent parameters.

- All three proposed algorithms use only piecewise constant control inputs, which have the benefit of reducing actuator updates and thus conserving energy resources. Furthermore, each agent only updates its control inputs at its own event times, and does not require knowledge of the trigger times of neighbouring agents.

Chapter 6 discusses cooperative stabilization control of distance-based formations via an event-triggered approach. We first design a centralized event-triggered formation control system, in which a central event controller determines the next triggering time and broadcasts the event signal to all the agents for control inputs update. We then build on this centralized approach to propose a distributed event control strategy, in which each agent can use its local trigger events and local information to update the control inputs at its own event times. For both cases, the triggering condition, triggering behaviour and system convergence are discussed in detail.

The contributions of this chapter are stated as follows:

- For the first time, we propose and apply event-triggered strategies to distance-based formation control tasks.
- We prove local stability of the formation system for both centralized and distributed event-based controllers, and show that, in fact, convergence is exponentially fast. The exponential stability of the formation control system has important implications relating to robustness issues.

Chapter 7 presents a short summary of the main results and contributions of this thesis, and indicates some possible topics/directions for future research.

Chapter 2

Preliminary

2.1 Notations

The notations used in this thesis are those standard in systems and control literature. We use $\mathbb{N}$ to denote the set of all natural numbers. Let $\mathbb{R}^n$ denote the n-dimensional Euclidean space and $\mathbb{R}^{m\times n}$ denote the set of $m \times n$ real matrices. The transpose of a vector or matrix $\boldsymbol{M}$ is given by $\boldsymbol{M}^\top$. The rank, image and null space of a matrix $\boldsymbol{M}$ are denoted by $\text{rank}(\boldsymbol{M})$, $\text{Im}(\boldsymbol{M})$ and $\ker(\boldsymbol{M})$, respectively.The i-th smallest eigenvalue of a symmetric matrix $\boldsymbol{M}$ is denoted by $\lambda_i(\boldsymbol{M})$. Let $\boldsymbol{x} = [\boldsymbol{x}_1, \ldots, \boldsymbol{x}_n]^\top$ where $\boldsymbol{x}_i \in \mathbb{R}^{n\times n}$ and $n > 1$. Then $\text{diag}\{\boldsymbol{x}\}$ denotes a (block) diagonal matrix with the (block) elements of $\boldsymbol{x}$ on its diagonal, i.e. $\text{diag}\{\boldsymbol{x}_1, ..., \boldsymbol{x}_n\}$. A symmetric matrix $\boldsymbol{A} \in \mathbb{R}^{n\times n}$ which is positive definite (respectively, non-negative definite) is denoted by $\boldsymbol{A} > 0$ (respectively, $\boldsymbol{A} \geq 0$). For two symmetric matrices $\boldsymbol{A}, \boldsymbol{B}$, the expression $\boldsymbol{A} > \boldsymbol{B}$ is equivalent to $\boldsymbol{A} - \boldsymbol{B} > 0$. The $n \times n$ identity matrix is $\boldsymbol{I}_n$ and $\boldsymbol{1}_n$ denotes an n-tuple column vector of all ones. The $n \times 1$ column vector of all zeros is denoted by $\boldsymbol{0}_n$. The symbol $\otimes$ denotes the Kronecker product. The Euclidean norm of a vector, and the matrix norm induced by the Euclidean norm, is denoted by $\|\cdot\|$. We let $\|\boldsymbol{M}\|_F$ denote the Frobenius norm for a matrix M. Note that there holds $\|\boldsymbol{M}\| \leq \|\boldsymbol{M}\|_F$ for any matrix M. For the space of piecewise continuous, bounded vector functions, the norm is defined as $\|f\|_{\mathcal{L}_\infty} = \sup \|f(t)\| < \infty$ and the space is denoted by $\mathcal{L}_\infty$. The space $\mathcal{L}_p$ for $1 \leq p < \infty$ is defined as the set of all piecewise continuous vector functions such that $\|f\|_{\mathcal{L}_p} = \left(\int_0^\infty \|f(t)\|^p dt\right)^{1/p} < \infty$ where p refers to the type of p-norm.

2.2 Event-triggered consensus: a revisit

2.2.1 The consensus problem

Consider a MAS consisting of n agents with continuous-time single-integrator dynamics

$$\dot{x}_i(t) = u_i(t) \tag{2.1}$$

where $x_i(t) \in \mathbb{R}$ is the state of agent i and $u_i(t)$ is the control input. The objective of consensus is to ensure all agents reach a common state value, i.e. $x_1 = x_2 = \cdots = x_n$.

It is required that agent i can only take local information (information between agent i and its neighbours) into account to reach consensus. For this purpose, we need to describe the interactions between the agents. A well-known approach is to model the neighbouring relations by a graph $\mathcal{G}$ with vertex set $\mathcal{V} = \{v_1, v_2, \ldots, v_n\}$ and edge set $\mathcal{E} = \{\epsilon_1, \epsilon_2, \ldots, \epsilon_m\} \subset \mathcal{V} \times \mathcal{V}$ [1]. The neighbour set $\mathcal{N}_i$ of vertex v_i is defined as $\mathcal{N}_i := \{v_j \in \mathcal{V} : (v_i, v_j) \in \mathcal{E}\}$. The unweighted adjacency matrix $\mathcal{A} = \mathcal{A}(\mathcal{G}) = (a_{ij})$ is a $n \times n$ matrix given by $a_{ij} = 1$, if and only if $(v_i, v_j) \in \mathcal{E}$, and $a_{ij} = 0$, otherwise. If there is an edge $(v_i, v_j) \in \mathcal{E}$, then vertexes v_i, v_j are said to be adjacent. A path of length r from a vertex v_i to a vertex v_j is a sequence of $r + 1$ distinct vertices starting with v_i and ending with v_j such that consecutive vertices are adjacent. If there is a path between any two vertices of the graph $\mathcal{G}$, then $\mathcal{G}$ is called connected. Let $\mathcal{D}$ be the $n \times n$ diagonal matrix of d_i's, where the degree d_i of each vertex i is defined as $d_i = \sum_{j=1}^{n} a_{ij}$. The Laplacian matrix of $\mathcal{G}$ is a symmetric positive semi-definite matrix given by $\mathcal{L} = \mathcal{D} - \mathcal{A}$. For a connected graph, the Laplacian matrix $\mathcal{L}$ has a single zero eigenvalue and the corresponding eigenvector is the vector of ones. All other eigenvalues are positive and real. The eigenvalues of $\mathcal{L}$ can be ordered as $0 = \lambda_1(\mathcal{L}) < \lambda_2(\mathcal{L}) \leq \ldots \leq \lambda_n(\mathcal{L})$ [Ren and Beard, 2008].

We define an auxiliary variable $g_i(t)$ for agent i:

$$g_i(t) = \sum_{j \in \mathcal{N}_i} (x_i(t) - x_j(t)) \tag{2.2}$$

The consensus controller is typically designed as follows:

$$u_i(t) = -g_i(t) \tag{2.3}$$

or some variation of the above. By using the Laplacian matrix $\mathcal{L}$, the closed loop form of the MAS with agents having dynamics (2.1) and control inputs (2.3) can be written as

$$\dot{\boldsymbol{x}}(t) = -\boldsymbol{g}(t) = -\mathcal{L}\boldsymbol{x}(t) \tag{2.4}$$

where $\boldsymbol{g}(t) = [g_1(t) \cdots g_n(t)]^\top \in \mathbb{R}^n$ and $\boldsymbol{x}(t) = [x_1(t) \cdots x_n(t)]^\top \in \mathbb{R}^n$.

Another important matrix representation of an undirected graph $\mathcal{G}$ is the incidence matrix $\mathcal{H} = h_{ri} \in \mathbb{R}^{m \times n}$ (for more information, see [Zelazo and Mesbahi, 2011; Bapat, 2010; Mesbahi and Egerstedt, 2010]. The incidence matrix relates the edges to the vertexes, whose entries are defined as (with arbitrarily chosen edge orientations):

[1] For simplicity and because it is for illustrative purposes, we assume $\mathcal{G}$ is undirected in this chapter.

$$h_{ri} = \begin{cases} -1, & \text{if vertex } v_i \text{ is the terminal vertex of edge } \epsilon_r \\ 1, & \text{if vertex } v_i \text{ is the initial vertex of edge } \epsilon_r \\ 0, & \text{otherwise} \end{cases} \tag{2.5}$$

Note that the Laplacian matrix for an undirected graph can be written as $\mathcal{L} = \mathcal{H}^\top \mathcal{H}$. The incidence matrix $\mathcal{H}$ can be divided into two sub matrices: the in-incidence matrix and the out-incidence matrix. Following the definitions in [Zeng et al., 2016], each entry of the $m \times n$ in-incidence matrix $\mathcal{H}_\odot$ is denoted as

$$(h_\odot)_{ri} = \begin{cases} -1, & \text{if vertex } v_i \text{ is the terminal node of } r\text{-th edge} \\ 0, & \text{otherwise} \end{cases} \tag{2.6}$$

and each entry of the $m \times n$ out-incidence matrix $\mathcal{H}_\otimes$ is denoted as

$$(h_\otimes)_{ri} = \begin{cases} 1, & \text{if vertex } v_i \text{ is the initial node of } r\text{-th edge} \\ 0, & \text{otherwise} \end{cases} \tag{2.7}$$

It is obvious that $\mathcal{H} = \mathcal{H}_\odot + \mathcal{H}_\otimes$.

By using the incidence matrix $\mathcal{H}$, we can construct the relative state vector as an image of $\mathcal{H}$ from the state vector $\boldsymbol{x}$:

$$\boldsymbol{z}(t) = \mathcal{H}\boldsymbol{x}(t) \tag{2.8}$$

where $\boldsymbol{z}(t) = [z_1(t) \cdots z_m(t)]^\top \in \mathbb{R}^m$ with $z_r \in \mathbb{R}$ being the relative state for the vertex pair defined by the r-th edge ϵ_r. Then, the consensus dynamics (2.4) can also be reformulated as:

$$\dot{\boldsymbol{x}}(t) = -\mathcal{H}^\top \boldsymbol{z}(t) \tag{2.9}$$

We use **Example** 1 to show how to construct the Laplacian matrix, incidence matrix, in-incidence matrix and out-incidence matrix for a given undirected graph.

For an undirected graph $\mathcal{G}$ and its corresponding Laplacian matrix and incidence matrix, we have the following lemmas.

Lemma 1 ([Dimarogonas and Johansson, 2010])**.** *If $\mathcal{G}$ is undirected and connected, the matrix $\mathcal{H}\mathcal{H}^\top$ and the Laplacian matrix $\mathcal{L}$ both have non-negative eigenvalues and moreover the same positive ones.*

Lemma 2 ([Guo and Dimarogonas, 2013])**.** *If $\mathcal{G}$ is undirected and connected, then $\boldsymbol{z}^\top \mathcal{H}\mathcal{H}^\top \boldsymbol{z} \geq \lambda_2(\mathcal{L})\|\boldsymbol{z}\|^2$.*

Remark 1. *Though the continuous-time controller* (2.3) *only involves relative information, how the controller is implemented on practical agents, e.g. ground robots or UAVs, results in different requirements of the coordinate systems. There are two approaches to implement the control algorithms. The first one is to equip wireless communication devices to each agent*

and broadcast the self-state ($x_i(t)$) to its neighbours. This approach requires agents to be aligned with a common coordinate system. Another approach is to let each agent sense the relative states ($x_j(t) - x_i(t)$) between its neighbours and itself by using sensors, for example, stereo cameras. In this approach, only local coordinate systems are required. To equip both wireless communication devices and relative state sensors on agents for consensus tasks can be regarded as a waste of resources on hardware cost and energy/process resource consumption, since we usually assume low cost and limited on-board resources for one agent when studying a distributed multi-robot system.

Example 1. *An example of the Laplacian matrix and the incidence matrix:*

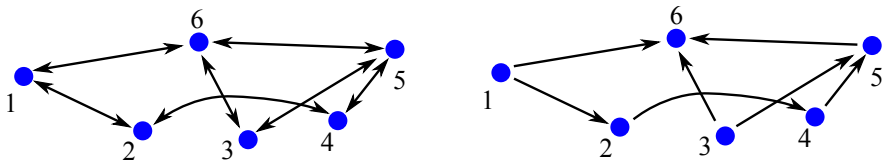

Figure 2.1: Left: An undirected graph. Right: A corresponding directed graph with arbitrarily chosen edge orientations for constructing the incidence matrix.

The Laplacian matrix of the undirected graph in ***Fig.*** *2.1 can be written as*

$$\mathcal{L} = \begin{bmatrix} 2 & -1 & 0 & 0 & 0 & -1 \\ -1 & 2 & 0 & -1 & 0 & 0 \\ 0 & 0 & 2 & 0 & -1 & -1 \\ 0 & -1 & 0 & 2 & -1 & 0 \\ 0 & 0 & -1 & -1 & 3 & -1 \\ -1 & 0 & -1 & 0 & -1 & 3 \end{bmatrix}$$

By defining

$$z = \begin{bmatrix} x_1 - x_2 \\ x_2 - x_4 \\ x_3 - x_5 \\ x_3 - x_6 \\ x_4 - x_5 \\ x_5 - x_6 \\ x_1 - x_6 \end{bmatrix}$$

we can construct an incidence matrix as follows:

$$\mathcal{H} = \begin{bmatrix} 1 & -1 & 0 & 0 & 0 & 0 \\ 0 & 1 & 0 & -1 & 0 & 0 \\ 0 & 0 & 1 & 0 & -1 & 0 \\ 0 & 0 & 1 & 0 & 0 & -1 \\ 0 & 0 & 0 & 1 & -1 & 0 \\ 0 & 0 & 0 & 0 & 1 & -1 \\ 1 & 0 & 0 & 0 & 0 & -1 \end{bmatrix}$$

where the in-incidence matrix and out-incidence matrix can be separately constructed as

$$\mathcal{H}_{\odot} = \begin{bmatrix} 0 & -1 & 0 & 0 & 0 & 0 \\ 0 & 0 & 0 & -1 & 0 & 0 \\ 0 & 0 & 0 & 0 & -1 & 0 \\ 0 & 0 & 0 & 0 & 0 & -1 \\ 0 & 0 & 0 & 0 & -1 & 0 \\ 0 & 0 & 0 & 0 & 0 & -1 \\ 0 & 0 & 0 & 0 & 0 & -1 \end{bmatrix} \quad \mathcal{H}_{\otimes} = \begin{bmatrix} 1 & 0 & 0 & 0 & 0 & 0 \\ 0 & 1 & 0 & 0 & 0 & 0 \\ 0 & 0 & 1 & 0 & 0 & 0 \\ 0 & 0 & 1 & 0 & 0 & 0 \\ 0 & 0 & 0 & 1 & 0 & 0 \\ 0 & 0 & 0 & 0 & 1 & 0 \\ 1 & 0 & 0 & 0 & 0 & 0 \end{bmatrix}$$

It can be verified that $\mathcal{L} = \mathcal{H}^{\top}\mathcal{H}$ *and* $\mathcal{H} = \mathcal{H}_{\odot} + \mathcal{H}_{\otimes}$.

2.2.2 Basic trigger schemes

Event-triggered consensus algorithms are usually designed based on the fundamental continuous-time controller (2.3), for which there are two main steps:

- Design a control input which only uses the agents' state values (x_i or z_i) at some discrete-time instants.
- Define a state mismatch between the continuous states and the discrete-time state values, then design trigger conditions to determine the time instants for updating the control input.

How to define the state mismatch variable (it is called measurement error in some papers) plays a very important role in the design of event-triggered algorithms, according to which we can classify widely-adopted event-triggered consensus algorithms in the vast number of literature regarding event-triggered consensus into three types, namely self-measurement-based, edge-measurement-based and local-measurement-based schemes.

2.2.2.1 Self-measurement-based scheme

The self-measurement-based scheme is the first trigger scheme reported in the literature (see [Dimarogonas and Johansson, 2009a,b; Dimarogonas et al., 2012] for some early work) and has been widely developed in the studies of event-triggered consensus problem investigating different agent dynamics [Mu et al., 2015; Yang et al., 2016; Garcia et al., 2014; Liu et al., 2016d], and information constraints (e.g. graph topology, information quantization, communication delays) [Seyboth et al., 2013; Garcia et al., 2013; Yi et al., 2016; Mu et al., 2015; Zhang et al., 2015].

In this scheme, each agent is required to monitor its own state ($x_i(t)$) continuously in a global coordinate system. The interactions among the agents rely on on-board wireless communication devices. Let the event time instants for agent i be denoted as $t_0^i = 0, \cdots, t_{k^i}^i, \cdots$. The state mismatch for agent i is defined as

$$e_i(t) = x_i(t_{k^i}^i) - x_i(t), \quad t \in [t_{k^i}^i, t_{k^i+1}^i) \tag{2.10}$$

Every time an event is triggered, $e_i(t)$ is reset to be equal to zero. The control input is described by

$$u_i(t) = -\sum_{j\in\mathcal{N}_i}\left(x_i(t^i_{k^i}) - x_j(t^j_{k^j})\right) \tag{2.11}$$

where $k^j = \arg\min_{l\in\mathbb{N}} : t \geq t^j_l$. For $t \in [t^i_{k^i}, t^i_{k^i+1})$, $t^j_{k^j}$ is the last event time of agent j. Each agent takes into account the last update value of each of its neighbours in its control law (see **Example** 2). The control input for agent i is updated both at its own event times $t^i_0, t^i_1, \ldots$, as well as at the event times of its neighbours $t^j_0, t^j_1, \ldots$, $j \in \mathcal{N}_i$. The closed loop form of the MAS with agent dynamics (2.1) and control input (2.11) can be written as

$$\dot{\boldsymbol{x}}(t) = -\mathcal{L}\begin{bmatrix} x_1(t^1_{k^1}) \\ x_2(t^2_{k^2}) \\ \vdots \\ x_n(t^n_{k^n}) \end{bmatrix}$$

Note that $x_i(t^i_{k^i}) = x_i(t) + e_i(t)$. By substituting this to the above closed-loop form, we obtain

$$\dot{\boldsymbol{x}}(t) = -\mathcal{L}\boldsymbol{x}(t) - \mathcal{L}\boldsymbol{e}(t) \tag{2.12}$$

This closed loop form is of great importance for the design of trigger conditions and represents the main difference of the self-measurement-based scheme from the other two triggering schemes. We now show how to design a basic, distributed trigger function by using Lyapunov analysis and the closed loop form (2.12).

Consider the following Lyapunov function

$$V(t) = \frac{1}{2}\boldsymbol{x}(t)^\top\mathcal{L}\boldsymbol{x}(t) \tag{2.13}$$

Its time derivative along the solution of (2.12) is

$$\begin{aligned}\dot{V}(t) &= \boldsymbol{x}(t)^\top\mathcal{L}\dot{\boldsymbol{x}}(t) \\ &= -\boldsymbol{x}(t)^\top\mathcal{L}\mathcal{L}\boldsymbol{x}(t) - \boldsymbol{x}(t)^\top\mathcal{L}\mathcal{L}\boldsymbol{e}(t)\end{aligned}$$

Since $\mathcal{L}$ is symmetric, we obtain $\boldsymbol{g}(t)^\top = \boldsymbol{x}(t)^\top\mathcal{L}$. Then we can upper bound $\dot{V}(t)$ as

$$\dot{V}(t) \leq -\|\boldsymbol{g}(t)\|^2 + \|\mathcal{L}\|\|\boldsymbol{g}(t)\|\|\boldsymbol{e}(t)\|$$

To guarantee $\dot{V}(t) < 0$ ($\dot{V}(t) < 0$ means $\lim_{t\to\infty}\mathcal{L}\boldsymbol{x}(t) = 0$, which implies consensus), we must ensure that $\|\boldsymbol{e}(t)\| \leq \|\boldsymbol{g}(t)\|/\|\mathcal{L}\|$. For this purpose, we can design a distributed trigger function as follows:

$$f_i(t) = \|e_i(t)\| - \beta_i\|g_i(t)\| \tag{2.14}$$

where $\beta_i > 0$. The trigger condition can be simply formulated as follows: an event for agent i is triggered as soon as the trigger function $f_i(t) = 0$ is satisfied. Note that $e_i(t)$ is reset at each event time, the trigger condition thus ensures $\|e_i(t)\| \leq \beta_i \|g_i(t)\|$. By using a properly selected β_i, the trigger condition can ensure $\|\boldsymbol{e}(t)\| \leq \|\boldsymbol{g}(t)\|/\|\mathcal{L}\|$ holds for all $t \geq 0$, meaning consensus can be achieved.

Remark 2. *The above design procedures follow the ideas proposed in [Dimarogonas and Johansson, 2009a,b; Dimarogonas et al., 2012]. The trigger function* (2.14) *involves two terms, the error term e_i and the comparison term g_i, where g_i can be calculated by using continuous communication or measured by relative state sensors (e.g. cameras). To avoid continuous communication, [Dimarogonas and Johansson, 2009a,b; Dimarogonas et al., 2012] assumes each agent monitors the relative states using additional sensors. However, this assumption increases the cost for constructing the system since both wireless communication devices and relative state sensors are equipped. We note that the requirement of continuous relative measurement has been removed in [Garcia et al., 2013; Seyboth et al., 2013], by replacing the comparison term (g_i) with state values measured at discrete-time instants and time-dependent functions, respectively. The two ideas were then widely adopted in the follow-up work (e.g. [Yang et al., 2016; Liu et al., 2016d]) using agent-measurement-based scheme. According to this, we choose to say that, when using the self-measurement-based scheme, each agent only needs to monitor its self state continuously rather than measuring relative states continuously.*

Now we record two features of the self-measurement-based scheme and present both its advantages and disadvantages.

- Each agent uses discrete-time state values at both its own and its neighbours' event time instants to update the control input. For this purpose, each agent is assumed to be equipped with wireless communication devices to broadcast the discrete-time state values to its neighbours.

- Each agent monitors its own state continuously to calculate the state mismatch (2.10) and determine event time instants. The state measurement for each agent has to be with respect to a global coordinate system. For example, UAVs use Global Positioning System (GPS) to measure their own position information.

Advantages: Each agent only needs to broadcast its discrete-time state values at specific time instants, and therefore continuous communications among the agents are avoided. On-board communication resources can be saved significantly.

Disadvantages: The control input (2.11) of each agent has to be updated at its own event times, as well as at the event times of its neighbours. This may result in a very frequent control input updates, especially when one agent has a large number of neighbours. Moreover, though measuring the self state in a continuous-time manner is simpler from the viewpoint of practical applications, the requirement of a global coordinate system restricts the application circumstances of the self-measurement-based scheme, for example, in a GPS-denied area.

2.2.2.2 Edge-measurement-based scheme

The edge-measurement-based scheme is firstly proposed in [Xiao et al., 2012, 2015] and has been further developed by numerous papers, e.g. [Cao et al., 2015; Wei et al., 2016; Cao et al., 2016; Wei et al., 2017; Xu et al., 2017].

In the edge-measurement-based scheme, it is assumed that for each edge ϵ_r connecting agents i and j, both agents i and j measure the relative state z_r over ϵ_r continuously. The sequence of event-triggered executions for edge ϵ_r (meaning agents i, j linked by ϵ_r) is denoted by $t_{0_r} = 0, t^r_{1_r}, \cdots, t^r_{k_r}, \cdots$. At $t^r_{k_r}$, the two linked agents update their control inputs simultaneously. For time $t \in [t^r_{k_r}, t^r_{k_r+1})$, the relative state mismatch over edge ϵ_r is defined as

$$e_r(t) = z_r(t^r_{k_r}) - z_r(t), \ \ r = 1, \ldots, m \tag{2.15}$$

We note that $e_r(t)$ is actually calculated by agents i and j linked by ϵ_r separately using their own on-board processors. For agent i, which is one of the agent pair (i, j) linked by ϵ_r, the control input is designed as follows:

$$u_i(t) = \sum_{j \in \mathcal{N}_i} \left(x_j(t^r_{k_r}) - x_i(t^r_{k_r}) \right) \tag{2.16}$$

for $t \in [t^r_{k_r}, t^r_{k_r+1})$. Note that only partial information $x_j(t^r_{k_r}) - x_i(t^r_{k_r})$ in the control input is updated at $t^r_{k_r}$ (see **Example** 2).

According to (2.9), we can construct the closed loop form of agent (2.1) with control input (2.16) as

$$\dot{\boldsymbol{x}}(t) = -\mathcal{H}^\top \begin{bmatrix} z_1(t^1_{k_1}) \\ z_2(t^2_{k_2}) \\ \vdots \\ z_m(t^m_{k_m}) \end{bmatrix} \tag{2.17}$$

Substituting the state mismatch (2.15) into (2.17) leads to

$$\dot{\boldsymbol{x}}(t) = -\mathcal{H}^\top \boldsymbol{z}(t) - \mathcal{H}^\top \boldsymbol{e}(t) \tag{2.18}$$

where $\boldsymbol{z}(t) = [z_1(t), z_2(t), \ldots, z_m(t)]^\top \in \mathbb{R}^m$ and $\boldsymbol{e}(t) = [e_1(t), e_2(t), \ldots, e_m(t)]^\top \in \mathbb{R}^m$. We now show how to use this closed loop form and the Lyapunov function (2.13) to design a basic edge trigger function.

The time derivative of (2.13) along the solution of (2.18) yields

$$\begin{aligned} \dot{V}(t) &= \boldsymbol{x}(t)^\top \mathcal{L} \dot{\boldsymbol{x}}(t) \\ &= -\boldsymbol{z}(t)^\top \mathcal{H}\mathcal{H}^\top \boldsymbol{z}(t) - \boldsymbol{z}(t)^\top \mathcal{H}\mathcal{H}^\top \boldsymbol{e}(t) \end{aligned}$$

Since $\mathcal{G}$ is undirected and connected, by applying **Lemma** 2, we have

$$\dot{V}(t) \leq -\lambda_2(\mathcal{L})\|z(t)\|^2 + \|z(t)\|\|\mathcal{H}\mathcal{H}^\top\|e(t)\|$$

We then design an edge trigger function as follows:

$$f_r(t) = \|e_r(t)\| - \beta_r\|z_r(t)\| \tag{2.19}$$

with $\beta_r > 0$. The selection of β_r must guarantee $\dot{V}(t) < 0$, which means consensus can be achieved.

We also record two features of the edge-measurement-based scheme and summarize both its advantages and disadvantages.

- The trigger events are defined over edges rather than agents. An agent may have multiple edge trigger conditions, whose number is determined by the amount of its edges links. Every time an edge trigger condition is satisfied, two agents linked by this edge must update their control inputs simultaneously.

- Each agent measures the relative states over its connected edges to determine edge events. The measurement is executed in each agent's own local coordinate system.

Advantages: The algorithms based on the edge-event-based scheme can be implemented in a totally coordinate-free manner, which extends the application circumstances.

Disadvantages: The control input (2.16) of agent i has to be updated at the event times of all edges it links. This may also result in a very frequent control input updates. Furthermore, measuring relative states is more complicated and unreliable when compared to measuring self states in practical applications.

2.2.2.3 Local-measurement-based scheme

The local-measurement-based scheme was first proposed in [Fan et al., 2013]. After that, the trigger scheme was widely used and developed by researchers, e.g. in [Liu et al., 2016b,c,a; Hu et al., 2016, 2017; Fan et al., 2015; Li et al., 2015; Zhu et al., 2014; Zhu and Jiang, 2015].

In the local-measurement-based scheme, we let $g_i(t)$ (defined in (2.2)) represent the real-time average state of agent i and its neighbours in agent i's local coordinate system. Agent i monitors $g_i(t)$ continuously. The sequence of event-triggered executions for agent i is $t_0^i = 0, t_1^i, \ldots, t_{k^i}^i, \ldots$. The state mismatch for agent i is defined as

$$e_i(t) = g_i(t_{k^i}^i) - g_i(t), \quad i = 1, \ldots, n, \quad t \in [t_{k^i}^i, t_{k^i+1}^i) \tag{2.20}$$

The control input is designed as follows:

$$\begin{aligned} u_i(t) &= -g_i(t^i_{k^i}) \\ &= \sum_{j\in\mathcal{N}_i}\Big(x_j(t^i_{k^i}) - x_i(t^i_{k^i})\Big) \end{aligned} \tag{2.21}$$

for $t \in [t^i_{k^i}, t^i_{k^i+1})$. The control input is only updated at agent i's own event times. The closed loop form of agent dynamics (2.1) with control input (2.21) is formulated as follows:

$$\dot{\boldsymbol{x}}(t) = -\begin{bmatrix} g_1(t^1_{k^1}) \\ g_2(t^2_{k^2}) \\ \vdots \\ g_n(t^n_{k^n}) \end{bmatrix} \tag{2.22}$$

By substituting (2.20) into (2.22), we obtain

$$\dot{\boldsymbol{x}}(t) = -\boldsymbol{g}(t) - \boldsymbol{e}(t) \tag{2.23}$$

where $\boldsymbol{e}(t) = [e_1(t), e_2(t), \ldots, e_n(t)]^\top \in \mathbb{R}^n$. We now design a trigger function according to the Lyapunov function (2.13) and the dynamics (2.23). The derivative of (2.13) along the solution of (2.23) is

$$\dot{V}(t) = -\boldsymbol{g}(t)^\top \boldsymbol{g}(t) - \boldsymbol{g}(t)\boldsymbol{e}(t) \tag{2.24}$$

Then the upper bound of $\dot{V}(t)$ can be simply calculated as

$$\dot{V}(t) \leq -\|\boldsymbol{g}(t)\|^2 + \|\boldsymbol{g}(t)\|\|\boldsymbol{e}(t)\| \tag{2.25}$$

It is then straightforward to design the trigger function as

$$f_i(t) = \|e_i(t)\| - \beta_i\|g_i(t)\| \tag{2.26}$$

where $\beta_i \in (0,1)$. Every time $f_i(t) = 0$ is satisfied, $e_i(t)$ is reset and thus $\dot{V}(t) < 0$ can be guaranteed.

As before, we record the features of the local-measurement-based scheme and summarise both its advantages and disadvantages.

- Each agent has its own isolated trigger conditions. The updates of each agent's control input are only determined by its own trigger conditions.
- The state mismatch is defined according to each agent's measurements of relative states in its own local coordinate system.

Advantages: 1) The algorithms designed according to the local-measurement-based scheme can be implemented in a coordinate-free manner, which is the same as the edge-measurement-based scheme. 2) Each agent only needs to update its

control input at its own event times; thus the control input updating times can be significantly reduced.

Disadvantages: Similarly, to obtain accurate relative state measurements is complicated in practical applications.

We now present an example to intuitively display the differences of the control input updates in the three trigger schemes.

Example 2. *Now we present three examples to illustrate the control input updates for the three trigger schemes.*

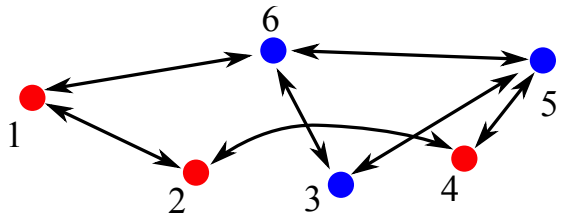

Figure 2.2: Communication topology for the illustration of the self-measurement-based scheme.

Firstly, we describe the updates of agent 2*'s control input in* ***Fig.*** *2.2 to illustrate the self-measurement-based scheme. At time* $t_0, t_0 = 0$*, the control input of agent* 2 *can be written as*

$$u_2(t) = x_1(t_0) - x_2(t_0) + x_3(t_0) - x_2(t_0)$$

Assuming that the starting trigger times (t_1^1, t_1^2, t_1^3) *for agents* $1, 2, 3$ *satisfy* $t_1^1 < t_1^2 < t_1^3 < \min\{t_2^1, t_2^2, t_2^3\}$*. At* t_1^1*, agent* 2 *receives the state update* $x_1(t_1^1)$ *from agent* 1*, and then the control input changes to*

$$u_2(t) = x_1(t_1^1) - x_2(t_0) + x_3(t_0) - x_2(t_0)$$

At t_1^2*, agent* 2 *updates its own state, then*

$$u_2(t) = x_1(t_1^1) - x_2(t_1^2) + x_3(t_0) - x_2(t_1^2)$$

At t_1^3*, agent* 2 *receives the state update* $x_3(t_1^3)$ *from agent* 3 *and changes the control input as*

$$u_2(t) = x_1(t_1^1) - x_2(t_1^2) + x_3(t_1^3) - x_2(t_1^2)$$

Secondly, we turn to the edge-measurement-based scheme. As shown in ***Fig.*** *2.3. Agent* 2 *measures the relative states* $x_1 - x_2$ *over* ϵ_1 *(linking agents 1 and 2) and* $x_2 - x_4$ *over* ϵ_2 *(linking agents 2 and 4) in its own local coordinate system. At time* t_0*, the control input is*

$$u_2(t) = x_1(t_0) - x_2(t_0) + x_3(t_0) - x_2(t_0)$$

Let the first trigger times for edges ϵ_1, ϵ_2 *be denoted by* t_1^1 *and* t_1^2*, which satisfy* $t_1^1 < t_1^2 <$

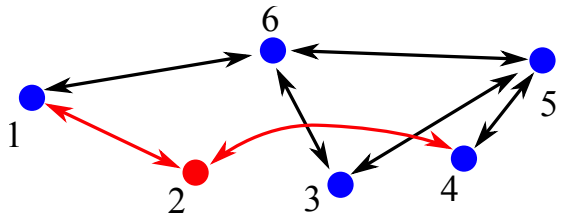

Figure 2.3: Sensing topology for the illustration of both the edge-measurement-based scheme and the local-measurement-based scheme.

$\min\{t_2^1, t_2^2\}$. *At* t_1^1, *the control input changes to*

$$u_2(t) = x_1(t_1^1) - x_2(t_1^1) + x_3(t_0) - x_2(t_0)$$

Then at t_1^2, *the control input is*

$$u_2(t) = x_1(t_1^1) - x_2(t_1^1) + x_3(t_1^2) - x_2(t_1^2)$$

Lastly, we move to illustrate the local-measurement-based scheme. Agent 2 *measures* $x_1 - x_2$ *and* $x_2 - x_4$ *in its own local coordinate system. At* t_0, *the control input for agent* 2 *is:*

$$u_2(t) = x_1(t_0) - x_2(t_0) + x_3(t_0) - x_2(t_0)$$

At t_1^2, *which is the first trigger time of agent* 2, *the control input is updated as*

$$u_2(t) = x_1(t_1^2) - x_2(t_1^2) + x_3(t_1^2) - x_2(t_1^2)$$

At the second trigger time t_2^2, *the control input changes to*

$$u_2(t) = x_1(t_2^2) - x_2(t_2^2) + x_3(t_2^2) - x_2(t_2^2)$$

2.2.3 Zeno behaviour

Zeno behaviour is a key issue when designing event-scheduled control systems. We first provide a formal definition of Zeno behaviour:

Definition 1. *Let a finite time interval be* $t_{\mathcal{Z}} = [a, b]$ *where* $0 \leq a < b < \infty$. *If, for some finite* $k \geq 0$, *there is a sequence of event triggers* $\{t_k^i, ..., t_\infty^i\} \in [a, b]$ *then the system exhibits Zeno behaviour.*

Definition 1 follows [Zhang et al., 2001; Ames et al., 2006], where Zeno behaviour is defined in finite time, i.e. $t \in [0, b], b < \infty$. The intuitive explanation of **Definition** 1 is that Zeno behaviour occurs if there is an infinite number of events take place in a finite time interval. However, there exists another concept on the definition of Zeno behaviour (see e.g. [Seyboth, 2010; Qin et al., 2017b]), in which Zeno behaviour is seen as an accumulation point of events on the complete time axis, i.e. $t \in [0, \infty)$. The accumulation point means the inter-event time $t_{k+1}^i - t_k^i \to 0$. Since formal

definitions of this concept of Zeno behaviour are not provided in [Seyboth, 2010; Qin et al., 2017b] or in other literature, we call this concept of Zeno behaviour as **Concept** 2, noting it is different from **Definition** 1, for later reference.

An example presented in [Qin et al., 2017b] can be used to illustrate the differences between **Definition** 1 and **Concept** 2: if the inter-event time $t^i_{k+1} - t^i_k$ is bounded below by $\frac{1}{t}$, where t denotes a continuous time, then the lower bound $\frac{1}{t}$ tends to 0 when $t \to \infty$. There might be accumulation events as $t \to \infty$. In **Concept** 2, this accumulation of trigger events at $t \to \infty$ is also called Zeno behaviour. However, in **Definition** 1, this is not Zeno behaviour as the definition is only valid in at finite time.

Remark 3. *In this thesis, we adopt **Definition** 1 as the formal definition of Zeno behaviour. however, it is also obvious that, if we can exclude Zeno behaviour according to **Concept** 2, then Zeno behaviour defined in **Definition** 1 does not exist, either.*

In the sequel, we will follow the idea presented in [Sun et al., 2016a] to show that how Zeno behaviour may happen when using the basic event-triggered consensus schemes introduced above.

We first use a simulation to show the trigger performance of agents with dynamics (2.1) and with control inputs (2.21) and trigger functions (2.26).

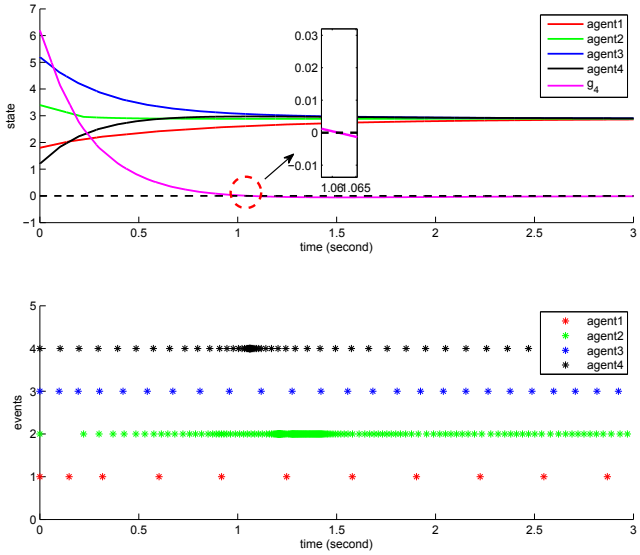

Figure 2.4: State trajectories and trigger performance of agents with dynamics (2.1) and with control input (2.21) and trigger function (2.26).

From **Fig.** 2.4, it is observed that agent 4 shows a dense trigger phenomenon when the comparison term g_4 crosses zero at some finite time [2]. Referring to the

[2]We emphasis that g_i is the i-th element of vector $\boldsymbol{g}$, which may cross zero several times at some finite times instants before $\boldsymbol{g}$ goes to zero when $t \to \infty$.

numerical data in the simulation shows that the minimum inter-event time is 0.00005 seconds, which is equal to the fixed time step of our settings in MATLAB. From the viewpoint of the experiment, this dense trigger phenomenon can be seen as Zeno behaviour. We note that the issue of Zeno behaviour at zero-crossing points of the state-dependent comparison threshold has been theoretically proved in [Sun et al., 2017]. We refer interested readers to this comment paper.

For three basic trigger schemes, all of the comparison terms might behave zero-crossing phenomenon, which means Zeno behaviour cannot be completed excluded by each agent when using the basic trigger schemes. Now we show three Zeno-free approaches proposed in the literature.

2.2.4 Zeno-free approaches

In the last subsection we have concluded that Zeno behaviour occurs when $t^i_{k+1} - t^i_k \to 0$ at some finite time instants and the reason is that the comparison thresholds in the trigger functions cross zero. Thus there are two intuitive idea to exclude Zeno behaviour. One is to modify the comparison thresholds for which zero-crossing phenomenon does not appear. By following this idea, we will introduce two modified trigger functions with either a time-dependent comparison threshold or a static comparison threshold. Another idea is to directly add a strictly positive inter-event time interval. We will talk about this at the end of this subsection.

2.2.4.1 Time-dependent trigger function

The intuitive idea of the time-dependent trigger function is to replace the state-dependent comparison term in the trigger functions, e.g. (2.14), (2.19), (2.26), by a non-negative, time-dependent continuous function $h_i(t)$, which can be formulated as

$$f_i(t) = \|e_i(t)\| - h_i(t) \tag{2.27}$$

In [Sun et al., 2016a], a general type of $h_i(t)$ is designed and analysed, which satisfies $h_i(t) \in L_\infty$, $h_i(t) > 0$ for all finite time t and $h_i(\infty) = 0$. Since $h_i(t)$ is strictly positive at any finite time, it takes time for $\|e_i(t)\|$ to increase from zero at t^i_k to be equal to $h_i(t)$ so that Zeno behaviour is excluded. By finding an upper bound b_i of the evolution speed $\frac{d}{dt}\|e_i(t)\|$, a lower bound for the inter-event time $t^i_{k+1} - t^i_k$ can be simply calculated as $h_i(t^i_{k+1})/b_i$, which is strictly positive for any finite time t^i_{k+1}, and thus Zeno behaviour is excluded.

We note that the general type time-dependent trigger function (2.27) can only exclude Zeno behaviour as defined in **Definition** 1. The lower bound of the inter-event time interval is however time-dependent and tends to zero as $t \to \infty$. We provide a simulation exapmle in **Fig.** 2.5 to show the trigger performance of using a time-dependent trigger function with a relative fast evolution speed. We can observe there exists very dense trigger events when consensus is close to be reached. And the inter-event time interval is also identified as 0.00005s in this dense trigger behaviour.

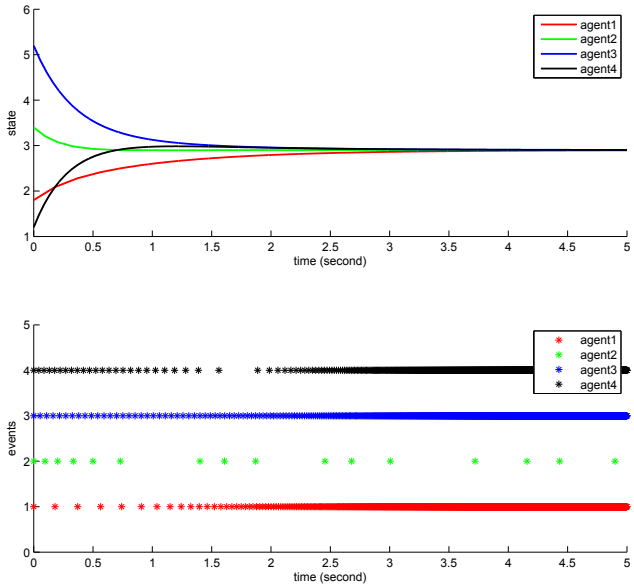

Figure 2.5: State trajectories and trigger performance of agents (2.1) with control input (2.21) and time-dependent trigger function (2.28). We set $\alpha_i = 3$ for all agents .

We conclude that the trigger behaviour in **Fig.** 2.5 is Zeno-free in terms of **Definition** 1, but is not Zeno-free in terms of **Concept** 2. It is still possible to use a time-dependent trigger function to exclude Zeno behaviour as presented in **Concept** 2 by carefully designing the decay rate of $h_i(t)$. This idea is first proposed in [Seyboth, 2010; Seyboth et al., 2013], where $h_i(t)$ is chosen as

$$h_i(t) = c_i \exp^{-\alpha_i t} \tag{2.28}$$

with $c_i, \alpha_i > 0$. The exponential decay rate α_i is required to be less than a specific upper bound, which is calculated according to the system evolution rate (e.g. related to the network connectivity λ_2). By using carefully designed, time-dependent trigger function, a strictly positive, constant lower bound of the inter-event time $t^i_{k+1} - t^i_k$ can be obtained, which excludes the possibility of accumulation events when $t \in [0, \infty)$ (see **Fig.** 2.6 for the trigger performance when α_i is selected small enough).

Though using a pre-designed time-dependent trigger function shows nice trigger performance, there exist two constraints:

- The studied system has to be exponential stable.
- The design of the decay rate requires global informations.

which may restrict its applied scenarios.

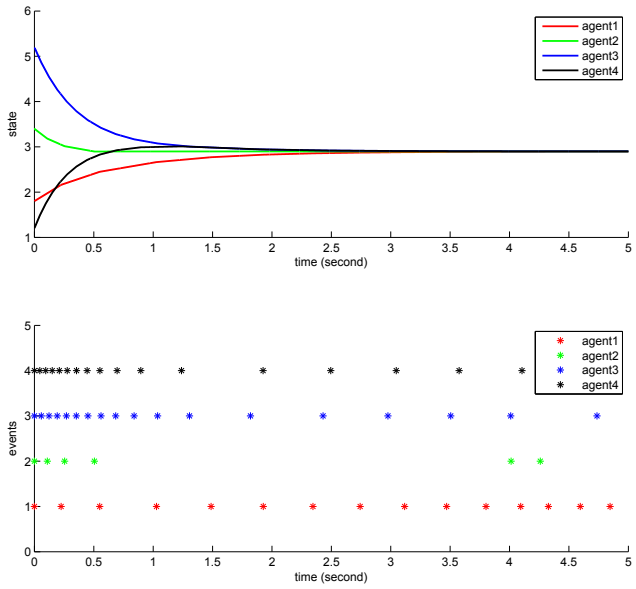

Figure 2.6: State trajectories and trigger performance of agents (2.1) with control inputs (2.21) and time-dependent trigger functions (2.28). The parameter α_i is set as 1.5 for all agents .

2.2.4.2 Static trigger function

The idea of using a static trigger function to exclude Zeno behaviour can be found in [Zhu et al., 2014; Mu et al., 2014; Seyboth, 2010].

A static trigger function is usually designed as

$$f_i(t) = \|e_i(t)\| - c_i \tag{2.29}$$

where c_i is a strictly positive constant. The idea of introducing static trigger function is actually the same with that using time-dependent trigger function (2.27), which is to make the comparison term be strictly positive, then the lower bound of the inter-event time $t^i_{k+1} - t^i_k$ is straightforwardly calculated as c_i/b_i, where b_i denotes the upper bound of the evolution speed of $e_i(t)$. Since c_i is a constant, this lower bound is valid for $t \in [0, \infty)$ thus Zeno behaviour presented in **Concept** 2 can be excluded for each agent. The drawback of using static trigger function is that complete consensus cannot be achieved. The agents' state values will converge to a ball instead of a point. Moreover, when using static trigger function, the control input for each agent cannot reach zero, which means static consensus cannot be guaranteed, as shown in **Fig.** 2.7.

Remark 4. *In the literature, the state-dependent comparison threshold, time-dependent threshold and the static threshold are usually combined together as a general comparison threshold. However, in the analysis, the exclusion of Zeno behaviour is only respect to the time-dependent term or the static term.*

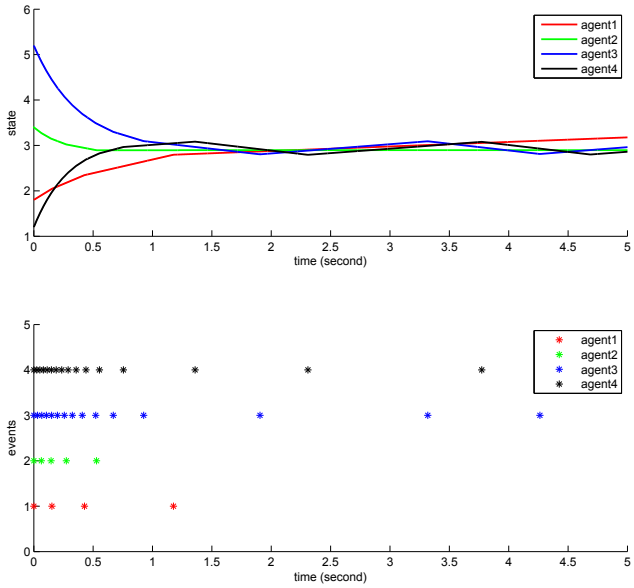

Figure 2.7: State trajectories and trigger performance of agents (2.1) with control input (2.21) and static trigger function (2.29). c_i is chosen to be 0.5 for all agents.

2.2.4.3 Time-regulation trigger condition

The time regulation idea is originally proposed in [Nowzari and Cortés, 2014; Fan et al., 2015] and is gaining attention.

We use the equations in [Fan et al., 2015] to illustrate the idea of using time-regulation trigger condition. The next event time t_{k_i+1} for agent i is determined by

$$t_{k_i+1} = t_{k_i} + \max\{\tau_{k_i}, c_i\} \tag{2.30}$$

where c_i is a strictly positive and τ_{k_i} is determined by

$$\tau_{k_r} = \inf_{t>t_{k_r}} \{t - t_{k_r} | f_i(t) = 0\} \tag{2.31}$$

where $f_i(t)$ is the trigger function (2.26).

By observing the above equations, we see that the time-regulation idea is straightforward by directly adding a strictly positive, minimum inter-event time c_i between two consecutive trigger events, thus Zeno behaviour (**Concept** 2) can be well excluded by each agent. To ensure convergence, the minimum inter-event time has to be less than a finite upper bound. Though this is a straightforward idea, how to calculate the upper bound of c_i is actually quite challenging, especially when the studied system has complex agent dynamics or network topology.

Remark 5. *In this thesis, the above three ideas to exclude Zeno behaviour are all used, depending on different research topics.*

2.3 Chapter summary

In this chapter, we first introduce mathematical notations that used throughout this thesis. After that, we provide a general review to the event-triggered consensus problem where we start from the classical consensus algorithms for single-integrator agents with an introduction to some knowledge of graph theory that will be used in **Chapters** 2-4. Then we discuss how to construct three widely-used event-triggered schemes for consensus, including self-measurement-based, edge-measurement-based and local-measurement-based schemes. Their features as well as advantages and disadvantages when being implemented in the practical applications are all recorded. At last, we talk about Zeno behaviour, which is a main difficulty when designing an event-triggered control algorithm. We compare the difference between the two viewpoints of Zeno behaviour existed in literature. We also list three Zeno-free trigger approaches and discuss the trade-off when using these approahes, respectively.

Chapter 3

Event-Triggered Consensus with Quantized Relative Information

3.1 Introduction

Event-triggered consensus [Dimarogonas et al., 2012; Seyboth et al., 2013; Fan et al., 2013] and quantized consensus [Nedić et al., 2009; Liu et al., 2012; Guo, 2011; Ceragioli et al., 2011] have been widely investigated in recent years. Note that quantized algorithms are considered because they reduce the requirement of measurement, and event-triggered algorithms are designed to reduce the requirement of control updates. However, implementing both of them together to further minimize the processing and actuating burden is still relatively unexplored. Some existing work in this area can be found in [Yu and Antsaklis, 2012], [Garcia et al., 2013] and [Zhang et al., 2015]. The work in [Yu and Antsaklis, 2012] first uses quantized *absolute* state measurements to design event-triggered consensus algorithms for undirected networks with single integrator agent dynamics. The authors prove that the quantized states of agents achieve consensus asymptotically. In [Garcia et al., 2013], the authors consider a uniform quantizer and prove that all agents will converge to a certain ball whose radius is related to the quantization error. However, both [Yu and Antsaklis, 2012] and [Garcia et al., 2013] do not provide any analysis on the exclusion of Zeno behaviour [Zhang et al., 2001], which is a key issue when designing event-scheduled systems as Zeno behaviour can cause the collapse of the entire system. In addition, the proposed schemes in [Yu and Antsaklis, 2012] and [Garcia et al., 2013] require each agent to update its own control input at both its own and its neighbours' trigger time and this may increase the updating frequency significantly. Moreover, the information shared among the agents in these work is measured with respect to a global coordinate. However, for multi-robot systems in 2-dimensional or 3-dimensional space, the assumption that all robots align with a global coordinate system is undesirable for implementing consensus controllers in e.g. a GPS-denied environment. The work in [Zhang et al., 2015] is built on [Garcia et al., 2013], in which the authors further investigate the case of logarithmic quantizer and provide analysis which shows Zeno behaviour does not occur. However, it is worth pointing out that the trigger conditions proposed in this work use *ideal* state information

instead of quantized state information. This strong assumption makes the exclusion of Zeno behaviour easier but is not reflective of real world applications since agents with digital sensors and processors actually will not have access to the ideal state information.

In this chapter, we present event-triggered algorithms for solving the consensus problem with *quantized sum of relative states* and *sum of quantized relative states*, respectively. The agent dynamic is described by single integrator and the sensing graph is undirected. Both uniform and logarithmic quantizers are considered, which, together with two different controllers, yield four cases of study in this chapter. The quantized information is used to update the control input as well as to determine the next trigger event. We show that approximate consensus can be achieved by the proposed algorithms and Zeno behaviour can be completely excluded if constant offsets with some computable lower bounds are added to the trigger conditions.

3.2 Additional Preliminaries

3.2.1 Quantizer functions

In this chapter, $q(\cdot) : \mathbb{R} \to \mathbb{R}$ represents a generalised quantization function which includes two types of quantization models, namely uniform quantization and logarithmic quantization. We follow the definitions of [Guo, 2011] for these quantizers.

Definition 2. *A uniform quantizer $q_u : \mathbb{R} \to \mathbb{R}$ is defined as:*

$$q_u(x) = \Delta_u \lfloor \frac{x}{\Delta_u} \rceil \tag{3.1}$$

where $\lfloor \cdot \rceil$ denotes the nearest integer operation and $\lfloor \frac{1}{2} \rceil = 1$. Δ_u is the quantization gain.

Definition 3. *A logarithmic quantizer $q_l : \mathbb{R} \to \mathbb{R}$ is defined as:*

$$q_l(x) = sign(x) \cdot e^{q_u(ln(|x|))} \quad (x \neq 0) \tag{3.2}$$

where q_u is the uniform quantizer with gain Δ_u, as defined in (3.1)*. In particular, $q_l(0)$ is defined to be zero.*

3.2.2 Quantizer properties

Let $\delta(x) = q(x) - x$ denote the quantization error function. For the uniform quantizer q_u, the following relation holds

$$|\delta_u(x)| = |q_u(x) - x| \leq \frac{\Delta_u}{2} \tag{3.3}$$

For the logarithmic quantizer q_l, we have $\delta_l(x) = q_l(x) - x$. Then

$$|\delta_l(x)| \leq \Delta_l |x|, \quad \Delta_l = e^{\frac{\Delta_u}{2}} - 1 \tag{3.4}$$

where Δ_u is the gain of uniform quantizer in (3.1).

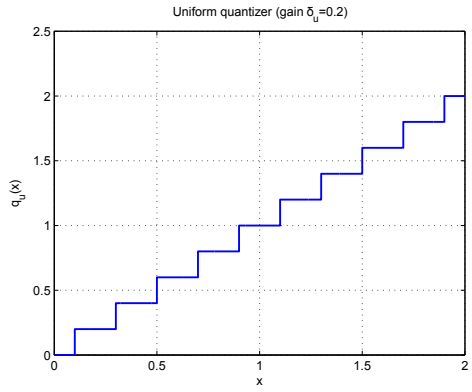

Figure 3.1: Uniform quantizer function with the gain $\delta_u = 0.2$.

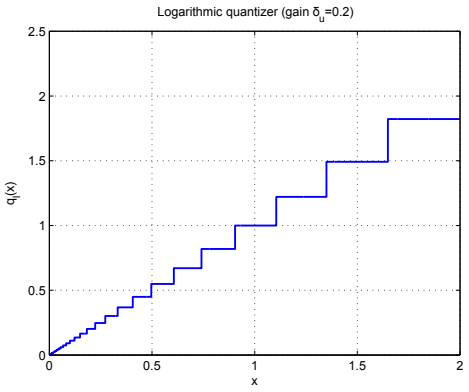

Figure 3.2: Logarithmic quantizer function with the gain $\delta_u = 0.2$.

3.3 Problem formulation

Assume that each agent is equipped with sensors which allow measurement of relative states (e.g. $x_i - x_j$). We further assume that the relative state sensors have their own processors and can collect the relative state information $x_i - x_j$ continuously. The sensing graph topology for the relative states is captured by a fixed, undirected graph $\mathcal{G}$ with associated incidence matrix $\mathcal{H}$ and Laplacian matrix $\mathcal{L}$. That is, if for agent i we have $a_{ij} = 1$, i.e. the sensors on agent i can sense $x_i - x_j$. The control unit of agent i can only receive quantized information from its sensors and update the control input at its own event time. The sequence of event-triggered executions for agent i is $t_0^i = 0, t_1^i, \ldots, t_k^i, \ldots$.

Assume agent i is described by single-integrator dynamics

$$\dot{x}_i(t) = u_i(t) \tag{3.5}$$

for all $i \in 1, \ldots, n$. Since the way of quantizing information is determined by the relative state sensors, the control input can either be the *quantized sum of relative states* or *the sum of quantized relative states*. Accordingly, we design two controllers. The control input 1 is designed as

$$u_i(t) = q\left(\sum_{j\in\mathcal{N}_i}(x_i(t_k^i) - x_j(t_k^i))\right) \tag{3.6}$$

while the control input 2 is designed as

$$u_i(t) = \sum_{j\in\mathcal{N}_i} q\left(x_i(t_k^i) - x_j(t_k^i)\right) \tag{3.7}$$

for $t \in [t_k^i, t_{k+1}^i)$.

Problem 1. *Consider the multi-agent system consisting of $n > 1$ agents with dynamics described by* (3.5)*, driven by control input* (3.6)*. Find triggering conditions for each agent, such that approximate consensus can be achieved and each agent does not exhibit Zeno behaviour.*

Problem 2. *Consider the multi-agent system consisting of $n > 1$ agents with dynamics described by* (3.5)*, driven by control input* (3.7)*. Find triggering conditions for each agent, such that approximate consensus can be achieved and each agent does not exhibit Zeno behaviour.*

3.4 Input quantization case

Let $g_i(t) = \sum_{j\in\mathcal{N}_i}(x_i(t) - x_j(t))$ represent the real-time average states of agent i and its neighbours in agent i's coordinate system. Agent i obtains $q(g_i(t))$ continuously. At time t_k^i, agent i takes $q(g_i(t_k^i))$ as the control input, which remains unchanged until the next trigger time t_{k+1}^i comes. The state mismatch is defined as

$$e_i^q(t) = q(g_i(t_k^i)) - q(g_i(t)), \quad i = 1, \ldots, n, \quad t \in [t_k^i, t_{k+1}^i) \tag{3.8}$$

We have $e_i^{q_u}(t) = q_u(g_i(t_k^i)) - q_u(g_i(t))$ for the uniform quantizer case and $e_i^{q_l}(t) = q_l(g_i(t_k^i)) - q_l(g_i(t))$ for the logarithmic quantizer case. The system model with quantized control input is written as:

$$\dot{x}_i(t) = -q(g_i(t_k^i)), \quad i = 1, \ldots, n, \quad t \in [t_k^i, t_{k+1}^i) \tag{3.9}$$

For controller (3.6), and for both uniform and logarithmic quantizers. We propose the following universal trigger condition:

$$f_i(e_i^q(t), q(g_i(t))) = \|e_i^q(t)\|^2 - \beta_i^2\|q(g_i(t))\|^2 - c_i^2 > 0 \tag{3.10}$$

where $f_i(e_i^q(t), q(g_i(t)))$ is the *trigger function*, $\beta_i, c_i > 0$ and c_i is a constant *offset*. An event for agent i is triggered as soon as the trigger condition $f_i(e_i^q(t), q(g_i(t))) > 0$ is fulfilled. Furthermore, every time an event is triggered, and in accordance with its definition, the state mismatch $e_i^q(t)$ is reset to be equal to zero. It is obvious that the trigger function only contains quantized information. Let $\beta_{\max} = \max_{1\le i\le n}\{\beta_i\}$, $c_{\max} = \max_{1\le i\le n}\{c_i\}$. Now we are ready for our main theorem.

Theorem 1. *Consider system* (3.9) *with trigger condition* (3.10) *and assume that $\mathcal{G}$ is connected.*

- *In the case of uniform quantizer, $z(t)$ converges to a ball of radius*

$$\frac{(1+\beta_{\max})\sqrt{n}\Delta_u\|\mathcal{H}\| + 2\sqrt{n}c_{\max}\|\mathcal{H}\|}{2(1-\beta_{\max})\lambda_2(\mathcal{L})}$$

  around the origin ($z = 0$) without Zeno behaviour if $\beta_i < 1$ and $c_i > \Delta_u$ for all $i \in 1, \ldots, n$.

- *In the case of logarithmic quantizer, $\boldsymbol{z}(t)$ converges to a ball of radius*

$$\frac{\sqrt{n}c_{\max}\|\mathcal{H}\|}{(1-\beta_{\max}-\Delta_l-\beta_{\max}\Delta_l)\lambda_2(\mathcal{L})}$$

around the origin ($\boldsymbol{z}=0$) without Zeno behaviour if $\beta_i+\Delta_l+\beta_i\Delta_l<1$ and $c_i>2\Delta_l\|\mathcal{H}^T\boldsymbol{z}(0)\|$ for all $i\in 1,\ldots,n$.

Proof. The proof is mainly composed of two parts: we first construct a Lyapunov function to perform the stability analysis which covers the two cases with different quantizers. Then, the convergence conditions and regions will be shown separately for different cases. In the second part, we will prove that Zeno behaviour can be excluded by adding certain offsets to the trigger functions. The principles for choosing the offsets will be discussed for different cases of quantizers.

Considering the following Lyapunov function :

$$V(t)=\frac{1}{2}\boldsymbol{x}^\top(t)\mathcal{L}\boldsymbol{x}(t) \tag{3.11}$$

where $\mathcal{L}$ is the Lapalacian matrix of $\mathcal{G}$.[1] By the definition of state mismatch (3.8), the derivative of (3.11) along the solution of (3.9) is

$$\begin{aligned}\dot{V}(t)&=\boldsymbol{x}^\top(t)\mathcal{L}\dot{\boldsymbol{x}}(t)\\&=-\boldsymbol{x}^\top(t)\mathcal{L}\begin{bmatrix}q(g_1(t))+e_1^q(t)\\q(g_2(t))+e_2^q(t)\\\vdots\\q(g_n(t))+e_n^q(t)\end{bmatrix}\end{aligned}$$

Note that $\mathcal{L}$ is symmetric and $q(g_i)=\boldsymbol{g_i}+\delta(g_i)$. Then straightforward calculations show that the derivative of the Lyapunov function can be rewritten as

$$\dot{V}(t)=-\boldsymbol{g}^\top(t)\begin{bmatrix}g_1(t)+\delta(g_1(t))+e_1^q(t)\\g_2(t)+\delta(g_2(t))+e_2^q(t)\\\vdots\\g_n(t)+\delta(g_N(t))+e_n^q(t)\end{bmatrix}$$

where $\boldsymbol{g}(t)=[g_1(t)\ g_2(t)\ \ldots\ g_n(t)]^\top$. Then $\dot{V}(t)$ satisfies:

$$\dot{V}(t)\leq-\|\boldsymbol{g}(t)\|^2+\|\boldsymbol{g}(t)\|\|\delta(\boldsymbol{g}(t))\|+\|\boldsymbol{g}(t)\|\|\boldsymbol{e}^q(t)\| \tag{3.12}$$

where $\delta(\boldsymbol{g}(t))=[\delta(g_1(t))\ \delta(g_2(t))\ \ldots\ \delta(g_n(t))]^\top$ and $\boldsymbol{e}^q(t)=[e_1^q(t)\ e_2^q(t)\ \ldots\ e_n^q(t)]^\top$. According to the updating rules of controller, the state mismatch $e_i^q(t)$ is reset to zero as soon as the trigger condition (3.10) is satisfied, which means $\|e_i^q(t)\|^2\leq\beta_i^2\|q(g_i(t))\|^2+c_i^2$ holds through the evolution of the corresponding i-th agent's state.

[1] The Lyapunov function can also be reformed as $V(t)=\frac{1}{2}\|\boldsymbol{z}(t)\|^2$ since $\boldsymbol{z}=\mathcal{H}\boldsymbol{x}$ and $\mathcal{L}=\mathcal{H}^\top\mathcal{H}$.

Let $q(\boldsymbol{g}(t)) = [q(g_1(t)), \ldots, q(g_n(t))]^T$, then $\|e^q(t)\| \leq \beta_{\max}\|q(g(t))\| + \sqrt{n}c_{\max}$ holds. Meanwhile, it is easy to obtain that $\|q(\boldsymbol{g}(t))\|$ can be bounded from above by $\|\boldsymbol{g}(t)\| + \|\delta(\boldsymbol{g}(t))\|$.

From above discussions, we obtain

$$\dot{V}(t) \leq (\beta_{\max} - 1)\|\boldsymbol{g}(t)\|^2 + (1 + \beta_{\max})\|\boldsymbol{g}(t)\|\|\delta(\boldsymbol{g}(t))\| + \sqrt{n}c_{\max}\|\boldsymbol{g}(t)\|$$

According to **Lemma** 2, we have that $\|\boldsymbol{g}(t)\|^2 \geq \lambda_2(\mathcal{L})\|\boldsymbol{z}(t)\|^2$ if graph $\mathcal{G}$ is connected, then $(\beta_{\max} - 1)\|\boldsymbol{g}(t)\|^2 \leq (\beta_{\max} - 1)\lambda_2(\mathcal{L})\|z(t)\|^2$ holds if $0 < \beta_{\max} < 1$. Furthermore, by rewriting $\boldsymbol{g}(t) = \mathcal{L}\boldsymbol{x}(t) = \mathcal{H}^\top \boldsymbol{z}(t)$, we can obtain $\|\boldsymbol{g}(t)\| \leq \|\mathcal{H}\|\|\boldsymbol{z}(t)\|$.

In the following, we will state the convergence results for both uniform and logarithmic cases.

In the *uniform quantizer* case, according to (3.3), we have

$$\dot{V}(t) \leq (\beta_{\max} - 1)\lambda_2(\mathcal{L})\|\boldsymbol{z}(t)\|^2 + (1 + \beta_{\max})\frac{\sqrt{n}}{2}\Delta_u\|\mathcal{H}\|\|\boldsymbol{z}(t)\| + \sqrt{n}c_{\max}\|\mathcal{H}\|\|\boldsymbol{z}(t)\|$$

when $0 < \beta_{\max} < 1$, we can obtain that $\boldsymbol{z}(t)$ converges to a ball around the origin. The radius of the ball is defined as follows:

$$R_{u1} = \frac{(1 + \beta_{\max})\sqrt{n}\Delta_u\|\mathcal{H}\| + 2\sqrt{n}c_{\max}\|\mathcal{H}\|}{2(1 - \beta_{\max})\lambda_2(\mathcal{L})} \tag{3.13}$$

In the *logarithmic quantizer* case, by using the property of logarithmic quantizer (3.4), we obtain

$$\dot{V}(t) \leq (\beta_{\max} + \Delta_l + \beta_{\max}\Delta_l - 1)\,\lambda_2(\mathcal{L})\|\boldsymbol{z}(t)\|^2 + \sqrt{n}c_{\max}\|\mathcal{H}\|\|\boldsymbol{z}(t)\|$$

if $0 < \beta_{\max} + \Delta_l + \beta_{\max}\Delta_l < 1$. Then we obtain that $\boldsymbol{z}(t)$ converges to a ball of radius

$$R_{l1} = \frac{\sqrt{n}c_{\max}\|\mathcal{H}\|}{(1 - \beta_{\max} - \Delta_l - \beta_{\max}\Delta_l)\lambda_2(\mathcal{L})} \tag{3.14}$$

around the origin.

Now we turn to prove that no Zeno behaviour occur throughout the evolution of the agent i's state.

We apply the commonly-used method to prove that an event-based control system does not show Zeno behaviour, which is to find a strictly positive lower bound for the inter-event time. Here we need to introduce a continuous measurement error:

$$e_i(t) = g_i(t_k^i) - g_i(t), \quad i = 1, \ldots, n, \quad t \in [t_k^i, t_{k+1}^i) \tag{3.15}$$

$e_i(t)$ is also reset to zero as long as the trigger condition (3.10) is satisfied. It is

obvious that $\frac{d}{dt}\|e_i(t)\| \leq \|\dot{g}_i(t)\|$. Thus

$$\begin{aligned}\frac{d}{dt}\|e_i(t)\| &\leq \left\|\sum_{j\in N_i}(\dot{x}_i(t)-\dot{x}_j(t))\right\| \\ &\leq \left\|\sum_{j\in N_i} q(g_i(t^i_{k_i}))\right\| + \left\|\sum_{j\in N_i} q(g_j(t^j_{k_j}))\right\|\end{aligned}$$

Note that $t^i_{k_i}$ is equal to t^i_k, and further note that $t^j_{k_j}$ denotes the latest event time instant of agent j before the current time t. Furthermore, there holds

$$\begin{aligned}\|e_i(t)\| &= \|g_i(t^i_k) - g_i(t) + q(g_i(t)) - q(g_i(t))\| \\ &= \|g_i(t^i_k) - q(g_i(t)) + q(g_i(t)) - g_i(t)\| \\ &= \|q(g_i(t^i_k)) - q(g_i(t)) - \delta(g_i(t^i_k)) + \delta(g_i(t))\| \\ &= \|e^q_i(t) - \delta(g_i(t^i_k)) + \delta(g_i(t))\|\end{aligned} \tag{3.16}$$

and this transformation will be used later.

For the *uniform quantizer* case, we have

$$\begin{aligned}\frac{d}{dt}\|e_i(t)\| &\leq \left\|\sum_{j\in N_i} q_u(g_i(t^i_{k_i}))\right\| + \left\|\sum_{j\in N_i} q_u(g_j(t^j_{k_j}))\right\| \\ &\leq \left\|\sum_{j\in N_i} g_i(t^i_{k_i})\right\| + \left\|\sum_{j\in N_i}\delta_u(g_i(t^i_{k_i}))\right\| + \left\|\sum_{j\in N_i} g_j(t^j_{k_j})\right\| + \left\|\sum_{j\in N_i}\delta_u(g_j(t^j_{k_j}))\right\|\end{aligned} \tag{3.17}$$

Note that $g(t^i_k) = \mathcal{H}^T z(t^i_k)$, so $\|g_i(t^i_k)\| \leq \|g(t^i_k)\| \leq \|\mathcal{H}\|\|z(t^i_k)\|$. Meanwhile, since $V(t) = \frac{1}{2}\|\boldsymbol{z}(t)\|^2$ is decreasing before entering the ball of radius (3.13) around zero, $\|g_i(t^i_k)\|$ can be bounded from above by $\|H\|\|z(0)\|$. The same analysis can be applied to $g_j(t^j_k)$ directly. Now we have that

$$\frac{d}{dt}\|e_i(t)\| \leq 2n_i\|\mathcal{H}\|\|\boldsymbol{z}(0)\| + n_i\Delta_u$$

where n_i denotes the number of neighbours of agent i. For any $t \in [t^i_k, t^i_{k+1})$, the following inequality always holds

$$t - t^i_k \geq \frac{\|e_i(t)\| - \|e_i(t^i_k)\|}{(2n_i\|\mathcal{H}\|\|\boldsymbol{z}(0)\| + n_i\Delta_u)} \tag{3.18}$$

According to (3.3) and (3.16), it is easy to obtain

$$\|e_i(t)\| - \|e_i(t^i_k)\| \geq \|e^{q_u}_i(t)\| - \Delta_u \tag{3.19}$$

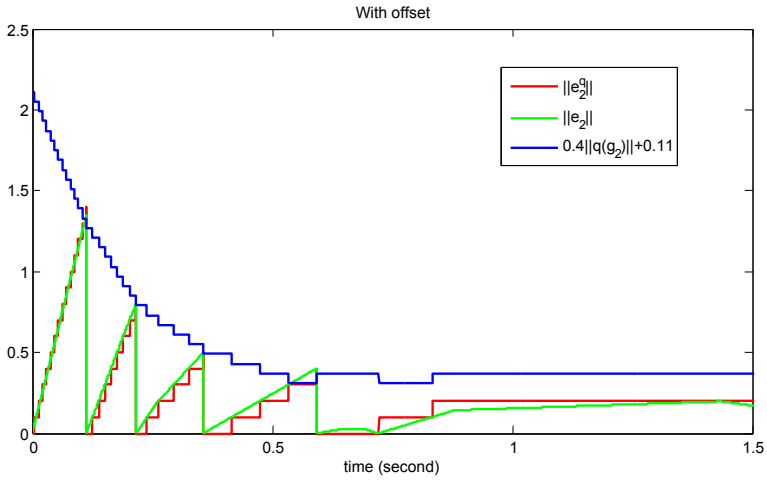

Figure 3.3: Evolution of the comparison states

since $e_i(t_k^i) = 0$. According to the trigger condition (3.10), we know that $\|e_i^{q_u}(t)\|^2 > \beta_i^2\|q_u(g_i(t))\|^2 + c_i^2$ holds at the trigger time t_{k+1}^i. Since $q_u(g_i(t))$ may be equal to zero, we obtain that the inter-event time $t_{k+1}^i - t_k^i$ is lower bounded by a strictly positive value $\frac{c_i - \Delta_u}{(2n_i\|\mathcal{H}\|\|z_0\| + n_i\Delta_u)}$ if $c_i > \Delta_u$, which completes the proof of the uniform quantizer case.

For the *logarithmic quantizer* case, by (3.4) and following the analysis steps which start from (3.17) to (3.18), we have

$$t - t_k^i \geq \frac{\|e_i(t)\| - \|e_i(t_k^i)\|}{2(1+\Delta_l)n_i\|\mathcal{H}\|\|z(0)\|}$$

By rewriting $\|e_i(t)\| = \|e_i^{q_l}(t) - \delta_l(g_i(t_k^i)) + \delta_l(g_i(t))\|$ according to (3.16), we obtain

$$\|e_i(t)\| \geq \|e_i^{q_l}(t)\| - \Delta_l\|g_i(t)\| - \Delta_l\|g_i(t_k^i)\|$$

At the trigger time t_{k+1}^i, $\|e_i^{q_l}(t)\|^2 > \beta_i^2\|q_l(g_i(t))\|^2 + c_i^2$ holds and $\|q_l(g_i(t))\|$ may be zero. So the inter-event time is bounded from below by a strictly positive value if $c_i - \Delta_l\|g_i(t)\| - \Delta_l\|g_i(t_k^i)\| > 0$ holds. Since the agent cannot obtain $g_i(t)$ and $g_i(t_k^i)$ directly, we use $\|g(0)\|$, the information of initial states to be the upper bound for $g_i(t)$ and $\|g_i(t_k^i)\|$. Note that $g(0) = \mathcal{H}^T z(0)$. Finally, we can conclude that no Zeno behaviour occur when using a logarithmic quantizer with controller (3.6) if $c_i > 2\Delta_l\|\mathcal{H}^T vectz(0)\|$.

□

3.5 Edge quantization case

Now we turn to the control input (3.7) (correspond to **Problem** 2). Let $p_i(t) = \sum_{j\in\mathcal{N}_i} q(x_i(t) - x_j(t))$, agent i obtains $p_i(t)$ continuously. Here we redefine the state

mismatch as

$$e_i^q(t) = p_i(t_k^i) - p_i(t), \;\; i = 1, \ldots, n \;\; t \in [t_k^i, t_{k+1}^i) \tag{3.20}$$

The network system model is then written as:

$$\dot{x}_i(t) = -p_i(t_k^i), \;\; i = 1, \ldots, n \;\; t \in [t_k^i, t_{k+1}^i) \tag{3.21}$$

The trigger condition is designed as:

$$f(e_i^q(t), p_i(t)) = \|e_i^q(t)\|^2 - \beta_i^2 \|p_i(t)\|^2 - c_i^2 > 0 \tag{3.22}$$

where $f(e_i^q(t), p_i(t))$ is the trigger function, $\beta_i, c_i > 0$ and c_i is a constant offset. The k-th event for agent i is triggered as soon as the trigger condition $f_i(e_i^q(t), p_i(t)) > 0$ is fulfilled at $t = t_k^i$. From (3.21) and (3.22), it is obvious that each agent only uses quantized relative information, as well.

Let $\beta_{\max} = \max_{1 \le i \le n}\{\beta_i\}$, $c_{\max} = \max_{1 \le i \le n}\{c_i\}$ and n_i denote the number of neighbours of agent i, as well. The main result of this subsection is summarised as follows:

Theorem 2. *Consider system* (3.21) *with trigger condition* (3.22) *and assume that* $\mathcal{G}$ *is connected.*

- *In the case of uniform quantizer,* $z(t)$ *converges to a ball of radius*

$$\frac{(1+\beta_{\max})\sqrt{m}\Delta_u \|\mathcal{H}\|^2 + 2\sqrt{n}c_{\max}\|\mathcal{H}\|}{2(\lambda_2(\mathcal{L}) - \beta_{\max}\|\mathcal{H}\|^2)}$$

  around the origin without Zeno behaviour if $\beta_i < \frac{\lambda_2(\mathcal{L})}{\|\mathcal{H}\|^2}$ *and* $c_i > n_i\Delta_u$ *for all* $i \in 1, \ldots, n$.

- *In the case of logarithmic quantizer,* $z(t)$ *converges to a ball of radius*

$$\frac{\sqrt{n}c_{\max}\|\mathcal{H}\|}{\lambda_2(\mathcal{L}) - (\beta_{\max} + \Delta_l + \beta_{\max}\Delta_l)\|\mathcal{H}\|^2}$$

  around the origin without Zeno behaviour if $\beta_i + \Delta_l + \beta_i\Delta_l < \frac{\lambda_2(\mathcal{L})}{\|\mathcal{H}\|^2}$ *and* $c_i > 2\Delta_l\|\mathcal{H}\|\|\boldsymbol{z}(0)\|$ *for all* $i \in 1, \ldots, n$.

Proof. The proof is also composed of two parts and has the same structure as the proof of **Theorem** 1.

Let $V(t) = \frac{1}{2}\boldsymbol{z}^\top(t)\boldsymbol{z}(t)$ be a Lyapunov function. Then

$$\begin{aligned}\dot{V}(t) &= \boldsymbol{z}^\top(t)\dot{\boldsymbol{z}}(t) \\ &= -\boldsymbol{z}^\top(t)\mathcal{H}\begin{bmatrix} p_1(t)+e_1^q(t) \\ p_2(t)+e_2^q(t) \\ \vdots \\ p_n(t)+e_n^q(t)\end{bmatrix} \\ &= -\boldsymbol{z}^\top(t)\mathcal{H}\boldsymbol{p}(t) - \boldsymbol{z}^\top(t)\mathcal{H}\boldsymbol{e}^q(t)\end{aligned}$$

Substituting $\boldsymbol{p}(t) = \mathcal{H}^\top q(\boldsymbol{z}(t))$ into the above equation and noting that $q(\boldsymbol{z}(t)) = \boldsymbol{z}(t) + \delta(\boldsymbol{z}(t))$, then $\dot{V}(t)$ can be rewritten as:

$$\dot{V}(t) = -\boldsymbol{z}^\top(t)\mathcal{H}\mathcal{H}^\top\boldsymbol{z}(t) - \boldsymbol{z}^\top(t)\mathcal{H}\mathcal{H}^\top\delta(\boldsymbol{z}(t)) - \boldsymbol{z}^\top(t)\mathcal{H}\boldsymbol{e}^q(t)$$

Note that the trigger condition (3.22) guarantees that $\|e_i^q(t)\|^2 \leq \beta_i^2\|p_i(t)\|^2 + c_i^2$. Then with **Lemma** 2, we have

$$\begin{aligned}\dot{V}(t) \leq& -\lambda_2(\mathcal{L})\|\boldsymbol{z}(t)\|^2 + \|\boldsymbol{z}(t)\|\|\mathcal{H}\|^2\|\delta(\boldsymbol{z}(t))\| \\ &+ \beta_{\max}\|\boldsymbol{z}(t)\|\|\mathcal{H}\|\|\boldsymbol{p}(t)\| + \sqrt{n}c_{\max}\|\boldsymbol{z}(t)\|\|\mathcal{H}\|\end{aligned}$$

In the case of *uniform quantizer*, we have

$$\begin{aligned}\dot{V}(t) &\leq -\lambda_2(\mathcal{L})\|\boldsymbol{z}(t)\|^2 + \frac{\sqrt{m}}{2}\Delta_u\|\boldsymbol{z}(t)\|\|\mathcal{H}\|^2 + \frac{\sqrt{m}}{2}\beta_{\max}\Delta_u\|\boldsymbol{z}(t)\|\|\mathcal{H}\|^2 \\ &\quad + \beta_{\max}\|\boldsymbol{z}(t)\|^2\|\mathcal{H}\|^2 + \sqrt{n}c_{\max}\|\boldsymbol{z}(t)\|\|\mathcal{H}\| \\ &\leq \left(\beta_{\max}\|\mathcal{H}\|^2 - \lambda_2(\mathcal{L})\right)\|\boldsymbol{z}(t)\|^2 + (1+\beta_{\max})\frac{\sqrt{m}}{2}\Delta_u\|\boldsymbol{z}(t)\|\|\mathcal{H}\|^2 \\ &\quad + \sqrt{n}c_{\max}\|\boldsymbol{z}(t)\|\|\mathcal{H}\| \qquad (3.23)\end{aligned}$$

if $0 < \beta_i < \frac{\lambda_2(\mathcal{L})}{\|\mathcal{H}\|^2}$. Then we can obtain that $z(t)$ converges to a ball of radius

$$R_{u2} = \frac{(1+\beta_{\max})\sqrt{m}\Delta_u\|\mathcal{H}\|^2 + 2\sqrt{n}c_{\max}\|\mathcal{H}\|}{2(\lambda_2(\mathcal{L}) - \beta_{\max}\|\mathcal{H}\|^2)} \qquad (3.24)$$

around the origin.

In the case of *logarithmic quantizer*, we have

$$\begin{aligned}\dot{V}(t) \leq& \left((\beta_{\max} + \Delta_l + \beta_{\max}\Delta_l)\|\mathcal{H}\|^2 - \lambda_2(\mathcal{L})\right)\|\boldsymbol{z}(t)\|^2 \\ &+ \sqrt{n}c_{\max}\|\mathcal{H}\|\|\boldsymbol{z}(t)\|\end{aligned}$$

if $\beta_{\max} + \Delta_l + \beta_{\max}\Delta_l < \frac{\lambda_2(\mathcal{L})}{\|\mathcal{H}\|^2}$, $z(t)$ converges to a ball of radius

$$R_{l2} = \frac{\sqrt{n} c_{\max} \|\mathcal{H}\|}{\lambda_2(\mathcal{L}) - (\beta_{\max} + \Delta_l + \beta_{\max}\Delta_l)\|\mathcal{H}\|^2} \tag{3.25}$$

around the origin.

We follow the same method used in **Theorem** 1 to exclude Zeno behaviour in this part. The analysis will again focus on $\|e_i(t)\|$, which is defined in (3.16). For both cases, we have

$$\begin{aligned} \frac{d}{dt}\|e_i(t)\| &\leq \|\dot{g}_i(t)\| \\ &\leq \sum_{j\in N_i} \left\| p(t^i_{k_i}) \right\| + \sum_{j\in\mathcal{N}_i} \left\| p(t^j_{k_j}) \right\| \\ &\leq n_i \|\mathcal{H}\| \|q(z(t^i_{k_i}))\| + n_i \|\mathcal{H}\| \|q(z(t^j_{k_j}))\| \end{aligned} \tag{3.26}$$

We rewrite $\|e_i(t)\|$ as follows:

$$\|e_i(t)\| = \|g_i(t^i_k) - g_i(t) + p_i(t) - p_i(t)\|$$

Further note that

$$\begin{aligned} p_i(t) &= \sum_{j\in\mathcal{N}_i} q(x_i(t) - x_j(t)) \\ &= \sum_{j\in\mathcal{N}_i} \big(x_i(t) - x_j(t)\big) + \sum_{j\in\mathcal{N}_i} \delta\left(x_i(t) - x_j(t)\right) \\ &= g_i(t) + \sum_{j\in\mathcal{N}_i} \delta\left(x_i(t) - x_j(t)\right) \end{aligned}$$

Let $d_i(t) = \sum_{j\in\mathcal{N}_i} \delta(x_i(t) - x_j(t))$, then $p_i(t) = g_i(t) + d_i(t)$ and $g_i(t^i_k) = p_i(t^i_k) - d_i(t^i_k)$. By several manipulations, $\|e_i(t)\|$ can be rewritten as

$$\|e_i(t)\| = \|e^q_i(t) - d_i(t^i_k) + d_i(t)\| \tag{3.27}$$

For the *uniform quantizer* case, we have

$$\begin{aligned} \frac{d}{dt}\|e_i(t)\| &\leq n_i \|\mathcal{H}\| \|q_u(z(t^i_{k_i}))\| + n_i \|\mathcal{H}\| \|q_u(z(t^j_{k_j}))\| \\ &\leq 2n_i \|\mathcal{H}\| \|z(0)\| + n_i \sqrt{m} \|\mathcal{H}\| \Delta_u \end{aligned}$$

since $\|z(t)\|$ is decreasing before entering the ball around zero, which means

$$t - t^i_k \geq \frac{\|e_i(t)\| - \|e_i(t^i_k)\|}{2n_i \|\mathcal{H}\| \|z(0)\| + n_i \sqrt{m} \|\mathcal{H}\| \Delta_u}$$

for any $t \in [t_k^i, t_{k+1}^i)$. From (3.27), we can easily obtain $\|e_i(t)\| \geq \|e_i^{q_u}(t)\| - n_i\Delta_u$ at time t_{k+1}^i. By using the same analysis steps as in **Theorem** 1, we know that Zeno behaviour will not occur when using the uniform quantizer with controller (3.7) if $c_i > n_i\Delta_u$.

For the *logarithmic quantizer* case, we have

$$\begin{aligned}\frac{d}{dt}\|e_i(t)\| &\leq n_i\|H\|\|q_l(z(t_{k_i}^i))\| + n_i\|\mathcal{H}\|\|q_l(\boldsymbol{z}(t_{k_j}^j))\| \\ &\leq 2\Delta_l n_i\|\mathcal{H}\|\|\boldsymbol{z}(0)\|\end{aligned}$$

which means

$$t - t_k^i \geq \frac{\|e_i(t)\| - \|e_i(t_k^i)\|}{2\Delta_l n_i\|\mathcal{H}\|\|\boldsymbol{z}(0)\|}$$

Now we turn to calculate the lower bound for $\|e_i(t)\|$ at t_{k+1}^i. Note that $d_i(t)$ can be seen as an element of the vector $\mathcal{H}^T\delta(\boldsymbol{z}(t))$. Then by applying (3.4), (3.27) and the fact that $\|\boldsymbol{z}(t)\|$ is decreasing before entering the ball around the origin of zero, we obtain

$$\|e_i(t)\| - \|e_i(t_k^i)\| \geq \|e_i^{q_l}(t)\| - 2\Delta_l\|\mathcal{H}\|\|\boldsymbol{z}(0)\|$$

which means no Zeno behaviour occurs when using a logarithmic quantizer with controller (3.7) if $c_i > 2\Delta_l\|\mathcal{H}\|\|\boldsymbol{z}(0)\|$.

□

Remark 6. *All of our analysis on exclusion of Zeno behaviour is built on studying* $\|e_i(t)\|$ *dynamics. Notice that* $\|e_i(t)\|$ *is not used in the trigger condition* (3.10) *and the growth of* $\|e_i(t)\|$ *does not trigger the event. Although this is true, we stress that it is hard to study the time derivative of* $\|e_i^q(t)\|$ *since* $e_i^q(t)$ *is discontinuous. However,* $\|e_i(t)\|$ *is continuous, so we can obtain the lower bound of time interval* $t_{k+1}^i - t_k^i$*, that* $\|e_i(t)\|$ *grows from* 0 *to* $\|e_i(t_{k+1}^i)\|$*. Note that* $t_{k+1}^i - t_k^i$ *also represents the time interval that* $\|e_i^q(t)\|$ *changes from* 0 *to* $\|e_i^q(t_{k+1}^i)\|$*. Thus by proving that the lower bound of* $t_{k+1}^i - t_k^i$ *obtained from the analysis of* $\|e_i(t)\|$ *is strictly positive, Zeno behaviour can be excluded. It is worth noting that, Zeno behaviour excluded in this chapter is actually the one presented in* ***Concept*** *2 in* ***Section*** *2.2*

3.6 Simulation examples

Consider a 4-agent system with the corresponding incidence matrix

$$\mathcal{H} = \begin{bmatrix} 1 & -1 & 0 & 0 \\ 0 & 1 & -1 & 0 \\ 0 & 1 & 0 & -1 \end{bmatrix}$$

For all the four cases, the initial states for agents are chosen as $x_1(0) = 1.8$, $x_2(0) = 3.4$, $x_3(0) = 5.2$ and $x_4(0) = 6.2$, the gain of the uniform quantizer is chosen as $\Delta_u = 0.05$ and thus the gain of the logarithmic quantizer is calculated as $\Delta_l = 0.0253$, respectively. Moreover, we set $\beta_i = 0.6$ for all i for all the simulation experiments. For input quantization case, the constant offset c_i is set to be 0.06 in the uniform quantizer case while $c_i = 0.096$ in the logarithmic case. For edge quantization case, we let $c_1 = c_3 = c_4 = 0.06$ and $c_2 = 0.16$ (agent 2 has three neighbours) in the uniform quantizer case while $c_i = 0.096$ in the logarithmic case.

For comparison, each figure contains the performance of controller whose trigger function does not contain offset. From all these figures, one can find that with the offsets, Zeno behaviour is avoided and there is the additional benefit of a reduction in the number of trigger events.

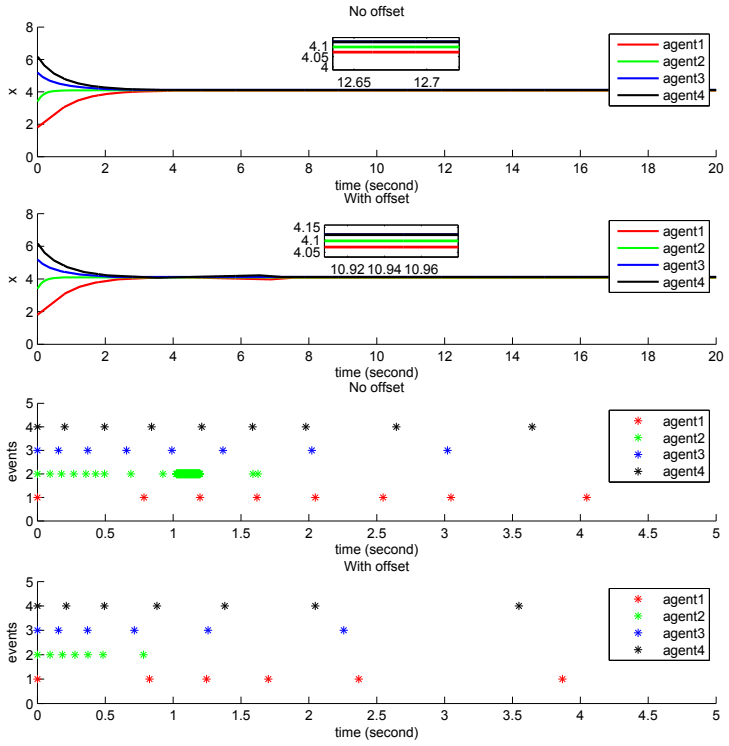

Figure 3.4: Input quantization case with uniform quantizer

3.7 Concluding remarks

In this chapter, we propose two types of event-based controllers for consensus with quantized, relative measurements. Explicit convergence results are derived for both uniform quantizer and logarithmic quantizer cases. Moreover, the addition of constant offsets to the trigger functions is discussed to ensure Zeno behaviour is avoided

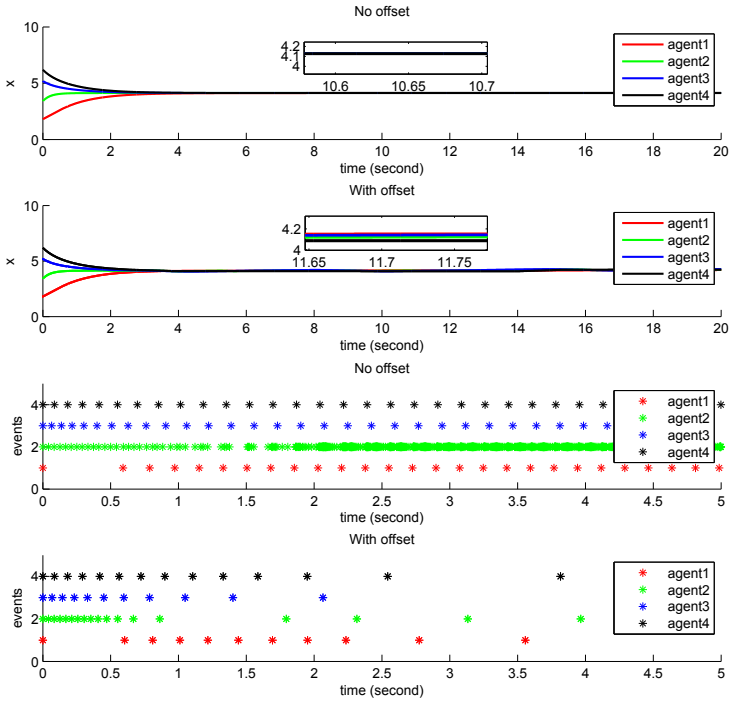

Figure 3.5: Input quantization case with logarithmic quantizer

if the agent is only able to access to quantized relative information. Numerical simulations are provided to show the the algorithms' effectiveness.

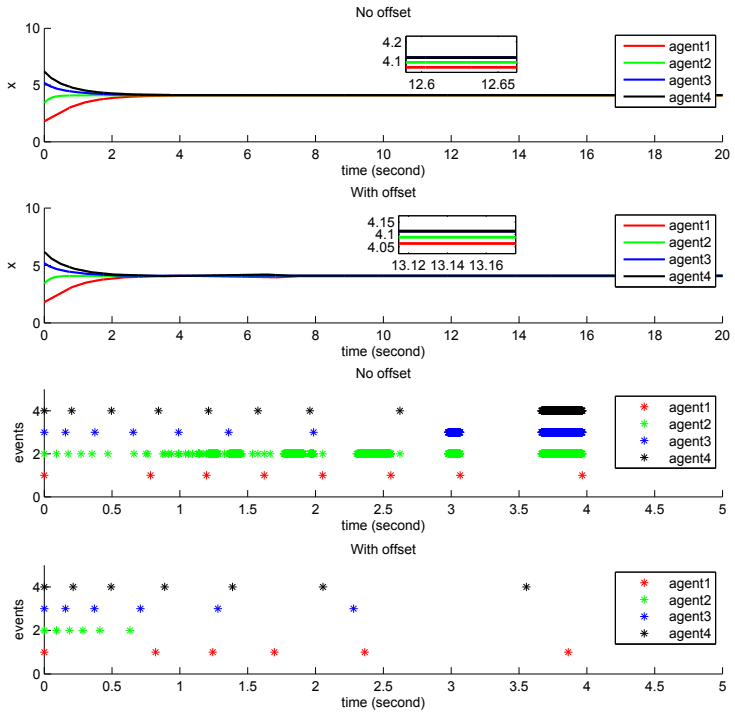

Figure 3.6: Edge quantization case with uniform quantizer

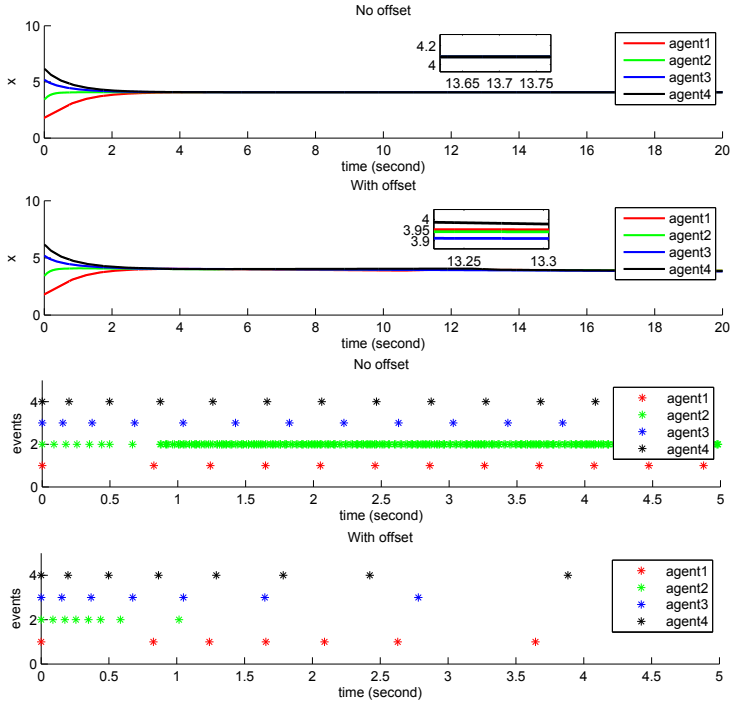

Figure 3.7: Edge quantization case with logarithmic quantizer

Chapter 4

Edge-Event-Triggered Consensus under Synchronized and Unsynchronized Clocks

4.1 Introduction

In this chapter, we present novel edge-event-triggered consensus algorithms (based on edge-measurement-based scheme reviewed in **Section** 2.2) to achieve multi-agent consensus with Zeno-free triggers under both synchronized and unsynchronized clocks. The agent's dynamics are modelled by single integrators and the graph topology is assumed to be fixed, undirected and connected. The contributions of this chapter is two-fold.

Firstly, as compared to [Xiao et al., 2012, 2015], the synchronized clock case studied in **Section** 4.2 provides another point of view with much simpler trigger conditions. In our framework, agents only use relative information measured in its own local coordinate frame to achieve *average consensus*. This is in contrast to prior work [Xiao et al., 2012; Seyboth et al., 2013; Nowzari and Cortés, 2016] (a global coordinate frame is required for all agents) and [Fan et al., 2013, 2015] (average consensus cannot be achieved). We also apply the time regulation idea from [Fan et al., 2015] to guarantee Zeno-free triggers, which differs from the time-dependent trigger condition used in [Wei et al., 2017].

Secondly, the unsynchronized clock case studied in **Section** 4.3 provides a generalised framework for edge-measurement-based trigger scheme. We note that the edge-measurement-based trigger scheme reviewed in **Section** 2.2 requires synchronous controller updates for two linked agents. To achieve this synchronous requirement, all agents in the network have to share a global clock and are activated simultaneously, i.e. $t_0^i = 0, i = 1, \cdots, n$. In the generalised framework, each agent measures the relative information and updates the control input under its own isolated clock. An edge event is defined over an individual agent rather than two linked agents, i.e. two agents linked by one edge do not update their control inputs synchronously.

4.1.1 Problem formulation

The MAS we study in this chapter consists of n single integrators that are labelled from 1 to n. The n agents are connected by m edges (sensing links). Let $x_i(t) \in \mathbb{R}$ denote the state of agent i, $i = 1, 2, \dots n$. The dynamics of agent i are described by

$$\dot{x}_i(t) = u_i(t), \ i = 1, \cdots, n \tag{4.1}$$

where $u_i(t)$ is the control input. We assume that each agent is only equipped with relative position sensors, e.g. sonar or ToF (time-of-flight) camera, to measure the relative states between its neighbours and itself, in its own local coordinate frame. The sensing topology is captured by a fixed, undirected and connected graph $\mathcal{G}$ with corresponding incidence matrix $\mathcal{H}$, Laplacian matrix $\mathcal{L}$ and adjacency matrix $\mathcal{A}$. For each edge ϵ_r connecting agent i and agent j, both agent i and agent j measure the relative state z_r continuously.

In the synchronized clock case, we further assume that all agents share a global clock t, i.e. each agent in the MAS are activated simultaneously. The sequence of event-triggered executions for edge ϵ_r is $t_{0_r} = 0, t_{1_r}, \dots, t_{k_r}, \dots$. At t_{k_r}, agent i and agent j (correspond to vertexes v_i and v_j in graph $\mathcal{G}$) linked by edge ϵ_r update their control input simultaneously. For agent i, which is one agent of the agent pair (i, j) linked by edge ϵ_r, the control input is designed as follows:

$$u_i(t) = \sum_{j \in \mathcal{N}_i} \left(x_j(t_{k_r}) - x_i(t_{k_r}) \right) \tag{4.2}$$

for $t \in [t_{k_r}, t_{k_r+1})$.

In the unsynchronized clock case, we let t, $t(0) = 0$ denote a global clock. However, each agent i has its own isolated, local clock t^i, $i = 1, 2, \dots, n$. Let $t^i(0) \geq 0$ denote the initial value for each t^i and $t^i(0), \forall i$ is not necessarily identical. That is to say, agents i and j linked by edge ϵ_r start to measure the relative information and update their control inputs under their own clocks with non-identical initial time. Because of this, agent i and j linked by ϵ_r do not update their control inputs synchronously.

Since the trigger times of agents i and j linked by ϵ_r are non-identical, we define two time sequences of event-triggered executions for agents i and j, respectively, which are $t^i_{0^i_r}, t^i_{1^i_r}, \dots, t^i_{k^i_r}, \dots$ for agent i under t^i and $t^j_{0^j_r}, t^j_{1^j_r}, \dots, t^j_{k^j_r}, \dots$ for agent j under t^j. $t^i_{k^i_r}$ denotes the time of k-th edge event of agent i triggered over edge ϵ_r under agent i's clock. Both agents update their control inputs at their own edge event times. For agent i, which is one agent of the agent pair (i, j) linked by ϵ_r, the control input is designed as follows:

$$u_i(t^i) = \sum_{j \in \mathcal{N}_i} \left(x_j(t^i_{k^i_r}) - x_i(t^i_{k^i_r}) \right), \ i = 1, 2, \dots, n \tag{4.3}$$

for $t^i \in [t^i_{k^i_r}, t^i_{k^i_r+1})$.

Problem 3. *Consider the multi-agent system consisting of $n > 1$ agents whose dynamics are described by* (4.1)*. We assume each agent is driven by* (4.2) *in the synchronized clock case. In the unsynchronized clock case, the control input is designed as* (4.3)*. For both cases, the aims are to find triggering conditions for each agent, such that complete consensus can be achieved and each agent does not exhibit Zeno behaviour.*

4.2 Synchronized clock case

We first introduce a time-varying error $e_r(t)$. For time $t \in [t_{k_r}, t_{k_r+1})$, the relative state mismatch over edge ϵ_r is defined as

$$e_r(t) = z_r(t_{k_r}) - z_r(t), \ r = 1, \dots, m \tag{4.4}$$

We note that $e_r(t)$ is actually calculated by agents i and j linked by ϵ_r separately using their own on-board processors. However, since agents i and j share a global clock and start simultaneously, the values of $\|e_r(t)\|$ calculated inside their processors are identical. We then define the Zeno-free edge-event-based trigger algorithm by following the idea proposed in [Fan et al., 2015]. The next event time for edge ϵ_r is determined by

$$t_{k_r+1} = t_{k_r} + \max\{\tau_{k_r}, b_r\} \tag{4.5}$$

where b_r is strictly positive and τ_{k_r} is determined by the trigger condition

$$f(e_r(t), z_r(t)) = \|e_r(t)\| - \beta_r \|z_r(t)\| = 0, \tag{4.6}$$

where $\beta_r > 0$. Every time an event is triggered, $e_r(t)$ resets to zero. Mathematically, τ_{k_r} is determined by

$$\tau_{k_r} = \inf_{t > t_{k_r}} \{t - t_{k_r} | f(e_r(t), z_r(t)) = 0\}.$$

Now we state the main result of this section.

Theorem 3. *Consider a multi-agent system where each agent's dynamics are described by* (4.1) *with control input* (4.2) *and edge-event trigger condition* (4.5)*. Let η_1 and η_2 be positive real numbers satisfying $\eta_1 + \eta_2 < 1$. If $\beta_r \leq \eta_1(\lambda_2(\mathcal{L})/\|\mathcal{H}\|^2)$ for all edges* [1]*, b_r is strictly positive and satisfies $b_r \leq \frac{\eta_2\lambda_2(\mathcal{L})}{\|H\|^2\left(\sqrt{m}\|\mathcal{H}\|^2+\eta_2\lambda_2(\mathcal{L})\right)}$. Then*

- *(Average consensus) All agents' states converge to their initial average.*
- *(Zeno-free triggers) At any time $t > 0$, no edge will exhibit Zeno behaviour.*

Proof. (Consensus and determination of b_r) It is well-known that the compact form of continuous-time consensus dynamic is constructed $\dot{\boldsymbol{x}} = -\mathcal{L}\boldsymbol{x} = -\mathcal{H}^T\boldsymbol{z}$. Following

[1] In synchronized clock case, "edge" means two agents linked by an edge

this construction, the compact form of (4.2) can be written as

$$u(t) = -\mathcal{H}^\top \begin{bmatrix} z_1(t_{k_1}) \\ z_2(t_{k_2}) \\ \vdots \\ z_m(t_{k_m}) \end{bmatrix} \tag{4.7}$$

where $k_r = \arg\max_{k_r \in \mathbb{N}}\{t_{k_r} | t_{k_r} \leq t\}, r = 1, \ldots, m$. By substituting the error term (4.4), the compact form of the consensus dynamic can be written as

$$\dot{\boldsymbol{x}}(t) = -\mathcal{H}^\top \boldsymbol{z}(t) - \mathcal{H}^\top \boldsymbol{e}(t) \tag{4.8}$$

where $\boldsymbol{z}(t) = [z_1(t), z_2(t), \ldots, z_m(t)]^\top$ and $\boldsymbol{e}(t) = [e_1(t), e_2(t), \ldots, e_m(t)]^\top$.

Consider the Lyapunov function $V(t) = \frac{1}{2}\boldsymbol{z}(t)^\top \boldsymbol{z}(t)$, whose time derivative along (4.8) is

$$\dot{V}(t) = \boldsymbol{z}(t)^\top \dot{\boldsymbol{z}}(t) = -\boldsymbol{z}(t)^\top \mathcal{H}\mathcal{H}^\top \boldsymbol{z}(t) - \boldsymbol{z}(t)^\top \mathcal{H}\mathcal{H}^\top \boldsymbol{e}(t)$$

By applying **Lemma** 2, we further obtain

$$\begin{aligned} \dot{V}(t) &\leq -\lambda_2(\mathcal{L})\|\boldsymbol{z}(t)\|^2 + \|\mathcal{H}\|^2 \|\boldsymbol{e}(t)\| \|\boldsymbol{z}(t)\| \\ &= -\left(\lambda_2(\mathcal{L}) \sqrt{\sum_{r=1}^{m} \|z_r(t)\|^2} - \|\mathcal{H}\|^2 \sqrt{\sum_{r=1}^{m} \|e_r(t)\|^2}\right) \|\boldsymbol{z}(t)\| \end{aligned}$$

If we can guarantee that

$$\sum_{r=1}^{m} \|e_r(t)\|^2 \leq \eta^2 \left(\frac{\lambda_2(\mathcal{L})}{\|\mathcal{H}\|^2}\right)^2 \sum_{r=1}^{m} \|z_r(t)\|^2 \tag{4.9}$$

with $\eta \in (0, 1)$, then it yields

$$\dot{V}(t) \leq -\left((1-\eta)\lambda_2(\mathcal{L}) \sqrt{\sum_{r=1}^{m} \|z_r(t)\|^2}\right) \|\boldsymbol{z}(t)\| < 0 \tag{4.10}$$

According to (4.5), we know that at any time $t > 0$, the determination of inter-edge-event time of edge ϵ_r is either by τ_{k_r} or b_r. Let $S_1(t)$ and $S_2(t)$ be the edge sets consisting of edges whose next inter-edge-event time at t is τ_{k_r} and b_r, respectively. Then it is obvious that $S_1(t) \bigcup S_2(t) = \{\epsilon_1, \ldots, \epsilon_m\}$ and $S_1(t) \bigcap S_2(t) = \emptyset$. To guarantee (4.10), we further propose the following two conditions:

$$\sum_{\epsilon_r \in S_1(t)} \|e_r(t)\|^2 \leq \eta_1^2 \left(\frac{\lambda_2(\mathcal{L})}{\|\mathcal{H}\|^2}\right)^2 \sum_{r=1}^{m} \|z_r(t)\|^2 \tag{4.11}$$

and

$$\sum_{\epsilon_r \in S_2(t)} \|e_r(t)\|^2 \leq \eta_2^2 \left(\frac{\lambda_2(\mathcal{L})}{\|\mathcal{H}\|^2}\right)^2 \sum_{r=1}^{m} \|z_r(t)\|^2 \tag{4.12}$$

where η_1 and η_2 are strictly positive real numbers under the condition that $\eta_1 + \eta_2 = \eta < 1$. For each edge in $S_1(t)$, if we let $\beta_r \leq \eta_1(\lambda_2(\mathcal{L})/\|\mathcal{H}\|^2)$, then condition (4.11) will holds for all t. For condition (4.12), if we can guarantee

$$\|e_r(t)\| \leq \sqrt{\zeta}\|\boldsymbol{z}(t)\| \tag{4.13}$$

where $\zeta = \frac{\eta_2^2}{m}\left(\frac{\lambda_2(\mathcal{L})}{\|\mathcal{H}\|^2}\right)^2$, then condition (4.12) can be ensured.

Since ζ is strictly positive, the evolution time of $\|e_r(t)\|/\|\boldsymbol{z}(t)\|$ from 0 to $\sqrt{\zeta}$ is strictly positive (because $\|\boldsymbol{z}(t)\| \neq 0$, $\|e_r(t)\|$ evolutes from 0 at t_{k_r}). By finding an upper bound B_r of this evolution time, we can determine a strictly positive time $b_r \leq B_r$. Then condition (4.13) can always be guaranteed if the evolution time of $\|e_r(t)\|/\|\boldsymbol{z}(t)\|$ is b_r. To find B_r, we first estimate the time derivative of $\|e_r(t)\|/\|\boldsymbol{z}(t)\|$:

$$\frac{d}{dt}\frac{\|e_r\|}{\|\boldsymbol{z}\|} \leq \frac{\|\dot{e}_r\|}{\|\boldsymbol{z}\|} + \frac{\|e_r\|}{\|\boldsymbol{z}\|}\frac{\|\dot{\boldsymbol{z}}\|}{\|\boldsymbol{z}\|} \tag{4.14}$$

According to (4.4), one can deduce that $\dot{e}_r = -\dot{z}_r$. So it is obvious that $\frac{d}{dt}\frac{\|e_r\|}{\|\boldsymbol{z}\|} \leq \|\mathcal{H}\|^2(1+\frac{\|e\|}{\|\boldsymbol{z}\|})^2$. Similar time derivative of $\|\boldsymbol{e}\|/\|\boldsymbol{z}\|$ yields $\frac{d}{dt}\frac{\|\boldsymbol{e}\|}{\|\boldsymbol{z}\|} \leq \|\mathcal{H}\|^2(1+\frac{\|\boldsymbol{e}\|}{\|\boldsymbol{z}\|})^2$. It is noticed that $\|\boldsymbol{e}\|/\|\boldsymbol{z}\|$ always upper bounds $\|e_r\|/\|\boldsymbol{z}\|$ and both of them are non-negative. Now we conclude that $\|e_r\|/\|\boldsymbol{z}\| < g(t, g_0)$, where $g(t, g_0)$ is the solution of $\dot{g}(t) = \|\mathcal{H}\|^2(1+g(t))^2$, $g_0 = 0$. Thus the lower bound of evolution time of $\|e_r\|/\|\boldsymbol{z}\|$ from 0 to $\sqrt{\zeta}$ is

$$B_r = \frac{\eta_2\lambda_2(\mathcal{L})}{\|\mathcal{H}\|^2\left(\sqrt{m}\|\mathcal{H}\|^2 + \eta_2\lambda_2(\mathcal{L})\right)} \tag{4.15}$$

We can choose a strictly positive real time b_r which is satisfied with $b_r \leq B_r$ to guarantee (4.12) for each edge in $S_2(t)$. Since b_r is strictly positive, it is straightforward to conclude that Zeno behaviour is excluded for each edge. Moreover, since condition (4.10) can be ensured, we also conclude that consensus can be reached.

(Average preservation) Define an average variable

$$\bar{x}(t) = \frac{1}{n}\sum_{i=1}^{n} x_i(t).$$

The time derivative of $\bar{x}(t)$ is

$$\begin{aligned}\dot{\bar{x}}(t) &= \frac{1}{n}\sum_{i=1}^{n}\dot{x}_i(t) = \frac{1}{n}\sum_{i=1}^{n}u_i(t)\\ &= \frac{1}{n}\sum_{i=1}^{n}\sum_{j\in\mathcal{N}_i}\left(x_j(t_{k_r}) - x_i(t_{k_r})\right)\end{aligned}$$

Since $j \in \mathcal{N}_i$ represents the adjacency relation between agent i and agent j, the above equation can be reformulated as

$$\dot{\bar{x}}(t) = \frac{1}{n}\sum_{i=1}^{n}\sum_{j=1}^{n}a_{ij}\left(x_j(t_{k_r}) - x_i(t_{k_r})\right)$$

Applying the symmetric property of undirected graph shows:

$$\begin{aligned}\dot{\bar{x}}(t) &= \frac{1}{2n}\sum_{i=1}^{n}\sum_{j=1}^{n}a_{ij}\left(x_j(t_{k_r}) - x_i(t_{k_r})\right) + \frac{1}{2n}\sum_{j=1}^{n}\sum_{i=1}^{n}a_{ji}\left(x_i(t_{k_r}) - x_j(t_{k_r})\right)\\ &= \frac{1}{2n}\sum_{i=1}^{n}\sum_{j=1}^{n}\Big(a_{ij}(x_j(t_{k_r}) - x_i(t_{k_r})) + a_{ji}(x_i(t_{k_r}) - x_i(t_{k_r}))\Big)\\ &= 0,\end{aligned} \tag{4.16}$$

which indicates that average state $\bar{x}(t)$ remains a constant. Note that the previous analysis has shown that the consensus can be reached, so it is obvious that the final consensus value is their initial average.

□

4.3 Unsynchronized clock case

For time $t^i \in [t^i_{k^i_r}, t^i_{k^i_r+1})$, agent i, which is one agent of edge ϵ_r, measures the relative states $z^i_r(t^i)$ continuously along its own time axis and the relative state mismatch is defined as

$$e^i_r(t^i) = z^i_r(t^i_{k^i_r}) - z^i_r(t^i) \tag{4.17}$$

Since $t^i_{0^i_r} = t^j_{0^j_r}$ can not be guaranteed for agents i and j linked by ϵ_r, it is obvious that $e^i_r(t^i)$ is not supposed to be equal to $e^j_r(t^j)$. When combined the trigger conditions proposed below, it is implied that the linked agents i and j update their controllers asynchronously.

We follow the same method used in the synchronized clock case to determine the next edge event time over ϵ_r for agent i:

$$t^i_{k^i_r+1} = t^i_{k^i_r} + \max\{\tau^i_{k^i_r}, b_r\} \tag{4.18}$$

The trigger function used to determine $\tau^i_{k^i_r}$ is

$$f(e^i_r(t^i), z^i_r(t^i)) = \|e^i_r(t^i)\| - \beta^i_r \|z^i_r(t^i)\| \tag{4.19}$$

where $\beta^i_r > 0$. As usual, every time the trigger condition (4.18) is satisfied, $e^i_r(t^i)$ is reset to be equal to zero.

Theorem 4. *Consider system* (4.1) *with control input* (4.3)*, trigger condition* (4.18)*. Let* η_1 *and* η_2 *be positive real numbers and* $\eta_1 + \eta_2 < 1$*. Let* $\alpha = \max\{\|\mathcal{H}\mathcal{H}^\top_\otimes\|, \|\mathcal{H}\mathcal{H}^\top_\odot\|\}$*. If* $\beta^i_r \le \eta_1\lambda_2(\mathcal{L})/2\alpha$ *for all edges,* b_r *is strictly positive and satisfies* $b_r \le \frac{\eta_2\lambda_2(\mathcal{L})}{2\alpha(2m\alpha+\eta_2\lambda_2(\mathcal{L}))}$*. Then*

- *(Consensus) All agents' states will reach consensus.*
- *(Zeno-free triggers) No agent will exhibit Zeno behaviour.*

Proof. It is obvious that we do not need to consider the convergence of the system before all agents are activated. Thus we introduce a new global clock t', where $t'(0) = \max\{t^i(0) : i = 1, 2, \ldots, n\}$ indicates the time point that all agents are activated to achieve consensus. Note that the compact form (4.7) cannot be used here because agents i and j linked by edge ϵ_r update asynchronously. New variables are required to be defined to construct the compact form of the system.

Note that all the state variables used and defined in the proof are with respect to a global coordinate frame. We start the analysis from the continuous-time consensus dynamic $\dot{x}(t') = -\mathcal{H}^\top z(t')$, as well. In this dynamic, the entry $h^\top_{ir}$ of $\mathcal{H}^\top$ can be explained as follows:

$$h^\top_{ir} = \begin{cases} 1, & \text{agent } i\text{'s knowledge of } z_r(t') \text{ is } -z_r(t') \\ -1, & \text{agent } i\text{'s knowledge of } z_r(t') \text{ is } z_r(t') \\ 0, & \text{agent } i \text{ does not access } z_r(t') \end{cases} \tag{4.20}$$

Note that $h^\top_{ir} = h_{ra}$, h_{ra} is the entry of $\mathcal{H}$. According to the definition of h_{ri} in (4.20), we have the following conclusions: if agent i is the terminal agent of edge ϵ_r, its knowledge of $z_r(t')$ is $-z_r(t')$; if agent i is the initial agent of edge ϵ_r, its knowledge of z_r is $z_r(t')$. Let the relative states assigned to initial agent i and terminal agent j linked by edge ϵ_r be respectively described by z^μ_r and z^ν_r, where the initial agent and terminal agent are pre-assigned by incidence matrix H. It is obvious that $z^\mu_r(t') = z^\nu_r(t') = z_r(t')$. Note that there are m initial agents and m terminal agents in the MAS since the graph $\mathcal{G}$ has m edges. Then it is reasonable to rewrite the consensus dynamic as $\dot{\boldsymbol{x}} = -\mathcal{H}^\top_\otimes \boldsymbol{z}^\mu(t') - \mathcal{H}^\top_\odot \boldsymbol{z}^\nu(t')$, where $\boldsymbol{z}^\mu = [z^\mu_1, z^\mu_2, \ldots, z^\mu_m]^\top$ and $\boldsymbol{z}^\nu = [z^\nu_1, z^\nu_2, \ldots, z^\nu_m]^\top$.

Let $t'_{k^\mu_r}$ and $t'_{k^\nu_r}$ re-denote the latest r-th edge event time instants of initial agent i and terminal agent j linked by edge ϵ_r, respectively. It is assumed that $t'_{k^\mu_r}, t'_{k^\nu_r} \ge t'(0)$. Following the consensus dynamic constructed in the last paragraph, the compact

form of the control input (4.3) can be expressed as:

$$u(t') = -\mathcal{H}_{\otimes}^{\top} \begin{bmatrix} z_1^{\mu}(t'_{k_1^{\mu}}) \\ z_2^{\mu}(t'_{k_2^{\mu}}) \\ \vdots \\ z_m^{\mu}(t'_{k_m^{\mu}}) \end{bmatrix} - \mathcal{H}_{\odot}^{\top} \begin{bmatrix} z_1^{\nu}(t'_{k_1^{\nu}}) \\ z_2^{\nu}(t'_{k_2^{\nu}}) \\ \vdots \\ z_m^{\nu}(t'_{k_m^{\nu}}) \end{bmatrix} \tag{4.21}$$

This is a key step of the proof.

According to (4.17), we define two stack state mismatch $e^{\mu} = [e_1^{\mu}, e_2^{\mu}, \ldots, e_m^{\mu}]^{\top}$ and $e^{\nu} = [e_1^{\nu}, e_2^{\nu}, \ldots, e_m^{\nu}]^{\top}$ are defined for all of the initial agents and terminal agents, respectively. The compact form of the consensus dynamic at t' can be formulated as

$$\begin{aligned} \dot{\boldsymbol{x}}(t') &= -\mathcal{H}_{\otimes}^{\top}\boldsymbol{z}(t') - \mathcal{H}_{\odot}^{\top}\boldsymbol{z}(t') - \mathcal{H}_{\otimes}^{\top}\boldsymbol{e}^{\mu}(t') - \mathcal{H}_{\odot}^{\top}\boldsymbol{e}^{\nu}(t') \\ &= -\mathcal{H}^{\top}\boldsymbol{z}(t') - \mathcal{H}_{\otimes}^{\top}\boldsymbol{e}^{\mu}(t') - \mathcal{H}_{\odot}^{\top}\boldsymbol{e}^{\nu}(t') \end{aligned} \tag{4.22}$$

Now reconsider the Lyapunov function $V(t') = \frac{1}{2}\boldsymbol{z}(t')^{\top}\boldsymbol{z}(t')$. Its time derivative along (4.22) is

$$\begin{aligned} \dot{V}(t') &= \boldsymbol{z}(t')^{\top}\mathcal{H}\dot{\boldsymbol{x}}(t') \\ &= -\boldsymbol{z}(t')^{\top}\mathcal{H}\mathcal{H}^{\top}\boldsymbol{z}(t') - \boldsymbol{z}(t')^{\top}\mathcal{H}\mathcal{H}_{\otimes}^{\top}\boldsymbol{e}^{\mu}(t') - \boldsymbol{z}(t')^{\top}\mathcal{H}\mathcal{H}_{\odot}^{\top}\boldsymbol{e}^{\nu}(t') \end{aligned}$$

By recalling **Lemma** 2, it yields that

$$\begin{aligned} \dot{V}(t') &\leq -\lambda_2(\mathcal{L})\|\boldsymbol{z}(t')\|^2 + \|\mathcal{H}\mathcal{H}_{\otimes}^{\top}\|\|\boldsymbol{z}(t')\|\|\boldsymbol{e}^{\mu}(t')\| + \|\mathcal{H}\mathcal{H}_{\odot}^{\top}\|\|\boldsymbol{z}(t')\|\|\boldsymbol{e}^{\nu}(t')\| \\ &= -\left(\lambda_2(\mathcal{L})\|\boldsymbol{z}(t')\| - \|\mathcal{H}\mathcal{H}_{\otimes}^{\top}\|\|\boldsymbol{e}^{\mu}(t')\| - \|\mathcal{H}\mathcal{H}_{\odot}^{\top}\|\|\boldsymbol{e}^{\nu}(t')\|\right)\|\boldsymbol{z}(t')\| \end{aligned}$$

Note that $\|e^{\mu}(t')\| = \sqrt{\sum_{r=1}^{m}\|e_r^{\mu}(t')\|^2}$ and $\|e^{\nu}(t')\| = \sqrt{\sum_{r=1}^{m}\|e_r^{\nu}(t')\|^2}$. Let $\alpha = \max\{\|\mathcal{H}\mathcal{H}_{\otimes}^{\top}\|, \|\mathcal{H}\mathcal{H}_{\odot}^{\top}\|\}$. If we can ensure the following condition

$$\sqrt{\sum_{r=1}^{m}\|e_r^{\mu}(t')\|^2} + \sqrt{\sum_{r=1}^{m}\|e_r^{\nu}(t')\|^2} \leq \frac{\lambda_2(\mathcal{L})}{\alpha}\|\boldsymbol{z}(t')\| \tag{4.23}$$

then consensus will be achieved.

At t', let $S_{\mu}^1(t')$ and $S_{\mu}^2(t')$ be the edge sets that their linked initial agents will trigger the edge events at $t'_{k_r^{\mu}} + \tau_{k_r^{\mu}}$ and $t'_{k_r^{\mu}} + b_r$, respectively. It is satisfied that $S_{\mu}^1(t') \bigcup S_{\mu}^2(t') = \{\epsilon_1, \ldots, \epsilon_m\}$ and $S_{\mu}^1(t') \bigcap S_{\mu}^2(t') = \emptyset$. Similarly, let $S_{\nu}^1(t')$ and $S_{\nu}^2(t')$ denote the edge sets that their linked terminal agents will trigger the edge events at $t'_{k_r^{\mu}} + \tau_{k_r^{\mu}}$ and $t'_{k_r^{\mu}} + b_r$, respectively. it is also satisfied that $S_{\nu}^1(t') \bigcup S_{\nu}^2(t') = \{\epsilon_1, \ldots, \epsilon_m\}$

and $S_\mu^1(t') \bigcap S_\mu^2(t') = \emptyset$. Note that condition (4.23) can be guaranteed if

$$\sqrt{\sum_{r\in S_\mu^1(t')} \|e_r^\mu(t')\|^2} + \sqrt{\sum_{r\in S_\nu^1(t')} \|e_r^\nu(t')\|^2} \leq \frac{\eta_1\lambda_2(\mathcal{L})}{\alpha}\|z(t')\| \tag{4.24}$$

and

$$\sqrt{\sum_{r\in S_\mu^2(t')} \|e_r^\mu(t')\|^2} + \sqrt{\sum_{r\in S_\nu^2(t')} \|e_r^\nu(t')\|^2} \leq \frac{\eta_2\lambda_2(\mathcal{L})}{\alpha}\|z(t')\| \tag{4.25}$$

where $\eta_1, \eta_2 > 0$ and $\eta_1 + \eta_2 < 1$.

According to the trigger function (4.19) and the fact that the state mismatch (4.17) is reset as soon as the value of the trigger function reaches zero, it is enough to imply $\|e_r^\mu(t')\| \leq \beta_{\max}\|z_r(t')\|$ and $\|e_r^\nu(t')\| \leq \beta_{\max}\|z_r(t')\|$, where $\beta_{\max} = \max\{\beta_r^i\}$. Furthermore, by recalling that $S_\mu^1(t')$ and $S_\nu^1(t')$ are subsets of edge set $\mathcal{E}$, we obtain $\mathbf{card}\{S_\mu^1(t')\}, \mathbf{card}\{S_\nu^1(t')\} \leq m$. The above analysis indicates that the upper bound of the left-hand side term in (4.24) can be calculated as $2\sqrt{\sum_{r=1}^m \beta_{\max}^2\|z_r(t')\|^2}$, which is equal to $2\beta_{\max}\|z(t')\|$. If we enforce β_r^i to satisfy $\beta_r^i < \frac{\eta_1\lambda_2(\mathcal{L})}{2\alpha}$, then condition (4.24) is always satisfied.

For condition (4.25), since $\mathbf{card}\{S_\mu^2(t')\} \leq m$, we obtain $\sqrt{\sum_{r\in S_\mu^2(t')} \|e_r^\mu(t')\|^2} \leq \sum_{r=1}^m \|e_r^\mu(t')\|$. According to the same arguments, we also get $\sqrt{\sum_{r\in S_\nu^2(t')} \|e_r^\mu(t')\|^2} \leq \sum_{r=1}^m \|e_r^\nu(t')\|$. The upper bound of the left-hand side term in (4.25) is thus obtained as $\sum_{r=1}^m \|e_r^\mu(t')\| + \sum_{r=1}^m \|e_r^\nu(t')\|$. Note that $e_r^\mu(t')$ and $e_r^\nu(t')$ are actually the mismatch $e_r^i(t')$ defined in (4.17). By enforcing $\|e_r^i(t')\| \leq \frac{\eta_2\lambda_2(\mathcal{L})}{2m\alpha}\|z(t')\|$, condition (4.25) can be ensured. Now we are ready to determine B_r. By following the similar process from (4.14) to (4.15) in the last subsection, the lower bound B_r is obtained as

$$B_r = \frac{\eta_2\lambda_2(\mathcal{L})}{2\alpha(2m\alpha + \eta_2\lambda_2(\mathcal{L}))}$$

For each agent i, the next edge-triggering time $t_{k_r^i+1}^i$ can be set as $t_{k_r^i}^i + b_r$, where $b_r \leq B_r$, if $\tau_{k_r^i}^i$ determined by trigger function (4.19) is less than b_r. By choosing suitable β_r and b_r, the aims of both consensus and Zeno-free triggers can be achieved. □

Remark 7. *In both cases, we regulate that each agent use the measurements of the relative states between its neighbours and itself to update its control input. This 'measurement-driven' principle makes the achievement of average consensus impossible since evolutions of two neighbouring agents are asynchronous. Take a two-agent group as an example. Assume that agent 1 and agent 2 are activated at $t1$ and $t2$, $t1 < t2$, respectively. Then between $t1$ and $t2$, agent 1 measure the relative states $x1 - x2$ and updating its control input while agent 2 remains still. This results in a pursuit phenomenon, that agent 1's states converge to agent 2' static states $x_2(t1)$ until $t2$. At $t2$, agent 2 is activated. However, it is obvious*

that $x_1(t2) \neq x_1(t1)$*, which means the final the consensus value is* $\frac{x_1(t2)+x_2(t2)}{2}$ *rather than the initial average* $\frac{x_1(t1)+x_2(t2)}{2}$*. Moreover, since we are utilising a distributed system, where global state values for all agents are unknown. This makes the final consensus value be unpredictable.*

4.4 Simulation examples

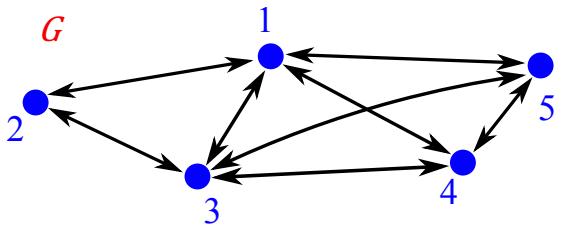

Figure 4.1: Graph topology

The MAS considered in the simulation consists of 5 agents. The sensing topology is described by **Fig.** 4.1 whose incidence matrix is chosen as

$$\mathcal{H} = \begin{bmatrix} -1 & 1 & 0 & 0 & 0 \\ 0 & -1 & 1 & 0 & 0 \\ -1 & 0 & 1 & 0 & 0 \\ 0 & 0 & 1 & 0 & -1 \\ 0 & 0 & -1 & 1 & 0 \\ 0 & 0 & 0 & -1 & 1 \\ 1 & 0 & 0 & 0 & -1 \\ -1 & 0 & 0 & 1 & 0 \end{bmatrix} \tag{4.26}$$

In the synchronized clock case, the initial states for all agents are set as $x_1(0) = -6.4$, $x_2(0) = 2.1$, $x_3(0) = -2.7$, $x_4(0) = 5.3$ and $x_5(0) = 0.6$. The parameters η_1 and η_2 are chosen as $\eta_1 = 0.85$ and $\eta_2 = 0.14$. We set $\beta_r = 0.34$ for the trigger function. The minimum inter-event time b_r is chosen to be $0.0039s$. The trajectories of each agent, the controller update times for each agent and the edge event times for each edge are depicted in **Fig.** 4.2.

In the unsynchronized clock case, the parameters are chosen as $\eta_1 = 0.8$ and $\eta_2 = 0.19$. $\beta_r^i, i = 1, \cdots, n$ and b_r are selected as $\beta_r^i = 0.22$ and $b_r = 0.0011s$, respectively. The activated times are chosen as $t^1(0) = 0.4$, $t^2(0) = 0.75$, $t^3(0) = 0.1$, $t^4(0) = 0.2$ and $t^5(0) = 0.8$. **Fig.** 4.3 illustrates the trajectory of each agent and the event times for both agent 1 and agent 2 linked by edge ϵ_1. It is verified that consensus can be reached and the event times of agents 1 and 2 triggered over ϵ_1 are asynchronous.

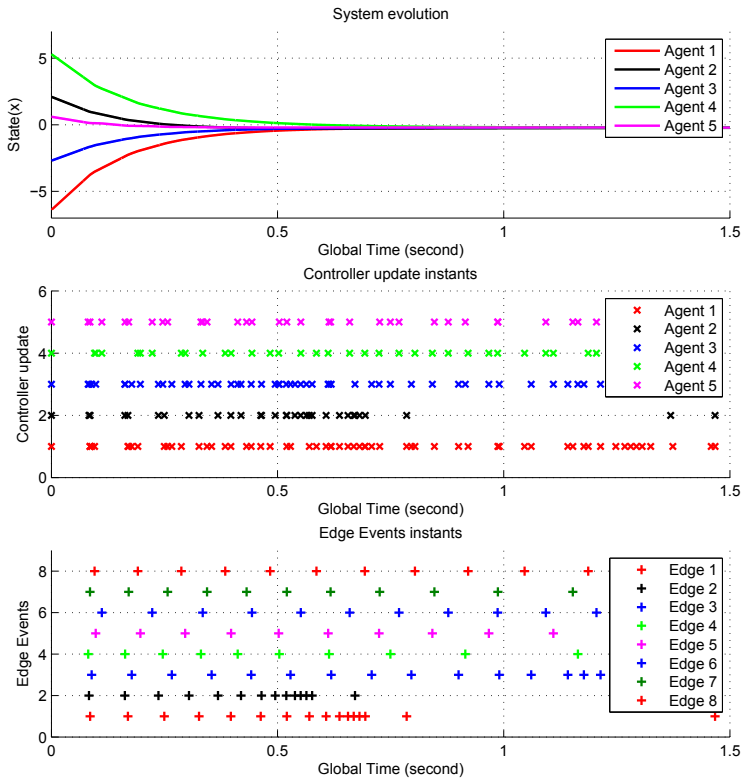

Figure 4.2: Comparison of state trajectories

4.5 Concluding remarks

In this chapter, we propose novel Zeno-free, edge-event-based algorithms to achieve multi-agent consensus under both synchronized clocks and unsynchronized clocks. In the synchronized clock case, we show that average consensus can be achieved under our algorithms even though each agent only measure the relative information via its own local coordinate frame. In the study of the unsynchronized clock case, each agent not only uses the relative information, but also works under its own clock that is not necessarily synchronized with others' clocks. We show that consensus can be achieved with Zeno-free triggers by using our proposed algorithm.

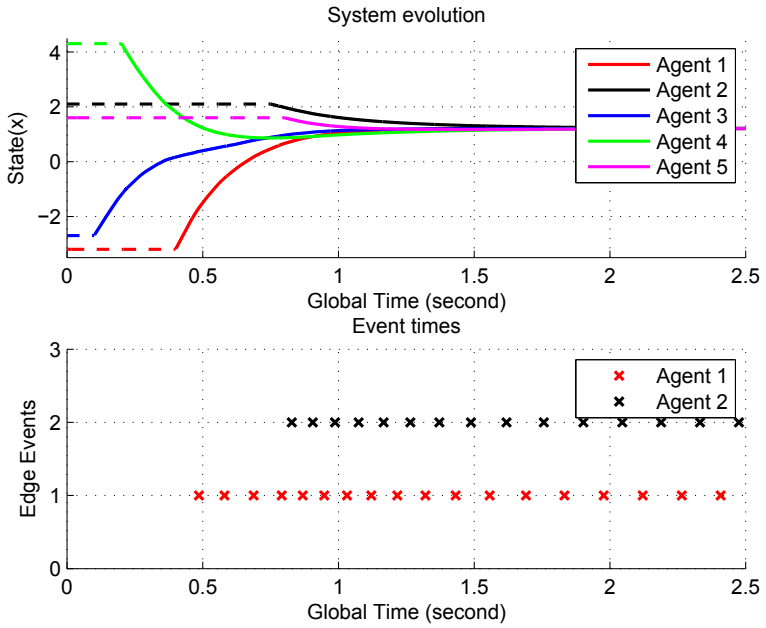

Figure 4.3: State trajectories for all agents and edge event times for agents 1 and 2 triggered over edge ϵ_1

Chapter 5

Event-Triggered Consensus for Networked Euler-Lagrange Agents

5.1 Introduction

The Euler-Lagrange equations describe the dynamics of a large class of nonlinear systems (including many mechanical systems such as robotic manipulators, spacecraft and marine vessels) [Kelly et al., 2006; Ortega et al., 2013]. As a result, there is motivation to study multi-agent coordination problems where each agent has Euler-Lagrange dynamics [Ren and Cao, 2011].

There have been relatively few results published studying event-triggered control for networks of Euler-Lagrange agents. Pioneering contributions studied leaderless consensus (but not leader-follower consensus) on an undirected network [Mu et al., 2014; Huang et al., 2016]. The dynamics studied in [Mu et al., 2014] and [Huang et al., 2016] are a subclass of Euler-Lagrange dynamics as they do not consider the presence of gravitational forces for each agent. While continuous model-independent algorithms e.g. [Ye et al., 2015] are easily adapted to be event-triggered, as shown in [Mu et al., 2014; Huang et al., 2016], they cannot guarantee the coordination objective in the presence of gravitational forces (which has an effect similar to a bounded disturbance). Typical control techniques required to deal with this term include feedback linearisation [Meng and Lin, 2012], adaptive control [Mei et al., 2013] and sliding mode control [Mei et al., 2011]. We note that these techniques have not been well studied in an event-triggered framework. In [Liu et al., 2016d], an adaptive, event-triggered controller is proposed to achieve flocking behaviour for undirected networks of Euler-Lagrange agents. This allows for gravitational forces omitted in [Mu et al., 2014; Huang et al., 2016]. However, the proposed controller in [Liu et al., 2016d] is piecewise continuous, which restricts its implementation in digital platforms. Moreover, it is worth noting that the trigger function used in [Liu et al., 2016d] cannot eliminate Zeno behaviour for each agent.

In this chapter, we present three different distributed event-triggered control algorithms to achieve leader-follower consensus for networked Euler-Lagrange agents; each algorithm has different strengths and their appropriateness of use may depend on the application scenario. Firstly, a globally asymptotically stable variable-gain al-

gorithm is proposed for agents on undirected graphs. The variable-gain controller allows for fully distributed and arbitrary design of parameters in both the control algorithm and trigger function. For the second control algorithm, which is applicable for directed graphs, we are motivated to use constant control gains. The algorithm achieves leader-follower consensus semi-globally, exponentially fast. Some limited knowledge of the bounds on the agent dynamic parameters, the network topology and a set of all possible initial conditions is required to centrally design the control gains. Lastly, we propose a globally asymptotically stable adaptive algorithm for use when the gravitational term is present in the agent self-dynamics. The adaptive algorithm is able to estimate uncertain dynamical parameters, but requires increased knowledge about the agent self-dynamics.

All three proposed controllers are piecewise constant, which has the benefit of reducing actuator updates and thus conserving energy resources. Furthermore, each agent only requires state, and relative state measurements, and does not require knowledge of the trigger times of neighbouring agents, which in general reduces the number of controller updates. For each algorithm, a trigger function is proposed and we show that Zeno behaviour can be excluded for every agent. All three trigger functions are of the same form with only minor modifications. Each term of the trigger function is carefully selected to ensure that the trigger function is more effective, when compared with existing trigger functions which do one of the following, but not both: 1) reduce the total number of events, and 2) eliminate Zeno behaviour for every agent. We show this by detailed comparison and analysis based on simulations. As a result of having multiple terms in the trigger function to achieve the aforementioned improvements, the stability analysis is significantly more complex. Each algorithm requires a different approach to proving stability, and the proposed methods may be useful for other problems in event-based control of multi-agent systems.

5.2 Additional preliminaries

We provide several theorems and lemmas, which will be used in this chapter. We also provide alternative preliminaries on graph theory which focus on directed graphs.

Theorem 5 (Mean Value Theorem for Vector-Valued Functions [Rudin et al., 1964])**.** *For a continuous vector-valued function $\boldsymbol{f}(s) : \mathbb{R} \to \mathbb{R}^n$ differentiable on $s \in [a, b]$, there exists $t \in (a, b)$ such that*

$$\left\| \frac{d\boldsymbol{f}}{ds}(t) \right\| \geq \frac{1}{b-a} \|\boldsymbol{f}(b) - \boldsymbol{f}(a)\|$$

Theorem 6 (The Schur Complement [Horn and Johnson, 2012])**.** *Consider a symmetric block matrix, partitioned as*

$$\boldsymbol{A} = \begin{bmatrix} \boldsymbol{B} & \boldsymbol{C} \\ \boldsymbol{C}^\top & \boldsymbol{D} \end{bmatrix} \tag{5.1}$$

Then $\boldsymbol{A} > 0$ if and only if $\boldsymbol{B} > 0$ and $\boldsymbol{D} - \boldsymbol{C}^\top \boldsymbol{B}^{-1} \boldsymbol{C} > 0$. Equivalently, $\boldsymbol{A} > 0$ if and only if $\boldsymbol{D} > 0$ and $\boldsymbol{B} - \boldsymbol{C}\boldsymbol{D}^{-1}\boldsymbol{C}^\top > 0$.

Lemma 3 ([Ioannou and Fidan, 2006])**.** *If a function $f(t)$ satisfies $f(t), \dot{f}(t) \in \mathcal{L}_\infty$, and $f(t) \in \mathcal{L}_p$ for some value of $p \in [1, \infty)$, then $f(t) \to 0$ as $t \to \infty$.*

Lemma 4. *Suppose $\boldsymbol{A} > 0$ is defined as in* (5.1)*. Let a quadratic function with arguments $\boldsymbol{x}, \boldsymbol{y}$ be expressed as $W = [\boldsymbol{x}^\top, \boldsymbol{y}^\top]\boldsymbol{A}[\boldsymbol{x}^\top, \boldsymbol{y}^\top]^\top$. Define $\boldsymbol{F} := \boldsymbol{B} - \boldsymbol{C}\boldsymbol{D}^{-1}\boldsymbol{C}^\top$ and $\boldsymbol{G} := \boldsymbol{D} - \boldsymbol{C}^\top \boldsymbol{B}^{-1}\boldsymbol{C}$. Then there holds*

$$\lambda_{\min}(\boldsymbol{F})\boldsymbol{x}^\top \boldsymbol{x} \leq \boldsymbol{x}^\top \boldsymbol{F}\boldsymbol{x} \leq W \tag{5.2a}$$

$$\lambda_{\min}(\boldsymbol{G})\boldsymbol{y}^\top \boldsymbol{y} \leq \boldsymbol{y}^\top \boldsymbol{G}\boldsymbol{y} \leq W \tag{5.2b}$$

Proof. The proof for (5.2b) is immediately obtained by recalling **Theorem** 6 and observing that

$$W = \boldsymbol{y}^\top \boldsymbol{G}\boldsymbol{y} + [\boldsymbol{y}^\top \boldsymbol{C}^\top \boldsymbol{B}^{-1} + \boldsymbol{x}^\top]\boldsymbol{B}[\boldsymbol{B}^{-1}\boldsymbol{C}\boldsymbol{y} + \boldsymbol{x}]$$

An equally straightforward proof yields (5.2a). □

Lemma 5. *Let $g(x, y)$ be a function given as*

$$g(x, y) = ax^2 + by^2 - cxy^2 - dxy \tag{5.3}$$

for real positive scalars $a, c, d > 0$. Then for a given $\mathcal{X} > 0$, there exist $b > 0$ such that $g(x, y) > 0$ for all $y \in [0, \infty)$ and $x \in [0, \mathcal{X}]$.

Proof. Observe that $cxy^2 \leq c\mathcal{X}y^2$ for all $x \in [0, \mathcal{X}]$. It follows that

$$g(x, y) \geq ax^2 + (b - c\mathcal{X})y^2 - dxy$$

if $y \in [0, \infty)$ and $x \in [0, \mathcal{X}]$ because $c > 0$. For any fixed value of $y = y_1 \in [0, \infty)$, write $\bar{g}(x) = ax^2 + (b - c\mathcal{X})y_1^2 - dxy_1$. The discriminant of $\bar{g}(x)$ is negative if

$$b > c\mathcal{X} + \frac{d^2}{4a} \tag{5.4}$$

which implies that the roots of $\bar{g}(x)$ are complex, i.e. $\bar{g}(x) > 0$ and this holds for any $y_1 \in [0, \infty)$. We thus conclude that for all $y \in [0, \infty)$ and $x \in [0, \mathcal{X}]$, if b satisfies (5.4), then $g(x, y) > 0$ except the case where $g(x, y) = 0$ if and only if $x = y = 0$. □

Corollary 1. *Let $h(x, y)$ be a function given as*

$$h(x, y) = ax^2 + by^2 - cxy^2 - dxy - ex - fy \tag{5.5}$$

where the real, strictly positive scalars c, d, e, f and two further positive scalars ε, ϑ are fixed. Suppose that for given $\mathcal{Y}, \varepsilon$ there holds $\mathcal{Y} - \varepsilon > 0$, and for a given $\mathcal{X} > 0$ there holds $\mathcal{X} - \vartheta > 0$. Define the sets $\mathcal{U} = \{x, y : x \in [\mathcal{X} - \vartheta, \mathcal{X}], y > 0\}$ and $\mathcal{V} = \{x, y : x > 0, y \in$

$[\mathcal{Y}-\varepsilon, \mathcal{Y}]\}$. *Define the region* $\mathcal{R} = \mathcal{U} \cup \mathcal{V}$. *Then there exist* $a, b > 0$ *such that* $h(x, y)$ *is positive definite in* $\mathcal{R}$.

Proof. Observe that $h(x, y) = g(x, y) - ex - fy$ where $g(x, y)$ is defined in **Lemma** 5. Let b^* be such that it satisfies condition (5.4) in **Lemma** 5 and thus $g(x, y) > 0$ for $x \in [0, \infty)$ and $y \in [0, \mathcal{Y}]$. Note that the positivity condition on $g(x, y)$ in **Lemma** 5 continues to hold for any $a \geq a^*$ and any $b \geq b^*$. Let a_1 and b_1 be positive scalars whose magnitudes will be determined later. Define $a = a_1 + a^*$ and $b = b_1 + b^*$. Define $z(x, y) \triangleq a_1 x^2 + b_1 y^2 - ex - fy$. Next, consider $(x, \bar{y}) \in \mathcal{V}$, where $\bar{y}$ is some fixed value. It follows that

$$z(x, \bar{y}) = a_1 x^2 - ex + (b_1 \bar{y}^2 - f\bar{y})$$

Note the discriminant of $z(x, \bar{y})$ is $\mathcal{D}_x = e^2 - 4a_1(b_1\bar{y}^2 - f\bar{y})$. It follows that $\mathcal{D}_x < 0$ if $b_1\bar{y}^2 > f\bar{y} + e/4a_1$. This is satisfied, independently of $\bar{y} \in [\mathcal{Y} - \varepsilon, \mathcal{Y}]$, for any $b_1 \geq b_{1,y}$, $a_1 \geq a_{1,y}$ where

$$b_{1,y} > \frac{e^2}{4a_{1,y}(\mathcal{Y}-\varepsilon)^2} + \frac{f}{\mathcal{Y}-\varepsilon}$$

because $\mathcal{Y} - \varepsilon \leq \bar{y}$. It follows that $\mathcal{D}_x < 0 \Rightarrow z(x, y) > 0$ in $\mathcal{V}$. Now, consider $(\bar{x}, y) \in \mathcal{U}$ for some fixed value $\bar{x}$. It follows that

$$z(\bar{x}, y) = b_1 y^2 - fy + (a_1\bar{x}^2 - e\bar{x})$$

and note the discriminant of $z(\bar{x}, y)$ is $\mathcal{D}_y = f^2 - 4b_1(a_1\bar{x}^2 - e\bar{x})$. Suppose that $a_1 > e/\mathcal{X}$, which ensures that $a_1\bar{x}^2 - e\bar{x} > 0$. Then, $\mathcal{D}_y < 0$ if $b_1(a_1\bar{x}^2 - e\bar{x}) > f/4$. This is satisfied, independently of $\bar{x} \in [\mathcal{X} - \vartheta, \mathcal{X}]$, for any $b_1 \geq b_{1,x}$, $a_1 \geq a_{1,x}$ where

$$b_{1,x} > \frac{f}{4(a_{1,x}(\mathcal{X}-\vartheta)^2 - e(\mathcal{X}-\vartheta))}$$

It follows that $\mathcal{D}_y < 0 \Rightarrow z(x, y) > 0$ in $\mathcal{U}$. We conclude that setting $b = b^* + \max[b_{1,x}, b_{1,y}]$ and $a = a^* + \max[a_{1,x}, a_{1,y}]$, implies $h(x, y) > 0$ in $\mathcal{R}$, except $h(0, 0) = 0$. □

5.2.1 Graph theory

We model the interactions among the leader and n followers by a weighted directed graph (digraph) $\mathcal{G} = (\mathcal{V}, \mathcal{E}, \mathcal{A})$ with vertex set $\mathcal{V} = \{v_0, v_1, \cdots, v_n\}$ and edge set $\mathcal{E} \subseteq \mathcal{V} \times \mathcal{V}$. Without loss of generality, the leader agent is numbered by v_0. We use $\mathcal{G}_F$ to describe the interactions among the n follower agents with vertex set $\mathcal{V}_F = \{v_1, \cdots, v_n\}$ and edge set $\mathcal{E}_F \subseteq \mathcal{V}_F \times \mathcal{V}_F$. An ordered edge set of $\mathcal{G}$ is $e_{ij} = (v_i, v_j)$. The weighted adjacency matrix $\mathcal{A} = \mathcal{A}(\mathcal{G}) = \{a_{ij}\}$ is the $(n+1) \times (n+1)$ matrix given by $a_{ij} > 0$, if $e_{ji} \in \mathcal{E}$ and $a_{ij} = 0$, otherwise. In this chapter, it is assumed that $a_{ii} = 0$, i.e. there are no self-loops. The edge e_{ij} is incoming with respect to v_j and outgoing with respect to v_i. A graph is undirected if $e_{ij} \in \mathcal{E} \Leftrightarrow e_{ji} \in \mathcal{E}$ and $a_{ij} = a_{ji}$. The neighbour set of v_i is denoted by $\mathcal{N}_i = \{v_j \in \mathcal{V} : (v_i, v_j) \in \mathcal{E}\}$. The

$(n+1) \times (n+1)$ Laplacian matrix, $\mathcal{L} = \{l_{ij}\}$, of the associated directed graph $\mathcal{G}$ is defined as $l_{ij} = -a_{ij}$ for all $i \neq j$ and $l_{ii} = \sum_{k=1, k\neq i}^{n} a_{ik}$ for all i. A digraph with $n+1$ vertices is called a directed spanning tree if it has n edges and there exists a root vertex with directed paths to every other vertex [Ren and Cao, 2011]. The following result holds for the Laplacian matrix associated with a directed graph.

Lemma 6 ([Ren and Cao, 2011])**.** *Let $\mathcal{L}$ be the Laplacian matrix associated with a directed graph $\mathcal{G}$. Then $\mathcal{L}$ has a simple zero eigenvalue and all other eigenvalues have positive real parts if and only if $\mathcal{G}$ has a directed spanning tree.*

Lemma 7 ([Song et al., 2012])**.** *Suppose a graph $\mathcal{G}$ contains a directed spanning tree, and there are no edges of $\mathcal{G}$ which are incoming to the root vertex v_0 of the tree. Then the Laplacian matrix associated with $\mathcal{G}$ has the following form:*

$$\mathcal{L} = \begin{bmatrix} 0 & \mathbf{0}_n^T \\ \mathcal{L}_{21} & \mathcal{L}_{22} \end{bmatrix}$$

and all eigenvalues of $\mathcal{L}_{22}$ have positive real parts. Moreover, there exists a diagonal positive definite matrix $\mathbf{\Gamma}$ such that $\boldsymbol{Q} := \mathbf{\Gamma}\mathcal{L}_{22} + \mathcal{L}_{22}^{\top}\mathbf{\Gamma} > 0$. In addition, if $\mathcal{G}_F$ is undirected, then $\mathcal{L}_{22}$ is symmetric positive definite.

5.2.2 Euler-Lagrange systems

A class of dynamical systems can be described using the Euler-Lagrange equations [Kelly et al., 2006]. The general form for the i-th agent equation of motion is:

$$\boldsymbol{M}_i(\boldsymbol{q}_i)\ddot{\boldsymbol{q}}_i + \boldsymbol{C}_i(\boldsymbol{q}_i, \dot{\boldsymbol{q}}_i)\dot{\boldsymbol{q}}_i + \boldsymbol{g}_i(\boldsymbol{q}_i) = \boldsymbol{\tau}_i \tag{5.6}$$

where $\boldsymbol{q}_i \in \mathbb{R}^p$ is a vector of the generalized coordinates, $\boldsymbol{M}_i(\boldsymbol{q}_i) \in \mathbb{R}^{p\times p}$ is the inertial matrix, $\boldsymbol{C}_i(\boldsymbol{q}_i, \dot{\boldsymbol{q}}_i) \in \mathbb{R}^{p\times p}$ is the Coriolis and centrifugal torque matrix, $\boldsymbol{g}_i(\boldsymbol{q}_i) \in \mathbb{R}^p$ is the vector of gravitational forces and $\boldsymbol{\tau}_i \in \mathbb{R}^p$ is the control input vector. For agent i, we have $\boldsymbol{q}_i = [\boldsymbol{q}_i^{(1)}, \ldots, \boldsymbol{q}_i^{(p)}]^{\top}$. We assume each agent is fully actuated. Throughout this chapter, the dynamics in (5.6) are assumed to satisfy the following properties, details of which are provided in [Kelly et al., 2006].

P1 The matrix $\boldsymbol{M}_i(\boldsymbol{q}_i)$ is symmetric positive definite.

P2 There exist constants $k_{\underline{m}}, k_{\overline{M}} > 0$ such that $k_{\underline{m}}\boldsymbol{I}_p \leq \boldsymbol{M}_i(\boldsymbol{q}_i) \leq k_{\overline{M}}\boldsymbol{I}_p, \forall\, i, \boldsymbol{q}_i$. It follows that $\sup_{\boldsymbol{q}_i} \|\boldsymbol{M}_i\|_2 \leq k_{\overline{M}}$ and $k_{\underline{m}} \leq \inf_{\boldsymbol{q}_i} \|\boldsymbol{M}_i^{-1}\|_2^{-1}\ \forall\, i$.

P3 There exists a constant $k_C > 0$ such that $\|\boldsymbol{C}_i\|_2 \leq k_C\|\dot{\boldsymbol{q}}_i\|_2, \forall\, i, \dot{\boldsymbol{q}}_i$.

P4 The matrix $\boldsymbol{C}_i(\boldsymbol{q}_i, \dot{\boldsymbol{q}}_i)$ is related to the inertial matrix $\boldsymbol{M}_i(\boldsymbol{q}_i, \dot{\boldsymbol{q}}_i)$ by the expression $\boldsymbol{x}^T(\frac{1}{2}\dot{\boldsymbol{M}}_i(\boldsymbol{q}_i) - \boldsymbol{C}_i(\boldsymbol{q}_i, \dot{\boldsymbol{q}}_i))\boldsymbol{x} = 0$ for any $\boldsymbol{q}, \dot{\boldsymbol{q}}, \boldsymbol{x} \in \mathbb{R}^p$. This implies that $\dot{\boldsymbol{M}}_i(\boldsymbol{q}_i) = \boldsymbol{C}_i(\boldsymbol{q}_i, \dot{\boldsymbol{q}}_i) + \boldsymbol{C}_i(\boldsymbol{q}_i, \dot{\boldsymbol{q}}_i)^{\top}$.

P5 There exists a constant $k_g > 0$ such that $\|\boldsymbol{g}_i(\boldsymbol{q}_i)\| < k_g$.

P6 Linearity in the parameters: $\boldsymbol{M}_i(\boldsymbol{q}_i)\boldsymbol{x} + \boldsymbol{C}_i(\boldsymbol{q}_i, \dot{\boldsymbol{q}}_i)\boldsymbol{y} + \boldsymbol{g}_i(\boldsymbol{q}_i) = \boldsymbol{Y}_i(\boldsymbol{q}_i, \dot{\boldsymbol{q}}_i, \boldsymbol{x}, \boldsymbol{y})\boldsymbol{\Theta}_i$ for all vectors $x, y \in \mathbb{R}^p$, where $\boldsymbol{Y}_i(\boldsymbol{q}_i, \dot{\boldsymbol{q}}_i, \boldsymbol{x}, \boldsymbol{y})$ is the known regressor matrix and $\boldsymbol{\Theta}_i$ is a vector of unknown but constant parameters associated with the i^{th} agent.

Assumption 1. *(Sub-class of dynamics) In* ***Sections*** *5.4 and 5.5, we assume that* $\boldsymbol{g}_i(\boldsymbol{q}_i) = \boldsymbol{0}, \forall\, i$. *In other words, the dynamics of the agents belong to a subclass of Euler-Lagrange equations which do not have a gravity term. That is,*

$$\boldsymbol{M}_i(\boldsymbol{q}_i)\ddot{\boldsymbol{q}}_i + \boldsymbol{C}_i(\boldsymbol{q}_i, \dot{\boldsymbol{q}}_i)\dot{\boldsymbol{q}}_i = \boldsymbol{\tau}_i \tag{5.7}$$

If the gravity term $\boldsymbol{g}_i(\boldsymbol{q}_i)$ is present, the adaptive controller proposed in **Section** 5.6 may be used.

5.3 Problem statement

Problem 4. *Denote the leader as agent 0 with* $\boldsymbol{q}_0$ *and* $\dot{\boldsymbol{q}}_0$ *being the generalised coordinates and generalised velocity of the leader, respectively. The aim is to develop event-triggered, distributed algorithms for each Euler-Lagrange follower agent, where the updates are such that* τ_i *is piecewise-constant. The distributed algorithms are designed to achieve leader-follower consensus to a stationary leader, i.e.* $\dot{\boldsymbol{q}}_0(t) = 0, \forall t \geq 0$. *Leader-follower consensus is said to be achieved if* $\lim_{t\to\infty} \|\boldsymbol{q}_i(t) - \boldsymbol{q}_0(t)\| = 0, \forall i = 1, \ldots, n$ *and* $\lim_{t\to\infty} \|\dot{\boldsymbol{q}}_i(t)\| = 0, \forall i = 1, \ldots, n$ *are satisfied. Another aim of this chapter is to exclude the possibility of Zeno behaviour, which we formally defined in* ***Definition*** *1.*

In this chapter, we assume that the follower agent $i \in 1, \ldots, n$ *is equipped with sensors which continuously measure the relative generalised coordinates to agent i's neighbours. In other words,* $\boldsymbol{q}_i(t) - \boldsymbol{q}_j(t), \forall j \in \mathcal{N}_i$ *is available to agent i. In* ***Section*** *5.5 we also assume that the relative generalised velocities are available, i.e.* $\dot{\boldsymbol{q}}_i(t) - \dot{\boldsymbol{q}}_j(t), \forall j \in \mathcal{N}_i$. *The scenario where agents collect relative information to execute algorithms can be found in many experimental testbeds, such as ground robots or UAVs equipped with high-speed cameras. It is also assumed that each agent i can measure its own generalised velocity continuously, i.e.* $\dot{\boldsymbol{q}}_i(t)$.

5.4 Variable-gain, model-independent algorithm

In this section, we introduce a variable-gain, event-triggered control algorithm for when the network model of the follower agents is described by an undirected graph. We show that the proposed algorithm does not require any knowledge of the multi-agent system (i.e totally distributed design) and is globally stable. Zeno behaviour is also excluded for each agent.

5.4.1 Main result

Define a new state variable for agent i as

$$\boldsymbol{z}_i(t) = \sum_{j=0}^{n} a_{ij}(\boldsymbol{q}_i(t) - \boldsymbol{q}_j(t)) + \mu_i(t)\dot{\boldsymbol{q}}_i(t), \qquad i = 1, \ldots, n$$

where a_{ij} is the (i,j)th element of the adjacency matrix $\mathcal{A}$ associated with the digraph $\mathcal{G}$. Note that the follower graph $\mathcal{G}_F$ is undirected. The variable control gain $\mu_i(t)$ is subject to the following updating law[1]:

$$\dot{\mu}_i(t) = \alpha_i \dot{\boldsymbol{q}}_i(t)^\top \dot{\boldsymbol{q}}_i(t) \tag{5.8}$$

The scalar α_i is strictly positive and may be independent for all agents. It is obvious that $\mu_i(t)$ is a monotonically increasing function. The variable-gain scalar function $\mu_i(t)$ is initialised at $t = 0$ with an arbitrary $\mu_i(0) \geq 0$, which implies that $\mu_i(t) \geq 0, \forall\, t > 0$.

The control algorithm is now proposed. Let the trigger time sequence of agent i be denoted as $t_0^i, t_1^i, \ldots, t_k^i, \ldots$ with $t_0^i := 0$ and we detail below how each trigger time is determined. The event-triggered controller for follower agent i is designed as:

$$\boldsymbol{\tau}_i(t) = -\boldsymbol{z}_i(t_k^i) \tag{5.9}$$

for $t \in [t_k^i, t_{k+1}^i)$. The control input for each agent is held constant and equal to the last control update $\boldsymbol{\tau}_i(t_k^i)$ in the time interval $[t_k^i, t_{k+1}^i)$.

We define a state mismatch for agent i between consecutive event times t_k^i and t_{k+1}^i as follows:

$$\boldsymbol{e}_i(t) = \boldsymbol{z}_i(t_k^i) - \boldsymbol{z}_i(t) \tag{5.10}$$

for $t \in [t_k^i, t_{k+1}^i)$. The trigger function is designed as follows:

$$f_i(t) = \|\boldsymbol{e}_i(t)\|^2 - \beta_i \|\dot{\boldsymbol{q}}_i(t)\|^2 - \omega_i(t) \tag{5.11}$$

where β_i is *an arbitrarily chosen positive constant* (see the Proof of **Theorem** 7 for the explanations), $\omega_i(t)$ is an offset function defined as $\omega_i(t) = \kappa_i \exp(-\varepsilon_i t)$ with arbitrarily chosen $\kappa_i, \varepsilon_i > 0$. The k-th event for agent i is triggered as soon as the trigger condition $f_i(t) = 0$ is satisfied. The control input $\boldsymbol{\tau}_i(t)$ is updated only when an event of agent i is triggered. Furthermore, every time an event is triggered, and in accordance with their definitions, the state mismatch $\boldsymbol{e}_i(t)$ is reset to be equal to zero

[1] In some existing works on multi-agent systems, similar controllers which have monotonically increasing gains have been termed "adaptive-gain controllers" or "adaptive controllers", see e.g. [Mei et al., 2014; Li et al., 2013; Mei et al., 2016]. While we acknowledge this terminology is correct, we choose to call the controller proposed in this section a "variable-gain controller" to differentiate, and avoid confusion with, the controller we will propose in **Section** 5.6, which adaptively estimates unknown, but constant, parameters of the agent dynamics. The variable-gain controller in this section and the adaptive controller in **Section** 5.6 are fundamentally different in design and ideology.

and thus the trigger function assumes a non-positive value, that is, $f_i(t) \leq 0$.

Remark 8. *In existing event-based multi-agent control literature, the parameters of the state-dependent term are typically restricted. For example, the authors of [Huang et al., 2016] studied leaderless consensus for undirected networked Euler-Lagrange agents. Different from our proposed variable-gain controller, their controller adopts fixed gains. As a result, the parameter ϱ_i (see the trigger function in [Huang et al., 2016]) of the state-dependent term has to be less than a computable upper bound. This bound requires knowledge of the control gains and graph topology (e.g. number of neighbours and degree of the agent). In comparison, our equivalent parameter β_i in our proposed trigger function* (5.11) *can be chosen as an arbitrarily positive constant. This provides a much greater flexibility in the implementation of the algorithm.*

We note that even in papers considering simple single integrator dynamics with a parameter for the state-dependent term, equivalent to our β_i, require an upper bound as well (see the seminal works of [Dimarogonas et al., 2012; Fan et al., 2013]). To the best of the authors' knowledge, the event-based controller proposed in this section is the first to allow for an arbitrarily chosen positive parameter for the state-dependent term in the trigger function.

By substituting the control input (5.9) into the system dynamics (5.7), the closed-loop system can be written as

$$\boldsymbol{M}_i(\boldsymbol{q}_i)\ddot{\boldsymbol{q}}_i(t) + \boldsymbol{C}_i(\boldsymbol{q}_i, \dot{\boldsymbol{q}}_i)\dot{\boldsymbol{q}}_i(t) = -\boldsymbol{z}_i(t_k^i) \tag{5.12}$$

Then by applying (5.10), we obtain

$$\boldsymbol{M}_i(\boldsymbol{q}_i)\ddot{\boldsymbol{q}}_i(t) + \boldsymbol{C}_i(\boldsymbol{q}_i, \dot{\boldsymbol{q}}_i)\dot{\boldsymbol{q}}_i(t) = -(\boldsymbol{z}_i(t) + \boldsymbol{e}_i(t)) \tag{5.13}$$

Define new state variables $\boldsymbol{u}_i = \boldsymbol{q}_i - \boldsymbol{q}_0$ and $\boldsymbol{v}_i = \dot{\boldsymbol{q}}_i$ and we henceforth drop the argument t for brevity, and where there is no confusion. Define the stacked column vectors of all $\boldsymbol{u}_i, \boldsymbol{v}_i, \boldsymbol{q}_i, \boldsymbol{e}_i$ as $\boldsymbol{u} = [\boldsymbol{u}_1^\top, ..., \boldsymbol{u}_n^\top]^\top$, $\boldsymbol{v} = [\boldsymbol{v}_1^\top, ..., \boldsymbol{v}_n^\top]^\top$, $\boldsymbol{q} = [\boldsymbol{q}_1^\top, ..., \boldsymbol{q}_n^\top]^\top$, $\boldsymbol{z} = [\boldsymbol{z}_1^\top, ..., \boldsymbol{z}_n^\top]^\top$ and $\boldsymbol{e} = [\boldsymbol{e}_1^\top, ..., \boldsymbol{e}_n^\top]^\top$ respectively. It is easy to obtain that

$$\begin{aligned}\boldsymbol{z} &= (\mathcal{L}_{22} \otimes \boldsymbol{I}_p)(\boldsymbol{q} - \boldsymbol{1}_n \otimes \boldsymbol{q}_0) + \boldsymbol{K}\dot{\boldsymbol{q}} \\ &= (\mathcal{L}_{22} \otimes \boldsymbol{I}_p)\boldsymbol{u} + \boldsymbol{K}\boldsymbol{v}\end{aligned}$$

where $\boldsymbol{K} = \text{diag}[\mu_1 \boldsymbol{I}_p, ..., \mu_n \boldsymbol{I}_p]$. Define the following block diagonal matrices $\boldsymbol{M}(\boldsymbol{q}) = \text{diag}[\boldsymbol{M}_1(\boldsymbol{q}_1), ..., \boldsymbol{M}_n(\boldsymbol{q}_n)]$, $\boldsymbol{C}(\boldsymbol{q}, \dot{\boldsymbol{q}}) = \text{diag}[\boldsymbol{C}_1(\boldsymbol{q}_1, \dot{\boldsymbol{q}}_1), ..., \boldsymbol{C}_n(\boldsymbol{q}_n, \dot{\boldsymbol{q}}_n)]$. It is obvious that $\boldsymbol{M}$ is symmetric positive definite since $\boldsymbol{M}_i > 0, \forall\, i$. With these notations, the compact form of system (5.13) can be expressed as

$$\begin{aligned}\dot{\boldsymbol{u}} &= \boldsymbol{v} \\ \dot{\boldsymbol{v}} &= -\boldsymbol{M}(\boldsymbol{q})^{-1}\left[\boldsymbol{C}(\boldsymbol{q}, \boldsymbol{v})\boldsymbol{v} + (\mathcal{L}_{22} \otimes \boldsymbol{I}_p)\boldsymbol{u} + \boldsymbol{K}\boldsymbol{v} + \boldsymbol{e}\right] \\ \dot{\boldsymbol{K}} &= \boldsymbol{\Xi} \otimes \boldsymbol{I}_p\end{aligned} \tag{5.14}$$

where $\boldsymbol{\Xi} = \text{diag}[\alpha_1 \|\boldsymbol{v}_1\|_2^2, \alpha_2 \|\boldsymbol{v}_2\|_2^2, ..., \alpha_n \|\boldsymbol{v}_n\|_2^2]$. The leader-follower objective is achieved when there holds $\boldsymbol{u} \equiv \boldsymbol{v} \equiv \boldsymbol{0}_{np}$. We now present the main result for this

Section.

Theorem 7. *Suppose that each follower agent with dynamics* (5.7)*, under Assumption 1, employs the controller* (5.9) *with trigger function* (5.11)*. Suppose further that the directed graph $\mathcal{G}$ contains a directed spanning tree, with the leader agent* 0 *as the root node (thus with no incoming edges) and the follower graph $\mathcal{G}_F$ is undirected. Then the leader-follower consensus objective is globally asymptotically achieved and no agent will exhibit Zeno behaviour.*

Proof. We divide our proof into two parts. In the first part, we focus on the stability analysis of the system (5.14). In the second part, analysis is provided to show the exclusion of Zeno behaviour *for each agent*.

5.4.1.1 Stability analysis

Consider the following Lyapunov-like function

$$\begin{aligned} V &= \frac{1}{2}\boldsymbol{u}^\top(\mathcal{L}_{22}\otimes \boldsymbol{I}_p)\boldsymbol{u} + \frac{1}{2}\boldsymbol{v}^\top \boldsymbol{M}\boldsymbol{v} + \sum_{i=1}^{n}\frac{1}{2\alpha_i}(\mu_i-\bar{\mu})^2 \\ &= V_1 + V_2 + V_3 \end{aligned} \tag{5.15}$$

where $\bar{\mu}$ is a strictly positive constant. The choice of $\bar{\mu}$ will be presented below. Since $\mathcal{G}$ contains a directed spanning tree and $\mathcal{G}_F$ is undirected, according to **Lemma** 7, $\mathcal{L}_{22}$ is positive definite. Note that $\boldsymbol{M}$ is positive definite and V_3 is non-negative, we conclude that V is strictly positive for nonzero $\boldsymbol{u}$ and $\boldsymbol{v}$.

Taking the derivative of V with respect to time, along the trajectory of system (5.14), there holds $\dot{V} = \dot{V}_1 + \dot{V}_2 + \dot{V}_3$. Evaluating $\dot{V}_1$ yields $\dot{V}_1 = \boldsymbol{u}^\top(\mathcal{L}_{22}\otimes \boldsymbol{I}_p)\boldsymbol{v}$. Next, the derivative $\dot{V}_2$ is evaluated to be $\dot{V}_2 = \boldsymbol{v}^\top \boldsymbol{M}\dot{\boldsymbol{v}} + \frac{1}{2}\boldsymbol{v}^\top \dot{\boldsymbol{M}}\boldsymbol{v}$, which on further analysis, yields

$$\begin{aligned} \dot{V}_2 &= -\boldsymbol{v}^\top \boldsymbol{C}\boldsymbol{v} - \boldsymbol{v}^\top(\mathcal{L}_{22}\otimes \boldsymbol{I}_p)\boldsymbol{u} - \boldsymbol{v}^\top \boldsymbol{K}\boldsymbol{v} - \boldsymbol{v}^\top \boldsymbol{e} + \frac{1}{2}\boldsymbol{v}^\top \dot{\boldsymbol{M}}\boldsymbol{v} \\ &= -\boldsymbol{v}^\top(\mathcal{L}_{22}\otimes \boldsymbol{I}_p)\boldsymbol{u} - \boldsymbol{v}^\top \boldsymbol{K}\boldsymbol{v} - \boldsymbol{v}^\top \boldsymbol{e} \end{aligned}$$

Lastly, we obtain $\dot{V}_3 = \sum_{i=1}^{n}(\mu_i-\bar{\mu})\boldsymbol{v}_i^\top \boldsymbol{v}_i = \boldsymbol{v}^\top \boldsymbol{K}\boldsymbol{v} - \bar{\mu}\boldsymbol{v}^\top \boldsymbol{v}$. Since $\mathcal{L}_{22}$ is symmetric, summing $\dot{V}_1$, $\dot{V}_2$ and $\dot{V}_3$ yields $\dot{V} = -\bar{\mu}\boldsymbol{v}^\top \boldsymbol{v} + \boldsymbol{v}^\top \boldsymbol{e}$. By using the inequality $\boldsymbol{v}^\top \boldsymbol{e} \leq \frac{a}{2}\|\boldsymbol{v}\|^2 + \frac{1}{2a}\|\boldsymbol{e}\|^2, \forall a > 0$, we obtain

$$\dot{V} \leq (\frac{a}{2} - \bar{\mu})\|\boldsymbol{v}\|^2 + \frac{1}{2a}\|\boldsymbol{e}\|^2$$

Note that the non-positivity of the trigger function f_i guarantees that $\|\boldsymbol{e}\|^2 \leq \beta\|\boldsymbol{v}\|^2 + \bar{\omega}(t)$, where $\beta = \max_i\{\beta_i\}$ and $\bar{\omega}(t) = \sum_{i=1}^{n}\omega_i(t)$. It follows that $\dot{V}$ satisfies

$$\dot{V} \leq (\frac{a}{2} + \frac{\beta}{2a} - \bar{\mu})\|\boldsymbol{v}\|^2 + \bar{\omega}(t)$$

For notation simplicity, we define $\chi = \bar{\mu} - \frac{a}{2} - \frac{\beta}{2a}$. Note that for any given a and β,

we can find a sufficiently large $\bar{\mu}$ to ensure $\chi > 0$ and thus

$$\dot{V} \leq -\chi \|\boldsymbol{v}\|^2 + \bar{\omega}(t)$$

and it is straightforward to conclude that the parameter β_i in the trigger function (5.11) can be selected as an arbitrarily positive constant. Integrating both sides of the above equation from zero to t, for any $t > 0$, yields

$$V(t) + \chi \int_0^t \|\boldsymbol{v}(\epsilon)\|^2 . \mathrm{d}\epsilon \leq V(0) + \sum_{i=1}^{n} \frac{\kappa_i}{\varepsilon_i}$$

which implies that $V(t)$ and $\chi \int_0^t \|\boldsymbol{v}(\epsilon)\|^2 . \mathrm{d}\epsilon$ are bounded since $V(0), \kappa_i, \varepsilon_i$ are all bounded. By recalling (5.15), it is straightforward to conclude that $\boldsymbol{u}, \boldsymbol{v}, \mu_i$ are all bounded. Now we turn to $\dot{\boldsymbol{v}}_i$. Notice that $\dot{\boldsymbol{q}}_0 = 0$ and from (5.12), we have

$$\dot{\boldsymbol{v}}_i = -\boldsymbol{M}_i(\boldsymbol{q}_i)^{-1}[\boldsymbol{C}_i(\boldsymbol{q}_i, \dot{\boldsymbol{q}}_i)\dot{\boldsymbol{q}}_i + \boldsymbol{z}_i(t_k^i)] \tag{5.16}$$

Since $\boldsymbol{u}, \boldsymbol{v}, \mu_i$ are bounded, $\dot{\boldsymbol{q}}_i$ and $\boldsymbol{z}_i(t_k^i)$ are bounded. Then by recalling properties P2 and P3, we conclude that $\dot{\boldsymbol{v}}$ is bounded. From the fact that both $\boldsymbol{v}$ and $\dot{\boldsymbol{v}}$ are bounded, we obtain $\boldsymbol{v}, \dot{\boldsymbol{v}} \in \mathcal{L}_\infty$. Moreover, the boundedness of $\chi \int_0^t \|\boldsymbol{v}(\epsilon)\|^2 . \mathrm{d}\epsilon$ indicates $\boldsymbol{v} \in \mathcal{L}_2$. By applying **Lemma** 3, we conclude that $\boldsymbol{v} \to \boldsymbol{0}_{np}$ as $t \to \infty$. From (5.8) we observe that μ_i is strictly monotonically increasing. Combining this with the fact that $\mu_i(0) \geq 0$ is bounded, we conclude that $\mu_i(t), \forall\, i$ tends to a finite constant value as $t \to \infty$.

Now we turn to prove that $\boldsymbol{u} \to \boldsymbol{0}_{np}$. Due to the difficulty arising from the term $\omega_i(t)$ (which makes the system non-autonomous), and the second-order non-linear dynamics, the proof is more complex than existing proofs for showing convergence to the consensus objective. We discuss the intuition behind the following steps in **Remark** 9 below. Consider firstly $\boldsymbol{e}$ and $\boldsymbol{K}$. By recalling the definitions of $\boldsymbol{e}_i$ and the trigger function f_i, we observe that $\|\boldsymbol{e}\|^2 \leq \beta \|\boldsymbol{v}\|^2 + \bar{\omega}(t), \forall\, t$. We concluded above that $\lim_{t\to\infty} \|\boldsymbol{v}\|, \bar{\omega}(t) = 0$ which implies that $\lim_{t\to\infty} \boldsymbol{e} = \boldsymbol{0}_{np}$. Recalling the definition of $\boldsymbol{K}$ above (5.14), and the fact that $\mu_i, \forall\, i$ tends to a constant value as $t \to \infty$, we conclude that $\lim_{t\to\infty} \boldsymbol{K} = \bar{\boldsymbol{K}}$ where $\bar{\boldsymbol{K}}$ is some finite constant matrix. Rewrite the second equation of (5.14) as

$$\dot{\boldsymbol{v}} = \boldsymbol{f}(t) + \boldsymbol{r}(t) \tag{5.17}$$

where $\boldsymbol{f}(t) = -\boldsymbol{M}(\boldsymbol{q})^{-1}(\mathcal{L}_{22} \otimes \boldsymbol{I}_p)\boldsymbol{u}$ and $\boldsymbol{r}(t) = -\boldsymbol{M}(\boldsymbol{q})^{-1}\big[\boldsymbol{C}(\boldsymbol{q}, \boldsymbol{v})\boldsymbol{v} + \boldsymbol{K}\boldsymbol{v} + \boldsymbol{e}\big]$ are both vector functions. Since $\lim_{t\to\infty} \boldsymbol{v}, \boldsymbol{e} = \boldsymbol{0}_{np}$, $\bar{\boldsymbol{K}}$ is finite, and $\boldsymbol{M}, \boldsymbol{C}$ are bounded according to Properties P2 and P3, it is obvious that $\lim_{t\to\infty} \boldsymbol{r}(t) = \boldsymbol{0}_{np}$. Then by integrating both sides of (5.17) from t to $t + \Delta$, where Δ is a finite positive constant and $t \geq 0$, we obtain

$$\boldsymbol{v}(t + \Delta) - \boldsymbol{v}(t) = \int_t^{t+\Delta} \boldsymbol{f}(s)\mathrm{d}s + \int_t^{t+\Delta} \boldsymbol{r}(s).\mathrm{d}s \tag{5.18}$$

This implies that there holds

$$\left\| \int_t^{t+\Delta} \boldsymbol{f}(s)\mathrm{d}s \right\| \leq \|\boldsymbol{v}(t+\Delta) - \boldsymbol{v}(t)\| + \left\| \int_t^{t+\Delta} \boldsymbol{r}(s)\mathrm{d}s \right\| \tag{5.19}$$

Consider the term $\| \int_t^{t+\Delta} \boldsymbol{f}(s)\mathrm{d}s\|$. By applying **Theorem** 5, we conclude that there holds

$$\left\| \int_t^{t+\Delta} \boldsymbol{f}(s)\mathrm{d}s \right\| \leq \Delta \|\boldsymbol{f}(t+\theta(t))\|$$

where $\theta(t) \in (0, \Delta)$. Subtracting $\Delta\|\boldsymbol{f}(t)\|$ from the both sides of the above inequality yields

$$\left\| \int_t^{t+\Delta} \boldsymbol{f}(s)\mathrm{d}s \right\| - \Delta\|\boldsymbol{f}(t)\| \leq \Delta \left(\|\boldsymbol{f}(t+\theta(t))\| - \|\boldsymbol{f}(t)\| \right)$$

Considering the above right hand side, we observe that $\Delta \left(\|\boldsymbol{f}(t+\theta(t))\| - \|\boldsymbol{f}(t)\| \right) \leq \Delta\|\boldsymbol{f}(t+\theta(t)) - \boldsymbol{f}(t)\| = \Delta\| \int_t^{t+\theta(t)} \dot{\boldsymbol{f}}(s)\mathrm{d}s\|$, which implies that

$$\left\| \int_t^{t+\Delta} \boldsymbol{f}(s)\mathrm{d}s \right\| - \Delta\|\boldsymbol{f}(t)\| \leq \Delta \left\| \int_t^{t+\theta(t)} \dot{\boldsymbol{f}}(s)\mathrm{d}s \right\| \tag{5.20}$$

Note that $\mathrm{d}(\boldsymbol{M}^{-1})/\mathrm{d}t = -\boldsymbol{M}^{-1}\dot{\boldsymbol{M}}\boldsymbol{M}^{-1}$ because $\mathrm{d}(\boldsymbol{M}^{-1}\boldsymbol{M})/\mathrm{d}t = \boldsymbol{M}^{-1}\dot{\boldsymbol{M}} + (\mathrm{d}(\boldsymbol{M}^{-1})/\mathrm{d}t)\boldsymbol{M} = \boldsymbol{0}$. From Properties P3 and P4, we observe that $\lim_{t\to\infty} \|\dot{\boldsymbol{M}}\| \leq 2k_C\|\boldsymbol{v}\| = 0$. Observe that

$$\dot{\boldsymbol{f}} = -\left(\frac{\mathrm{d}(\boldsymbol{M}(\boldsymbol{q})^{-1})}{\mathrm{d}t} (\mathcal{L}_{22} \otimes \boldsymbol{I}_p)\boldsymbol{v} + \boldsymbol{M}(\boldsymbol{q})^{-1}(\mathcal{L}_{22} \otimes \boldsymbol{I}_p)\boldsymbol{v} \right)$$

We proved below (5.16) that $\boldsymbol{u}$ is bounded and $\lim_{t\to\infty} \boldsymbol{v} = \boldsymbol{0}_{np}$. Recall also that $\|\boldsymbol{M}(\boldsymbol{q})^{-1}\|$ is bounded according to Property P2. It follows that $\lim_{t\to\infty} \|\dot{\boldsymbol{f}}\| = 0$ because $\lim_{t\to\infty} \|\boldsymbol{v}\| = 0$. This implies $\| \int_t^{t+\theta(t)} \dot{\boldsymbol{f}}(s)\mathrm{d}s\| = 0$ since $\theta(t) \in (0, \Delta)$ is finite. The inequality (5.20) then implies that $\lim_{t\to\infty} \left\| \int_t^{t+\Delta} \boldsymbol{f}(s)\mathrm{d}s \right\| = \Delta\|\boldsymbol{f}(t)\|$. By substituting this into the left hand side of (5.19), we obtain

$$\Delta\|\boldsymbol{f}(t)\| \leq \|\boldsymbol{v}(t+\Delta) - \boldsymbol{v}(t)\| + \left\| \int_t^{t+\Delta} \boldsymbol{r}(s)\mathrm{d}s \right\| \tag{5.21}$$

as $t \to \infty$. Immediately above (5.18), we showed that $\lim_{t\to\infty} \boldsymbol{r} = \boldsymbol{0}_{np}$. In addition, $\lim_{t\to\infty} \boldsymbol{v} = \boldsymbol{0}_{np}$ and Δ is a positive constant. We conclude that $\lim_{t\to\infty} \|\boldsymbol{v}(t+\Delta) - \boldsymbol{v}(t)\| + \left\| \int_t^{t+\Delta} \boldsymbol{r}(s)\mathrm{d}s \right\| = 0$, which according to (5.21) implies that $\lim_{t\to\infty} \|\boldsymbol{f}(t)\| = 0$. By recalling that $\boldsymbol{f}(t) = -\boldsymbol{M}(\boldsymbol{q})^{-1}(\mathcal{L}_{22} \otimes \boldsymbol{I}_p)\boldsymbol{u}$, we conclude $\lim_{t\to\infty} \boldsymbol{u} = \boldsymbol{0}_{np}$ since both $\boldsymbol{M}(\boldsymbol{q})^{-1}$ and $\mathcal{L}_{22}$ are non-singular. It is obvious that $\lim_{t\to\infty} \boldsymbol{u}, \boldsymbol{v} = \boldsymbol{0}_{np}$ implies the leader-follower objective is asymptotically achieved.

5.4.1.2 Absence of Zeno behaviour

According to **Definition** 1, we can prove that Zeno behaviour does not occur for $t \in [0, b], b < \infty$ by showing that for all $k \geq 0$ there holds $t_{k+1}^i - t_k^i \geq \xi$ where $\xi > 0$ is a strictly positive constant.

Let ξ_i denote the lower bound of the inter-event interval $t_{k+1}^i - t_k^i$ for agent i, i.e. $t_{k+1}^i - t_k^i \geq \xi_i \ , \forall k : t_k^i \in [0, b]$. In this part of the proof, we show that ξ_i is strictly positive for $k < \infty$ and thus no Zeno behaviour can occur. From the definition of $\boldsymbol{e}_i(t)$ in (5.10) and the fact that $\boldsymbol{z}_i(t_k^i)$ is a constant, we observe that the derivative of $\|\boldsymbol{e}_i(t)\|$ with respect to time satisfies

$$\frac{d}{dt}\|\boldsymbol{e}_i(t)\| \leq \|\dot{\boldsymbol{z}}_i(t)\| \tag{5.22}$$

where $\dot{\boldsymbol{z}}_i(t) = \sum_{j=0}^n a_{ij}(\dot{\boldsymbol{q}}_i(t) - \dot{\boldsymbol{q}}_j(t)) + \dot{\mu}_i(t)\dot{\boldsymbol{q}}_i(t) + \mu_i(t)\ddot{\boldsymbol{q}}_i(t),\ i = 1, \ldots, n$. Note that it is straightward to conclude $\dot{\boldsymbol{q}}_i(t), \ddot{\boldsymbol{q}}_i(t), \dot{\mu}_i(t), \mu_i(t)$ are bounded according to the arguments in *Part* 1). This implies $\dot{\boldsymbol{z}}_i(t)$ is bounded. By letting a positive constant B_e represent the upper bound of $\|\dot{\boldsymbol{z}}_i(t)\|$, we obtain

$$\frac{d}{dt}\|\boldsymbol{e}_i(t)\| \leq B_e$$

It follows that

$$\|\boldsymbol{e}_i(t)\| \leq \int_{t_k^i}^t B_e dt = B_e(t - t_k^i) \tag{5.23}$$

for $t \in [t_k^i, t_{k+1}^i)$ and for any k. It is obvious that the next event time t_{k+1}^i is determined both by the changing rate of $\|\boldsymbol{e}_i(t)\|$ and by the value of the comparison term $\beta_i\|\boldsymbol{v}_i(t)\|^2 + \omega_i(t)$ at t_{k+1}^i. Moreover, t_{k+1}^i is the time that

$$\|\boldsymbol{e}_i(t)\|^2 = \beta_i\|\boldsymbol{v}_i(t)\|^2 + \omega_i(t), \quad t > t_k^i \tag{5.24}$$

holds. In *Part* 1) we conclude that global state variable $\boldsymbol{v}(t) \to \boldsymbol{0}_{np}$ as $t \to \infty$ but notice that in the evolution of the system (5.14), the state variable $\boldsymbol{v}_i(t)$ may be equal to $\boldsymbol{0}_p$ instantaneously ($\boldsymbol{v}_i(t)$ is a component of $\boldsymbol{v}(t)$) at t_{k+1}^i. However, this does not imply leader-follower consensus is reached since $\dot{\boldsymbol{v}}_i(t)$ can be non-zero at t_{k+1}^i. We refer to such points in time as "zero-crossing points" for convenience. Here we provide Fig. 5.2 to show the trigger performance at the zero-crossing points of $\boldsymbol{v}_i(t)$ when $\omega_i(t) = 0$. *It is observed that dense trigger behaviour occurs whenever $\boldsymbol{v}_i(t)$ crosses zero. Theoretically, it can be proved that Zeno behaviour takes place at these zero-crossing points. We refer interested readers to [Sun et al., 2016a] with detailed arguments of the Zeno triggering issues at zero-crossing points.*

Now we return to the trigger time interval analysis. By recalling (5.24), we conclude that at t_{k+1}^i, the triggering of the event can only occur for the following two cases:

- Case 1: If $\|\boldsymbol{v}_i(t_{k+1}^i)\| \neq 0$, the equality $\|\boldsymbol{e}_i(t_{k+1}^i)\| = \beta_i\|\boldsymbol{v}_i(t_{k+1}^i)\|^2 + \omega_i(t_{k+1}^i)$ is

satisfied.

- Case 2: If $\|\boldsymbol{v}_i(t^i_{k+1})\| = 0$, the equality $\|\boldsymbol{e}_i(t^i_{k+1})\| = \omega_i(t^i_{k+1})$ is satisfied.

Compare the above two cases, and note that $\|\boldsymbol{v}_i(t^i_{k+1})\| > 0$ for any $\|\boldsymbol{v}_i(t^i_{k+1})\| \neq 0$. By recalling that $\boldsymbol{e}_i(t)$ is equal to zero at t^i_k, it is straightforward to conclude that it takes longer for the quantity $\|\boldsymbol{e}_i(t)\|^2$ to increase to be equal to the quantity $\beta_i\|\boldsymbol{v}_i(t^i_{k+1})\|^2 + \omega_i(t^i_{k+1})$ (i.e. Case 1) than to increase to be equal to the quantity $\omega_i(t^i_{k+1})$ (i.e. Case 2), and thus trigger an event and resetting $\boldsymbol{e}_i(t)$. This implies that $\xi_{Case\,2} < \xi_{Case\,1}$ and proving that there exists a strictly positive $\xi_{Case\,2}$ allows us to draw the conclusion that no Zeno behaviour occurs. According to (5.23), we have

$$B_e\xi_{Case\,2} \geq \omega_i(t) = \exp(-\kappa_i(t^i_k + \xi_{Case\,2}))$$

This implies that the inter-event time $\xi_{Case\,2}$ is lower bounded by the solution $\bar{\xi}_{Case\,2}$ of the following equation

$$B_e\bar{\xi}_{Case\,2} = \exp(-\kappa_i(t^i_k + \bar{\xi}_{Case\,2})) \tag{5.25}$$

The solution is time-dependent and strictly positive for any finite time since B_e is strictly positive and upper bounded. Zeno behaviour is thus excluded for all agents. □

Remark 9. *The reader will have noticed the complexity and length of argument required to go from concluding* $\lim_{t\to\infty}\boldsymbol{v} = \boldsymbol{0}_{np}$ *below* (5.16)*, to concluding* $\lim_{t\to\infty}\boldsymbol{u} = \boldsymbol{0}_{np}$ *below* (5.21)*. The key reason is the combination of second-order non-linear dynamics and the non-autonomous nature of* (5.14) *resulting from the offset term* $\omega_i(t)$ *in* (5.11)*. We now explain the intuition for the steps from* (5.17) *to immediately below* (5.21)*. Between* (5.19) *and* (5.21)*, we use* ***Theorem*** *5 (mean value inequality for vector-valued functions) and the definition of* $\boldsymbol{f}$ *to obtain the key equality* $\lim_{t\to\infty}\left\|\int_t^{t+\Delta}\boldsymbol{f}(s)ds\right\| = \Delta\|\boldsymbol{f}(t)\|$*. This allows us to use* (5.19) *to show a key result:* $\lim_{t\to\infty}\boldsymbol{f} = \boldsymbol{0}_{np}$ *(because we established earlier the both terms on the right of* (5.19) *tend to zero). We then use the definition of* $\boldsymbol{f}$ *to show that* $\boldsymbol{f} = \boldsymbol{0}_{np} \Rightarrow \boldsymbol{u} = \boldsymbol{0}_{np}$*.*

The authors in [Huang et al., 2016] use a similar trigger function with the same offset term, and claim that $\lim_{t\to\infty}\boldsymbol{v} = \boldsymbol{0}_{np}$ *implies that* $\lim_{t\to\infty}\dot{\boldsymbol{v}} = \boldsymbol{0}_{np}$*. This is not correct since the system is non-autonomous. The paper [Li et al., 2015] uses a trigger function without the offset term, and thus they are able to avoid the non-autonomous issue. However, the lack of the offset term can yield Zeno behaviour, something which was not recorded by [Li et al., 2015]. We explore the use of the offset term for avoiding Zeno behaviour in the next section.*

Remark 10. *Unfortunately, we cannot find a constant lower bound for the inter-event time interval (Zeno behaviour in* ***Concept*** *2 cannot be excluded). The lower bound* ξ_{Case2} *found by solving* (5.25) *is time-dependent and tends to zero as* $t \to \infty$*. The avoidance of Zeno behaviour depends on the exponential decay offset completely and the trigger performance when* $t \to \infty$ *is not discussed in the theoretical analysis. However, we note that the state-dependent term in* (5.11) *provides a performance advantage when* $t \to \infty$ *due to its own specific effects and should not be removed. We will provide detail explanations for the advantages of our proposed trigger function* (5.11) *in the following subsection.*

Remark 11. *As with other variable-gain controllers that have monotonically increasing gain, e.g. [Mei et al., 2014; Li et al., 2013; Mei et al., 2016], there is a chance that $\mu_i(t)$ becomes large. This is a fundamental aspect of such controllers, and might be considered a trade-off for being able to design the parameters of the trigger function in a distributed manner. An interesting future work to remedy this problem is to consider an "adaptive σ-modification" algorithm which allows the gain to both increase and decrease, as studied in [Mei et al., 2016, Section III-C].*

5.4.2 Discussions on the choice of trigger functions

In this subsection, we provide discussions regarding the trigger performance of controller (5.9) using the following three trigger functions

- State-dependent trigger function (SDTF)

$$f_i = \|\boldsymbol{e}_i(t)\| - \beta_i\|\boldsymbol{v}_i(t)\| \tag{5.26}$$

- Time-dependent trigger function (TDTF)

$$f_i = \|\boldsymbol{e}_i(t)\| - \kappa_i \exp(-\varepsilon_i t) \tag{5.27}$$

- Mixed trigger function (MTF), which is the proposed (5.11)

$$f_i = \|\boldsymbol{e}_i(t)\|^2 - \beta_i\|\boldsymbol{v}_i(t)\|^2 - \kappa_i \exp(-\varepsilon_i t) \tag{5.28}$$

from both the viewpoints of theoretical analysis and numerical simulations. In doing so, we highlight the advantages of our proposed trigger function (5.11). Note that it is hard, but not impossible, to observe the zero-crossing phenomenon for $\boldsymbol{v}_i(t) \in \mathbb{R}^p, p \geq 2$ (i.e. when $\boldsymbol{v}_i(t) = \boldsymbol{0}_p$ occurs, Zeno behaviour is observed as discussed in the proof of **Theorem** 7 and in [Sun et al., 2016a]). This is because each entry of $\boldsymbol{v}_i(t)$ must be simultaneously equal to 0. For purposes of illustration, in this subsection we therefore simulate using dynamics of a one-arm mechanic manipulator ($\boldsymbol{v}_i(t) \in \mathbb{R}^1$). The dynamics are described by equation 3.5 in [Kelly et al., 2006]. For all simulations presented in this subsection, we set a constant step size in MATLAB to be 0.00005 seconds (the numerical accuracy of the simulation) and the running time to be 30 seconds. In order to compare performance, we require the following two definitions

Definition 4 (Minimum Inter-Event Time for Agent i)**.** *For $j = \{$SDTF,TDTF,MTF$\}$, and for $i = \{1, \ldots, n\}$ define the minimum inter-event time for Agent i Δ_j^i as $\Delta_j^i \triangleq \min_k\{t_{k+1}^i - t_k^i\}$.*

Definition 5 (Infimum Time of Δ_j^i For Agent i)**.** *For $j = \{$SDTF,TDTF,MTF$\}$, and for $i = \{1, \ldots, n\}$, define the "infimum time of Δ_j^i for Agent i" as $t_{\Delta_j^i} \triangleq \inf_{t_k^i} t_k^i : t_{k+2}^i - t_{k+1}^i = t_{k+1}^i - t_k^i = \Delta_j^i, \forall k$.*

In other words, for Agent i, $t_{\Delta_j^i}$ is the infimum of all event times $t_k^i, \forall\, k$ such that the inter-event time between consecutive events $k+1$ and $k+2$ is equal to the minimum inter-event time Δ_j^i. If there are multiple consecutive events (e.g. 10 events) with inter-event time Δ_j^i then we call this a *dense triggering of events*. Note that $\Delta_j^i > 0$ for (5.27) and (5.28) because we can theoretically rule out Zeno behaviour. In these two cases, dense triggering is not Zeno behaviour, but is nevertheless undesirable.

Due to space limitations and the similarity of the proofs, we omit the proofs of convergence of system (5.12) under trigger functions (5.26) and (5.27). **Figures** 5.3 and 5.4 illustrate the controller (5.9) using SDTF (5.26), and TDTF (5.27), respectively. The figures show leader-follower consensus is achieved, the evolutions of comparison terms ($\beta_i\|\boldsymbol{v}_i(t)\|$ in SDTF and $\kappa_i \exp(-\varepsilon_i t)$ in TDTF) and event times. **Fig.** 5.5 shows the performance of controller (5.9) using MTF. We also provide three tables to compare the trigger performance when using SDTF, TDTF and MTF. **Table** 5.1 records the total number of events which occur when using the three different trigger functions. **Table** 5.2 records the minimum inter-event time, Δ_j^i. **Table** 5.3 records the infimum time value, $t_{\Delta_j^i}$, which was defined in **Definition** 5 above.

Note that SDTF and TDTF are widely adopted in event-based multi-agent consensus literature. We hereby review and illustrate the advantages and disadvantages regarding the trigger performance using SDTF and TDTF.

5.4.2.1 SDTF

The papers [Dimarogonas et al., 2012; Fan et al., 2013; Garcia et al., 2013; Hu et al., 2016; Liu et al., 2016d] used SDTF to determine the event times. The disadvantage of using SDTF is that Zeno behaviour can occur when the local state-dependent term crosses zero at a finite time value as indicated in [Sun et al., 2016a] (i.e. in (5.26), the term $v_i(t) = 0$ instantaneously, for $t < \infty$). According to the first column of **Table** 5.2, the minimum inter-event time is $\Delta_{\text{SDTF}}^i = 0.00005$ seconds, for all i, which is equal to the fixed time step of the MATLAB simulations. From the first column of **Table** 5.3 and the second sub-graph of **Fig.** 5.3, we observe that Zeno behaviour occurs at the time instants that $v_i(t)$ crosses 0, which supports the conclusion of [Sun et al., 2016a]. However, according to the arguments in [Dimarogonas et al., 2012; Sun et al., 2016a], if each agent uses SDTF, then at any time t, there exists at least one agent for which the next inter-event interval is strictly positive at any time t. In other words, for all $t \in [0, \infty)$, some agents may exhibit Zeno behaviour, *but at least one agent will have a constant lower bound on its inter-event time.*

5.4.2.2 TDTF

In [Seyboth et al., 2013; Yang et al., 2016; Wei et al., 2017], by using carefully-designed TDTF (typically the decay rate ε_i in (5.27) must be upper bounded), a strictly positive and *constant lower bound* on the inter-event time interval for each agent can be obtained. However, the use of the TDTF has the following two limitations: 1) the applied system has to be exponentially stable, and 2) accurate information (agent's dy-

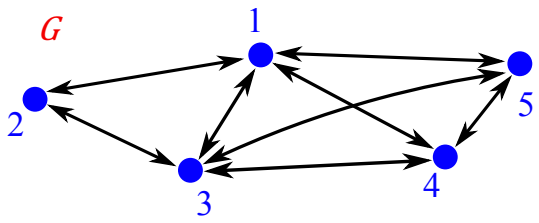

Figure 5.1: Graph topology used in simulations

Table 5.1: Number of events for three different trigger functions

	State-dependent	Time-dependent	Mixed
Agent 1	259	5581	74
Agent 2	184	8106	63
Agent 3	575	2251	168
Agent 4	94	7365	101
Agent 5	438	3845	200
Total	1550	27148	606

Table 5.2: Minimum inter-event time Δ_j^i under three trigger functions

	State-dependent	Time-dependent	Mixed
Agent 1	0.00005	0.00005	0.0388
Agent 2	0.00005	0.00005	0.0235
Agent 3	0.00005	0.00005	0.0010
Agent 4	0.00005	0.00005	0.0037
Agent 5	0.00005	0.00005	0.0006

Table 5.3: The infimum Time of Δ_j, $t_{\Delta_j^i}$ as defined in **Definition** 5

	State-dependent	Time-dependent	Mixed
Agent 1	0.6736	29.8177	18.0246
Agent 2	0.3042	29.6469	2.3991
Agent 3	0.4722	29.8398	14.0583
Agent 4	1.3219	29.6458	1.3182
Agent 5	0.0798	29.9830	15.435

namic model and network topology) is required to design the decay rate of $\exp(-\varepsilon_i t)$. We emphasise that the use of TDTF with arbitrary decay rate for $\exp(-\varepsilon_i t)$ is enough to exclude Zeno behaviour (see the second part of the proof of **Theorem** 7). However, if the decay rate is not selected to be sufficiently slow, the lower bound on the inter-event time cannot be guaranteed to be constant, but instead becomes time de-

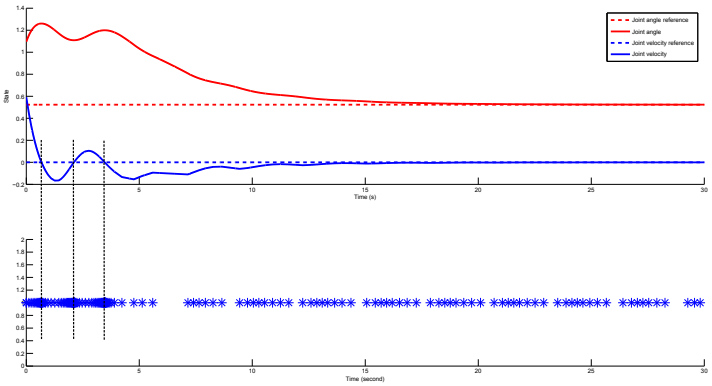

Figure 5.2: Top: the evolutions of the generalized coordinate and velocity of agent 1. Bottom: the trigger event times of agent 1

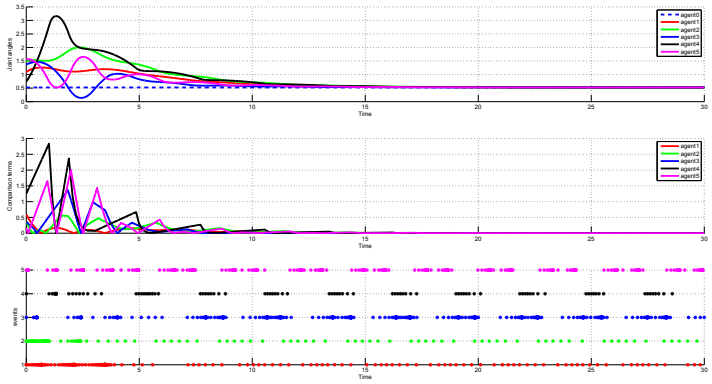

Figure 5.3: Performance of controller (5.9) using SDTF (5.26). We set $\beta_i = 2.4$. From top to bottom: 1) the rendezvous of the generalized coordinates; 2) the evolution of $\beta_i \|v_i(t)\|$; 3) event times for each agent.

pendent. This results in dense triggering behaviour as consensus is almost reached, i.e. multiple events occur in a very short time interval (see **Fig.** 5.4). From the second columns of **Table** 5.2 and **Table** 5.3, it is observed that Δ^i_{TDTF} occurs around $29s$, for all i, which is when the system is close to consensus. Note that dense triggering as $t \to \infty$ is not Zeno behaviour (See **Definition** 1). However, it can be observed from Table 5.1 that unsuitably chosen trigger function parameters will introduce a large amount of events, which is obviously undesirable. This is in contrast to the SDTF, which ensures that a constant lower bound exists on the inter-event time of at least one agent. In other words, a poorly designed TDTF will result in multiple events in sequence with inter-event time equal to Δ^i_{TDTF} when agents near consensus. In comparison SDTF ensures that for $t = [0, \infty)$, there will always be at least one agent whose inter-event time is lower bounded by a positive constant, even as agents near consensus. See **Fig.** 5.4 in comparison to **Fig.** 5.3.

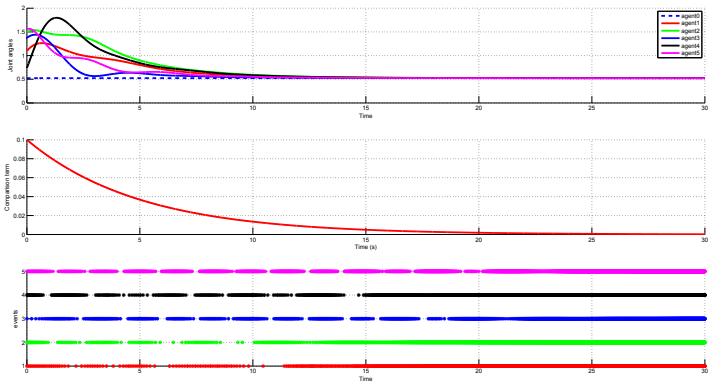

Figure 5.4: Performance of controller (5.9) using TDTF (5.27). We set $\kappa_i \exp(-\varepsilon_i t) = 0.1\exp(-0.2t)$. From top to bottom: 1) the rendezvous of the generalized coordinates; 2) the evolution of $\kappa_i \exp(-\varepsilon_i t)$; 3) event times for each agent.

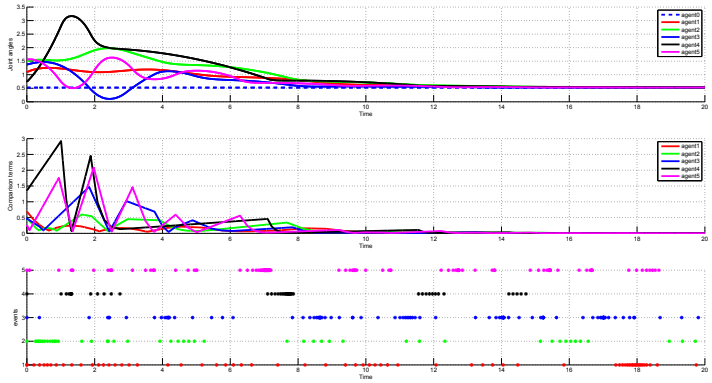

Figure 5.5: Performance of controller (5.9) with MTF (5.28). We set $\beta_i = 2.4$ and $\kappa_i \exp(-\varepsilon_i t) = 0.1\exp(-0.2t)$. From top to bottom: 1) the rendezvous of the generalized coordinates; 2) the evolution of $\beta_i \|v_i(t)\| + \kappa_i \exp(-\varepsilon_i t)$; 3) event times for each agent.

5.4.2.3 MTF

According to **Table** 5.1, it is straightforward to conclude that using MTF shows the best trigger performance with the least number of total events. According to **Table** 5.1, using MTF also shows that the minimum inter-event time, Δ^i_{MTF} is greater than the constant MATLAB step size of 0.00005 seconds, which indicates Zeno behaviour is excluded. These observations reveal that MTF is able to combine the advantages of using SDTF and TDTF separately, i.e., the exclusion of Zeno behaviour in finite time (TDTF) and guarantee that dense triggering does not occur as consensus is reached (SDTF). This can also be observed from **Fig.** 5.5 in comparison to **Fig.** 5.3 and **Fig.** 5.4. We conducted a large number of simulations with arbitrarily chosen $\kappa_i \exp(-\varepsilon_i t)$,

all of which show the above observations. However, a thorough analysis to find a *constant* lower bound on Δ_j^i when using MTF remains an open challenge (we can find a time-dependent bound).

Remark 12. *The intuition behind the MTF is straightforward. The time-dependent term $\kappa_i \exp(-\varepsilon_i t)$ (strictly positive for any $t < \infty$) in the MTF ensures that the error term $\|\boldsymbol{e}_i(t)\|$ will not compare to a zero threshold when the state-dependent term $\boldsymbol{v}_i(t)$ crosses zero, thus avoiding possible Zeno behaviour that may occur using SDTF. Meanwhile, by using numerical simulation examples, it is observed that using SDTF shows better trigger performance near consensus. Although theoretical explanations about this cannot be provided at this stage, simulations show that using MTF combines the benefits of separately using SDTF and TDTF.*

Note that it is not guaranteed that using MTF will always result in better trigger performance (larger Δ_i^j and fewer trigger events) compared to using SDTF or TDTF. For example, it is possible that $\boldsymbol{v}_i(t)$ does not cross zero at any $t < \infty$, depending on the initial conditions and network dynamics. In this case, Zeno behaviour will not occur even when using SDTF. Another example is that using a well-designed TDTF (suitably chosen decay rate ε_i based on accurate model knowledge) may also have better trigger performance than using MTF. Nevertheless, zero-crossing phenomenon cannot always be avoided when using SDTF and it is difficult to find a suitable TDTF in our proposed controller. In general, using MTF is the most suitable way for all three proposed event-triggered controllers.

Remark 13. *The work [Zhu and Jiang, 2015; Wang et al., 2017b] also use MTF. However, the authors design the evolution speeds of the exponential functions using exact knowledge of agent dynamic models and the graph topology. The effects of adding state-dependent terms to the trigger functions were not well-addressed by the authors of [Zhu and Jiang, 2015; Wang et al., 2017b].*

5.5 Fixed gain, model-independent algorithm

In this section, we propose and analyse a distributed event-triggered algorithm for a directed network where each fully-actuated agent has self-dynamics described by the Euler-Lagrange equation (5.7). For design of the control laws, the following assumption is required.

Assumption 2 (Limited Use of Centralised Design)**.** *Three parameters in the algorithm in this Section must be designed to exceed several lower bounding inequalities. These inequalities require knowledge of the constants $k_{\underline{m}}, k_{\overline{M}}, k_C$ defined in the properties P2 and P3 and the matrices $\boldsymbol{Q}$, $\mathcal{L}_{22}$ and $\boldsymbol{\Gamma}$ as defined in Lemma 7. We therefore assume these constants are known to the designer.*

Let the triggering time sequence of agent i be $t_0^i, t_1^i, \ldots, t_k^i, \ldots$ with $t_0^i := 0$. Consider a model-independent, event-triggered algorithm for the i^{th} follower agent of

the form

$$\boldsymbol{\tau}_i(t) = -\sum_{j\in\mathcal{N}_i} a_{ij}\Big((\boldsymbol{q}_i(t_k^i) - \boldsymbol{q}_j(t_k^i)) + \mu(\dot{\boldsymbol{q}}_i(t_k^i) - \dot{\boldsymbol{q}}_j(t_k^i))\Big)$$
$$t \in [t_k^i, t_{k+1}^i) \tag{5.29}$$

where a_{ij} is the weighted (i,j) entry of the adjacency matrix $\mathcal{A}$ associated with the weighted directed graph $\mathcal{G}$. The control gain scalar $\mu > 0$ is universal to all agents. To ensure the control objective is achieved, μ must be designed to satisfy several inequalities, which will be detailed below. Note that if the leader is a neighbour of agent i then for $j = 0$ we have $\mu(\dot{\boldsymbol{q}}_i(t_k^i) - \dot{\boldsymbol{q}}_0(t_k^i)) = \mu(\dot{\boldsymbol{q}}_i(t_k^i))$, which is simply a damping term.

Define a new variable

$$\boldsymbol{z}_i(t) = \sum_{j\in\mathcal{N}_i} a_{ij}\Big((\boldsymbol{q}_i(t) - \boldsymbol{q}_j(t)) + \mu(\dot{\boldsymbol{q}}_i(t) - \dot{\boldsymbol{q}}_j(t))\Big)$$

We define a state mismatch for agent i between consecutive event times t_k^i and t_{k+1}^i as follows:

$$\boldsymbol{e}_i(t) = \boldsymbol{z}_i(t_k^i) - \boldsymbol{z}_i(t) \tag{5.30}$$

for $t \in [t_k^i, t_{k+1}^i)$.

The trigger function is proposed as follows:

$$f_i(t) = \|\boldsymbol{e}_i(t)\|^2 - \mu^{-2}{\beta_1}^2\|\sum_{j\in\mathcal{N}_i} a_{ij}(\boldsymbol{q}_i(t) - \boldsymbol{q}_j(t))\|^2$$
$$- {\beta_2}^2\|\sum_{j\in\mathcal{N}_i} a_{ij}(\boldsymbol{v}_i(t) - \boldsymbol{v}_j(t))\|^2 - \omega_i(t) \tag{5.31}$$

where $\omega_i(t) = a_i\exp(-\kappa_i t)$ with $a_i, \kappa_i > 0$. The parameters β_1 and β_2 are to be determined in the sequel. The k-th event for agent i is triggered as soon as the trigger condition $f_i(t) = 0$ is fulfilled at $t = t_k^i$. For $t \in [t_k^i, t_{k+1}^i)$, the control input is $\tau_i(t) = \tau_i(t_k^i)$; the control input is updated when the next event is triggered. Furthermore, every time an event is triggered, and in accordance with their definitions, the state mismatch $\boldsymbol{e}_i(t)$ is reset to be equal to zero and thus the trigger function assumes a negative value. One can immediately observe that for all t

$$\|\boldsymbol{e}_i(t)\|^2 \le \mu^{-2}{\beta_1}^2\|\sum_{j\in\mathcal{N}_i} a_{ij}(\boldsymbol{q}_i(t) - \boldsymbol{q}_j(t))\|^2$$
$$+ {\beta_2}^2\|\sum_{j\in\mathcal{N}_i} a_{ij}(\boldsymbol{v}_i(t) + \boldsymbol{v}_j(t))\|^2 + \omega_i(t)$$

and note that $\sum_{j\in\mathcal{N}_i} a_{ij}(\boldsymbol{q}_i(t) - \boldsymbol{q}_j(t)) = \sum_{j\in\mathcal{N}_i} a_{ij}[(\boldsymbol{q}_i(t) - \boldsymbol{q}_0) - (\boldsymbol{q}_j(t) - \boldsymbol{q}_0)] = \boldsymbol{l}_i^\top\boldsymbol{u}$ where $\boldsymbol{l}_i^\top$ is the i-th row of $\mathcal{L}_{22}$. Likewise, $\sum_{j\in\mathcal{N}_i} a_{ij}(\boldsymbol{v}_i(t) - \boldsymbol{v}_j(t)) = \boldsymbol{l}_i^\top\boldsymbol{v}$. The stacked

column vector $\boldsymbol{e} = [\boldsymbol{e}_1^\top, \ldots, \boldsymbol{e}_n^\top]^\top$ then has the following property

$$\begin{aligned}\|\boldsymbol{e}\|^2 &= \sum_{i=1}^{n} \|\boldsymbol{e}_i(t)\|^2 \\ &\leq \sum_{i=1}^{n} \left(\mu^{-2}{\beta_1}^2 \|\boldsymbol{l}_i^\top \boldsymbol{u}\|^2 + {\beta_2}^2 \|\boldsymbol{l}_i^\top \boldsymbol{v}\|^2 + \omega_i(t)\right)\end{aligned} \tag{5.32}$$

It is straightforward to verify that $\sum_{i=1}^{n} \|\boldsymbol{l}_i^\top \boldsymbol{u}\|^2 = \|\mathcal{L}_{22}\boldsymbol{u}\|^2$, and $\sum_{i=1}^{n} \|\boldsymbol{l}_i^\top \boldsymbol{v}\|^2 = \|\mathcal{L}_{22}\boldsymbol{v}\|^2$. It then follows that

$$\|\boldsymbol{e}\|^2 \leq \mu^{-2}{\beta_1}^2 \|\mathcal{L}_{22}\boldsymbol{u}\|^2 + {\beta_2}^2 \|\mathcal{L}_{22}\boldsymbol{v}\|^2 + \bar{\omega}(t)^2 \tag{5.33}$$

$$\|\boldsymbol{e}\| \leq \mu^{-1}\beta_1 \|\mathcal{L}_{22}\| \|\boldsymbol{u}\| + \beta_2 \|\mathcal{L}_{22}\| \|\boldsymbol{v}\| + \bar{\omega}(t) \tag{5.34}$$

where $\bar{\omega}(t) = (\sum_{i=1}^{n} \omega_i(t))^{\frac{1}{2}}$

It is obvious that

$$\boldsymbol{\tau}_i(t) = \boldsymbol{z}_i(t) + \boldsymbol{e}_i(t)$$

Applying control law (5.29) to each agent we can express the networked system using the new variables $\boldsymbol{u}, \boldsymbol{v}$ as below

$$\boldsymbol{M}(\boldsymbol{q})\dot{\boldsymbol{v}} + \boldsymbol{C}(\boldsymbol{q}, \boldsymbol{v})\boldsymbol{v} + (\mathcal{L}_{22} \otimes \boldsymbol{I}_p)(\boldsymbol{u} + \mu\boldsymbol{v}) + \boldsymbol{e} = \boldsymbol{0} \tag{5.35}$$

and expressed as the non-autonomous system

$$\begin{aligned}\dot{\boldsymbol{u}} &= \boldsymbol{v} \\ \dot{\boldsymbol{v}} &= -\boldsymbol{M}(\boldsymbol{q})^{-1}\left[\boldsymbol{C}(\boldsymbol{q}, \boldsymbol{v})\boldsymbol{v} + (\mathcal{L}_{22} \otimes \boldsymbol{I}_p)(\boldsymbol{u} + \mu\boldsymbol{v}) + \boldsymbol{e}\right]\end{aligned} \tag{5.36}$$

By using arguments like those of usual Lyapunov theory, we will be able to prove the stability of (5.36). Before we present the main theorem of this section, we state a mild assumption used *only in this Section*.

Assumption 3. *All possible initial conditions lie in some fixed but arbitrarily large set, which is known a priori. In particular,* $\|\boldsymbol{u}_i(0)\| \leq k_a/\sqrt{n}$ *and* $\|\boldsymbol{v}_i(0)\| \leq k_b/\sqrt{n}$*, where* k_a, k_b *are known a priori.*

This assumption is entirely reasonable; many Euler-Lagrange systems will have an expected operating range for $\boldsymbol{q}$ and $\dot{\boldsymbol{q}}$.

Theorem 8. *Suppose that each follower agent with dynamics* (5.7)*, under Assumption 1, employs the controller* (5.29) *with trigger function* (5.31)*. Suppose further that the directed graph* $\mathcal{G}$ *contains a directed spanning tree, with the leader agent* 0 *as the root node (and thus with no incoming edges). Then there exists a sufficiently large* μ*, and sufficiently small* β_1, β_2 *which ensures that the leader-follower consensus objective is achieved semi-globally exponentially fast.*

Proof. Before we present the main proof of **Theorem** 8, we need to compute an upper bound using limited information about the initial conditions.

5.5.1 An upper bound using initial conditions

Suppose that initial conditions are bounded as $\|\boldsymbol{u}(0)\| \leq k_a$ and $\|\boldsymbol{v}(0)\| \leq k_b$ with k_a, k_b known a priori. Before we proceed with the main proof, we provide a method to calculate a non-tight upper bound on the initial states expressed as $\|\boldsymbol{u}(0)\| < \mathcal{X}$ and $\|\boldsymbol{v}(0)\| < \mathcal{Y}$, with the property that as shown in the sequel, there holds $\|\boldsymbol{u}(t)\| < \mathcal{X}$ and $\|\boldsymbol{v}(t)\| < \mathcal{Y}$ for all $t \geq 0$, and exponential convergence results. Due to spatial limitations, we show only the bound on $\boldsymbol{v}$ and leave the reader to follow an identical process for $\boldsymbol{u}$. In keeping with the model-independent nature, define a function as

$$\bar{V}_\mu = \begin{bmatrix} \boldsymbol{u} \\ \boldsymbol{v} \end{bmatrix}^\top \begin{bmatrix} \lambda_{\max}(\boldsymbol{Q})\boldsymbol{I}_{np} & \frac{1}{2}\mu^{-1}\bar{\gamma}(k_{\overline{M}}+\delta)\boldsymbol{I}_{np} \\ \frac{1}{2}\mu^{-1}\bar{\gamma}(k_{\overline{M}}+\delta)\boldsymbol{I}_{np} & \frac{1}{2}\bar{\gamma}(k_{\overline{M}}+\delta)\boldsymbol{I}_{np} \end{bmatrix} \begin{bmatrix} \boldsymbol{u} \\ \boldsymbol{v} \end{bmatrix} \tag{5.37}$$

where $\boldsymbol{Q} = \boldsymbol{\Gamma}\mathcal{L}_{22} + \mathcal{L}_{22}^\top\boldsymbol{\Gamma}$, $\underline{\gamma} = \min_i \gamma_i$ and $\bar{\gamma} = \max_i \gamma_i$. Here, γ_i are the diagonal entries of $\boldsymbol{\Gamma}_p$. The constant $\delta > 0$ is arbitrarily small and fixed. Note that $(k_{\overline{M}} + \delta)\boldsymbol{I}_{np} > \boldsymbol{M}$ and that $\bar{V}_\mu$ is *not* a Lyapunov function. Let the matrix in (5.37) be $\boldsymbol{L}_\mu$. Then according to **Theorem** 6, $\boldsymbol{L}_\mu > 0$ if and only if $\lambda_{\max}(\boldsymbol{Q})\boldsymbol{I}_{np} - \frac{1}{2}\mu^{-2}\bar{\gamma}(k_{\overline{M}} + \delta)\boldsymbol{I}_{np} > 0$ which is implied by $\lambda_{\max}(\boldsymbol{Q}) - \frac{1}{2}\mu^{-2}\bar{\gamma}(k_{\overline{M}} + \delta) > 0$. Then $\boldsymbol{L}_\mu > 0$ for any $\mu \geq \mu_1^*$ where

$$\mu_1^* > \sqrt{\frac{\bar{\gamma}(k_{\overline{M}} + \delta)}{2\lambda_{\max}(\boldsymbol{Q})}}$$

While $\bar{V}_\mu$ is a function of $\boldsymbol{u}(t)$ and $\boldsymbol{v}(t)$, we use $\bar{V}_\mu(t)$ to denote $\bar{V}_\mu(\boldsymbol{u}(t), \boldsymbol{v}(t))$. Lastly, observe that

$$\begin{aligned} \bar{V}_\mu \leq \lambda_{\max}(\boldsymbol{Q})\|\boldsymbol{u}\|^2 + \frac{1}{2}\bar{\gamma}(k_{\overline{M}} + \delta)\|\boldsymbol{v}\|^2 \\ + \mu^{-1}\bar{\gamma}(k_{\overline{M}} + \delta)\|\boldsymbol{u}\|\|\boldsymbol{v}\| \end{aligned}$$

Next, let

$$\underline{V}_\mu = \begin{bmatrix} \boldsymbol{u} \\ \boldsymbol{v} \end{bmatrix}^\top \begin{bmatrix} \frac{1}{4}\lambda_{\min}(\boldsymbol{Q})\boldsymbol{I}_{np} & \frac{1}{2}\mu^{-1}\underline{\gamma}(k_{\underline{m}}-\delta)\boldsymbol{I}_{np} \\ \frac{1}{2}\mu^{-1}\underline{\gamma}(k_{\underline{m}}-\delta)\boldsymbol{I}_{np} & \frac{1}{2}\underline{\gamma}(k_{\underline{m}}-\delta)\boldsymbol{I}_{np} \end{bmatrix} \begin{bmatrix} \boldsymbol{u} \\ \boldsymbol{v} \end{bmatrix} \tag{5.38}$$

Call the matrix in (5.38) $\boldsymbol{N}_\mu$. Let the arbitrarily small δ be such that $(k_{\underline{m}} - \delta) > 0$. Analysis using **Theorem** 6, similar to above, is used to conclude that $\boldsymbol{N}_\mu > 0$ for any $\mu \geq \mu_2^*$ where

$$\mu_2^* > \sqrt{\frac{2\underline{\gamma}(k_{\underline{m}} - \delta)}{\lambda_{\min}(\boldsymbol{Q})}}$$

Set $\mu_3^* = \max\{\mu_1^*, \mu_2^*\}$. Define

$$\rho_1(\mu) = \frac{1}{2}(k_{\overline{M}} + \delta) - \frac{1}{4}\mu^{-2}(k_{\overline{M}} + \delta)^2\lambda_{\max}(\boldsymbol{Q})^{-1}$$
$$\rho_2(\mu) = \frac{1}{2}(k_{\underline{m}} - \delta) - \mu^{-2}(k_{\underline{m}} - \delta)^2\lambda_{\min}(\boldsymbol{Q})^{-1}$$
$$\rho_3(\mu) = \frac{1}{2}(k_{\underline{m}} - \delta) - \frac{1}{2}\mu^{-2}(k_{\overline{M}})^2\|\boldsymbol{Q}^{-1}\|$$

and observe that for sufficiently large μ there holds $\rho_1 \geq \rho_3 > \rho_2$. Assume without loss of generality that $\rho_1 \geq \rho_3 > \rho_2$ (if not, one can always replace μ_3^* by a μ_4^* with $\mu_4^* > \mu_3^*$, and such that $\rho_1 \geq \rho_3 > \rho_2$). Note that for any $\mu \geq \mu_3^*$ there holds $\rho_i(\mu_3^*) \leq \rho_i(\mu), i = 1, 2$. Compute now

$$\bar{V}^* = \lambda_{\max}(\boldsymbol{Q})k_a^2 + \frac{1}{2}\bar{\gamma}(k_{\overline{M}} + \delta)k_b^2 + \mu_3^{*-1}\bar{\gamma}(k_{\overline{M}} + \delta)k_a k_b$$

One can verify that for any $\mu \geq \mu_3^*$ that $\bar{V}_\mu(0) \leq \bar{V}^*$. It follows from **Lemma** 4 and (5.2b) that

$$\|\boldsymbol{v}(0)\|_2 \leq \sqrt{\frac{\bar{V}_\mu(0)}{\rho_1(\mu)}} \leq \sqrt{\frac{\bar{V}_\mu(0)}{\rho_1(\mu_3^*)}} < \sqrt{\frac{\bar{V}^*}{\rho_2(\mu_3^*)}} := \mathcal{Y}_1 \tag{5.39}$$

Follow a similar method to obtain $\mathcal{X}_1$. Next, compute

$$\widehat{V}^* = \lambda_{\max}(\boldsymbol{Q})\mathcal{X}_1{}^2 + \frac{1}{2}\bar{\gamma}(k_{\overline{M}} + \delta)\mathcal{Y}_1{}^2 + \mu_3^{*-1}\bar{\gamma}(k_{\overline{M}} + \delta)\mathcal{X}_1\mathcal{Y}_1$$

Finally, compute the bound $\mathcal{Y} = \sqrt{\widehat{V}^*/\rho_2(\mu_3^*)}$, and note that $\bar{V}_{\mu_3^*} \leq \widehat{V}^*$. Note also that $\bar{V}_\mu, \bar{V}^*, \rho_2(\mu_3^*)$ are independent of μ. Thus $\|\boldsymbol{v}(0)\|_2 < \mathcal{Y}$ (and similarly $\|\boldsymbol{u}(0)\|_2 < \mathcal{X}$) can be used for all $\mu \geq \mu_3^*$. We now proceed to the proof of **Theorem** 8.

5.5.2 Main proof

We divide the proof into three parts.

Part 1: Consider the Lyapunov-like candidate function

$$V = \frac{1}{2}\boldsymbol{u}^\top\boldsymbol{Q}\boldsymbol{u} + \frac{1}{2}\boldsymbol{v}^\top\boldsymbol{\Gamma}_p\boldsymbol{M}\boldsymbol{v} + \mu^{-1}\boldsymbol{u}^\top\boldsymbol{\Gamma}_p\boldsymbol{M}\boldsymbol{v} \tag{5.40}$$

where $\boldsymbol{\Gamma}_p = \boldsymbol{\Gamma} \otimes \boldsymbol{I}_p$. It may also be expressed as a quadratic in the variables $\boldsymbol{u}$ and $\boldsymbol{v}$

$$V = \begin{bmatrix}\boldsymbol{u}\\ \boldsymbol{v}\end{bmatrix}^\top \begin{bmatrix}\frac{1}{2}\boldsymbol{Q} & \frac{1}{2}\mu^{-1}\boldsymbol{\Gamma}_p\boldsymbol{M}\\ \frac{1}{2}\mu^{-1}\boldsymbol{\Gamma}_p\boldsymbol{M} & \frac{1}{2}\boldsymbol{\Gamma}_p\boldsymbol{M}\end{bmatrix}\begin{bmatrix}\boldsymbol{u}\\ \boldsymbol{v}\end{bmatrix} \tag{5.41}$$

Theorem 6 is used to conclude that V is positive definite if

$$\frac{1}{2}\boldsymbol{Q} - \frac{1}{2}\mu^{-2}\boldsymbol{\Gamma}_p\boldsymbol{M} > 0 \tag{5.42}$$

which is implied by

$$\lambda_{\min}(\boldsymbol{Q}) - \mu^{-2}\bar{\gamma}\lambda_{\max}(\boldsymbol{M}) > 0 \tag{5.43}$$

Observe that (5.43) is implied by

$$\mu > \sqrt{\frac{\bar{\gamma}k_{\overline{M}}}{\lambda_{\min}(\boldsymbol{Q})}} \tag{5.44}$$

because there holds $\lambda_{\max}(\boldsymbol{M}) \leq k_{\overline{M}}$. Since $\lambda_{\min}(\boldsymbol{Q}) > 0$ then there can always be found a $\mu > 0$ which satisfies (5.44). Define μ_5^* such that μ_5^* satisfies (5.44) and $\mu_5^* \geq \mu_3^*$. Therefore V is positive definite in $\boldsymbol{u}$ and $\boldsymbol{v}$ for all $\mu \geq \mu_5^*$. Denote the matrix in (5.41) as $\boldsymbol{G}$. Following the method outlined in the appendix of **?**, it is straightforward to show that $V(t) < \bar{V}_\mu(t)$ for all t because $\boldsymbol{L}_\mu > \boldsymbol{G} > \boldsymbol{N}_\mu$ for all $\mu \geq \mu_5^*$. Lastly, observe that

$$\begin{aligned} V(t) \leq \frac{1}{2}\lambda_{\max}(\boldsymbol{Q})\|\boldsymbol{u}(t)\|^2 + \frac{1}{2}\bar{\gamma}k_{\overline{M}}\|\boldsymbol{v}(t)\|^2 \\ + \mu^{-1}\bar{\gamma}k_{\overline{M}}\|\boldsymbol{u}(t)\|\|\boldsymbol{v}(t)\| \end{aligned} \tag{5.45}$$

Taking the derivative of V with respect to time along the trajectories of the system (5.36), we have

$$\begin{aligned} \dot{V} &= \boldsymbol{u}^\top \boldsymbol{Q}\boldsymbol{v} + \boldsymbol{v}^\top \boldsymbol{\Gamma}_p \boldsymbol{M}\dot{\boldsymbol{v}} + \frac{1}{2}\boldsymbol{v}^\top \boldsymbol{\Gamma}_p \dot{\boldsymbol{M}}\boldsymbol{v} \\ &\quad + \mu^{-1}\boldsymbol{v}^\top \boldsymbol{\Gamma}_p \boldsymbol{M}\boldsymbol{v} + \mu^{-1}\boldsymbol{u}^\top \boldsymbol{\Gamma}_p \dot{\boldsymbol{M}}\boldsymbol{v} + \mu^{-1}\boldsymbol{u}^\top \boldsymbol{\Gamma}_p \boldsymbol{M}\dot{\boldsymbol{v}} \qquad (5.46) \\ &= -\frac{1}{2}\mu\boldsymbol{v}^\top \boldsymbol{Q}\boldsymbol{v} - \frac{1}{2}\mu^{-1}\boldsymbol{u}^\top \boldsymbol{Q}\boldsymbol{u} + \mu^{-1}\boldsymbol{v}^\top \boldsymbol{\Gamma}_p \boldsymbol{M}\boldsymbol{v} \\ &\quad + \mu^{-1}\boldsymbol{u}^\top \boldsymbol{\Gamma}_p \boldsymbol{C}^\top \boldsymbol{v} - \boldsymbol{v}^\top \boldsymbol{\Gamma}_p \boldsymbol{e} - \mu^{-1}\boldsymbol{u}^\top \boldsymbol{\Gamma}_p \boldsymbol{e} \qquad (5.47) \end{aligned}$$

We obtain (5.47) by substituting in $\boldsymbol{M}\dot{\boldsymbol{v}}$ from (5.35) noting that $\dot{\boldsymbol{M}} - 2\boldsymbol{C}$ is skew-symmetric, or equivalently $\dot{\boldsymbol{M}} = \boldsymbol{C} + \boldsymbol{C}^\top$. Using the properties of the Euler-Lagrange system (P1 to P5), the following upper bound on $\dot{V}$ is obtained.

$$\begin{aligned} \dot{V} \leq -(\frac{1}{2}\mu\lambda_{\min}(\boldsymbol{Q}) - \mu^{-1}k_{\overline{M}}\bar{\gamma})\|\boldsymbol{v}\|^2 - \frac{1}{2}\mu^{-1}\lambda_{\min}(\boldsymbol{Q})\|\boldsymbol{u}\|^2 \\ + \mu^{-1}k_C\bar{\gamma}\|\boldsymbol{v}\|^2\|\boldsymbol{u}\| + \bar{\gamma}\|\boldsymbol{v}\|\|\boldsymbol{e}\| + \mu^{-1}\bar{\gamma}\|\boldsymbol{u}\|\|\boldsymbol{e}\| \end{aligned} \tag{5.48}$$

Using the bound on $\|\boldsymbol{e}\|$ computed in (5.34), we then evaluate (5.48) to be

$$\begin{aligned}\dot{V} &\leq -(\frac{1}{2}\mu\lambda_{\min}(\boldsymbol{Q}) - \mu^{-1}k_{\overline{M}}\bar{\gamma})\|\boldsymbol{v}\|^2 - \frac{1}{2}\mu^{-1}\lambda_{\min}(\boldsymbol{Q})\|\boldsymbol{u}\|^2 \\ &\quad + \mu^{-1}k_C\bar{\gamma}\|\boldsymbol{v}\|^2\|\boldsymbol{u}\| + \mu^{-1}\beta_1\bar{\gamma}\|\mathcal{L}_{22}\|\|\boldsymbol{u}\|\|\boldsymbol{v}\| \\ &\quad + \beta_2\bar{\gamma}\|\mathcal{L}_{22}\|\|\boldsymbol{v}\|^2 + \mu^{-2}\beta_1\bar{\gamma}\|\mathcal{L}_{22}\|\|\boldsymbol{u}\|^2 \\ &\quad + \mu^{-1}\beta_2\bar{\gamma}\|\mathcal{L}_{22}\|\|\boldsymbol{u}\|\|\boldsymbol{v}\| + \mu^{-1}\bar{\omega}(t)\bar{\gamma}\|\boldsymbol{u}\| + \bar{\omega}(t)\bar{\gamma}\|\boldsymbol{v}\| \qquad (5.49) \\ &= -\mu^{-1}\Bigg[A_1\|\boldsymbol{u}\|^2 + A_2\|\boldsymbol{v}\|^2 - A_3\|\boldsymbol{v}\|^2\|\boldsymbol{u}\| - A_4\|\boldsymbol{v}\|\|\boldsymbol{u}\| \\ &\quad - A_5\|\boldsymbol{u}\| - A_6\|\boldsymbol{v}\|\Bigg] := -\mu^{-1}p(\|\boldsymbol{u}\|, \|\boldsymbol{v}\|) \qquad (5.50)\end{aligned}$$

where $A_1(\mu) = \lambda_{\min}(\boldsymbol{Q})/2 - \mu^{-1}\bar{\gamma}\beta_1\|\mathcal{L}_{22}\|$, $A_2(\mu) = \mu^2\lambda_{\min}(\boldsymbol{Q})/2 - \bar{\gamma}(k_{\overline{M}} + \mu\beta_2)$, $A_3 = k_C\bar{\gamma}$, $A_4 = \|\boldsymbol{\Gamma}\mathcal{L}_{22}\|\bar{\gamma}(\beta_1 + \beta_2)$, $A_5(t) = \bar{\gamma}\bar{\omega}(t)$, and $A_6(\mu, t) = \mu\bar{\gamma}\bar{\omega}(t)$. By designing β_1 such that

$$\beta_1 < \frac{\mu_5^*\lambda_{\min}(\boldsymbol{Q})}{2\bar{\gamma}\|\mathcal{L}_{22}\|}$$

then $A_1(\mu) > 0$ for any $\mu \geq \mu_5^*$. Observe that $A_2(\mu_5^*) > 0$ if $(\mu_5^*)^2\lambda_{\min}(\boldsymbol{Q})/2 - \gamma k_{\overline{M}} - \mu_5^*\beta_2 > 0$. Rearranging for β_2, this is implied by

$$\beta_2 < \frac{\mu_5^*\lambda_{\min}(\boldsymbol{Q})}{2} - \frac{\bar{\gamma}k_{\overline{M}}}{\mu_5^*} \qquad (5.51)$$

and note that any β_2 satisfying (5.51) continues to satisfy (5.51) for any $\mu \geq \mu_5^*$. If the right hand side of (5.51) is negative, it is still possible to ensure that $A_2(\mu_5^*) > 0$ by increasing the size of μ_5^* and setting β_2 sufficiently small because the coefficient of μ^2 in A_2 is positive. Lastly, observe that as $\mu \to \infty$ then $A_1(\mu) \to \lambda_{\min}(\boldsymbol{Q})/2$, $A_2(\mu) = \mathcal{O}(\mu^2)$ and $A_6(\mu) = \mathcal{O}(\mu)$. Notice that $\bar{\omega}(t)$ decays to 0 exponentially fast. In other words, the coefficients $A_5(t)$ and $A_6(\mu, t)$ decay to zero exponentially fast.

Part 2: We now show that the trajectories of the system are bounded for all time by carefully designing μ. For *Part 2* and *Part 3* of the proof, a diagram is included in **Fig.** 5.6 to aid in the explanation of the proof. Notice that $p(\|\boldsymbol{u}\|, \|\boldsymbol{v}\|)$ in (5.50) is of the same form as $h(x, y)$ in **Corollary** 1 with $\|\boldsymbol{u}\| = x$, $\|\boldsymbol{v}\| = y$ and $A_1(\mu) = a$, $A_2(\mu) = b$, $A_3 = c$, $A_4 = d$, $A_5(0) = e$ and $A_6(\mu, 0) = f$. Note that $A_5(t_1) > A_5(t_2)$ and $A_6(\mu, t_1) > A_6(\mu, t_2)$ for any $t_1 < t_2$. Because of this, we proceed using $A_5(0), A_6(\mu, 0)$: any $A_2(\mu)$ satisfying the inequalities on b in **Corollary** 1 for $t = 0$ will continue to satisfy the inequalities for $t > 0$. This will be come clear in the sequel. We now use the values $\mathcal{X}, \mathcal{Y}$ computed in **Subsection** 5.5.1. Choose $\vartheta_0 > \mathcal{X} - \mathcal{X}_1$ and $\varphi_0 > \mathcal{Y} - \mathcal{Y}_1$, and ensure that $\mathcal{X} - \vartheta_0, \mathcal{Y} - \varphi_0 > 0$. Note the fact that $\mathcal{X} \geq \mathcal{X}_1$ and $\mathcal{Y} \geq \mathcal{Y}_1$ implies $\vartheta_0, \varphi_0 > 0$. We assume without loss of generality that $\mathcal{X}$ found in **Section** 5.5.1 is such that $\mathcal{X} - \vartheta_0 > A_5(0)/A_1(\mu)$. If this inequality were not satisfied, one would replace $\mathcal{X}$ by a $\bar{\mathcal{X}} > \mathcal{X}$ such that $\bar{\mathcal{X}} - \vartheta_0 > e/a$ and proceed

with the stability proof using $\bar{\mathcal{X}}$.

Define the sets $\mathcal{U}, \mathcal{V}$ and the region $\mathcal{R}$ as in **Corollary** 1 with $\|\boldsymbol{u}\| = x$, $\|\boldsymbol{v}\| = y$. Define further the sets $\bar{\mathcal{U}} = \{\|\boldsymbol{u}\| : \|\boldsymbol{u}\| > \mathcal{X}\}$ and $\bar{\mathcal{V}} = \{\|\boldsymbol{v}\| : \|\boldsymbol{v}\| > \mathcal{X}\}$. Define the compact region $\mathcal{S} = \mathcal{U} \cup \mathcal{V} \backslash \bar{\mathcal{U}} \cup \bar{\mathcal{V}}$ (refer to Fig. 5.6 for details). Since $\mathcal{S} \subset \mathcal{R}$, there exists a $\mu_6^* \geq \mu_5^*$ such that $A_2(\mu_6^*)$ satisfies the requirement on b in **Corollary** 1, which ensures that $p(\|\boldsymbol{u}\|, \|\boldsymbol{v}\|) > 0$. This in turn implies that $\dot{V} < 0$ in $\mathcal{S}$. Lastly, define the region $\|\boldsymbol{u}(t)\| \in [0, \mathcal{X} - \vartheta_0)$ and $\|\boldsymbol{v}(t)\| \in [0, \mathcal{Y} - \varphi_0)$ as $\mathcal{T}$. In this part of the proof, we are trying to show that the trajectories of (5.36) remain bounded for all time. For purposes of explanation, we therefore temporarily assume that $\mathcal{S}$ and $\mathcal{T}$ are time-invariant, as opposed to **Fig.** 5.6. In the latter *Part 3*, we will discuss the time-varying nature of $\mathcal{S}(t)$ and $\mathcal{T}(t)$ and show that the boundedness arguments developed here continue to hold.

We are now ready to show that the trajectory of the system (5.36) remains in $\mathcal{T} \cup \mathcal{S}$ for all $t \geq 0$. We define T_1 as the infimum of time values for which either $\|\boldsymbol{u}(t)\| < \mathcal{X}$ or $\|\boldsymbol{v}(t)\| < \mathcal{Y}$ fail to hold. We show that the existence of T_1 creates a contradiction, and thus conclude that the bounds $\|\boldsymbol{u}(t)\| < \mathcal{X}$ or $\|\boldsymbol{v}(t)\| < \mathcal{Y}$ hold for all t.

Observe that $\dot{V}$ may be sign indefinite in $\mathcal{T}$, which means if the trajectory of the system is in $\mathcal{T}$ (the blue region in **Fig.** 5.6) then $V(t)$ can increase. However, from (5.45) we obtain that in $\mathcal{T}$

$$\begin{aligned} V(t) \leq \frac{1}{2}\lambda_{\max}(\boldsymbol{Q})(\mathcal{X} - \vartheta_0)^2 + \frac{1}{2}\bar{\gamma}(k_{\overline{M}} + \delta)(\mathcal{Y} - \varphi_0)^2 \\ + \mu^{-1}\bar{\gamma}(k_{\overline{M}} + \delta)(\mathcal{X} - \vartheta_0)(\mathcal{Y} - \varphi_0) := \mathcal{Z} \end{aligned}$$

One can easily verify that $\mathcal{Z} < \widehat{V}^*$ because we selected ϑ_0, φ_0 such that $\mathcal{X}_1 > \mathcal{X} - \vartheta_0$ and $\mathcal{Y}_1 > \mathcal{Y} - \varphi_0$. Note that any trajectory of (5.36) beginning[2] in $\mathcal{S} \cup \mathcal{T}$ must satisfy $V(t) \leq \max\{\mathcal{Z}, V(0)\} < \widehat{V}^*$ for $t \in [0, T_1]$. This is because $\dot{V} < 0$ in $\mathcal{S}$; any trajectory starting in $\mathcal{S}$ (respectively $\mathcal{T}$) has $V(t) < V(0)$ (respectively $V(t) < \mathcal{Z}$). If the trajectory leaves $\mathcal{T}$ and enters $\mathcal{S}$ at some t, consider the crossover point, which is in the closure of $\mathcal{T}$. By the virtue that V is continuous, we have $V(t) < Z$ and by virtue of entering $\mathcal{S}$, $V(t + \delta) \leq V(t) < \mathcal{Z}$, for some arbitrarily small δ. Define $\zeta = \lambda_{\min}(\boldsymbol{M} - \mu^{-1}\boldsymbol{M}\boldsymbol{Q}^{-1}\boldsymbol{M})/2$ and verify that $\zeta \geq \rho_3(\mu_3^*) > \rho_2(\mu_3^*)$. In accordance with **Lemma** 4 we have

$$\|\boldsymbol{v}(T_1)\|_2 \leq \sqrt{\frac{V(T_1)}{\zeta}} < \sqrt{\frac{\widehat{V}^*}{\zeta}} < \sqrt{\frac{\widehat{V}^*}{\rho_2(\mu_3^*)}} = \mathcal{Y} \tag{5.52}$$

Paralleling the argument leading to (5.52), one can also show that $\|\boldsymbol{u}(T_1)\| < \mathcal{X}$. We omit this due to spatial limitations and similarity of argument. The existence of (5.52) and a similar inequality for $\|\boldsymbol{u}(T_1)\|$ contradict the definition of T_1. In other words, T_1 does not exist, and therefore $\|\boldsymbol{u}(t)\| < \mathcal{X}$ and $\|\boldsymbol{v}(t)\| < \mathcal{Y}$ for all t, as depicted in **Fig.** 5.6.

[2]The definitions of $\mathcal{S}$ and $\mathcal{T}$ ensure that $\boldsymbol{u}(0), \boldsymbol{v}(0) \in \mathcal{S} \cup \mathcal{T}$ as evident in (5.39).

Part 3: We now show that the leader-follower consensus objective is achieved. In order to do this, we firstly explore how the time-varying nature of $A_5(t)$ and $A_6(\mu, t)$ affects $\dot{V}$. As discussed in **Fig.** 5.6, $A_5(t)$ and $A_6(\mu, t)$ decay to zero exponentially fast due to the presence of $\bar{\omega}(t)$. Therefore, at $t = \infty$, $p(\|\boldsymbol{u}\|, \|\boldsymbol{v}\|)$ is of the form of $g(x, y)$ in **Lemma** 5 and is thus positive definite (and therefore $\dot{V} = -\mu^{-1}p$ is negative definite) for $\|\boldsymbol{u}\| \in [0, \mathcal{X}]$ and $\|\boldsymbol{v}\| \in [0, \infty)$. This is because μ_6^* as designed according to **Corollary** 1 also satisfies the requirements detailed in **Lemma** 5. It is also straightforward to conclude that the sign indefiniteness of $\dot{V}(t)$ in $\mathcal{T}(t)$ arises due to the terms linear in $\|\boldsymbol{u}\|$ and $\|\boldsymbol{v}\|$ in (5.49), i.e. the terms containing $\bar{\omega}(t)$, which are precisely the coefficients $A_5(t)$ and $A_6(\mu, t)$ in (5.50).

Now that we have established that $A_5(t)\|\boldsymbol{u}\|$ and $A_6(\mu, t)\|\boldsymbol{v}\|$ give rise to the region $\mathcal{T}(t)$, we now establish the precise behaviour of $\mathcal{T}(t)$ and $\mathcal{S}(t)$ as functions of time. Now examine the inequalities on the coefficient b as detailed in **Corollary** 1, applied to $p(\|\boldsymbol{u}\|, \|\boldsymbol{v}\|)$ in (5.50). We conclude that for a fixed μ_6^*, the strictly monotonically decreasing nature of A_5, A_6 then implies that, for fixed $A_2(\mu_6^*)$, the region in which $p(\|\boldsymbol{u}\|, \|\boldsymbol{v}\|) > 0$ (respectively sign indefinite) as defined by $\mathcal{S}(t)$ (respectively $\mathcal{T}(t)$), is time-varying. *Specifically, $\vartheta(t)$ and $\varphi(t)$ are strictly monotonically increasing.* Moreover, because $A_5 = A_6 = 0$ at $t = \infty$, we conclude that $\lim_{t\to\infty} \vartheta(t) = \mathcal{X}$ and $\lim_{t\to\infty} \varphi(t) = \mathcal{Y}$, at which point $\mathcal{T}(t) = [0, 0]$.

It is straightforward to show that appropriate functions are given by $\vartheta(t) = -a_1 e^{-a_2 t} + \mathcal{X}$ and $\varphi(t) = -b_1 e^{-b_2 t} + \mathcal{Y}$. Here, a_1, a_2, b_1, b_2 are positive constants associated with $\mathcal{X}_0$, $\mathcal{Y}_0$ and the decay rate of $\bar{\omega}(t)$. Moreover, because $\vartheta(t), \varphi(t)$ are strictly monotonically increasing, it is easy to verify that $\mathcal{S}(t_1) \subset \mathcal{S}(t_2)$ and $\mathcal{T}(t_1) \supset \mathcal{T}(t_2)$ for any $t_1 < t_2$. These properties ensure that the boundedness arguments developed in *Part 2* remain valid for time-varying $\mathcal{S}(t)$ and $\mathcal{T}(t)$ due to the nature of the time variation.

Now we have established the behaviour of $\mathcal{S}(t)$ and $\mathcal{T}(t)$, we move on to show that leader-follower consensus is achieved. Suppose that at some T_2, the trajectory of the system (5.36) leaves $\mathcal{T}(t)$ and does not enter $\mathcal{T}(t)$ for all $t \geq T_2$. In other words, for $t \geq T_2$, the trajectory is in $\mathcal{S}(t)$ (recall that in *Part 2* we established that $\|\boldsymbol{u}(t)\| < \mathcal{X}$ and $\|\boldsymbol{v}(t)\| < \mathcal{Y}$ for all t). This is illustrated in **Fig.** 5.6.

Firstly, consider the case where $T_2 = \infty$. From the form of $\vartheta(t), \varphi(t)$, we conclude that $\mathcal{T}(t)$ shrinks exponentially fast towards the origin $\boldsymbol{u} = \boldsymbol{v} = 0$. If $T_2 = \infty$ then there is some $T_3 < \infty$ such that the trajectory of the system (5.36) is in $\mathcal{T}(t)$ for all $t \in [T_3, \infty)$. From the limiting behaviour of $\mathcal{T}(t)$, we conclude that the trajectory of (5.36) also converges to the equilibrium $\|\boldsymbol{u}\| = \|\boldsymbol{v}\| = 0$, which implies that the leader-follower consensus objective has been achieved. Moreover, the convergence rate is exponential for $t \in [T_3, \infty)$.

Secondly, consider the case where T_2 is finite. Note that T_2 is initial condition dependent, but the initial condition set is bounded according to **Assumption** 3. It follows that there exists a $\bar{T}_2$ *independent of initial conditions* such that, for every initial condition satisfying Assumption 3, $T_2 < \bar{T}_2 < \infty$. Define the time interval $t_p = [\bar{T}_2, \infty)$. Because the trajectory of the system (5.36) is in $\mathcal{S}(t)$ for all $t \in t_p$ then $\dot{V}(t) < 0$ for all $t \in t_p$. Consider some arbitrary time $t_1 \in t_p$. We observe that

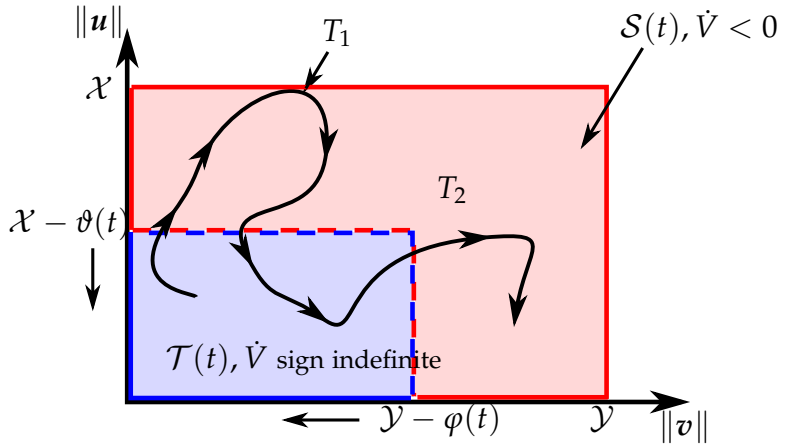

Figure 5.6: Diagram for proof of **Theorem** 8. The red region is $\mathcal{S}(t)$, in which $\dot{V}(t) < 0$ for all $t \geq 0$. The blue region is $\mathcal{T}(t)$, in which $\dot{V}(t)$ is sign indefinite. A trajectory of (5.36) is shown with the black curve. At $t = T_1$, it is shown in *Part 2* that the trajectory of (5.36) is such that $\|\boldsymbol{u}(T_1)\| < \mathcal{X}, \|\boldsymbol{v}(T_1)\| < \mathcal{Y}$ and thus the trajectory does not leave $\mathcal{S}(t)$. The sign indefiniteness of $\dot{V}(t)$ in $\mathcal{T}(t)$ arises due to the terms linear in $\|\boldsymbol{u}\|$ and $\|\boldsymbol{v}\|$ in (5.49), i.e. the terms containing $\bar{\omega}(t)$ (coefficients $A_5(t)$ and $A_6(\mu, t)$ in (5.50)). Because $\bar{\omega}(t)$ goes to zero at an exponential rate, so do the coefficients $A_5(t)$ and $A_6(\mu, t)$. Examining the inequalities detailed in **Corollary** 1 as applied to $p(\|\boldsymbol{u}\|, \|\boldsymbol{v}\|)$ in (5.50), it is straightforward to conclude that for a fixed μ_6^*, the exponential decay of A_5, A_6 implies that the region $\mathcal{T}(t)$ shrinks towards the origin at an exponential rate. In other words, $\vartheta(t)$ and $\varphi(t)$ monotonically increase until $\vartheta(t) = \mathcal{X}$ and $\varphi(t) = \mathcal{Y}$, at which point $\mathcal{T}(t) = [0, 0]$. This corresponds to the dotted red and blue lines, which show, respectively, the time-varying boundaries of $\mathcal{S}(t)$ and $\mathcal{T}(t)$. The solid red and blue lines show respectively, the boundaries of $\mathcal{S}(t)$ and $\mathcal{T}(t)$, which are time-invariant. Exponential convergence to the leader-follower objective is discussed in *Part 3* making using of T_2.

$p(\|\boldsymbol{u}\|, \|\boldsymbol{v}\|) > 0$ (i.e. positive definite) in the compact region $\mathcal{S}(t_1)$. One can therefore find a scalar $a_{1,t_1} > 0$ such that $p(\|\boldsymbol{u}\|, \|\boldsymbol{v}\|) \geq a_{1,t_1} \|[\boldsymbol{u}^\top, \boldsymbol{v}^\top]^\top\|$ for all $\|\boldsymbol{u}\|, \|\boldsymbol{v}\| \in \mathcal{S}(t_1)$. Furthermore, by recalling that A_5, A_6 are positive and strictly monotonically decreasing, we conclude that $p(\|\boldsymbol{u}\|, \|\boldsymbol{v}\|, t_1) < p(\|\boldsymbol{u}\|, \|\boldsymbol{v}\|, t_2)$ for any $\boldsymbol{u}, \boldsymbol{v}$, and for any $t_1 \leq t_2$ where $t_1, t_2 \in t_p$. It follows that there exists some constant $\bar{a}_1 > 0$ such that $p(\|\boldsymbol{u}\|, \|\boldsymbol{v}\|) \geq \bar{a}_1 \|[\boldsymbol{u}^\top, \boldsymbol{v}^\top]^\top\|$ for all $\boldsymbol{v}, \boldsymbol{u}$ in $\mathcal{S}(t)$, for all $t \in t_p$. This implies that, in $\mathcal{S}(t)$ we have $\dot{V} \leq -\bar{a}_1 \|[\boldsymbol{u}^\top, \boldsymbol{v}^\top]^\top\| < 0$ for all $t \in t_p$. The eigenvalues of the constant matrices $\boldsymbol{L}_\mu$ and $\boldsymbol{N}_\mu$ (the matrices introduced in **subsection** 5.5.1) are finite and strictly positive. Our earlier conclusion that $\boldsymbol{L}_\mu > \boldsymbol{G} > \boldsymbol{N}_\mu$ for all $\mu \geq \mu_3^*$ then implies that the eigenvalues of $\boldsymbol{G}$ (which vary with $\boldsymbol{q}(t)$) are upper bounded away from infinity and lower bounded away from zero. It follows that there exist scalars $a_2, a_3 > 0$ such that $a_2 \|[\boldsymbol{u}^\top, \boldsymbol{v}^\top]^\top\| \leq V(t) \leq a_3 \|[\boldsymbol{u}^\top, \boldsymbol{v}^\top]^\top\|$. This implies that $\dot{V}(t) \leq -\psi V(t)$ in $\mathcal{S}(t)$ for $t \in t_p$ where $\psi = \bar{a}_1 / a_3$. From this, we conclude that V decays exponentially fast to zero, with a minimum rate $e^{-\psi t}$, for $t \in t_p$. Since V

is positive definite in $\boldsymbol{u}, \boldsymbol{v}$, this implies that $\|[\boldsymbol{u}^\top, \boldsymbol{v}^\top]^\top\|$ decays to zero exponentially fast for $t \in t_p$, and the leader-follower consensus objective is achieved.

□

Remark 14. *We do not provide analysis of the exclusion of Zeno behaviour in this section since the trigger function is designed according to the MTF proposed in* ***Section*** *5.4, in which the offset term can ensure no Zeno behaviour for each agent.*

5.6 Adaptive, model-dependent algorithm

In this section, we propose an adaptive, distributed event-triggered controller to achieve leader-follower consensus for a directed network of Euler-Lagrange agents. This allows for uncertain parameters in each agent, e.g. the mass of a robotic manipulator arm, and includes the gravitational forces.

5.6.1 Main result

Before we present the main results, we introduce variables which allow us to rewrite the multi-agent system in a way which facilitates stability analysis. A lemma on stability is also provided. To begin, we introduce the following auxiliary variables $\boldsymbol{q}_{ri}$ and $\boldsymbol{s}_i$, which appeared in [Mei et al., 2013, 2012] studying leader-follower problems in directed Euler-Lagrange networks. Define

$$\dot{\boldsymbol{q}}_{ri}(t) = -\alpha \sum_{j=0}^{n} a_{ij}(\boldsymbol{q}_i(t) - \boldsymbol{q}_j(t)), \tag{5.53}$$

$$\boldsymbol{s}_i(t) = \dot{\boldsymbol{q}}_i(t) - \dot{\boldsymbol{q}}_{ri}(t) = \dot{\boldsymbol{q}}_i(t) + \alpha \sum_{j=0}^{n} a_{ij}(\boldsymbol{q}_i(t) - \boldsymbol{q}_j(t)), \quad i = 1, \ldots, n \tag{5.54}$$

where α is a positive constant, a_{ij} is the weighted (i, j) entry of the adjacency matrix $\mathcal{A}$ associated with the directed graph $\mathcal{G}$ that characterises the sensing flows among the n followers. Utilising **Lemma** 7, one can then verify that the compact form of (5.54) can be written as:

$$\dot{\boldsymbol{q}}(t) = -\alpha(\boldsymbol{\mathcal{L}}_{22} \otimes \boldsymbol{I}_p)(\boldsymbol{q}(t) - \boldsymbol{1}_n \otimes \boldsymbol{q}_0) + \boldsymbol{s}(t) \tag{5.55}$$

The following lemma will later be used for stability analysis of the networked system.

Lemma 8. *(From [Mei et al., 2012]) Suppose that, for the system* (5.55)*, the graph $\mathcal{G}$ contains a directed spanning tree with the leader as the root vertex. Then system* (5.55) *is input-to-state stable with respect to input $\boldsymbol{s}(t)$. If $\boldsymbol{s}(t) \to \boldsymbol{0}_p$ as $t \to \infty$, then $\dot{\boldsymbol{q}}_i(t) \to \boldsymbol{0}_p$ and $\boldsymbol{q}_i(t) \to \boldsymbol{q}_0$ as $t \to \infty$.*

Note that the proof of the above lemma is part of the proof of **Corollary** 3.7 in [Mei et al., 2012].

From P(6) and the definition of $\dot{\boldsymbol{q}}_{ri}$, we obtain

$$\boldsymbol{M}_i(\boldsymbol{q}_i)\ddot{\boldsymbol{q}}_{ri} + \boldsymbol{C}_i(\boldsymbol{q}_i, \dot{\boldsymbol{q}}_i)\dot{\boldsymbol{q}}_{ri} + \boldsymbol{g}_i(\boldsymbol{q}_i) = \boldsymbol{Y}_i(\boldsymbol{q}_i, \dot{\boldsymbol{q}}_i, \ddot{\boldsymbol{q}}_{ri}, \dot{\boldsymbol{q}}_{ri})\boldsymbol{\Theta}_i \tag{5.56}$$

Note that $\boldsymbol{\Theta}_i$ is an unknown but constant vector for agent i. Let $\hat{\boldsymbol{\Theta}}_i(t)$ be the estimate of $\boldsymbol{\Theta}_i$ at time t. We update $\hat{\boldsymbol{\Theta}}_i(t)$ by the following adaptation law:

$$\dot{\hat{\boldsymbol{\Theta}}}_i(t) = -\boldsymbol{\Lambda}_i \boldsymbol{Y}_i^{\top}(t)\boldsymbol{s}_i(t) \tag{5.57}$$

where $\boldsymbol{\Lambda}_i$ is a symmetric positive-definite matrix.

The control algorithm is now proposed. Let the triggering time sequence of agent i be $t_0^i, t_1^i, \ldots, t_k^i, \ldots$ with $t_0^i := 0$. The event-triggered controller for follower agent i is designed as:

$$\boldsymbol{\tau}_i(t) = -\boldsymbol{K}_i \boldsymbol{s}_i(t_k^i) + \boldsymbol{Y}_i(t_k^i)\hat{\boldsymbol{\Theta}}_i(t_k^i), \quad t \in [t_k^i, t_{k+1}^i) \tag{5.58}$$

where $\boldsymbol{K}_i > 0$ is a symmetric positive definite matrix. It is observed that the control torque remains constant in the time interval $[t_k^i, t_{k+1}^i)$, i.e. $\boldsymbol{\tau}_i(t)$ is a piecewise-constant function in time. From the definitions of $\boldsymbol{q}_{ri}$ and $\boldsymbol{s}_i$, calculations show that the system in (5.6) can be written as

$$\boldsymbol{M}_i(\boldsymbol{q}_i)\dot{\boldsymbol{s}}_i(t) + \boldsymbol{C}_i(\boldsymbol{q}_i, \dot{\boldsymbol{q}}_i)\boldsymbol{s}_i(t) = -\boldsymbol{K}_i \boldsymbol{s}_i(t_k^i) + \boldsymbol{Y}_i(t_k^i)\hat{\boldsymbol{\Theta}}_i(t_k^i) - \boldsymbol{Y}_i(t)\boldsymbol{\Theta}_i \tag{5.59}$$

Before the trigger function is presented, we define two types of state mismatch:

$$\begin{aligned} \boldsymbol{e}_i(t) &= \boldsymbol{s}_i(t_k^i) - \boldsymbol{s}_i(t); \\ \boldsymbol{\varepsilon}_i(t) &= \boldsymbol{Y}_i(t_k^i)\hat{\boldsymbol{\Theta}}_i(t_k^i) - \boldsymbol{Y}_i(t)\hat{\boldsymbol{\Theta}}_i(t); \end{aligned} \tag{5.60}$$

The trigger function is proposed as follows:

$$f_i(t) = \|\boldsymbol{\varepsilon}_i(t)\| + \lambda_{\max}(\boldsymbol{K}_i)\|\boldsymbol{e}_i(t) - \frac{\gamma_i}{2}\lambda_{\min}(\boldsymbol{K}_i)\|\boldsymbol{s}_i(t)\| - \omega_i(t) \tag{5.61}$$

where $0 < \gamma_i < 1$, $\omega_i(t) = \sigma_i\sqrt{\lambda_{\min}(\boldsymbol{K}_i)}\exp(-\kappa_i t)$ with $\sigma_i, \kappa_i > 0$. The k^{th} event for agent i is triggered as soon as the trigger condition $f_i(t) = 0$ is fulfilled at $t = t_k^i$. For $t \in [t_k^i, t_{k+1}^i)$, the control input is $\boldsymbol{\tau}_i(t) = \boldsymbol{\tau}_i(t_k^i)$; the control input is updated when the next event is triggered. Furthermore, every time an event is triggered, and in accordance with their definitions, the state mismatches $\boldsymbol{\varepsilon}_i(t)$ and $\boldsymbol{e}_i(t)$ are reset to be equal to zero. Thus $f_i(t) \leq 0$ for all $t \geq 0$.

We now present our main result.

Theorem 9. *Consider the multi-agent system* (5.6) *with control law* (5.58). *If $\mathcal{G}$ contains a directed spanning tree with the leader as the root vertex (and thus with no incoming edges), then leader-follower consensus ($\|\boldsymbol{q}_i - \boldsymbol{q}_0\| \to 0$ and $\|\dot{\boldsymbol{q}}_i\| \to 0$, $i = 1, \ldots, n$) is globally asymptotically achieved as $t \to \infty$ and no agent will exhibit Zeno behaviour.*

Proof. In this part, we focus on the stability analysis of the system (5.59). The proof on the exclusion of Zeno behaviour is omitted since the idea is the same with that in Part 2) of the proof of **Theorem** 7. Notice that (5.59) is non-autonomous in the sense that it is not self-contained ($\boldsymbol{M}_i, \boldsymbol{C}_i$ depend on $\boldsymbol{q}_i$ and $\boldsymbol{q}_i, \dot{\boldsymbol{q}}_i$ respectively). However, study of a Lyapunov-like function shows leader-follower consensus is achieved.

We make use of abuse of notation by omitting the argument of time t for time-dependent functions when appropriate, e.g. $\boldsymbol{q}_i$ denotes $\boldsymbol{q}_i(t)$.

Consider the following Lyapunov-like function

$$V = \frac{1}{2}\sum_{i=1}^{N} \boldsymbol{s}_i^\top \boldsymbol{M}_i(\boldsymbol{q}_i)\boldsymbol{s}_i + \frac{1}{2}\sum_{i=1}^{N} \tilde{\boldsymbol{\Theta}}_i^\top \boldsymbol{\Lambda}_i^{-1}\tilde{\boldsymbol{\Theta}}_i \tag{5.62}$$

where

$$\tilde{\boldsymbol{\Theta}}_i = \boldsymbol{\Theta}_i - \hat{\boldsymbol{\Theta}}_i \tag{5.63}$$

The derivative of V along the solution of (5.59) is

$$\begin{aligned}
\dot{V} &= \frac{1}{2}\sum_{i=1}^{N} \boldsymbol{s}_i^\top \dot{\boldsymbol{M}}_i(\boldsymbol{q}_i)\boldsymbol{s}_i + \sum_{i=1}^{N} \boldsymbol{s}_i^\top \boldsymbol{M}_i(\boldsymbol{q}_i)\dot{\boldsymbol{s}}_i + \sum_{i=1}^{N} \tilde{\boldsymbol{\Theta}}_i^\top \boldsymbol{\Lambda}_i^{-1}\dot{\tilde{\boldsymbol{\Theta}}} \\
&= \sum_{i=1}^{N} \boldsymbol{s}_i^\top \left(\frac{1}{2}\dot{\boldsymbol{M}}_i(\boldsymbol{q}_i) - \boldsymbol{C}_i(\boldsymbol{q}_i, \dot{\boldsymbol{q}}_i)\right)\boldsymbol{s}_i - \sum_{i=1}^{N} \boldsymbol{s}_i^\top \boldsymbol{K}_i \boldsymbol{s}_i(t_k^i) \\
&\quad + \sum_{i=1}^{N} \boldsymbol{s}_i^\top \boldsymbol{Y}_i(t_k^i)\hat{\boldsymbol{\Theta}}_i(t_k^i) - \sum_{i=1}^{N} \boldsymbol{s}_i^\top \boldsymbol{Y}_i\boldsymbol{\Theta}_i + \sum_{i=1}^{N} \tilde{\boldsymbol{\Theta}}_i^\top \boldsymbol{Y}_i^\top \boldsymbol{s}_i
\end{aligned}$$

From P(4) we have $\frac{1}{2}\dot{\boldsymbol{M}}_i(\boldsymbol{q}_i) - \boldsymbol{C}_i(\boldsymbol{q}_i)$ is skew-symmetric and with $\boldsymbol{\Theta}_i = \tilde{\boldsymbol{\Theta}}_i + \hat{\boldsymbol{\Theta}}_i$, we obtain

$$\dot{V} = -\sum_{i=1}^{N} \boldsymbol{s}_i^\top \boldsymbol{K}_i \boldsymbol{s}_i(t_k^i) + \sum_{i=1}^{N} \boldsymbol{s}_i^\top \boldsymbol{Y}_i(t_k^i)\hat{\boldsymbol{\Theta}}_i(t_k^i) - \sum_{i=1}^{N} \boldsymbol{s}_i^\top \boldsymbol{Y}_i(\tilde{\boldsymbol{\Theta}}_i + \hat{\boldsymbol{\Theta}}_i) + \sum_{i=1}^{N} \tilde{\boldsymbol{\Theta}}_i^\top \boldsymbol{Y}_i^\top \boldsymbol{s}_i$$

By recalling the definition of $\boldsymbol{e}_i$ and $\boldsymbol{\varepsilon}_i$ in (5.60), we have

$$\dot{V} = -\sum_{i=1}^{N} \boldsymbol{s}_i^\top \boldsymbol{K}_i \boldsymbol{s}_i - \sum_{i=1}^{N} \boldsymbol{s}_i^\top \boldsymbol{K}_i \boldsymbol{e}_i + \sum_{i=1}^{N} \boldsymbol{s}_i^\top \boldsymbol{\varepsilon}_i$$

Since $\boldsymbol{K}_i$ is a symmetric positive definite matrix, the upper bound of $\dot{V}$ is expressed

as

$$\dot{V} \leq -\sum_{i=1}^{N} \lambda_{\min}(\boldsymbol{K}_i)\|\boldsymbol{s}_i\|^2 + \sum_{i=1}^{N} \lambda_{\max}(\boldsymbol{K}_i)\|\boldsymbol{s}_i\|\|\boldsymbol{e}_i\| + \sum_{i=1}^{N} \|\boldsymbol{s}_i\|\|\boldsymbol{\varepsilon}_i\|$$

Note that the trigger condition $f_i(t) = 0$ guarantees that $\|\boldsymbol{\varepsilon}_i\| + \lambda_{\max}(\boldsymbol{K}_i)\|\boldsymbol{e}_i\| \leq \frac{\gamma_i}{2}\lambda_{\min}(\boldsymbol{K}_i)\|\boldsymbol{s}_i\| + \omega_i(t)$ holds throughout the evolution of system (5.59). By further introducing the definition of $\omega_i(t)$ in (5.61), we obtain

$$\dot{V} \leq -\sum_{i=1}^{N} \lambda_{\min}(\boldsymbol{K}_i)\|\boldsymbol{s}_i\|^2 + \sum_{i=1}^{N} \frac{\gamma_i}{2}\lambda_{\min}(\boldsymbol{K}_i)\|\boldsymbol{s}_i\|^2 + \sum_{i=1}^{N} \sqrt{\lambda_{\min}(\boldsymbol{K}_i)}\|\boldsymbol{s}_i\|\sigma_i \exp(-\kappa_i t)$$

Because there holds $|xy| \leq \frac{\gamma_i}{2}x^2 + \frac{1}{2\gamma_i}y^2, \forall x, y \in \mathbb{R}$, for $0 < \gamma_i < 1$, analysis of the right hand side of the above inequality implies that $\dot{V}$ can be further upper bounded as

$$\dot{V} \leq \sum_{i=1}^{N}(\gamma_i - 1)\lambda_{\min}(K_i)\|\boldsymbol{s}_i\|^2 + \sum_{i=1}^{N} \frac{\sigma_i^2}{2\gamma_i} \exp(-2\kappa_i t) \tag{5.64}$$

Integrating both sides of (5.64) for any $t > 0$ yields:

$$V + \sum_{i=1}^{N}(1 - \gamma_i)\lambda_{\min}(\boldsymbol{K}_i) \int_0^t \|\boldsymbol{s}_i(\tau)\|^2 d\tau \leq V(0) + \sum_{i=1}^{N} \frac{\sigma_i^2}{4\gamma_i\kappa_i} \tag{5.65}$$

which implies that V is bounded. Since V is bounded, according to (5.62), both s_i and $\tilde{\boldsymbol{\Theta}}_i(t)$, for all $i \in \{1, ..., n\}$, are bounded. Now we return to (5.56) and obtain that

$$\|\boldsymbol{Y}_i\boldsymbol{\Theta}_i\| \leq \|\boldsymbol{M}_i\|\|\ddot{\boldsymbol{q}}_{ri}\| + \|\boldsymbol{C}_i\|\|\dot{\boldsymbol{q}}_{ri}\| + \|\boldsymbol{g}_i\|$$

By recalling that the linear system (5.55) is input-to-state stable and the fact that s is bounded, we conclude that $\boldsymbol{q}_i$ and $\dot{\boldsymbol{q}}_i$ are both bounded. Because $\boldsymbol{q}_i$ and $\dot{\boldsymbol{q}}_i$ are bounded then, from their definitions, so are $\dot{\boldsymbol{q}}_{ri}$ and $\ddot{\boldsymbol{q}}_{ri}$. Then from P(2), P(3) and P(5), the assumed properties of Euler-Lagrange equations, we have that $\|\boldsymbol{Y}_i\|$ is upper bounded by a positive value. From the above conclusions, it is straightforward to see that the right hand side of (5.59), $\boldsymbol{M}_i$, $\boldsymbol{C}_i$ and $\boldsymbol{s}_i$ are all bounded. We thus obtain that $\dot{\boldsymbol{s}}_i$ is bounded. From this, it is obvious that $\boldsymbol{s}_i, \dot{\boldsymbol{s}}_i \in L_\infty$. Turning to (5.65), it follows that

$$\sum_{i=1}^{N}(1 - \gamma_i)\lambda_{\min}(\boldsymbol{K}_i) \int_0^t \|\boldsymbol{s}_i(\tau)\|^2 d\tau \leq V(0) + \sum_{i=1}^{N} \frac{\sigma_i^2}{4\gamma_i\kappa_i} \tag{5.66}$$

which indicates that $\int_0^t \|s_i(\tau)\|^2 d\tau$ is bounded and thus $s_i \in \mathcal{L}_2$. By applying **Lemma** 3, we have that $s_i \to \boldsymbol{0}_p$ as $t \to \infty$. Then by applying **Lemma** 8, we conclude that $\boldsymbol{q}_i - \boldsymbol{q}_0 \to \boldsymbol{0}_p$ and $\dot{\boldsymbol{q}}_i \to \boldsymbol{0}_p$ as $t \to \infty$. The leader-follower objective is globally

$$\Theta_i = \begin{bmatrix}(m_1+m_2)d_1^2+m_2d_2^2 & m_2d_1d_2 & m_2d_2^2 & (m_1+m_2)gd_1 & m_2gd_2\end{bmatrix}^T$$

$$Y_i = \begin{bmatrix} x_1 & 0 \\ 2x_1\cos(q_i^{(2)}) + x_2\cos(q_i^{(2)}) - y_1\sin(q_i^{(2)})\dot{q}_i^{(2)} - y_2\sin(q_i^{(2)})\dot{q}_i^{(2)} - y_2\sin(q_i^{(2)})\dot{q}_i^{(1)} & x_1\cos(q_i^{(2)}) + y_1\sin(q_i^{(2)})\dot{q}_i^{(1)} \\ x_2 & x_1+x_2 \\ \sin(q_i^{(1)}) & 0 \\ \sin(q_i^{(1)}+q_i^{(2)}) & \sin(q_i^{(1)}+q_i^{(2)}) \end{bmatrix}^T$$

asymptotically achieved.

□

5.7 Simulations

In this subsection, we will provide three simulations to respectively demonstrate the performance of the three proposed controllers in this chapter for application to industrial manipulators (See **Fig.** 5.7). Although the effectiveness of controller (5.9) is verified in **Subsection** 5.4.2, the applied system is simple one-arm manipulators. In this subsection we assume that all two-link manipulators share the same dynamic models and parameters. The Euler-Lagrange equations for the i^{th} two-link manipulator is:

$$\begin{bmatrix} M_i^{11} & M_i^{12} \\ M_i^{21} & M_i^{22} \end{bmatrix} \begin{bmatrix} \ddot{q}_i^{(1)} \\ \ddot{q}_i^{(2)} \end{bmatrix} + \begin{bmatrix} C_i^{11} & C_i^{12} \\ C_i^{21} & C_i^{22} \end{bmatrix} \begin{bmatrix} \dot{q}_i^{(1)} \\ \dot{q}_i^{(2)} \end{bmatrix} + \begin{bmatrix} g_i^{(1)} \\ g_i^{(2)} \end{bmatrix} = \begin{bmatrix} \tau_i^{(1)} \\ \tau_i^{(2)} \end{bmatrix}$$

The elements in M_i, C_i matrices and g_i vector are given below:

$$\begin{aligned}
M_i^{11} &= (m_1+m_2)d_1^2 + m_2d_2^2 + 2m_2d_1d_2\cos(q_i^{(2)}) \\
M_i^{12} &= M_i^{21} = m_2(d_2^2 + d_1d_2\cos(q_i^{(2)})) \\
M_i^{22} &= m_2d_2^2 \\
C_i^{11} &= -m_2d_1d_2\sin(q_i^{(2)})\dot{q}_i^{(2)} \\
C_i^{12} &= -m_2d_1d_2\sin(q_i^{(2)})\dot{q}_i^{(2)} - m_2d_1d_2\sin(q_i^{(2)})\dot{q}_i^{(1)} \\
C_i^{21} &= m_2d_1d_2\sin(q_i^{(2)})\dot{q}_i^{(1)} \\
C_i^{22} &= 0 \\
g_i^{(1)} &= (m_1+m_2)gd_1\sin(q_i^{(1)}) + m_2gd_2\sin(q_i^{(1)}+q_i^{(2)}) \\
g_i^{(2)} &= m_2gd_2\sin(q_i^{(1)}+q_i^{(2)})
\end{aligned}$$

where g is the acceleration due to gravity, d_1 and d_2 are lengths of the 1^{st} and 2^{nd} links of the manipulator, respectively; m_1 and m_2 are mass of the 1^{st} and 2^{nd} of the manipulator. The physical parameters of each manipulator are selected as $g = 9.8\,\text{m/s}^2$, $d_1 = 1.5\,\text{m}$, $d_2 = 1\,\text{m}$, $m_1 = 1\,\text{kg}$, $m_2 = 2\,\text{kg}$. The initial states of each manipulator are shown in **Table** 5.4. Note that in simulations 1 and 2, we assume that $g_i^{(1)}, g_i^{(2)} = 0$.

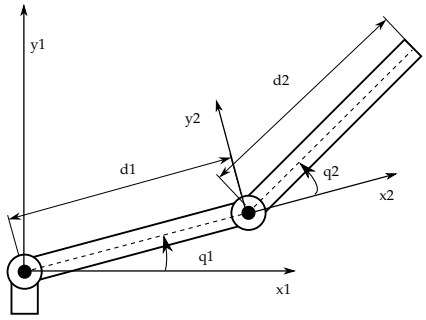

Figure 5.7: Two-link manipulator, generalized coordinates $\boldsymbol{q} = [q^1, q^2]^\top$
.

Table 5.4: Agents' initial states used in simulations

	$q_i^{(1)}(0)$	$q_i^{(1)}(0)$	$\dot{q}_i^{(1)}(0)$	$\dot{q}_i^{(1)}(0)$
Agent 0	$\pi/6$	$\pi/3$	0.0	0.0
Agent 1	$\pi/5$	$\pi/6$	0.8	0.2
Agent 2	$\pi/6$	$\pi/4$	-0.2	0.3
Agent 3	$\pi/9$	$\pi/6$	0.6	-0.4
Agent 4	$\pi/8$	$\pi/4$	0.5	0.1
Agent 5	$\pi/9$	$\pi/6$	0.1	0.0

Simulation 1. *This simulation will demonstrate the performance of controller* (5.9) *under trigger condition* (5.11). *The sensing graph $\mathcal{G}$ associated with the five follower manipulators and the leader manipulator has the following weighted Laplacian*

$$\mathcal{L} = \begin{bmatrix} 0 & 0 & 0 & 0 & 0 & 0 \\ -1 & 3.9 & -1.55 & 0 & -1.35 & 0 \\ -1 & -1.55 & 6.4 & -2.1 & -1.75 & 0 \\ 0 & 0 & -2.1 & 7.35 & -2.35 & -2.9 \\ 0 & -1.35 & -1.75 & -2.35 & 6.7 & -1.25 \\ 0 & 0 & 0 & -2.9 & -1.25 & 4.15 \end{bmatrix}$$

The initial value of the variable-gain scalar $\mu_(t)$ is chosen as $\mu_i(0) = 0$. The exponential function used in trigger function (5.11) *is selected as $\omega_i(t) = 1.8 * \exp(-0.2 * t)$. The performance of the controller is demonstrated in* ***Fig.*** *5.8.*

Simulation 2. *The directed sensing graph $\mathcal{G}$ associated with the five follower manipulators*

and the leader manipulator has the following weighted Laplacian

$$\mathcal{L} = \begin{bmatrix} 0 & 0 & 0 & 0 & 0 & 0 \\ -1 & 2.55 & -1.55 & 0 & 0 & 0 \\ -1 & 0 & 3.1 & -2.1 & 0 & 0 \\ 0 & 0 & -2.1 & 2.1 & 0 & 0 \\ 0 & -1.35 & -1.75 & -2.35 & 5.45 & 0 \\ 0 & 0 & 0 & -2.9 & -1.25 & 4.15 \end{bmatrix} \tag{5.67}$$

and it contains a directed spanning tree rooted at v_0. There are no incoming edges to v_0. The gain μ used in controller (5.29) *is selected as* 4*. The parameters β_1 and β_2 introduced in trigger function* (5.31) *are both chosen as* 0.6*. The performance of the proposed control algorithm is shown in* ***Fig.*** *5.9.*

Simulation 3. *The uncertain parameter vector Θ_i for each manipulator and the regression matrix are given at the top of the next page. Note that Θ_i is unknown for manipulator i. The Laplacian matrix is also chosen as* (5.67)*. The control gain matrix (in* (5.58)*) for all follower manipulators is chosen as $K_i = \mathrm{I}_2$. The parameter γ_i required in the trigger function* (5.61) *is selected as* 0.6 *for manipulator $i = 1, \ldots, 5$. Lastly, $\mu_i(t) = 5\exp(-0.6t)$ is used in the trigger functions for all manipulators in the follower network. The performance of controller* (5.58) *with trigger function* (5.61) *is presented in* ***Fig.*** *5.10.*

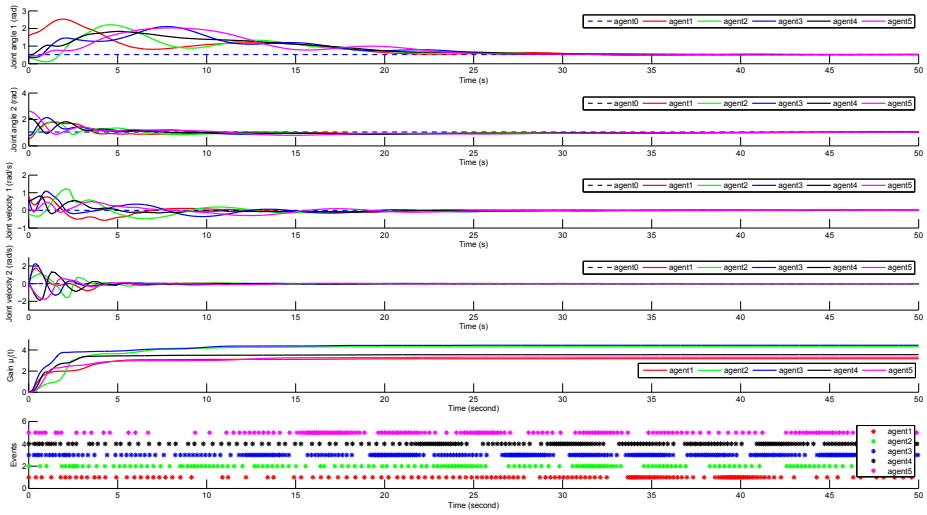

Figure 5.8: Simulation results for controller (5.9) under trigger function (5.11). From top to bottom: the plots the generalized coordinates; the plots of generalised velocities of all the follower manipulators; the plot of variable gain $\mu_i(t)$; the plot of trigger events

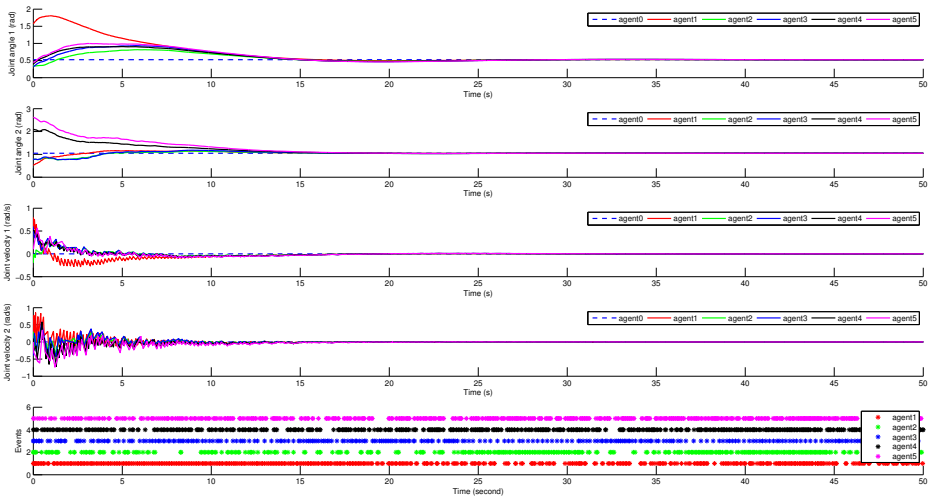

Figure 5.9: Simulation results for controller (5.29) under trigger function (5.31). From top to bottom: the plots the generalized coordinates; the plots of generalised velocities of all the follower manipulators; the plot of trigger events

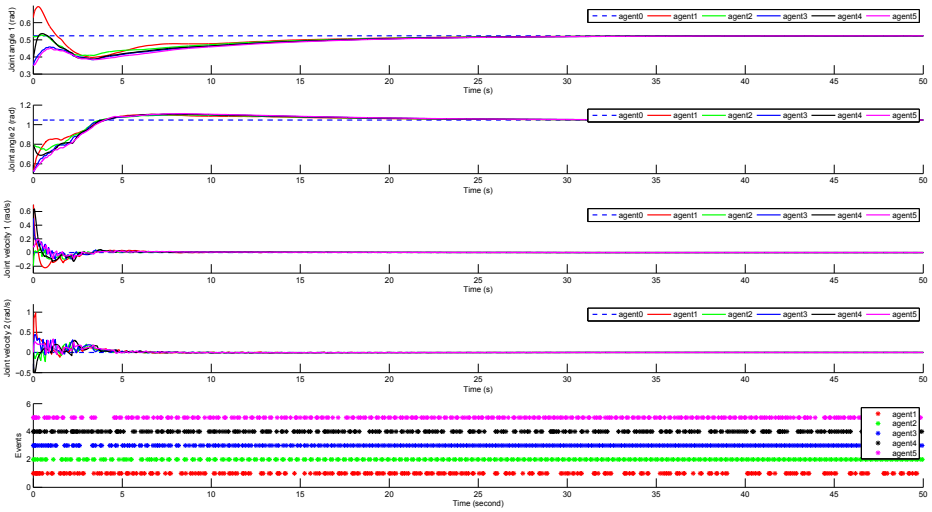

Figure 5.10: Simulation results for controller (5.58) under trigger function (5.61). From top to bottom: the plots the generalized coordinates; the plots of generalised velocities of all the follower manipulators; the plot of trigger events

5.8 Concluding remarks

This chapter proposed three different algorithms for achieving leader-follower consensus for a network of Euler-Lagrange agents. Each algorithm is suited for a different scenario and have their advantages and disadvantages, and can be chosen depending on the problem requirements. For each algorithm, we propose a mixed trigger function. The effectiveness of such a mixed trigger function is extensively explained via simulations.

Chapter 6

Event-Triggered Rigid Formation Control

6.1 Introduction

Formation control of multi-agent systems has received considerable attention in recent years due to its extensive applications in many areas including both civil and military fields. One problem of extensive interest is *formation shape control*, i.e. on designing controllers to achieve or maintain a geometrical shape for the formation [Oh et al., 2015]. By using rigid graph theory, the formation shape can be achieved by controlling a certain set of inter-agent distances [Anderson et al., 2008; Krick et al., 2009] and there is no requirement on a global coordinate system known to all the agents. This is in contrast to the linear *displacement-based* formation control approach, in which the target formation is defined by a certain set of relative positions and a global coordinate system is required for all the agents to implement the displacement-based formation control law (see detailed comparisons in [Oh et al., 2015]). Note that such coordinate alignment condition is a rather strict requirement, which is undesirable for implementing formation controllers in e.g. GPS-denied environment. Even if one assumes that such coordinate alignment is satisfied for all agents, slight coordinate misalignment would lead to a failure of formation control [Meng et al., 2015]. Motivated by all these considerations, in this chapter we focus on rigidity-based formation control.

There have been rich works on control algorithms design and stability analysis of rigid formation control (see e.g. [Krick et al., 2009; Dorfler and Francis, 2010; Oh and Ahn, 2014; Anderson and Helmke, 2014] and the review in [Oh et al., 2015]), most of which assume that the control input is updated in a continuous-time manner. The main objective of this chapter is to provide alternative controllers to stabilize rigid formation shapes based on an event-triggered approach. This kind of controller design is attractive for real-world robots/vehicles equipped with *digital* sensors or microprocessors [Aström, 2008; Heemels et al., 2012]. Furthermore, by using an event-triggered mechanism to update the control input, instead of using a continuous updating strategy as discussed in e.g. [Krick et al., 2009; Dorfler and Francis, 2010; Oh and Ahn, 2014; Anderson and Helmke, 2014], the formation system can save

resources in processors and thus can relax much computation/actuation burden for each agent.

The essential concepts and theoretical foundations in this chapter are based on rigidity theory, which differs from the graph theory used in other chapters. To clarify the difference, we introduce a new preliminary section.

6.2 Preliminaries

6.2.1 Basic concepts on rigidity theory

Consider an undirected graph with m edges and n vertices (or nodes), denoted by $\mathcal{G} = (\mathcal{V}, \mathcal{E})$ with vertex set $\mathcal{V} = \{1, 2, \cdots, n\}$ and edge set $\mathcal{E} \subset \mathcal{V} \times \mathcal{V}$. The neighbour set $\mathcal{N}_i$ of node i is defined as $\mathcal{N}_i := \{j \in \mathcal{V} : (i, j) \in \mathcal{E}\}$.

Let $\boldsymbol{p}_i \in \mathbb{R}^d$ where $d = \{2, 3\}$ denote a point that is assigned to $i \in \mathcal{V}$. The stacked vector $\boldsymbol{p} = [\boldsymbol{p}_1^\top, \boldsymbol{p}_2^\top, \cdots, \boldsymbol{p}_n^\top]^\top \in \mathbb{R}^{dn}$ represents the realization of $\mathcal{G}$ in $\mathbb{R}^d$. The pair $(\mathcal{G}, \boldsymbol{p})$ is said to be a framework of $\mathcal{G}$ in $\mathbb{R}^d$. By introducing the matrix $\bar{\mathcal{H}} := \mathcal{H} \otimes I_d \in \mathbb{R}^{dm \times dn}$ (the incidence matrix $\mathcal{H}$ is defined in **Section** 2.2, **Chapter** 2), one can construct the relative position vector as an image of $\bar{\mathcal{H}}$ from the position vector $\boldsymbol{p}$:

$$\boldsymbol{z} = \bar{\mathcal{H}}\boldsymbol{p} \tag{6.1}$$

where $\boldsymbol{z} = [\boldsymbol{z}_1^\top, \boldsymbol{z}_2^\top, \cdots, \boldsymbol{z}_m^\top]^\top \in \mathbb{R}^{dm}$, with $\boldsymbol{z}_k \in \mathbb{R}^d$ being the relative position vector for the vertex pair defined by the k-th edge.

Using the same ordering of the edge set $\mathcal{E}$ as in the definition of $\mathcal{H}$, the rigidity function $r_{\mathcal{G}}(p) : \mathbb{R}^{dn} \to \mathbb{R}^m$ associated with the framework $(\mathcal{G}, p)$ is given as:

$$r_{\mathcal{G}}(p) = \frac{1}{2}\left[\cdots, \|\boldsymbol{p}_i - \boldsymbol{p}_j\|^2, \cdots\right]^\top, \ \ (i, j) \in \mathcal{E} \tag{6.2}$$

where the k-th component in $r_{\mathcal{G}}(p)$, $\|\boldsymbol{p}_i - \boldsymbol{p}_j\|^2$, corresponds to the squared length of the relative position vector $\boldsymbol{z}_k$ which connects the vertices i and j.

The rigidity of frameworks is then defined as follows.

Definition 6. *(see [Asimow and Roth, 1979]) A framework $(\mathcal{G}, \boldsymbol{p})$ is rigid in $\mathbb{R}^d$ if there exists a neighbourhood $\mathbb{U}$ of $\boldsymbol{p}$ such that $r_{\mathcal{G}}^{-1}(r_{\mathcal{G}}(\boldsymbol{p})) \cap \mathbb{U} = r_{\mathcal{K}}^{-1}(r_{\mathcal{K}}(\boldsymbol{p})) \cap \mathbb{U}$ where $\mathcal{K}$ is the complete graph with the same vertices as $\mathcal{G}$.*

In the following, the set of all frameworks $(\mathcal{G}, \boldsymbol{p})$ which satisfies the distance constraints is referred to as the set of *target formations*. Let $d_{k_{ij}}$ denotes the desired distance in the target formation which links agent i and j. We further define

$$e_{k_{ij}} = \|\boldsymbol{p}_i - \boldsymbol{p}_j\|^2 - (d_{k_{ij}})^2$$

to denote the squared distance error for edge k. Note we will also use e_k and d_k occasionally for notational convenience if no confusion is expected. Define the distance square error vector $\boldsymbol{e} = [\boldsymbol{e}_1, \boldsymbol{e}_2, \cdots, \boldsymbol{e}_m]^\top$.

One useful tool to characterize the rigidity property of a framework is the rigidity matrix $\boldsymbol{R} \in \mathbb{R}^{m \times dn}$, which is defined as

$$\boldsymbol{R}(\boldsymbol{p}) = \frac{\partial r_{\mathcal{G}}(\boldsymbol{p})}{\partial \boldsymbol{p}} \tag{6.3}$$

It is not difficult to see that each row of the rigidity matrix R takes the following form

$$[\mathbf{0}_{1\times d}, \cdots, (\boldsymbol{p}_i - \boldsymbol{p}_j)^\top, \cdots, \mathbf{0}_{1\times d}, \cdots, (\boldsymbol{p}_j - \boldsymbol{p}_i)^\top, \cdots, \mathbf{0}_{1\times d}] \tag{6.4}$$

Each edge gives rise to a row of $\boldsymbol{R}$, and, if an edge links vertices i and j, then the non-zero entries of the corresponding row of $\boldsymbol{R}$ are in the columns from $di-(d-1)$ to di and from $dj-(d-1)$ to dj. The equation (6.1) shows that the relative position vector lies in the image of $\bar{\mathcal{H}}$. Thus one can redefine the rigidity function, $g_{\mathcal{G}}(z) : Im(\bar{\mathcal{H}}) \to \mathbb{R}^m$ as $g_{\mathcal{G}}(z) = \frac{1}{2}\left[\|z_1\|^2, \|z_2\|^2, \cdots, \|z_m\|^2\right]^\top$. From (6.1) and (6.3), one can obtain the following simple form for the rigidity matrix

$$\boldsymbol{R}(\boldsymbol{p}) = \frac{\partial r_{\mathcal{G}}(\boldsymbol{p})}{\partial \boldsymbol{p}} = \frac{\partial r_{\mathcal{G}}(\boldsymbol{z})}{\partial \boldsymbol{z}} \frac{\partial \boldsymbol{z}}{\partial \boldsymbol{p}} = \boldsymbol{Z}^\top \bar{\mathcal{H}} \tag{6.5}$$

where $\boldsymbol{Z} = \text{diag}\{z_1, z_2, \cdots, z_m\}$.

The rigidity matrix will be used to determine the infinitesimal rigidity of the framework, as shown in the following definition.

Definition 7. *(see [Hendrickson, 1992]) A framework $(\mathcal{G}, p)$ is infinitesimally rigid in d-dimensional space if*

$$rank(R(p)) = dn - d(d+1)/2 \tag{6.6}$$

Specifically, if the framework is infinitesimally rigid in $\mathbb{R}^2$ (resp. $\mathbb{R}^3$) and has exactly $2n-3$ (resp. $3n-6$) edges, then it is called a minimally and infinitesimally rigid framework. Fig. 6.1 shows several examples on rigid and non-rigid formations. In this chapter we focus on the stabilization problem of minimally and infinitesimally rigid formations. [1] From the definition of infinitesimal rigidity, one can easily prove the following lemma:

Lemma 9. *If the framework $(\mathcal{G}, \boldsymbol{p})$ is minimally and infinitesimally rigid in the d-dimensional space, then the matrix $\boldsymbol{R}(\boldsymbol{p})\boldsymbol{R}(\boldsymbol{p})^\top$ is positive definite.*

Another useful observation shows that there exists a smooth function which maps the distance set of a minimally rigid framework to the distance set of its corresponding framework modelled by a *complete* graph.

Lemma 10. *Let $r_{\mathcal{G}}(q)$ be the rigidity function for a given infinitesimally minimally rigid framework $(\mathcal{G}, q)$ with agents' position vector q. Further let $\bar{r}_{\bar{\mathcal{G}}}(q)$ denote the rigidity function for an associated framework $(\bar{\mathcal{G}}, q)$, in which the vertex set remains the same as $(\mathcal{G}, q)$ but the*

[1] With some complexity of calculation, the results extend to non-minimally rigid formations (see [Mou et al., 2015; Sun et al., 2016b]).

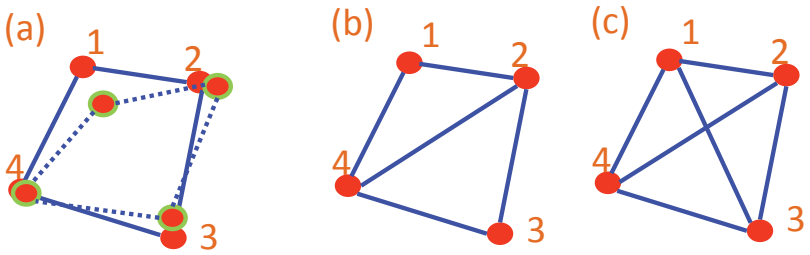

Figure 6.1: Examples on rigid and non-rigid formations. (a) non-rigid formation (a deformed formation with dashed lines is shown); (b) minimally rigid formation; (c) rigid but non-minimally rigid formation.

underlying graph is a complete one (i.e. there exist $n(n-1)/2$ edges which link any vertex pairs). Then there exists a continuously differentiable function $\pi : r_{\mathcal{G}}(q) \to \mathbb{R}^{n(n-1)/2}$ for which $\bar{r}_{\bar{\mathcal{G}}}(q) = \pi(r_{\mathcal{G}}(q))$ holds locally.

Lemma 10 indicates that all the edge distances in the framework $(\bar{\mathcal{G}}, q)$ modelled by a complete graph can be expressed locally in terms of the edge distances of a corresponding minimally infinitesimally rigid framework $(\mathcal{G}, q)$ via some smooth functions. The proof of the above Lemma is omitted here and can be found in [Mou et al., 2015]. We emphasize that **Lemma** 10 is important for later analysis of a distance error system (definition will be given in **Subsection** 6.3.1). **Lemma** 10 (together with **Lemma** 9) will enable us to obtain a self-contained distance error system so that the Lyapunov argument can be applied for convergence analysis.

6.2.2 Problem statement

The problem is formulated as follows.

Problem 5. *Consider a group of n agents in d-dimensional space modelled by single integrators*

$$\dot{\boldsymbol{p}}_i = \boldsymbol{u}_i, \quad i = 1, 2, \cdots, n \tag{6.7}$$

Design a distributed *control input $\boldsymbol{u}_i \in \mathbb{R}^n$ for each agent i in terms of $\boldsymbol{p}_i - \boldsymbol{p}_j$, $j \in \mathcal{N}_i$ with* event-triggered *control update such that $\|\boldsymbol{p}_i - \boldsymbol{p}_j\|$ converges to the desired distance $d_{k_{ij}}$ which forms a minimally and infinitesimally rigid formation.*

In this chapter, we propose two feasible event-triggered control algorithms (a centralized algorithm and a distributed algorithm) to solve this formation control problem.

6.3 Centralized control algorithm

This section focuses on the design of a feasible event-triggered formation control algorithm, by assuming that a centralized processor is available for collecting the

global information and broadcasting the trigger signal to all the agents such that their control inputs can be updated. The novel idea used for designing a simpler trigger function in this section will be useful for designing a feasible distributed version of an event-triggered formation control system, which will be reported in the next section.

6.3.1 Centralized algorithm design

We propose the following general form of event-triggered formation control system

$$\begin{aligned}\dot{\boldsymbol{p}}_i(t) &= \boldsymbol{u}_i(t) = \boldsymbol{u}_i(t_h) \\ &= \sum_{j\in\mathcal{N}_i}(\boldsymbol{p}_j(t_h) - \boldsymbol{p}_i(t_h))e_k(t_h)\end{aligned} \tag{6.8}$$

for $t \in [t_h, t_{h+1})$, where $h = 0, 1, 2, \cdots$ and t_h is the h-th trigger time for updating new information in the control input. Thus, the control input takes piecewise constant values in each time interval. In a compact form, the above position system can be written as

$$\dot{\boldsymbol{p}}(t) = -\boldsymbol{R}(\boldsymbol{p}(t_h))^\top \boldsymbol{e}(t_h) \tag{6.9}$$

Denote a vector $\boldsymbol{\delta}_i(t)$ as

$$\boldsymbol{\delta}_i(t) = \sum_{j\in\mathcal{N}_i}(\boldsymbol{p}_j(t) - \boldsymbol{p}_i(t))e_k(t) - \sum_{j\in\mathcal{N}_i}(\boldsymbol{p}_j(t_h) - \boldsymbol{p}_i(t_h))e_k(t_h) \tag{6.10}$$

for $t \in [t_h, t_{h+1})$. Then (6.8) can be equivalently stated as

$$\dot{\boldsymbol{p}}_i(t) = \boldsymbol{u}_i(t_h) = \sum_{j\in\mathcal{N}_i}(\boldsymbol{p}_j(t) - \boldsymbol{p}_i(t))e_k(t) - \boldsymbol{\delta}_i(t) \tag{6.11}$$

Define a vector $\boldsymbol{\delta}(t) = [\boldsymbol{\delta}_1(t)^\top, \boldsymbol{\delta}_2(t)^\top, \cdots, \boldsymbol{\delta}_n(t)^\top]^\top \in \mathbb{R}^{dn}$. Then there holds

$$\boldsymbol{\delta}(t) = \boldsymbol{R}(t_h)^\top \boldsymbol{e}(t_h) - \boldsymbol{R}(t)^\top \boldsymbol{e}(t) \tag{6.12}$$

which enables us to rewrite the compact form of the position system as

$$\dot{\boldsymbol{p}}(t) = -\boldsymbol{R}(t)^\top \boldsymbol{e}(t) - \boldsymbol{\delta}(t) \tag{6.13}$$

To deal with the position system with the event-triggered control input (6.8), we instead analyse the distance error system. By noting that $\dot{e}(t) = 2R(t)\dot{p}(t)$, the distance error system can be derived as

$$\begin{aligned}\dot{\boldsymbol{e}}(t) &= 2\boldsymbol{R}(t)\dot{\boldsymbol{p}}(t) \\ &= -2\boldsymbol{R}(t)\boldsymbol{R}(\boldsymbol{p}(t_h))^\top \boldsymbol{e}(t_h)) \ \ \forall t \in [t_h, t_{h+1})\end{aligned} \tag{6.14}$$

Note that all the entries of $\boldsymbol{R}(t)$ and $\boldsymbol{e}(t)$ contain the real-time values of $\boldsymbol{p}(t)$, and all the entries $\boldsymbol{R}(\boldsymbol{p}(t_h))$ and $\boldsymbol{e}(t_h)$ contain the piecewise-constant values $\boldsymbol{p}(t_h)$ during the

time interval $[t_h, t_{h+1})$.

The new form of the position system (6.13) also implies that the compact form of the distance error system can be written as

$$\dot{\boldsymbol{e}}(t) = -2\boldsymbol{R}(t)(\boldsymbol{R}(t)^\top \boldsymbol{e}(t) + \boldsymbol{\delta}(t)) \tag{6.15}$$

Consider the function $V = \frac{1}{4}\sum_{k=1}^{m} e_k^2$ as a Lyapunov-like function candidate for system (6.15). Similarly to the analysis in [Sun et al., 2015c], we define a sub-level set $\mathcal{B}(\rho) = \{\boldsymbol{e} : V(\boldsymbol{e}) \leq \rho\}$ for some suitably small ρ, such that when $\boldsymbol{e} \in \mathcal{B}(\rho)$ the formation is infinitesimally minimally rigid and $\boldsymbol{R}(\boldsymbol{p}(t))\boldsymbol{R}(\boldsymbol{p}(t))^\top$ is positive definite. Before giving the main proof, we record the following key result on the entries of the matrix $\boldsymbol{R}(\boldsymbol{p}(t))\boldsymbol{R}(\boldsymbol{p}(t))^\top$.

Lemma 11. *When the formation shape is close to the desired one such that the distance error e is in the set $\mathcal{B}(\rho)$, the entries of the matrix $\boldsymbol{R}(\boldsymbol{p}(t))\boldsymbol{R}(\boldsymbol{p}(t))^\top$ are continuously differentiable functions of $\boldsymbol{e}$.*

This lemma enables one to discuss the *self-contained* distance error system (6.15) and thus a Lyapunov argument can be applied to show the convergence of the distance errors. The proof of **Lemma** 11 can be found in [Mou et al., 2015] or [Sun et al., 2015d] and will not be presented here. From **Lemma** 11, one can show that

$$\begin{aligned}
\dot{V}(t) &= \frac{1}{2}\boldsymbol{e}(t)^\top \dot{\boldsymbol{e}}(t) = -\boldsymbol{e}(t)^\top \boldsymbol{R}(t)(\boldsymbol{R}(t)^\top \boldsymbol{e}(t) + \boldsymbol{\delta}(t)) \\
&= -\boldsymbol{e}(t)^\top \boldsymbol{R}(t)\boldsymbol{R}(t)^\top \boldsymbol{e}(t) - \boldsymbol{e}(t)^\top \boldsymbol{R}(t)\boldsymbol{\delta}(t) \\
&\leq -\|\boldsymbol{R}(t)^\top \boldsymbol{e}(t)\|^2 + \|\boldsymbol{e}(t)^\top \boldsymbol{R}(t)\|\|\boldsymbol{\delta}(t)\|
\end{aligned} \tag{6.16}$$

If we enforce the norm of $\boldsymbol{\delta}(t)$ to satisfy

$$\|\boldsymbol{\delta}(t)\| \leq \gamma \|\boldsymbol{R}(t)^\top \boldsymbol{e}(t)\| \tag{6.17}$$

and choose the parameter γ to satisfy $0 < \gamma < 1$, then we can guarantee that

$$\dot{V}(t) \leq (\gamma - 1)\|\boldsymbol{R}(t)^\top \boldsymbol{e}(t)\|^2 < 0 \tag{6.18}$$

This indicates that events are triggered when

$$f := \|\boldsymbol{\delta}(t)\| - \gamma \|\boldsymbol{R}(t)^\top \boldsymbol{e}(t)\| = 0 \tag{6.19}$$

The event time t_h is defined to satisfy $f(t_h) = 0$ for $h = 0, 1, \cdots$. For the time interval $t \in [t_h, t_{h+1})$, the control input is chosen as $\boldsymbol{u}(t) = \boldsymbol{u}(t_h)$ until the next event is triggered. Furthermore, every time an event is triggered, the event vector δ will be reset to zero.

We also show two key properties of the formation control system (6.8) with the above event function (6.19).

Lemma 12. *The formation centroid remains constant under the control of* (6.8) *with the event function* (6.19).

Proof. Denote by $\bar{\boldsymbol{p}}(t) \in \mathbb{R}^d$ the centre of the mass of the formation, i.e., $\bar{\boldsymbol{p}}(t) = \frac{1}{n}\sum_{i=1}^{n} \boldsymbol{p}_i(t) = \frac{1}{n}(\mathbf{1}_n \otimes I_d)^\top \boldsymbol{p}(t)$. One can show

$$\begin{aligned}\dot{\bar{\boldsymbol{p}}}(t) &= \frac{1}{n}(\mathbf{1}_n \otimes I_d)^\top \dot{\boldsymbol{p}}(t) \\ &= -\frac{1}{n}(\mathbf{1}_n \otimes I_d)^\top \boldsymbol{R}(\boldsymbol{p}(t_h))^\top \boldsymbol{e}(t_h) \\ &= -\frac{1}{n}\left(\boldsymbol{Z}(t_h)^\top \bar{\mathcal{H}}(\mathbf{1}_n \otimes I_d)\right)^\top \boldsymbol{e}(t_h) \end{aligned} \tag{6.20}$$

Note that $ker(\mathcal{H}) = span\{\mathbf{1}_n\}$ and therefore $ker(\bar{\mathcal{H}}) = span\{\mathbf{1}_n \otimes I_d\}$. Thus $\dot{\bar{\boldsymbol{p}}}(t) = 0$, which indicates that the formation centroid remains constant. □

The following lemma concerns the coordinate system requirement and enables each agent to use its local coordinate system to implement the control law, which is favourable for networked formation control systems in e.g. GPS denied environments.

Lemma 13. *To implement the controller* (6.8) *with the event-based control update condition in* (6.19)*, each agent can use its own local coordinate system which does not need to be aligned with a global coordinate system.*

The proof for the above lemma is omitted here, as it follows similar steps as in [Sun et al., 2015d, Lemma 4]. Note that **Lemma** 13 implies the event-based formation system (6.8) guarantees the $SE(N)$ invariance of the controller, which is a nice property to enable convenient implementation for networked control systems without coordinate alignment for each individual agent [Vasile et al., 2015].

We now arrive at the following main result of this section.

Theorem 10. *Suppose the target formation is infinitesimally and minimally rigid and the initial formation shape is close to the target one. By using the above control input* (6.8) *and the trigger function* (6.19)*, all the agents will reach the desired formation shape locally exponentially fast.*

Proof. The above analysis relating to Eq. (6.16)-(6.19) establishes boundedness of $\boldsymbol{e}(t)$ since $\dot{V}$ is non-positive. Now we show the exponential convergence of $\boldsymbol{e}(t)$ to zero will occur from a ball around the origin, which is equivalent to the desired formation shape being reached exponentially fast. According to **Lemma** 9, let $\bar{\lambda}_{\min}$ denote the smallest eigenvalue of $\boldsymbol{M}(\boldsymbol{e}) := \boldsymbol{R}(\boldsymbol{p})\boldsymbol{R}(\boldsymbol{p})^\top$ when $\boldsymbol{e}(\boldsymbol{p})$ is in the set $\mathcal{B}$ (i.e. $\bar{\lambda}_{\min} = \min_{e\in\mathcal{B}} \lambda(M(e)) > 0$). Note that $\bar{\lambda}_{\min}$ exists because the set $\mathcal{B}(\rho)$ is a compact set with respect to $\boldsymbol{e}$ and the eigenvalues of a matrix are continuous functions of the matrix elements. By recalling (6.18), there further holds

$$\dot{V}(t) \leq (\gamma - 1)\bar{\lambda}_{\min}\|\boldsymbol{e}(t)\|^2$$

Thus one concludes

$$\|\boldsymbol{e}(t)\| \leq \exp(-\kappa t)\|\boldsymbol{e}(0)\| \tag{6.21}$$

with the exponential decaying rate no less than $\kappa = 2(1-\gamma)\bar{\lambda}_{\min}$. □

Note that the convergence of the inter-agent distance error of itself does not directly guarantee the convergence of agents' positions $\boldsymbol{p}$ to some fixed points, even though it does guarantee convergence to a correct formation shape. This is because that the desired equilibrium corresponding to the correct rigid shape is not a single point, but is a set of equilibrium points induced by rotational and translation invariance (for a detailed discussion to this subtle point, see [Dorfler, 2008, Chapter 5]). A sufficient condition for this strong convergence to a stationary formation is guaranteed by the exponential convergence as proved above. To sum up, one has the following Lemma on the convergence of the position system (6.9) as a consequence of **Theorem** 10.

Lemma 14. *The event-triggered control law* (6.8) *and the event function* (6.19) *guarantee the convergence of* $\boldsymbol{p}(t)$ *to a fixed point.*

Remark 15. *We remark the above* ***Theorem*** *10 (as well as the subsequent results in later sections) concerns a* local *convergence. This is because that rigid formation shape control system is* non-linear *and exhibits* multiple *equilibria, which include the ones corresponding to correct shapes and those that do not correspond to the correct shape. It has been shown in [Anderson and Helmke, 2014] by using the tool of Morse Theory that multiple equilibria, including incorrect equilibria, are a consequence of any formation shape control algorithm which evolves in a steepest descent direction of a smooth cost function that is invariant under translations and rotations. A recent paper [Sun et al., 2015a] proves the instability of a set of degenerate equilibria that lives in a lower dimensional space. However, the stability property for more general equilibrium points is still unknown. It is in fact considered as a very challenging open problem to obtain an almost global convergence for general rigid formations, except for some special formation shapes such as 2-D triangular formation shape, or 2-D rectangular shape, or 3-D tetrahedral shape (see the review in [Oh et al., 2015]). We note that local convergence is still valuable in practice, if one assumes that initial shapes are close to the target ones (which is a very common assumption in most rigidity-based formation control works).*

6.3.2 Exclusion of Zeno behaviour

In the following we will show that the event-triggered system (6.8) does not exhibit Zeno behaviour. Note that the trigger function (6.19) involves the evolution of the term $\boldsymbol{R}(t)^\top \boldsymbol{e}(t)$, whose derivative is calculated as

$$\begin{aligned}\frac{\mathrm{d}(\boldsymbol{R}(t)^\top \boldsymbol{e}(t))}{\mathrm{d}t} =& \dot{\boldsymbol{R}}(t)^\top \boldsymbol{e}(t) + \boldsymbol{R}(t)^\top \dot{\boldsymbol{e}}(t) \\ =& \bar{\mathcal{H}}^\top \dot{\boldsymbol{Z}}(t)\boldsymbol{e}(t) \\ & - 2\boldsymbol{R}(t)^\top \boldsymbol{R}(t)(\boldsymbol{R}(t)^\top \boldsymbol{e}(t) + \boldsymbol{\delta}(t))\end{aligned}$$

According to the construction of the vector $\boldsymbol{\delta}(t)$ in (6.12), there also holds $\dot{\boldsymbol{\delta}}(t) = -\frac{\mathrm{d}(\boldsymbol{R}(t)^\top \boldsymbol{e}(t))}{\mathrm{d}t}$.

Before the proof, we first show a useful bound.

Lemma 15. *The following bound holds:*

$$\begin{aligned}\|\bar{\mathcal{H}}^\top \dot{\boldsymbol{Z}}(t)\boldsymbol{e}(t)\| &\leq \sqrt{d}\|\bar{\mathcal{H}}^\top\|\|\bar{\mathcal{H}}\|\|\boldsymbol{e}(t)\|\|\dot{\boldsymbol{p}}(t)\| \\ &\leq \sqrt{d}\|\bar{\mathcal{H}}^\top\|\|\bar{\mathcal{H}}\|\|\boldsymbol{e}(0)\|\|\boldsymbol{R}(t)^\top\boldsymbol{e}(t)+\boldsymbol{\delta}(t)\| \end{aligned} \tag{6.22}$$

Proof. We first show a trick to bound the term $\|\dot{\boldsymbol{Z}}(t)\boldsymbol{e}(t)\|$ by deriving an alternative expression for $\dot{\boldsymbol{Z}}(t)\boldsymbol{e}(t)$:

$$\begin{aligned}\dot{\boldsymbol{Z}}(t)\boldsymbol{e}(t) &= \operatorname{diag}\{\dot{\boldsymbol{z}}_1(t),\cdots,\dot{\boldsymbol{z}}_m(t)\}\boldsymbol{e}(t) \\ &= \begin{bmatrix} \boldsymbol{e}_1(t)\dot{\boldsymbol{z}}_1(t) \\ \boldsymbol{e}_2(t)\dot{\boldsymbol{z}}_2(t) \\ \vdots \\ \boldsymbol{e}_m(t)\dot{\boldsymbol{z}}_m(t) \end{bmatrix} \\ &= \left(\begin{bmatrix} \boldsymbol{e}_1(t) & 0 & \cdots & 0 \\ 0 & \boldsymbol{e}_2(t) & \cdots & 0 \\ \vdots & \vdots & \ddots & \vdots \\ 0 & 0 & \cdots & \boldsymbol{e}_m(t) \end{bmatrix} \otimes I_d\right) \begin{bmatrix} \dot{\boldsymbol{z}}_1(t) \\ \dot{\boldsymbol{z}}_2(t) \\ \vdots \\ \dot{\boldsymbol{z}}_m(t) \end{bmatrix} \\ &= (\boldsymbol{E}(t)\otimes I_d)\,\dot{\boldsymbol{z}}(t) \end{aligned} \tag{6.23}$$

where $\boldsymbol{E}(t)$ is defined as a diagonal matrix in the form $\boldsymbol{E}(t) = \operatorname{diag}\{\boldsymbol{e}_1(t),\boldsymbol{e}_2(t),\cdots,\boldsymbol{e}_m(t)\}$.

Note that $\boldsymbol{z}(t) = \bar{\mathcal{H}}\boldsymbol{p}(t)$ and thus $\dot{\boldsymbol{z}}(t) = \bar{\mathcal{H}}\dot{\boldsymbol{p}}(t)$. Then one has

$$\begin{aligned}\|\bar{\mathcal{H}}^\top \dot{\boldsymbol{Z}}(t)\boldsymbol{e}(t)\| &= \|\bar{\mathcal{H}}^\top\,(\boldsymbol{E}(t)\otimes I_d)\,\dot{\boldsymbol{z}}(t)\| \\ &\leq \|\bar{\mathcal{H}}^\top\|\|\,(\boldsymbol{E}(t)\otimes I_d)\,\|\|\bar{\mathcal{H}}\dot{\boldsymbol{p}}(t)\| \\ &\leq \|\bar{\mathcal{H}}^\top\|\|\bar{\mathcal{H}}\|\|\,(\boldsymbol{E}(t)\otimes I_d)\,\|_F\|\dot{\boldsymbol{p}}(t)\| \\ &\leq \sqrt{d}\|\bar{\mathcal{H}}^\top\|\|\bar{\mathcal{H}}\|\|\boldsymbol{e}(t)\|\|\boldsymbol{R}(t)^\top\boldsymbol{e}(t)+\boldsymbol{\delta}(t)\| \end{aligned} \tag{6.24}$$

where we have used the following facts

$$\begin{aligned}&\|\boldsymbol{E}(t)\| \leq \|\boldsymbol{E}(t)\|_F \\ &\|\,(\boldsymbol{E}(t)\otimes I_d)\,\|_F = \sqrt{d}\|\boldsymbol{E}(t)\|_F \\ &\|\boldsymbol{E}(t)\|_F = \|\boldsymbol{e}(t)\| \end{aligned}$$

The first inequality in (6.22) is thus proved. The second inequality in (6.22) is due to the fact that $\|\boldsymbol{e}(t)\| \leq \|\boldsymbol{e}(0)\|, \forall t > 0$ shown in (6.21). □

We now show that Zeno behaviour does not occur in the formation control system (6.8) with the trigger function (6.19) by proving a positive lower bound on the inter-event time interval.

Theorem 11. *The inter-event time interval* $\{t_{h+1} - t_h\}$ *is lower bounded by a positive value* τ

$$\tau = \frac{\gamma}{\alpha(1+\gamma)} > 0 \tag{6.25}$$

where

$$\alpha = \sqrt{d}\|\bar{\mathcal{H}}^\top\|\|\bar{\mathcal{H}}\|\|\boldsymbol{e}(0)\| + \sqrt{2}\bar{\lambda}_{max}(\boldsymbol{R}^\top\boldsymbol{R}(\boldsymbol{e})) > 0 \tag{6.26}$$

in which $\bar{\lambda}_{max}$ *denotes the largest eigenvalue of* $\boldsymbol{R}^\top\boldsymbol{R}(\boldsymbol{e})$ *when* $\boldsymbol{e}(\boldsymbol{p})$ *is in the set* $\mathcal{B}$ *(i.e.* $\bar{\lambda}_{max} = \max_{\boldsymbol{e}\in\mathcal{B}} \lambda(\boldsymbol{R}^\top\boldsymbol{R}(\boldsymbol{e})) > 0$*), and* γ *is a parameter designed in* (6.19) *which satisfies* $\gamma \in (0,1)$*. Thus, Zeno behaviour will not occur for the rigid formation control system* (6.8) *with the trigger function* (6.19).

Proof. We show the growth of $\|\delta\|$ from zero to the trigger threshold value $\gamma\|\boldsymbol{R}^\top\boldsymbol{e}\|$ needs to take a positive time interval. To show this, the relative growth rate on $\|\delta(t)\|/\|\boldsymbol{R}(t)^\top\boldsymbol{e}(t)\|$ is considered. The following proof is inspired by the one used in [Tabuada, 2007]. In the following derivation, we omit the argument of time t but it should be clear that each state variable and vector is considered as a function of t.

$$\begin{aligned}
\frac{\mathrm{d}}{\mathrm{d}t}\frac{\|\delta\|}{\|\boldsymbol{R}^\top\boldsymbol{e}\|} &\le \left(1+\frac{\|\delta\|}{\|\boldsymbol{R}^\top\boldsymbol{e}\|}\right)\frac{\|\dot{\boldsymbol{R}}^\top\boldsymbol{e}+\boldsymbol{R}^\top\dot{\boldsymbol{e}}\|}{\|\boldsymbol{R}^\top\boldsymbol{e}\|} \\
&= \left(1+\frac{\|\delta\|}{\|\boldsymbol{R}^\top\boldsymbol{e}\|}\right)\frac{\|\bar{\mathcal{H}}^\top\dot{\boldsymbol{Z}}\boldsymbol{e}+\boldsymbol{R}^\top\dot{\boldsymbol{e}}\|}{\|\boldsymbol{R}^\top\boldsymbol{e}\|} \\
&\le \left(1+\frac{\|\delta\|}{\|\boldsymbol{R}^\top\boldsymbol{e}\|}\right)\left(\frac{\sqrt{d}\|\bar{\mathcal{H}}^\top\|\|\bar{\mathcal{H}}\|\|\boldsymbol{e}\|\|\dot{\boldsymbol{p}}\| + \|2\boldsymbol{R}^\top\boldsymbol{R}(\boldsymbol{R}^\top\boldsymbol{e}+\delta)\|}{\|\boldsymbol{R}^\top\boldsymbol{e}\|}\right) \\
&\quad \text{(appealing to } \textbf{Lemma } 15\text{)} \\
&\le \left(1+\frac{\|\delta\|}{\|\boldsymbol{R}^\top\boldsymbol{e}\|}\right)\left((\sqrt{d}\|\bar{\mathcal{H}}^\top\|\|\bar{\mathcal{H}}\|\|\boldsymbol{e}(0)\| + \|2\boldsymbol{R}^\top\boldsymbol{R}\|)\left(1+\frac{\|\delta)\|}{\|\boldsymbol{R}^\top\boldsymbol{e}\|}\right)\right) \\
&\le \alpha\left(1+\frac{\|\delta\|}{\|\boldsymbol{R}^\top\boldsymbol{e}\|}\right)^2
\end{aligned} \tag{6.27}$$

where α is defined in (6.26). Note that $\bar{\lambda}_{\max}$ always exists and is finite (i.e. upper bounded) because the set $\mathcal{B}(\rho)$ is a compact set with respect to $\boldsymbol{e}$ and the eigenvalues of a matrix are continuous functions of the matrix elements. Thus, α defined in (6.26) exists, which is positive and upper bounded. If we denote $\frac{\|\delta\|}{\|\boldsymbol{R}^\top\boldsymbol{e}\|}$ by y we have the estimate $\dot{y}(t) \le \alpha(1+y(t))^2$. By the comparison principle there holds $y(t) \le \phi(t,\phi_0)$ where $\phi(t,\phi_0)$ is the solution of $\dot{\phi} = \alpha(1+\phi)^2$ with initial condition $\phi(0,\phi_0) = \phi_0$.

Solving the differential equation for ϕ in the time interval $t \in [t_h, t_{h+1})$ yields $\phi(\tau,0) = \frac{\tau\alpha}{1-\tau\alpha}$. The inter-execution time interval is thus bounded by the time it takes for ϕ to evolve from 0 to γ. Solving the above equation, one obtains a positive lower bound for the inter-event time interval $\tau = \frac{\gamma}{\alpha(1+\gamma)}$. Thus, Zeno behaviour is excluded

for the formation control system (6.8). The proof is completed. □

Remark 16. *We review several event-triggered formation strategies reported in the literature and highlight the advantages of the event-triggered algorithms proposed in this section. In [Sun et al., 2015c], the trigger function is based on the information of the distance error* $\boldsymbol{e}$ *only, which cannot guarantee a pure piecewise-constant update of the formation control input. The trigger function designed in [Liu et al., 2015] is based on the information of the relative position* $\boldsymbol{z}$*, while the trigger function designed [Bai et al., 2015] is based on the absolute position* $\boldsymbol{p}$*. It is noted that trigger conditions such as those in [Liu et al., 2015] and [Bai et al., 2015] are very complicated, which may limit their practical applications. The trigger function* (6.19) *designed in this section involves the term* $\boldsymbol{R}^\top \boldsymbol{e}$*, in which the information of the relative position* $\boldsymbol{z}$ *(involved in the entries of the rigidity matrix* $\boldsymbol{R}$*) and of the distance error* $\boldsymbol{e}$ *has been included. Such a trigger function greatly reduces the controller complexity while at the same time also maintains the discrete-time update nature of the control input.*

6.4 Distributed control algorithm

6.4.1 Distributed algorithm design

In this subsection we will further show how to design a distributed event-triggered formation control algorithm in the sense that each agent can use only local measurements in terms of relative positions with respect to its neighbours to determine the next event time and control update value. Denote the event time for each agent i as $t_0^i, t_1^i, \cdots, t_h^i, \cdots$. The dynamical system for agent i to achieve the desired inter-agent distances is now rewritten as

$$\dot{\boldsymbol{p}}_i(t) = \boldsymbol{u}_i(t) = \boldsymbol{u}_i(t_h^i), t \in [t_h^i, t_{h+1}^i) \tag{6.28}$$

and we aim to design a distributed trigger function such that the control input for agent i is updated at its own event times $t_0^i, t_1^i, \cdots, t_h^i, \cdots$ based on local information.

We consider the same Lyapunov function candidate as the one in **Section** 6.3, but calculate the derivative as follows:

$$\begin{aligned}
\dot{V}(t) =& \frac{1}{2}\boldsymbol{e}(t)^\top \dot{\boldsymbol{e}}(t) = -\boldsymbol{e}(t)^\top \boldsymbol{R}(t)(\boldsymbol{R}(t)^\top \boldsymbol{e}(t) + \boldsymbol{\delta}(t)) \\
=& -\boldsymbol{e}(t)^\top \boldsymbol{R}(t)\boldsymbol{R}(t)^\top \boldsymbol{e}(t) - \boldsymbol{e}^\top \boldsymbol{R}(t)\boldsymbol{\delta}(t) \\
\leq& -\|\boldsymbol{R}(t)^\top \boldsymbol{e}(t)\|^2 + \|\boldsymbol{e}(t)^\top \boldsymbol{R}(t)\boldsymbol{\delta}(t)\| \\
\leq& -\sum_{i=1}^{n} \|\{\boldsymbol{R}(t)^\top \boldsymbol{e}(t)\}_i\|^2 + \sum_{i=1}^{n} \|\{\boldsymbol{R}(t)^\top \boldsymbol{e}(t)\}_i\| \|\boldsymbol{\delta}_i(t)\|
\end{aligned} \tag{6.29}$$

where $\{\boldsymbol{R}(t)^\top \boldsymbol{e}(t)\}_i \in \mathbb{R}^d$ is a vector block taken from the $(di-d+1)$th to the (di)th entries of the vector $\boldsymbol{R}(t)^\top \boldsymbol{e}(t)$, and $\boldsymbol{\delta}_i(t)$ is a vector block taken from the $(di-d+1)$th to the (di)th entries of the vector $\boldsymbol{\delta}(t)$. According to the definition of the rigidity matrix in (6.4), it is obvious that $\{\boldsymbol{R}(t)^\top \boldsymbol{e}(t)\}_i$ only involves local information of

agent i in terms of relative position vectors $z_{k_{ij}}$ and distance errors $e_{k_{ij}}$ with $j \in \mathcal{N}_i$. Based on this, the control input for agent i is designed as

$$\begin{aligned}\dot{\boldsymbol{p}}_i(t) = \boldsymbol{u}_i(t_h^i) &= \sum_{j\in\mathcal{N}_i}(\boldsymbol{p}_j(t_h^i) - \boldsymbol{p}_i(t_h^i))e_k(t_h^i)) \\ &= \{\boldsymbol{R}(t_h^i)^\top \boldsymbol{e}(t_h^i)\}_i, \;\; t \in [t_h^i, t_{h+1}^i)\end{aligned} \tag{6.30}$$

Note that there holds

$$\boldsymbol{\delta}_i(t) = \{\boldsymbol{R}(t_h^i)^\top \boldsymbol{e}(t_h^i)\}_i - \{\boldsymbol{R}(t)^\top \boldsymbol{e}(t)\}_i \tag{6.31}$$

and we can rewrite (6.30) as $\dot{\boldsymbol{p}}_i(t) = -\{\boldsymbol{R}(t)^\top \boldsymbol{e}(t)\}_i - \boldsymbol{\delta}_i(t), t \in [t_h^i, t_{h+1}^i)$.

By using the inequality $\|\{\boldsymbol{R}(t)^\top \boldsymbol{e}(t)\}_i\|\|\boldsymbol{\delta}_i(t)\| \leq \frac{1}{2a_i}\|\boldsymbol{\delta}_i(t)\|^2 + \frac{a_i}{2}\|\{\boldsymbol{R}(t)^\top \boldsymbol{e}(t)\}_i\|^2$ with $a_i \in (0,1)$, the above inequality (6.29) on $\dot{V}$ can be further derived as

$$\begin{aligned}\dot{V}(t) \leq &-\sum_{i=1}^n \|\{\boldsymbol{R}(t)^\top \boldsymbol{e}(t)\}_i\|^2 \\ &+ \sum_{i=1}^n \frac{a_i}{2}\|\{\boldsymbol{R}(t)^\top \boldsymbol{e}(t)\}_i\|^2 + \sum_{i=1}^n \frac{1}{2a_i}\|\boldsymbol{\delta}_i(t)\|^2 \\ = &-\sum_{i=1}^n \frac{2-a_i}{2}\|\{\boldsymbol{R}(t)^\top \boldsymbol{e}(t)\}_i\|^2 + \sum_{i=1}^n \frac{1}{2a_i}\|\boldsymbol{\delta}_i(t)\|^2\end{aligned}$$

If we enforce the norm of $\boldsymbol{\delta}_i(t)$ to satisfy

$$\frac{1}{2a_i}\|\boldsymbol{\delta}_i(t)\|^2 \leq \gamma_i \frac{2-a_i}{2}\|\{\boldsymbol{R}(t)^\top \boldsymbol{e}(t)\}_i\|^2 \tag{6.32}$$

with $\gamma_i \in (0,1)$, we can guarantee

$$\dot{V}(t) \leq \sum_{i=1}^n (\gamma_i - 1)\frac{2-a_i}{2}\|\{\boldsymbol{R}(t)^\top \boldsymbol{e}(t)\}_i\|^2 \tag{6.33}$$

This implies that one can design a local trigger function for agent i as

$$f_i(t) := \|\boldsymbol{\delta}_i(t)\|^2 - \gamma_i a_i(2-a_i)\|\{\boldsymbol{R}(t)^\top \boldsymbol{e}(t)\}_i\|^2 \tag{6.34}$$

and the event time t_h^i for agent i is defined to satisfy $f_i(t_h^i) = 0$ for $h = 0, 1, 2, \cdots$. For the time interval $t \in [t_h^i, t_{h+1}^i)$, the control input is chosen as $\boldsymbol{u}_i(t) = \boldsymbol{u}_i(t_h^i)$ until the next event is triggered. Furthermore, every time when an event is triggered for agent i, the local event vector $\boldsymbol{\delta}_i$ will be reset to zero.

The convergence result is summarized as follows.

Theorem 12. *Suppose the target formation is infinitesimally and minimally rigid and the initial formation shape is close to the target one. By using the control input* (6.30) *and the distributed trigger function* (6.34)*, all the agents will reach the desired formation shape locally exponentially fast.*

Proof. The analysis is similar to **Theorem** 10 and we omit several steps here. Based on the derivation in Eqs. (6.29)-(6.34), one can conclude that

$$\|\boldsymbol{e}(t)\| \leq \exp(-\kappa t)\|\boldsymbol{e}(0)\| \tag{6.35}$$

with the exponential rate no less than $\kappa = 2\zeta_{\min}\bar{\lambda}_{\min}$ where $\zeta_{\min} = \min_i(1-\gamma_i)^{\frac{2-a_i}{2}}$. □

The exponential convergence of $\boldsymbol{e}(t)$ implies that the proposed distributed event-triggered control algorithm (6.30) also guarantees the convergence of $\boldsymbol{p}$ to a fixed point, by which one can conclude a similar result as the one in **Lemma** 14.

For the formation system with the distributed event-triggered control algorithm, an analogous result to **Lemma** 13 on coordinate system requirement is as follows.

Lemma 16. *To implement the distributed control input* (6.30)*, each agent can use its own local coordinate system to measure the relative positions to its neighbours and a global coordinate system is not required. Furthermore, to detect the distributed trigger condition* (6.32)*, a local coordinate system is sufficient which is not required to be aligned with the global coordinate system.*

Proof. The proof of the first statement on the distributed control input (6.30) follows similar steps as in [Sun et al., 2015d, Lemma 4] and is omitted here. We then prove the second statement on the event condition (6.32). Suppose agent i's position in a global coordinate system is measured as $\boldsymbol{p}_i^g$, while $\boldsymbol{p}_i^i$ and $\boldsymbol{p}_j^i$ stand for agent i and its neighbouring agent j's positions measured in agent i's local coordinate system. Clearly, there exist a rotation matrix $\mathcal{Q}_i \in \mathbb{R}^{d\times d}$ and a translation vector $\boldsymbol{\vartheta}_i \in \mathbb{R}^d$, such that $\boldsymbol{p}_j^i = \mathcal{Q}_i\boldsymbol{p}_j^g + \vartheta_i$. We also denote the relative position between agent i and agent j as $\boldsymbol{z}_{k_{ij}}^i$ measured by agent i's local coordinate system, and $\boldsymbol{z}_{k_{ij}}^g$ measured by the global coordinate system. Obviously there holds $\boldsymbol{z}_{k_{ij}}^i = \boldsymbol{p}_j^i - \boldsymbol{p}_i^i = \mathcal{Q}_i(\boldsymbol{p}_j^g - \boldsymbol{p}_i^g) = \mathcal{Q}_i\boldsymbol{z}_{k_{ij}}^g$ and thus $\|\boldsymbol{z}_{k_{ij}}^i\| = \|\boldsymbol{z}_{k_{ij}}^g\|$. Also notice that the trigger condition (6.32) involves the terms $\boldsymbol{\delta}_i$ and $\{\boldsymbol{R}(t)^\top\boldsymbol{e}(t)\}_i$ which are functions of the relative position vector $\boldsymbol{z}$, and thus event detection using (6.34) remains unchanged regardless of what coordinate systems are used. Since $\mathcal{Q}_i$ and $\boldsymbol{\vartheta}_i$ are chosen arbitrarily, the above analysis concludes that the detection of the local event condition (6.34) is independent of a global coordinate basis, which implies that agent i's local coordinate system is sufficient to implement (6.32). □

The above lemma indicates that the distributed event-triggered control input (6.30) and distributed trigger function (6.34) still guarantee the $SE(N)$ invariance property and enables a convenient implementation for the proposed formation control system without coordinate alignment for each individual agent.

Differently to **Lemma** 12, we show that the distributed event-based control algorithm proposed in this section cannot guarantee a fixed formation centroid.

Lemma 17. *The position of the formation centroid is not guaranteed to be fixed when the distributed event-based control algorithm* (6.30) *and trigger function* (6.34) *are applied.*

Proof. The dynamics for the formation centroid can be derived as

$$\dot{\bar{\boldsymbol{p}}}(t) = \frac{1}{n}(\mathbf{1}_n \otimes I_d)^\top \dot{\boldsymbol{p}}(t)$$

However, due to the *asymmetric* update of each agent's control input by using the local event function (6.34) to determine a local event time, one cannot decompose the vector $\dot{\boldsymbol{p}}(t)$ into terms involving $\bar{\mathcal{H}}$ and a single distance error vector as in (6.20). Thus $\dot{\bar{\boldsymbol{p}}}(t)$ is not guaranteed to be zero and there exist motions for the formation centroid when the distributed event-based control input (6.30) is applied. □

Remark 17. *We note a key property of the distributed event-triggered control algorithm* ((6.30) *and* (6.34)*) proposed in this section. It is obvious from* (6.30) *and* (6.34) *that each agent i updates its own control input by using only local information in terms of relative positions of its neighbours (which can be measured by agent i's local coordinate system), and is not affected by the control input updates from its neighbours. Thus, such local event-triggered algorithm does not require any communication between any two agents.*

6.4.2 Trigger behaviour analysis

In this subsection we will further discuss the possibility of Zeno behaviour in the distributed event-triggered formation system (6.30).

Theorem 13. *(Exclusion of Zeno behaviour) Consider the distributed formation system with the distributed event-triggered control input* (6.30) *and the distributed trigger function* (6.34)*.*

- *At least one agent does not exhibit Zeno behaviour.*
- *In addition, if there exists $\epsilon > 0$ such that $\|\{\boldsymbol{R}(t)^\top \boldsymbol{e}(t)\}_i\|^2 \geq \epsilon \|\boldsymbol{e}(t)\|^2$ for all $i = 1, 2, \cdots, n$ and $t \geq 0$, then there exists a common positive lower bound for any inter-event time interval for each agent. In this case, no agent will exhibit Zeno behaviour.*

Proof. Note that $\|\boldsymbol{\delta}_i(t)\|^2 \leq \|\boldsymbol{\delta}(t)\|^2$ for any i. In addition, there exists an agent i_* such that $\|\{\boldsymbol{R}(t)^\top \boldsymbol{e}(t)\}_{i_*}\|^2 \geq \frac{1}{m}\|\{\boldsymbol{R}(t)^\top \boldsymbol{e}(t)\}\|^2$. Then one has

$$\frac{\|\boldsymbol{\delta}_{i_*}(t)\|}{\|\{\boldsymbol{R}(t)^\top \boldsymbol{e}(t)\}_{i_*}\|} \leq \sqrt{m}\frac{\|\boldsymbol{\delta}(t)\|}{\|\{\boldsymbol{R}(t)^\top \boldsymbol{e}(t)\}\|} \tag{6.36}$$

By recalling the proof in **Theorem** 11, we can conclude that the inter-event interval for agent i_* is bounded from below by a time τ_{i_*} that satisfies

$$\sqrt{m}\frac{\tau_{i_*}\alpha}{1 - \tau_{i_*}\alpha} = \sqrt{\gamma_{i_*} a_{i_*}(2 - a_{i_*})} \tag{6.37}$$

So that $\tau_{i_*} = \frac{\sqrt{\gamma_{i_*} a_{i_*}(2-a_{i_*})}}{\alpha(\sqrt{m}+\sqrt{\gamma_{i_*} a_{i_*}(2-a_{i_*})})} > 0$. The first statement is proved.

We then prove the second statement. Denote $\bar{\lambda}_{\max}$ as the maximum of $\lambda_{\max}(R^T R(e))$ for all $e \in \mathcal{B}(\rho)$. Since $\mathcal{B}(\rho)$ is a compact set, $\bar{\lambda}_{\max}$ exists and is bounded. Then there

holds $\|\{\boldsymbol{R}(t)^\top \boldsymbol{e}(t)\}\|^2 \leq \bar{\lambda}_{\max}\|\boldsymbol{e}(t)\|^2$. One can further show

$$\|\{\boldsymbol{R}(t)^\top \boldsymbol{e}(t)\}_i\|^2 \geq \epsilon\|\boldsymbol{e}(t)\|^2 \geq \frac{\epsilon}{\bar{\lambda}_{\max}}\|\{\boldsymbol{R}(t)^\top \boldsymbol{e}(t)\}\|^2 \tag{6.38}$$

By following similar argument as above and using the analysis in the proof of **Theorem** 11, a lower bound of the inter-event interval $\bar{\tau}_i$ for each agent can be calculated as

$$\bar{\tau}_i = \frac{\sqrt{\varrho_i}}{\alpha\left(\sqrt{\frac{\bar{\lambda}_{\max}}{\epsilon}} + \sqrt{\varrho_i}\right)} > 0,\ i = 1, 2, \cdots, n \tag{6.39}$$

□

Remark 18. *The first part of* ***Theorem*** *13 is motivated by [Dimarogonas et al., 2012, Theorem 4], which guarantees the exclusion of Zeno behaviour for at least one agent. To improve the result for all the agents, we propose a condition in the second part of* ***Theorem*** *13. The above results in* ***Theorem*** *13 are more conservative than the centralized case. The condition on the existence of $\epsilon > 0$ essentially guarantees that $\|\{\boldsymbol{R}(t)^\top \boldsymbol{e}(t)\}_i\|$ cannot be zero at any finite time, and will be zero if and only if $t = \infty$. We have performed many simulations with different rigid formation shapes and observed that in most cases $\|\{\boldsymbol{R}(t)^\top \boldsymbol{e}(t)\}_i\|$ is non-zero. We conjecture that this may be due to the infinitesimal rigidity of the formation shape. In the next section, we will provide a simple modification of the distributed trigger function to remove the condition on ϵ.*

6.4.3 A modified distributed trigger function

The trigger function (6.34) for agent i involves the comparison of two terms, i.e. $\|\boldsymbol{\delta}_i(t)\|^2$ and $\gamma_i a_i(2 - a_i)\|\{\boldsymbol{R}(t)^\top \boldsymbol{e}(t)\}_i\|^2$. As noted above, the existence of $\epsilon > 0$ can guarantee $\|\{\boldsymbol{R}(t)^\top \boldsymbol{e}(t)\}_i\| \neq 0$ for any finite time t. To remove this condition in **Theorem** 13, we propose the following modified trigger function by including an exponential decay term:

$$\begin{aligned} f_i(t) := \|\boldsymbol{\delta}_i(t)\|^2 - \gamma_i a_i(2 - a_i)\|\{\boldsymbol{R}(t)^\top \boldsymbol{e}(t)\}_i\|^2 \\ - 2a_i v_i \exp(-\theta_i t) \end{aligned} \tag{6.40}$$

where $v_i > 0, \theta_i > 0$ are parameters that can be adjusted in the design to control the formation convergence speed. Note that $v_i \exp(-\theta_i t)$ is always positive and converges to zero when $t \to \infty$. Thus, even if $\{\boldsymbol{R}(t)^\top \boldsymbol{e}(t)\}_i$ exhibits crossing-zero scenario at some finite time instant, the addition of this decay term guarantees a positive threshold value in the event function which avoids the case of comparing $\|\boldsymbol{\delta}_i(t)\|^2$ to a zero threshold.

The main result in this subsection is to show that the above modified trigger function ensures Zeno-free trigger for all agents, and also drives the formation shape to reach the target one.

Theorem 14. *By using the proposed distributed event-based formation controller* (6.30) *and the modified distributed trigger function* (6.40)*, all the agents will reach the desired formation shape locally asymptotically and no agent will exhibit Zeno behaviour.*

Proof. We consider the same Lyapunov function as used in **Theorem** 10 and follow similar steps as above. The trigger condition from the modified trigger function (6.40) yields

$$\dot{V}(t) \leq \sum_{i=1}^{n}(\gamma_i - 1)\frac{2-a_i}{2}\|\{\boldsymbol{R}(t)^\top \boldsymbol{e}(t)\}_i\|^2 + v_i \exp(-\theta_i t) \tag{6.41}$$

which follows that

$$\dot{V}(t) \leq -4\zeta_{\min}\bar{\lambda}_{\min} V(t) + \sum_{i=1}^{n} v_i \exp(-\theta_i t) \tag{6.42}$$

where $\zeta_{\min}$ is defined as the same to the notation in **Theorem** 12 (i.e. $\zeta_{\min} = \min_i(1-\gamma_i)\frac{2-a_i}{2}$). For notational convenience, we define $\kappa = 2\zeta_{\min}\bar{\lambda}_{\min}$ (also the same to **Theorem** 12). By the well-known comparison principle [Khalil and Grizzle, 1996, Chapter 3.4], it further follows that

$$V(t) \leq \exp(-2\kappa t)V(0) + \sum_{i=1}^{n}\frac{v_i}{2\kappa - \theta_i}(\exp(-\theta_i t) - \exp(-2\kappa t)) \tag{6.43}$$

which implies that $V(t) \to 0$ as $t \to \infty$, or equivalently, $\|\boldsymbol{e}(t)\| \to 0$, as $t \to \infty$. In the following analysis of excluding Zeno behaviour we let $t \in [t_h^i, t_{h+1}^i)$. We first show a sufficient condition to guarantee $f_i(t) \leq 0$ when $f_i(t)$ is defined in (6.40). Note that $f_i(t) \leq 0$ can be equivalently stated as

$$\begin{aligned}&(\varrho_i + 1)\|\boldsymbol{\delta}_i(t)\|^2 \\ &\leq \varrho_i(\|\boldsymbol{\delta}_i(t)\|^2 + \|\{\boldsymbol{R}(t)^\top \boldsymbol{e}(t)\}_i\|^2) + 2a_i v_i \exp(-\theta_i t)\end{aligned} \tag{6.44}$$

where $\varrho_i := \gamma_i a_i(2-a_i)$. Note that

$$\begin{aligned}\|\{\boldsymbol{R}(t_h^i)^\top \boldsymbol{e}(t_h^i)\}_i\|^2 =& \|\boldsymbol{\delta}_i(t) + \{\boldsymbol{R}(t)^\top \boldsymbol{e}(t)\}_i\|^2 \\ \leq& 2(\|\boldsymbol{\delta}_i(t)\|^2 + \|\{\boldsymbol{R}(t)^\top \boldsymbol{e}(t)\}_i\|^2)\end{aligned} \tag{6.45}$$

Thus, a sufficient condition to guarantee the above inequality (6.44) (and the inequality $f_i(t) \leq 0$) is

$$\|\boldsymbol{\delta}_i(t)\|^2 \leq \frac{\varrho_i}{(2\varrho_i + 2)}\|\{\boldsymbol{R}(t_h^i)^\top \boldsymbol{e}(t_h^i)\}_i\|^2 + \frac{2a_i v_i}{\varrho_i + 1}\exp(-\theta_i t) \tag{6.46}$$

Note that from (6.12) there holds $\dot{\boldsymbol{\delta}}_i = -\frac{\mathrm{d}}{\mathrm{d}t}\{\boldsymbol{R}(t)^\top \boldsymbol{e}(t)\}_i$. It follows that

$$\begin{aligned}
\frac{\mathrm{d}}{\mathrm{d}t}\|\boldsymbol{\delta}_i(t)\| &\leq \frac{\|\boldsymbol{\delta}_i(t)^\top\|}{\|\boldsymbol{\delta}_i(t)\|}\|\dot{\boldsymbol{\delta}}_i(t)\| \\
&= \|\frac{\mathrm{d}}{\mathrm{d}t}\{\boldsymbol{R}(t)^\top \boldsymbol{e}(t)\}_i\| \\
&= \|\sum_{j\in\mathcal{N}_i}(\dot{\boldsymbol{p}}_j(t) - \dot{\boldsymbol{p}}_i(t))e_k(t) + \sum_{j\in\mathcal{N}_i}(\boldsymbol{p}_j(t) - \boldsymbol{p}_i(t))\dot{e}_k(t)\| \\
&= \|\sum_{j\in\mathcal{N}_i}(e_{k_{ij}}(t)\otimes I_d + 2\boldsymbol{z}_{k_{ij}}(t)\boldsymbol{z}_{k_{ij}}(t)^\top)(\dot{\boldsymbol{p}}_j(t) - \dot{\boldsymbol{p}}_i(t))\| \\
&= \|\sum_{j\in\mathcal{N}_i}\boldsymbol{Q}_{ij}(t)(\{\boldsymbol{R}(t^j_{h'})^\top e(t^j_{h'})\}_j - \{\boldsymbol{R}(t^i_h)^\top e(t^i_h)\}_i)\| \\
&\leq \sum_{j\in\mathcal{N}_i}\|\boldsymbol{Q}_{ij}(t)\|\|(\{\boldsymbol{R}(t^j_{h'})^\top e(t^j_{h'})\}_j - \{\boldsymbol{R}(t^i_h)^\top e(t^i_h)\}_i)\| \\
&:= \alpha_i
\end{aligned} \tag{6.47}$$

where $\boldsymbol{Q}_{ij}(t) := e_{k_{ij}}(t)\otimes I_d + 2\boldsymbol{z}_{k_{ij}}(t)\boldsymbol{z}_{k_{ij}}(t)^\top$, and $t^j_{h'} = \arg\max_h\{t^j_h | t^j_h \leq t, j\in\mathcal{N}_i\}$. Note that α_i is upper bounded by a positive constant which implies that $\frac{\mathrm{d}}{\mathrm{d}t}\|\boldsymbol{\delta}_i(t)\|$ is upper bounded. From the sufficient condition given in (6.46) which guarantees the event triggering condition $f_i(t)\leq 0$ shown in (6.40), the next inter-event interval for agent i is lower bounded by the solution τ^i_h of the following equation

$$\tau^i_h\alpha_i = \sqrt{\frac{\varrho_i}{(2\varrho_i+2)}\|\{\boldsymbol{R}(t^i_h)^\top \boldsymbol{e}(t^i_h)\}_i\|^2 + \frac{2a_iv_i}{\varrho_i+1}\exp(-\theta_i(t^i_h+\tau^i_h))} \tag{6.48}$$

such a solution always exists and is positive. Thus, no agents will exhibit Zeno behaviour with the modified event function (6.40). □

6.5 Simulation results

In this section we provide three simulation examples to show the performance of certain formations with centralized event-triggered control algorithm and distributed event-triggered control algorithm, respectively. Consider a double tetrahedron formation in the 3-D space, with the desired distances for each edge being 2. The initial conditions for each agent are chosen as $\boldsymbol{p}_1(0) = [0,-1.0,0.5]^\top$, $\boldsymbol{p}_2(0) = [1.8,1.6,-0.1]^\top$, $\boldsymbol{p}_3(0) = [-0.2,1.8,0.05]^\top$, $\boldsymbol{p}_4(0) = [1.2,1.9,1.7]^\top$ and $\boldsymbol{p}_5(0) = [-1.0,-1.5,-1.2]^\top$, so that the initial formation is close to the target one. The parameter γ in the trigger function is set as $\gamma = 0.6$. **Figs.** 6.2-6.4 illustrate formation convergence and event performance with centralized event triggering function. The trajectories of each agent, together with the initial shape and final shape are depicted in **Fig.** 6.2. The trajectories of each distance error are depicted in **Fig.** 6.3, which shows an exponential convergence to the origin. **Fig.** 6.4 shows the triggering time instant and the evolution of the norm of the vector $\boldsymbol{\delta}$ in the triggering function (6.19), which is

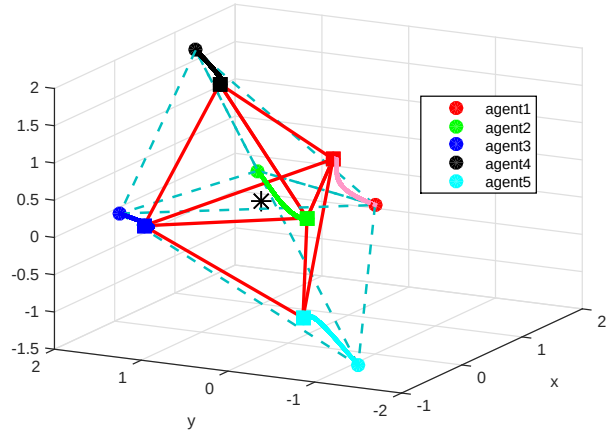

Figure 6.2: Simulation on stabilization control of a double tetrahedron formation in 3-D space with centralized algorithm. The initial and final positions are denoted by circles and squares, respectively. The initial formation is denoted by dashed lines, and the final formation is denoted by red solid lines. The black star denotes the formation centroid, which is stationary.

obviously bounded below by $\gamma\|\boldsymbol{R}(t)^\top \boldsymbol{e}(t)\|$ as required by (6.17).

We then perform another simulation on stabilizing the same formation shape by applying the proposed distributed event-triggered control input (6.30) and distributed trigger function (6.34). Agents' initial positions are set as same to the simulation with the centralized algorithm . The parameters $\gamma_i, i = 1, 2, \ldots, 5$ are set as 0.8 and $a_i, i = 1, 2, \ldots, 5$ are set as 0.6. The trajectories of each agent, together with the initial shape and final shape are depicted in **Fig.** 6.5. The event times for each agent and the exponential convergence of each distance error are depicted in **Fig.** 6.6. Note that no $\|\{\boldsymbol{R}(t)^\top \boldsymbol{e}(t)\}_i\|$ crosses zero values at any finite time and Zeno behaviour is excluded. Furthermore, the distance error system shown in **Fig.** 6.6 also demonstrates almost the same convergence property as shown in Fig. 6.3.

Lastly, we show simulations with the same formation shape by using the modified trigger function (6.40). The exponential decay term is chosen as $v_i \exp(-\theta_i t) = \exp(-10t)$ with $v_i = 1$ and $\theta_i = 10$ for each agent. **Fig.** 6.7 shows event times for each agent as well as the convergence of each distance error. As can be observed from **Fig.** 6.7, Zeno-triggering is strictly excluded with the modified event function (6.40), while the convergence of the distance error system behaves almost the same to **Fig.** 6.3 and **Fig.** 6.6. It should be noted that in comparison with the controller performance and simulation examples discussed in [Sun et al., 2015c; Liu et al., 2015; Bai et al., 2015], the proposed event-triggered rigid formation control algorithms in this chapter demonstrate equal or even better performance, while complicated controllers and unnecessary assumptions in [Sun et al., 2015c; Liu et al., 2015; Bai et al., 2015] are avoided.

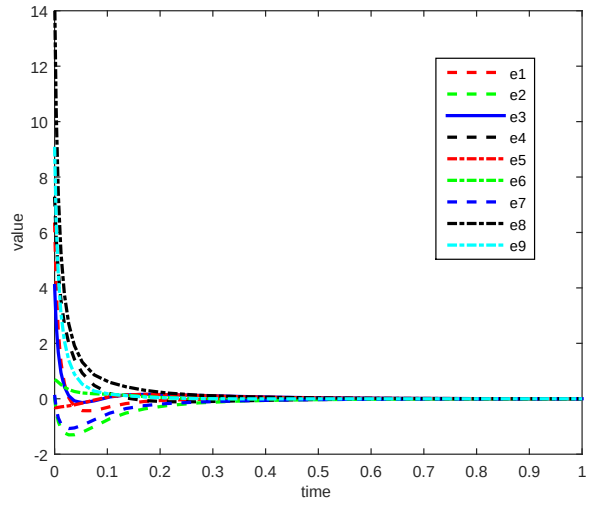

Figure 6.3: Exponential convergence of the distance errors with centralized algorithm.

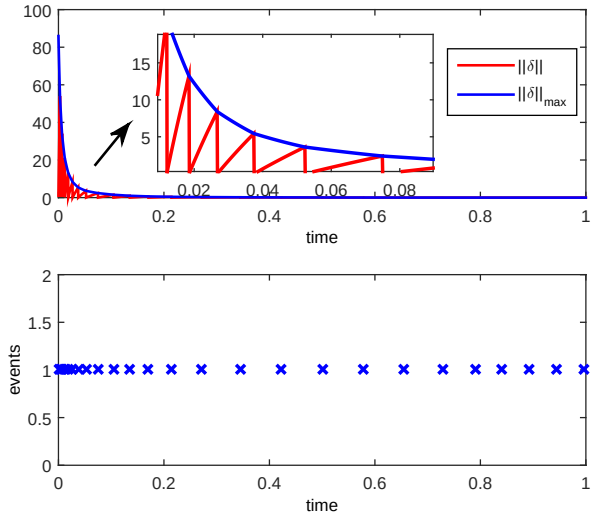

Figure 6.4: Performance of the centralized algorithm. Top: evolution of $\|\delta\|$ and $\|\delta\|_{\max} = \gamma\|R(t)^T e(t)\|$. Bottom: event triggering instants

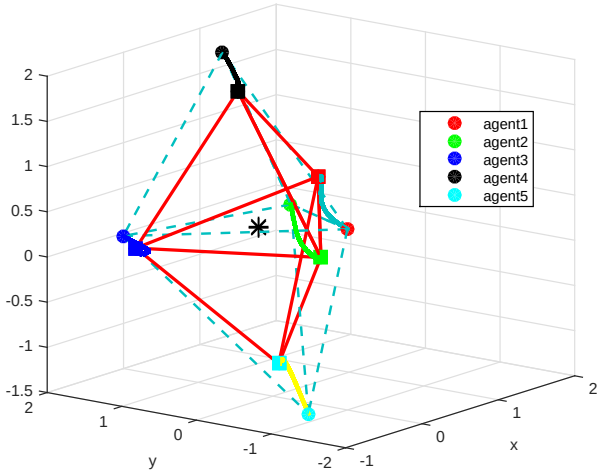

Figure 6.5: Simulation on stabilization control of a double tetrahedron formation in 3-D space with distributed algorithm. The initial and final positions are denoted by circles and squares, respectively. The initial formation is denoted by dashed lines, and the final formation is denoted by red solid lines. The black star denotes the formation centroid, which is *not* stationary.

6.6 Concluding remarks

In this chapter we have discussed in detail the design of feasible event-triggered control algorithms to stabilize rigid formation shapes. A centralized algorithm is proposed first, which guarantees the exponential convergence of distance errors and also excludes the existence of Zeno behaviour. Due to a careful design of the state mismatch and trigger function, the control algorithms are much simpler and require much less computation/measurement resources, compared with the results reported in [Bai et al., 2015; Sun et al., 2015c; Liu et al., 2015]. We then further propose a distributed algorithm such that each agent can trigger a local event to update its control input based on only local measurement. The event feasibility and trigger behaviour have been discussed in detail, which also guarantees Zeno-free behaviour for the event-triggered formation system and exponential convergence of the distance error system. A modified distributed event function is proposed, by which the Zeno behaviour is strictly excluded for each individual agent.

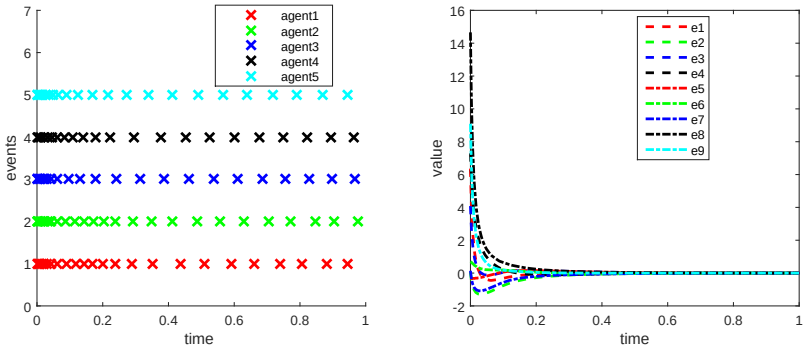

Figure 6.6: Controller performance of the distributed event-triggered formation system (6.30) with distributed trigger function (6.34). Left: Event instants for each agent. Right: Exponential convergence of the distance errors with distributed event controller.

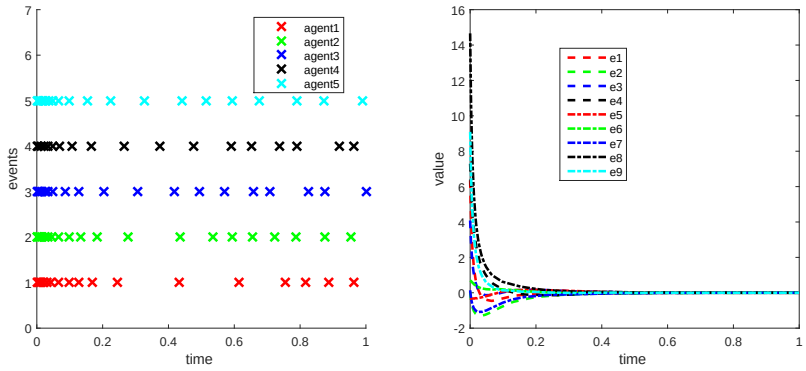

Figure 6.7: Controller performance of the distributed event-based formation system (6.30) (event function (6.40) with an exponential decay term). Left: Event triggering instants for each agent. Right: Exponential convergence of the distance errors with distributed event controller.

Chapter 7

Conclusions

In this chapter, we provide a summary and brief discussions of the main results in this thesis, and outline possible directions for future research.

7.1 Summary and contributions

We now show a brief summary of the main results and contributions of this thesis.

- The research of event-triggered control in MASs is an active area with numerous algorithms considering various situations. In **Chapter** 2, we provide a general review to the event-triggered consensus problem, in which the proposed trigger algorithms can be applied in different MAS tasks. We compare three types of trigger schemes, namely self-measurement-based, edge-measurement-based and local-measurement-based schemes, to classify the existing algorithms in literature, from the perspective of how the state mismatches are defined. For the three basic trigger schemes, we show how to deign their control inputs as well as trigger functions by using a classical Lyapunov function. The specific features for each trigger scheme are respectively presented with the statements of both its advantages and disadvantages. Moreover, we record two different concepts of Zeno behaviour in the literature and compare their differences by using an illustrative example. Zeno-free approaches in the existing literature are also concluded in this chapter with discussions on their basic ideas and restrictions.

- Motivated by practical constraints of digital platforms in MASs, we study event-triggered consensus problem under two different settings, namely agents using quantized information and agents under synchronized/unsynchronized working clocks. In **Chapter** 3, the convergence properties of the MAS with two types of quantized control inputs (input quantization and edge quantization) are investigated. We consider two kinds of quantizers, namely the uniform quantizer and the logarithmic quantizer. To completely exclude Zeno behaviour for each agent, we provide principles on how to add constant offsets to the trigger functions. The trade-off of using quantized information is also discussed in detail. In **Chapter** 4, the basic edge-measurement-based scheme for event-triggered

consensus is reconsidered with the concern of clock issues. In both synchronized and unsynchronized clock cases, we further investigate the requirement of the coordinate systems and present some much simpler, Zeno-free trigger conditions by using a time regulation idea (reviewed in **Section** 2). The main contribution of this chapter lies in the study of the unsynchronized clock case where we build a novel framework for constructing the closed-loop form of the MAS using edge-measurement-based scheme. This framework can deal with the situation that each agent is activated at different starting time.

- In **Chapter** 5, we design and investigate three event-triggered algorithms for networked Euler-Lagrange agents to achieve a specific leader-follower consensus task. The measurement requirement, convergence issues and the exclusion of Zeno behaviour for the three proposed algorithms are discussed in detail. We also provide simulation experiments to compare the trigger performance of our proposed algorithms under different trigger functions and point out the advantages of our adopted mixed trigger function. The first algorithm is built on a variable-gain approach with extremely flexible range of parameter selection in both control inputs and trigger functions. The second algorithm is proposed to deal with the difficulties introduced by considering directed network topologies. The proposed algorithm achieves leader-follower consensus semi-globally, exponentially fast. A trade-off in designing the algorithm is that some limited knowledge of the bounds on the agent dynamic parameters, the network topology and a set of all possible initial conditions are required to centrally design the control gains. The third algorithm is an adaptive algorithm, proposed under the situation that agent dynamics include the vector of gravitational potential forces. The design of the control inputs and trigger functions require more information about the agent dynamics but allow for the estimation of uncertain agent parameters.

- In **Chapter** 6, We provide alternative control algorithms to stabilize rigid formations based on an event-triggered strategy. Both centralized and distributed algorithms are proposed and studied in detail. In the centralized algorithms, a central event generator was designed to determine the next trigger time and broadcasts the event signal to all the agents for control inputs update. The distributed event-triggered algorithm is built on the centralized algorithm, in which each agent can use its local events and local information to update the control input at its own event times. For both algorithms, local exponential convergences to a target rigid formation are proved, which guarantees robustness to small disturbances. Our proposed algorithms show the lowest level of complexity when compared to the algorithms in relevant literature.

7.2 Future work

In this section we outline some future research problems.

- In **Chapter** 3, we apply the idea of adding constant offsets to the trigger functions to completely exclude Zeno behaviour for each agent. However, the offsets also sacrifice the convergence accuracy. In the analysis of logarithmic quantizer cases, it is observed that the offsets actually only need to be larger than some time-varying states, which tend to zero as $t \to \infty$. This observation reveals the possibility of designing a time-dependent offset (e.g. an exponential decay function) for the trigger function to exclude Zeno behaviour while ensuring a complete consensus, simultaneously. How to design the decay rate of the time-dependent offset should be the main challenge. Another interesting extension is to consider double integrator agent dynamics with both quantized relative positions and quantized relative velocities.

- In **Chapter** 4, we apply the time regulation idea (reviewed in **Chapter** 2) to exclude Zeno behaviour for each agent. However, the selection of the minimum trigger time interval and the control gain both require global knowledge of the applied MAS, which is not desirable for a distributed control system. The future focus of this work is to relax the requirement of using global knowledge in the parameter design procedure. Another extension is to consider different clock derivatives, i.e. the derivatives are not equal to one. This extension work is non-trivial because of the heterogeneity of the agent dynamics.

- In **Chapter** 5, we design and analyse event-triggered consensus algorithms for networked Euler-Lagrange agents. The difficulty mainly arises from the combination of highly non-linear agent dynamic models and the directed graph topology, which has not been addressed perfectly in this thesis. An important, also most challenging future work is to extend the variable-gain algorithm (see **Section** 5.4) to a directed graph case.

- In the study of the event-triggered consensus problem, the measurement of the states is usually assumed to be continuous so that state mismatches can be well defined. This assumption can be easily removed in consensus tasks, by using a so called self-triggered approach, due to the simplicity of the linear control inputs. In **Chapter** 6, we propose and investigate event-triggered rigid formation control algorithms, which also require continuous measurement of the relative positions among the agents. However, the complicated, highly non-linear control inputs bring a lot of difficulties in designing a self-triggered algorithm. We take the problem of designing self-triggered rigid formation control algorithms as the main future work of this chapter.

- In this thesis, the event-triggered algorithms are proposed to drive the agents to execute a single consensus task. However, in a practical MAS, it is common to require agents to execute multiple tasks simultaneously. This motivates us to think if it is possible to design event-triggered algorithms with multiple control aims, i.e., an event triggers multiple control updates. For example, we consider unsynchronized agent clocks in **Chapter** 4 where each agent's knowledge of its clock is predetermined and remains unchanged. However, it is acknowledged

that achieving clock synchronization might bring advantages for specific MASs, e.g. a wireless sensor network. What if we try to develop an event-triggered algorithm to drive agents to achieve both consensus and clock synchronizations simultaneously? This would be an interesting but also challenging problem.

Bibliography

Ames, A. D.; Tabuada, P.; and Sastry, S., 2006. On the stability of zeno equilibria. In *International Workshop on Hybrid Systems: Computation and Control*, 34–48. Springer. (cited on page 18)

Anderson, B. D. O. and Helmke, U., 2014. Counting critical formations on a line. *SIAM Journal on Control and Optimization*, 52, 1 (2014), 219–242. (cited on pages 91 and 98)

Anderson, B. D. O.; Yu, C.; Fidan, B.; and Hendrickx, J. M., 2008. Rigid graph control architectures for autonomous formations. *IEEE Control Systems Magazine*, 28, 6 (2008), 48–63. (cited on pages 1 and 91)

Araújo, J.; Mazo, M.; Anta, A.; Tabuada, P.; and Johansson, K. H., 2014. System architectures, protocols and algorithms for aperiodic wireless control systems. *IEEE Transactions on Industrial Informatics*, 10, 1 (2014), 175–184. (cited on page 2)

Asimow, L. and Roth, B., 1979. The rigidity of graphs, II. *Journal of Mathematical Analysis and Applications*, 68, 1 (1979), 171–190. (cited on page 92)

Aström, K. J., 2008. Event based control. In *Analysis and design of nonlinear control systems*, 127–147. Springer. (cited on page 91)

Bai, L.; Chen, F.; and Lan, W., 2015. Decentralized event-triggered control for rigid formation tracking. In *Proc. of the 34th Chinese Control Conference (CCC'15)*, 1262–1267. IEEE. doi:10.1109/ChiCC.2015.7259815. (cited on pages 101, 108, and 110)

Bapat, R. B., 2010. *Graphs and matrices*, vol. 27. Springer. (cited on page 8)

Cao, M.; Xiao, F.; and Wang, L., 2015. Event-based second-order consensus control for multi-agent systems via synchronous periodic event detection. *IEEE Transactions on Automatic Control*, 60, 9 (2015), 2452–2457. (cited on page 14)

Cao, M.; Xiao, F.; and Wang, L., 2016. Second-order consensus in time-delayed networks based on periodic edge-event driven control. *Systems & Control Letters*, 96 (2016), 37–44. (cited on page 14)

Cao, Y.; Yu, W.; Ren, W.; and Chen, G., 2013. An overview of recent progress in the study of distributed multi-agent coordination. *IEEE Transactions on Industrial informatics*, 9, 1 (2013), 427–438. (cited on page 1)

Carli, R. and Zampieri, S., 2010. Networked clock synchronization based on second order linear consensus algorithms. In *Decision and Control (CDC), 2010 49th IEEE Conference on*, 7259–7264. IEEE. (cited on page 1)

Ceragioli, F.; De Persis, C.; and Frasca, P., 2011. Discontinuities and hysteresis in quantized average consensus. *Automatica*, 47, 9 (2011), 1916–1928. (cited on page 25)

Dimarogonas, D. V.; Frazzoli, E.; and Johansson, K. H., 2012. Distributed event-triggered control for multi-agent systems. *Automatic Control, IEEE Transactions on*, 57, 5 (2012), 1291–1297. (cited on pages 11, 13, 25, 60, 67, and 105)

Dimarogonas, D. V. and Johansson, K. H., 2009a. Event-triggered control for multi-agent systems. In *Decision and Control, 2009 held jointly with the 2009 28th Chinese Control Conference. CDC/CCC 2009. Proceedings of the 48th IEEE Conference on*, 7131–7136. IEEE. (cited on pages 11 and 13)

Dimarogonas, D. V. and Johansson, K. H., 2009b. Event-triggered cooperative control. In *Control Conference (ECC), 2009 European*, 3015–3020. IEEE. (cited on pages 11 and 13)

Dimarogonas, D. V. and Johansson, K. H., 2010. Stability analysis for multi-agent systems using the incidence matrix: quantized communication and formation control. *Automatica*, 46, 4 (2010), 695–700. (cited on page 9)

Dong, X. and Hu, G., 2016. Time-varying formation control for general linear multi-agent systems with switching directed topologies. *Automatica*, 73 (2016), 47–55. (cited on page 1)

Donkers, M. and Heemels, W., 2012. Output-based event-triggered control with guaranteed-gain and improved and decentralized event-triggering. *IEEE Transactions on Automatic Control*, 57, 6 (2012), 1362–1376. (cited on page 2)

Dorfler, F., 2008. *Geometric analysis of the formation control problem for autonomous robots*. Diploma thesis, University of Toronto. Supervisor: Prof. Bruce Francis. (cited on page 98)

Dorfler, F. and Francis, B., 2010. Geometric analysis of the formation problem for autonomous robots. *IEEE Transactions on Automatic Control*, 55, 10 (2010), 2379–2384. (cited on page 91)

Fan, Y.; Feng, G.; Wang, Y.; and Song, C., 2013. Distributed event-triggered control of multi-agent systems with combinational measurements. *Automatica*, 49, 2 (2013), 671–675. (cited on pages 15, 25, 41, 60, and 67)

Fan, Y.; Liu, L.; Feng, G.; and Wang, L., 2015. Self-triggered consensus for multi-agent systemswith zeno-free triggers. *Automatic Control, IEEE Transactions on*, 60, 10 (2015), 2779 – 2784. (cited on pages 15, 23, 41, and 43)

Ferber, J., 1999. *Multi-agent systems: an introduction to distributed artificial intelligence*, vol. 1. Addison-Wesley Reading. (cited on page 1)

Gao, Y. and Wang, L., 2011. Sampled-data based consensus of continuous-time multi-agent systems with time-varying topology. *IEEE Transactions on Automatic Control*, 56, 5 (2011), 1226–1231. (cited on page 2)

Garcia, E.; Cao, Y.; and Casbeer, D. W., 2014. Decentralized event-triggered consensus with general linear dynamics. *Automatica*, 50, 10 (2014), 2633–2640. (cited on page 11)

Garcia, E.; Cao, Y.; Yu, H.; Antsaklis, P.; and Casbeer, D., 2013. Decentralised event-triggered cooperative control with limited communication. *International Journal of Control*, 86, 9 (2013), 1479–1488. (cited on pages 11, 13, 25, and 67)

Guinaldo, M.; Fábregas, E.; Farias, G.; Dormido-Canto, S.; Chaos, D.; Sánchez, J.; and Dormido, S., 2013. A mobile robots experimental environment with event-based wireless communication. *Sensors*, 13, 7 (2013), 9396–9413. (cited on page 2)

Guo, M., 2011. Quantized cooperative control. *Master's Degree Project, Stockholm, Sweden*, (2011). (cited on pages 25 and 26)

Guo, M. and Dimarogonas, D. V., 2013. Consensus with quantized relative state measurements. *Automatica*, 49, 8 (2013), 2531–2537. (cited on page 9)

Heemels, W.; Johansson, K. H.; and Tabuada, P., 2012. An introduction to event-triggered and self-triggered control. In *Proc. of the 51st Conference on Decision and Control*, 3270–3285. (cited on page 91)

Heemels, W.; Sandee, J.; and Van Den Bosch, P., 2008. Analysis of event-driven controllers for linear systems. *International journal of control*, 81, 4 (2008), 571–590. (cited on page 2)

Hendrickson, B., 1992. Conditions for unique graph realizations. *SIAM Journal on Computing*, 21, 1 (1992), 65–84. (cited on page 93)

Horn, R. A. and Johnson, C. R., 2012. *Matrix Analysis*. Cambridge University Press, New York. (cited on page 54)

Hu, W.; Liu, L.; and Feng, G., 2016. Consensus of linear multi-agent systems by distributed event-triggered strategy. *IEEE Transactions on Cybernetics*, 46, 1 (Jan 2016), 148–157. (cited on pages 15 and 67)

Hu, W.; Liu, L.; and Feng, G., 2017. Output consensus of heterogeneous linear multi-agent systems by distributed event-triggered/self-triggered strategy. *IEEE transactions on cybernetics*, (2017). (cited on page 15)

Huang, N.; Duan, Z.; and Zhao, Y., 2016. Distributed consensus for multiple Euler-Lagrange systems: An event-triggered approach. *Science China: Technological Sciences*, 59 (January 2016), 33–44. (cited on pages 53, 60, and 65)

Ioannou, P. A. and Fidan, B., 2006. *Adaptive Control Tutorial*. SIAM. (cited on page 55)

Isermann, R., 2013. *Digital control systems*. Springer Science & Business Media. (cited on page 2)

Kelly, R.; Davila, V. S.; and Perez, J. A. L., 2006. *Control of robot manipulators in joint space*. Springer Science & Business Media. (cited on pages 53, 57, and 66)

Khalil, H. K. and Grizzle, J., 1996. *Nonlinear systems*, vol. 3. Prentice hall New Jersey. (cited on page 106)

Knorn, S.; Chen, Z.; and Middleton, R. H., 2016. Overview: Collective control of multiagent systems. *IEEE Transactions on Control of Network Systems*, 3, 4 (2016), 334–347. (cited on page 1)

Krick, L.; Broucke, M. E.; and Francis, B. A., 2009. Stabilisation of infinitesimally rigid formations of multi-robot networks. *International Journal of Control*, 82, 3 (2009), 423–439. (cited on page 91)

Lehmann, D. and Lunze, J., 2009. Event-based control: A state-feedback approach. In *Control Conference (ECC), 2009 European*, 1716–1721. IEEE. (cited on page 2)

Li, H.; Liao, X.; Huang, T.; and Zhu, W., 2015. Event-triggering sampling based leader-following consensus in second-order multi-agent systems. *Automatic Control, IEEE Transactions on*, 60, 7 (July 2015), 1998–2003. doi:10.1109/TAC.2014.2365073. (cited on pages 15 and 65)

Li, Z.; Ren, W.; Liu, X.; and Fu, M., 2013. Consensus of Multi-Agent Systems With General Linear and Lipschitz Nonlinear Dynamics Using Distributed Adaptive Protocols. *IEEE Transactions on Automatic Control*, 58, 7 (2013), 1786–1791. (cited on pages 59 and 66)

Liu, H.; Cao, M.; and De Persis, C., 2012. Quantization effects on synchronized motion of teams of mobile agents with second-order dynamics. *Systems & Control Letters*, 61, 12 (2012), 1157–1167. (cited on page 25)

Liu, H.; Xie, G.; and Wang, L., 2010. Necessary and sufficient conditions for solving consensus problems of double-integrator dynamics via sampled control. *International Journal of Robust and Nonlinear Control*, 20, 15 (2010), 1706–1722. (cited on page 2)

Liu, Q.; Qin, J.; and Yu, C., 2016a. Event-based agreement protocols for complex networks with time delays under pinning control. *Journal of the Franklin Institute*, 353, 15 (2016), 3999–4015. (cited on page 15)

Liu, Q.; Qin, J.; and Yu, C., 2016b. Event-based multi-agent cooperative control with quantized relative state measurements. In *Decision and Control (CDC), 2016 IEEE 55th Conference on*, 2233–2239. IEEE. (cited on page 15)

Liu, Q.; Sun, Z.; Qin, J.; and Yu, C., 2015. Distance-based formation shape stabilisation via event-triggered control. In *Proc. of the 34th Chinese Control Conference(CCC'15)*, 6948–6953. IEEE. (cited on pages 101, 108, and 110)

Liu, Q.; Ye, M.; Qin, J.; and Yu, C., 2016c. Event-based leader-follower consensus for multiple euler-lagrange systems with parametric uncertainties. In *Decision and Control (CDC), 2016 IEEE 55th Conference on*, 2240–2246. IEEE. (cited on page 15)

Liu, X.; Du, C.; Lu, P.; and Yang, D., 2016d. Decentralised consensus for multiple lagrangian systems based on event-triggered strategy. *International Journal of Control*, 89, 6 (2016), 1111–1124. (cited on pages 11, 13, 53, and 67)

Mei, J.; Ren, W.; and Chen, J., 2016. Distributed Consensus of Second–Order Multi–Agent Systems with Heterogeneous Unknown Inertias and Control Gains Under a Directed Graph. *IEEE Transactions on Automatic Control*, 61, 8 (2016), 2019–2034. (cited on pages 59 and 66)

Mei, J.; Ren, W.; Chen, J.; and Anderson, B. D. O., 2014. Consensus of linear multi-agent systems with fully distributed control gains under a general directed graph. In *IEEE 53rd Annual Conference on Decision and Control*, 2993–2998. IEEE, Los Angeles, USA. (cited on pages 59 and 66)

Mei, J.; Ren, W.; Chen, J.; and Ma, G., 2013. Distributed adaptive coordination for multiple lagrangian systems under a directed graph without using neighborsâĂŹ velocity information. *Automatica*, 49, 6 (2013), 1723–1731. (cited on pages 53 and 81)

Mei, J.; Ren, W.; and Ma, G., 2011. Distributed Coordinated Tracking With a Dynamic Leader for Multiple Euler-Lagrange Systems. *IEEE Transactions on Automatic Control*, 56, 6 (2011), 1415–1421. (cited on page 53)

Mei, J.; Ren, W.; and Ma, G., 2012. Distributed Containment Control for Lagrangian Networks With Parametric Uncertainties Under a Directed Graph. *Automatica*, 48, 4 (2012), 653–659. (cited on pages 81 and 82)

Meng, Z.; Anderson, B. D. O.; and Hirche, S., 2015. Analysis of undirected formation shape control with directional mismatch. In *Proc. of the 54th Conference on Decision and Control*, 6773–6778. IEEE. (cited on page 91)

Meng, Z. and Lin, Z., 2012. Distributed Finite-time Cooperative Tracking of Networked Lagrange Systems via Local Interactions. In *American Control Conference (ACC), Montréal, Canada*, 4951–4956. IEEE. (cited on page 53)

Mesbahi, M. and Egerstedt, M., 2010. *Graph theoretic methods in multiagent networks*. Princeton University Press. (cited on page 8)

Mou, S.; Morse, A. S.; Belabbas, M. A.; Sun, Z.; and Anderson, B. D. O., 2015. Undirected rigid formations are problematic. *IEEE Transactions on Automatic Control, in press. DOI: 10.1109/TAC.2015.2504479*, (2015). (cited on pages 93, 94, and 96)

Mu, B.; Li, H.; Li, W.; and Shi, Y., 2014. Consensus for multiple euler-lagrange dynamics with arbitrary sampling periods and event-triggered strategy. In *Intelligent Control and Automation (WCICA), 2014 11th World Congress on*, 2596–2601. IEEE. (cited on pages 22 and 53)

Mu, N.; Liao, X.; and Huang, T., 2015. Event-based consensus control for a linear directed multiagent system with time delay. *Circuits and Systems II: Express Briefs, IEEE Transactions on*, 62, 3 (2015), 281–285. (cited on page 11)

Nagata, T. and Sasaki, H., 2002. A multi-agent approach to power system restoration. *IEEE transactions on power systems*, 17, 2 (2002), 457–462. (cited on page 1)

Nedić, A.; Olshevsky, A.; Ozdaglar, A.; and Tsitsiklis, J. N., 2009. On distributed averaging algorithms and quantization effects. *Automatic Control, IEEE Transactions on*, 54, 11 (2009), 2506–2517. (cited on page 25)

Nowzari, C. and Cortés, J., 2014. Zeno-free, distributed event-triggered communication and control for multi-agent average consensus. In *American Control Conference (ACC), 2014*, 2148–2153. IEEE. (cited on page 23)

Nowzari, C. and Cortés, J., 2016. Distributed event-triggered coordination for average consensus on weight-balanced digraphs. *Automatica*, 68 (2016), 237–244. (cited on page 41)

Oh, K.-K. and Ahn, H.-S., 2014. Distance-based undirected formations of single-integrator and double-integrator modeled agents in n-dimensional space. *International Journal of Robust and Nonlinear Control*, 24, 12 (2014), 1809–1820. (cited on pages 1 and 91)

Oh, K.-K.; Park, M.-C.; and Ahn, H.-S., 2015. A survey of multi-agent formation control. *Automatica*, 53 (2015), 424–440. (cited on pages 2, 91, and 98)

Oliva, G.; Setola, R.; and Hadjicostis, C. N., 2013. Distributed k-means algorithm. *arXiv preprint arXiv:1312.4176*, (2013). (cited on page 1)

Ortega, R.; Perez, J. A. L.; Nicklasson, P. J.; and Sira-Ramirez, H., 2013. *Passivity-based Control of Euler-Lagrange systems: Mechanical, Electrical and Electromechanical Applications*. Springer Science & Business Media. (cited on page 53)

Pan, X.; Han, C. S.; Dauber, K.; and Law, K. H., 2007. A multi-agent based framework for the simulation of human and social behaviors during emergency evacuations. *Ai & Society*, 22, 2 (2007), 113–132. (cited on page 1)

Qin, J.; Fu, W.; Gao, H.; and Zheng, W. X., 2017a. Distributed *k*-means algorithm and fuzzy *c*-means algorithm for sensor networks based on multiagent consensus theory. *IEEE transactions on cybernetics*, 47, 3 (2017), 772–783. (cited on page 1)

Qin, J.; Li, F.; Mou, S.; and Kang, Y., 2016. Multi-timer based event synchronization control for sensor networks and its application. *IEEE Transactions on Industrial Electronics*, 63, 12 (2016), 7765–7775. (cited on page 2)

Qin, J.; Ma, Q.; Shi, Y.; and Wang, L., 2017b. Recent advances in consensus of multi-agent systems: A brief survey. *IEEE Transactions on Industrial Electronics*, 64, 6 (2017), 4972–4983. (cited on pages 18 and 19)

Rahbari-Asr, N.; Ojha, U.; Zhang, Z.; and Chow, M.-Y., 2014. Incremental welfare consensus algorithm for cooperative distributed generation/demand response in smart grid. *IEEE Transactions on Smart Grid*, 5, 6 (2014), 2836–2845. (cited on page 1)

Ren, W., 2007. Consensus strategies for cooperative control of vehicle formations. *IET Control Theory & Applications*, 1, 2 (2007), 505–512. (cited on page 1)

Ren, W. and Beard, R. W., 2004. Decentralized scheme for spacecraft formation flying via the virtual structure approach. *Journal of Guidance, Control, and Dynamics*, 27, 1 (2004), 73–82. (cited on page 1)

Ren, W. and Beard, R. W., 2008. *Distributed consensus in multi-vehicle cooperative control*. Springer. (cited on pages 1 and 8)

Ren, W. and Cao, Y., 2011. *Distributed Coordination of Multi-agent Networks: Emergent Problems, Models and Issues*. Springer London. (cited on pages 53 and 57)

Rudin, W. et al., 1964. *Principles of mathematical analysis*, vol. 3. McGraw-Hill New York. (cited on page 54)

Seyboth, G., 2010. Event-based control for multi-agent systems. *Master's Degree Project, Stockholm, Sweden*, (2010). (cited on pages 2, 18, 19, 21, and 22)

Seyboth, G. S. and Allgower, F., 2013. Clock synchronization over directed graphs. In *Decision and Control (CDC), 2013 IEEE 52nd Annual Conference on*, 6105–6111. IEEE. (cited on page 1)

Seyboth, G. S.; Dimarogonas, D. V.; and Johansson, K. H., 2013. Event-based broadcasting for multi-agent average consensus. *Automatica*, 49, 1 (2013), 245–252. (cited on pages 11, 13, 21, 25, 41, and 67)

Song, Q.; Liu, F.; Cao, J.; and Yu, W., 2012. Pinning-controllability analysis of complex networks: an m-matrix approach. *Circuits and Systems I: Regular Papers, IEEE Transactions on*, 59, 11 (2012), 2692–2701. (cited on page 57)

Sun, Z.; Helmke, U.; and Anderson., B. D. O., 2015a. Rigid formation shape control in general dimensions: an invariance principle and open problems. In *Proc. of the 54th Conference on Decision and Control*, 6095–6100. IEEE. (cited on page 98)

Sun, Z.; Huang, N.; Anderson, B. D.; and Duan, Z., 2016a. A new distributed zeno-free event-triggered algorithm for multi-agent consensus. In *Decision and Control (CDC), 2016 IEEE 55th Conference on*, 3444–3449. IEEE. (cited on pages 19, 20, 64, 66, and 67)

Sun, Z.; Huang, N.; Anderson, B. D.; and Duan, Z., 2017. Comments on "distributed event-triggered control of multi-agent systems with combinational measurements". *In submission*, (2017). https://www.dropbox.com/s/umusynb4gjbldyx/2017_Automatica_Event_Comment.pdf?dl=0. (cited on page 20)

Sun, Z.; Liu, Q.; Qin, J.; and Yu, C., 2015b. Generalized controllers for rigid formation stabilization with application to event-based controller design. In *European Control Conference, 2015. ECC'15.*, 217–222. IEEE. (cited on page 1)

Sun, Z.; Liu, Q.; Yu, C.; and Anderson, B. D. O., 2015c. Generalized controllers for rigid formation stabilization with application to event-based controller design. In *Proc. of the 2015 European Control Conference (ECC'15)*, 217–222. IEEE. (cited on pages 96, 101, 108, and 110)

Sun, Z.; Mou, S.; Anderson, B. D.; and Cao, M., 2016b. Exponential stability for formation control systems with generalized controllers: A unified approach. *Systems & Control Letters*, 93 (2016), 50–57. (cited on page 93)

Sun, Z.; Mou, S.; Deghat, M.; and Anderson, B. D. O., 2015d. Finite time distributed distance-constrained shape stabilization and flocking control for d-dimensional undirected rigid formations. *International Journal of Robust and Nonlinear Control, in press. DOI: 10.1002/rnc.3477*, (2015). (cited on pages 96, 97, and 103)

Tabuada, P., 2007. Event-triggered real-time scheduling of stabilizing control tasks. *IEEE Transactions on Automatic Control*, 52, 9 (2007), 1680–1685. (cited on pages 2 and 100)

VanDyke, M. C. and Hall, C. D., 2006. Decentralized coordinated attitude control within a formation of spacecraft. *Journal of Guidance Control and Dynamics*, 29, 5 (2006), 1101–1109. (cited on page 1)

Vasile, C.-I.; Schwager, M.; and Belta, C., 2015. SE(N) Invariance in Networked Systems. In *Proc. of the 2015 European Control Conference (ECC'15)*, 186–191. IEEE. (cited on page 97)

Wang, A.; Mu, B.; and Shi, Y., 2017a. Consensus control for a multi-agent system with integral-type event-triggering condition and asynchronous periodic detection. *IEEE Transactions on Industrial Electronics*, 64, 7 (2017), 5629–5639. (cited on page 2)

Wang, X. and Lemmon, M. D., 2011. Event-triggering in distributed networked control systems. *IEEE Transactions on Automatic Control*, 56, 3 (2011), 586–601. (cited on page 2)

Wang, X.-F.; Deng, Z.; Ma, S.; and Du, X., 2017b. Event-triggered design for multi-agent optimal consensus of euler-lagrangian systems. *Kybernetika*, 53, 1 (2017), 179–194. (cited on page 71)

Wei, B.; Xiao, F.; and Dai, M.-Z., 2016. Edge event-triggered synchronization in networks of coupled harmonic oscillators. *IEEE transactions on cybernetics*, (2016). (cited on page 14)

Wei, B.; Xiao, F.; and Dai, M.-Z., 2017. Edge event-triggered control for multi-agent systems under directed communication topologies. *International Journal of Control*, (2017), 1–10. (cited on pages 14, 41, and 67)

Xiao, F. and Chen, T., 2012. Sampled-data consensus for multiple double integrators with arbitrary sampling. *IEEE Transactions on Automatic Control*, 57, 12 (2012), 3230–3235. (cited on page 2)

Xiao, F.; Meng, X.; and Chen, T., 2012. Average sampled-data consensus driven by edge events. In *Control Conference (CCC), 2012 31st Chinese*, 6239–6244. IEEE. (cited on pages 14 and 41)

Xiao, F.; Meng, X.; and Chen, T., 2015. Sampled-data consensus in switching networks of integrators based on edge events. *International Journal of Control*, 88, 2 (2015), 391–402. (cited on pages 14 and 41)

Xie, G.; Liu, H.; Wang, L.; and Jia, Y., 2009. Consensus in networked multi-agent systems via sampled control: fixed topology case. In *American Control Conference, 2009. ACC'09.*, 3902–3907. IEEE. (cited on page 2)

Xu, W.; Ho, D. W.; Zhong, J.; and Chen, B., 2017. Distributed edge event-triggered consensus protocol of multi-agent systems with communication buffer. *International Journal of Robust and Nonlinear Control*, 27, 3 (2017), 483–496. (cited on page 14)

Yang, D.; Ren, W.; Liu, X.; and Chen, W., 2016. Decentralized event-triggered consensus for linear multi-agent systems under general directed graphs. *Automatica*, 69 (2016), 242–249. (cited on pages 11, 13, and 67)

Ye, M.; Yu, C.; and Anderson, B. D. O., 2015. Model-Independent Rendezvous of Euler-Lagrange Agents on Directed Networks. In *Proceedings of IEEE 54th Annual Conference on Decision and Control, Osaka, Japan*, 3499–3505. (cited on page 53)

Yi, X.; Lu, W.; and Chen, T., 2016. Distributed event-triggered consensus for multi-agent systems with directed topologies. In *Control and Decision Conference (CCDC), 2016 Chinese*, 807–813. IEEE. (cited on page 11)

Yu, H. and Antsaklis, P. J., 2012. Quantized output synchronization of networked passive systems with event-driven communication. In *American Control Conference (ACC), 2012*, 5706–5711. IEEE. (cited on page 25)

Yu, W.; Zheng, W. X.; Chen, G.; Ren, W.; and Cao, J., 2011. Second-order consensus in multi-agent dynamical systems with sampled position data. *Automatica*, 47, 7 (2011), 1496–1503. (cited on page 2)

Zelazo, D. and Mesbahi, M., 2011. Edge agreement: Graph-theoretic performance bounds and passivity analysis. *IEEE Transactions on Automatic Control*, 56, 3 (2011), 544–555. (cited on page 8)

Zeng, Z.; Wang, X.; and Zheng, Z., 2016. Edge agreement of multi-agent system with quantised measurements via the directed edge laplacian. *Control Theory & Application, IET*, 10, 13 (August 2016), 1583 – 1589. doi:10.1049/iet-cta.2015.1068. (cited on page 9)

Zhang, J.; Johansson, K. H.; Lygeros, J.; and Sastry, S., 2001. Zeno hybrid systems. *International Journal of Robust and Nonlinear Control*, 11, 5 (2001), 435–451. (cited on pages 18 and 25)

Zhang, Z. and Chow, M.-Y., 2012. Convergence analysis of the incremental cost consensus algorithm under different communication network topologies in a smart grid. *IEEE Transactions on Power Systems*, 27, 4 (2012), 1761–1768. (cited on page 1)

Zhang, Z.; Zhang, L.; Hao, F.; and Wang, L., 2015. Distributed event-triggered consensus for multi-agent systems with quantisation. *International Journal of Control*, 88, 6 (2015), 1112–1122. (cited on pages 11 and 25)

Zhu, W. and Jiang, Z.-P., 2015. Event-based leader-following consensus of multi-agent systems with input time delay. *Automatic Control, IEEE Transactions on*, 60, 5 (May 2015), 1362–1367. (cited on pages 15 and 71)

Zhu, W.; Jiang, Z.-P.; and Feng, G., 2014. Event-based consensus of multi-agent systems with general linear models. *Automatica*, 50, 2 (2014), 552–558. (cited on pages 15 and 22)